الجمهورية الجزائرية الديمقراطية الشعبية
People's Democratic Republic of Algeria
وزارة التعليم العالي والبحث العلمي
Ministry of Higher Education Scientific Research

Mohamed Khider University– Biskra

Faculty of Sciences and Technology

Department: Civil and Hydraulic Engineering

Ref :……

جامعة محمد خيضر – بسكرة

جامعة محمد خيضر بسكرة

كلية العلوم والتكنولوجيا

قسم الهندسة المدنية والري :

المرجع.....:

Thesis Submitted for Obtaining the degree of

Doctor in Civil Engineering

Specialty: Materials

By

Hernoune Houria

Etude Expérimentale et Numérique du Comportement des Murs en Maçonnerie Renforcés par Matériau Composite

Experimental and Numerical Study of the Behaviour of Masonry Walls Reinforced with Composite Material

Thesis defended publicly on: ……

Jury members:

Mr. Rachid CHEBILI	Professor	President	University of Biskra
Mr. Abdelhamid GUETTALA	Professor	Supervisor	University of Biskra
Mr. Abdelkrim KADID	Professor	Examiner	University of Batna
Mr. Hocine CHABIL	Professor	Examiner	University of Constantine

ACKNOWLEDGMENTS

The work presented in this thesis would not have been possible without the contribution of many people who live close and far from me.

I wish to express my appreciation to my advisor Professor Guettala Abdelhamid who gave me the chance of going to the University of Biskra to conclude my research.

I would like also to express my special appreciation to Professor Benchaa Benabed for his guidance, advices and important suggestions.

A special thank goes also to my colleagues and friends Dr Herihiri Ouided, Dr Younes Ould Khaoua who supported and helped me during my research and, above all, with their friendship. I would also like to thank everyone who entered in the laboratory and helped me during the experimental campaign.

Last but not least, I would like to thank my parents for their love, support and patience.

Mrs. Houria.Hernoune

ملخص

هناك عدد كبير من المباني القديمة، بما في ذلك المعالم التاريخية والثقافية في جميع أنحاء العالم. والتي تم بناؤها بجدران بناء غير مدعمة، وهي معرضة للأضرار بسبب التحميل الزائد والتدهور الناجم عن المخاطر البيئية. لذلك يوصى بشدّة باقتراح تقنيات دعم مناسبة للحفاظ على هذا النوع من المبانيّ. تقنيات عديدة ومختلفة تم اقتراحها لتعزيز هذا النوع، باستعمال مواد مركّبة مختلفة، نذكر من بينها تقنية الدعم بشرائط البوليمار المقوى بألياف الكربون، ويتمّ استخدامها إما عن طريق تقنية (EB-CFRP) وهنا يكون الربط خارجيا مع الجدار، وإما عن طريق تقنية(NSM-CFRP) ،
وهنا يكون الربط عن طريق وضع قصّ داخل الجدار، ويكون قريبا من السّطح.

الهدف الرئيسيّ من الدراسة الحالية هو دراسة سلوك جدران البناء المصنوعة من الآجر المثقبة المعززة والغير معززة، باستعمال المواد المركبة من نوع (CFRP) تحت تأثير حمولة على المستوى، ولهذا الغرض تمّ دراسة أربعة أنواع مختلفة من عينات البناء.

تم اعتماد نهج النمذجة العددية الدقيقة والتفصيلية (DMM) باستعمال برنامج ABAQUS للقيام بنمذجة رقمية لسلوك جدران البناء المصنوع من الآجر. في هذه النمذجة الرقمية تم محاكاة التحليل الغير خطي للطوب والملاط بتقنية (CDP)، بحيث تسمح هذه التقنية بظهور التشققات والفشل على واجهة كل من الطوب والملاط، كما تمّ استخدام تقنية (XFEM) والتي من خلالها نتمكن من معرفة مكان ظهور الشقوق دون تعريف مبدئي لموقع التشقق. أظهرت النتائج المتحصّل عليها أن تقنيات التعزيز تعمل بشكل كبير على تحسن قوّة القص وقدرة التشوه، تمت مقارنة نتائج المحاكاة العددية مع النتائج التجريبية عن طريق مقارنة منحى تشوّه الإجهاد وأنماط التشقق. تم استنتاج أن النموذج المقترح يعطي تنبّؤا ممتازا لسلوك القصّ ووضع الفشل لجدران البناء المدعم بشرائط (CFRP) والغير مدعم، بالإضافة إلى ذلك استخدام تقنية العناصر المحدودة الممتدة (XFEM)، جيّد لتحليل عملية التصدّع وانتشار التشققات.

الكلمات المفتاحية: القص الثلاثي الغير مدعم؛ شرائط البوليمر المقوى بألياف الكربون؛ النمذجة الدقيقة المفصلة؛ اللدونة التالفة للخرسانة؛ طريقة العناصر المحدودة الممتدة.

Résumé

Il existe un grand nombre de bâtiments anciens, y compris des monuments historiques et culturels à travers le monde, qui sont construits avec de la maçonnerie non renforcée (URM) et qui sont extrêmement vulnérables en cas des actions environnementales.

Par conséquent, il est fortement recommandé de suggérer des techniques de renforcement adéquates afin de préserver ce type de structure. Différentes techniques de renforcement des structures URM ont été proposées, en utilisant une large gamme de matériaux tels que les matériaux composites. Parmi les techniques utilisées dans le renforcement des structures de maçonnerie, il y a la technique des polymères renforcés de fibres (FRP) à liaison externe (EB) et la technique des polymères renforcés de fibres (FRP) montés près de la surface (NSM).

L'objectif principal de la présente étude était d'étudier le comportement au cisaillement des assemblages de maçonnerie en briques renforcées par PRF sous une charge dans le plan. À cette fin, quatre types de spécimens de maçonnerie ont été étudiés. Afin de modéliser le comportement des murs de maçonnerie, l'approche de micro-modélisation détaillée (DMM) a été adoptée, qui est mise en œuvre dans le programme ABAQUS pour effectuer une simulation numérique de différents assemblages de maçonnerie. Dans cette étude, des modèles d'éléments finis ont été développés pour simuler le comportement de différents types d'essais d'assemblages de maçonnerie.

Le comportement non linéaire de la brique et du mortier a été simulé à l'aide des lois de comportement de plasticité endommagée du béton (CDP). Cependant, les bandes de FRP ont été connectées aux éléments de maçonnerie par modèle d'interface. Cette approche permet à la rupture de se produire sur brique, mortier et brique-mortier interface. De plus, une approche de zone cohésive basée sur la méthode des éléments finis étendus (XFEM) a été utilisée pour simuler l'initiation et la propagation de fissures arbitraires dans un mortier sans définition initiale de l'emplacement des fissures.

Les résultats des simulations numériques ont été comparés aux résultats expérimentaux. Il a été conclu que le modèle proposé présentait une excellente prédiction du comportement au cisaillement et du mode de rupture des murs de maçonnerie non renforcés et renforcés par FRP. Enfin, XFEM s'est révélé être une technique puissante à utiliser pour l'analyse du processus de fracture et de la propagation des fissures dans les murs de maçonnerie.

Mots clés : Triplet de cisaillement non renforcé ; Polymère renforcé par fibre de Carbon ; NSM-CFRP ; EB-CFRP ; Micro-modélisation détaillée (DMM) ; Plasticité endommagée du béton (CDP), Méthode des éléments finis étendus (XFEM).

Abstract

There is a large number of old buildings including historical and cultural monuments around the world, which are constructed with unreinforced masonry (URM) and they are exposed to damage due to overloading and deterioration caused by environmental hazards. Therefore, it is highly recommended that adequate retrofit techniques be suggested in order to preserve this type of structure. Different techniques for the reinforcement of URM structures have been proposed, using a wide range of materials such as composite materials. Among the techniques used in the reinforcement of masonry structures, there is the Externally Bonded (EB) fiber-reinforced polymer (FRP) technique and the Near-Surface Mounted (NSM) fiber-reinforced polymer (FRP) technique.

The main objective of the current study was to investigate the shear behavior of FRP strengthened brick masonry assemblages under in-plane loading. For this purpose, four masonry specimen types were investigated. The obtained results show that, the strengthening techniques had a considerable improvement in shear strength and deformation capacity.

In order to model the behaviour of masonry walls, the detailed micro-modelling (DMM) approach was adopted, which is implemented in ABAQUS program to perform a numeric simulation of different masonry assemblages. In this study, finite element models were developed to simulate the behavior of different test types of masonry assemblages. The nonlinearities behavior of brick and mortar was simulated using the Concrete Damaged Plasticity (CDP) constitutive laws. However, FRP strips were connected to masonry elements by interface model. This approach allows failure to occur on either the brick, mortar and brick-mortar interface. In addition, the Extended Finite Element Method (XFEM)-based cohesive zone approach was used to simulate the arbitrary crack initiation and crack propagation within a mortar without an initial definition of crack location.

The results of numerical simulations were compared with the experimental results. It was concluded that the proposed model presented an excellent prediction for shear behavior and failure mode of unreinforced and FRP-reinforced masonry walls. On the other hand, XFEM was found as a powerful technique to be used for the analysis of the fracture process and crack propagation in masonry walls.

Keywords: Unreinforced shear triplet; Carbon Fiber Reinforced Polymer (CFRP); NSM-CFRP; EB-CFRP; Detailed Micro-Modeling (DMM); Concrete Damaged Plasticity (CDP); Extended Finite Element Method (XFEM).

Contents

List of figures

List of Tables

List of abbreviations

(URM): unreinforced masonry

(FE): finite elements

(DEM): discrete element methods

(BEM): Boundary Element Method

(D-LAM): Discrete Limit Analysis Models

(CM): continuum model

(PM): particle model

(IT): resources all information technology resources and computer systems

(CPU): times process time

(DMM): Detailed Micro-Modeling

(CFRP): carbon fiber-reinforced polymer

(NSM-CFRP): Near-Surface Mounted with carbon fiber-reinforced polymer technique

(EB-FRP): externally bonded with carbon fiber-reinforced polymer

(XFEM): Extended Finite Element Method

(CDP): Concrete Damaged Plasticity

(COPEN): contact opening parameter

(STUXFEM): indicates the cracking status of the element

(FRP): fiber-reinforced polymer

(CFRP): Carbon Fiber Reinforced Polymer

(GFRP): Glass Fiber Reinforced Polymer

(AFRP): Aramid Fiber Reinforced Polymer

(URM): unreinforced masonry

(TRM): Textile reinforced mortar

(FRM) : Fiber Reinforced Mortar

(DAMAGET): tensile damage

(DAMAGEC): compression damage

(CSDMG): cohesive surface damage

(CSHEAR): contact shear

(LD): The masonry units with low unit volume mass

(HD): the masonry units with high unit volume mass

(Eb): elasticity module of clay bricks

(fb): compressive strength of bricks

(f_m): the average resistance of the mortar joint

(f_c): concrete resistance at 28 days

(C): Cement dosage

(Mf): Fineness module

(R_t): Tensile strength

(R_C) : Compressive strength

(E): Water dosage

(E/C) : Water / cement ratio

(μ): Apparent coefficient of friction

(σ_c) : Vertical pre-compression stress

(τ_0) : Pure shear strength

(τ): Average shear stress

(Mode I) : tensile failure

(Mode II) : shear failure

(ν_b):Poisson's ratio

(G_f): fracture energy for tension

(G_c): fracture energy for compression

(τ_u): shear strength of masonry assemblies

(ρ_h): the reinforcement ratio of FRP in the horizontal direction

(E_{FRP}): modulus of elasticity of FRP

(ε_{tu}): the ultimate strain of FRP

(k): efficiency factor

(t): wall thickness

(L): wall length.

(φ): The internal friction angles.

(c): cohesion value

(ft): the uniaxial tensile strength;

(fc): the ultimate uniaxial compressive strength;

(fcb): the ultimate biaxial compressive strength;

($f1$): the ultimate compressive strength for a state of biaxial compression superimposed on hydrostatic stress state failure surface proposed by William and Warnke in principal stress space

(F): function of the principal stress state,

(S): the failure surface expressed in terms of principal stresses and five input parameters ft, fc, fcb, $f1$ and $f2$.

(CoDIC): Concrete Drucker Prager - Ideal Spherical Compression Cap model

(ε_n): normal deformations

(ε_t): tangential deformations

(k_n): normal stiffnesses

(k_t): tangential stiffnesses

(G_b et G_m) : the shear modules of the bricks and the mortar

(E_b, E_m): elastic modules

(h_m): the thickness of the mortar

(PC): The portland cement

(NHL): Natural hydraulic lime

(P_{max}): the shear load at failure

($\mu = tan\,\varphi$): frictional coefficient between the unit and the mortar

($C = \tau_0$): the shear strength under zero compression loads and represents the cohesion (bond shear stress).

($\sigma_n = \sigma_0$) : the normal stress

(ST): the control triplet specimen

(SRV): masonry wall specimen reinforced with vertical FRP

(SRX): indicates an X pattern of FRP reinforcement applied to one side of the masonry wall specimen

(SR2X): indicates the specimen reinforced with FRP on two sides.

(C3D8R): eight node 3D continuum elements with four glass controls and reduced integration

($\frac{f_{bo}}{f_{co}}$): the ratio between the initial equilbiaxial compressive strength and uniaxial compressive strength of masonry.

(k): the ratio of second stress invariant on the tensile meridian.

(ψ): The dilation angle

(S4R): The Shell elements

(k_0): the initial stiffness

(t_i): the thickness of the resin

(t_c): the thickness of the masonry wall

(G_i, G_c): are the shear modulus of resin and masonry wall respectively.

(τ_s and τ_t): are the shear stresses of the interface, and n, s, t are the directions of the components of the constraint

(Gn): The opening fracture

(Gs): sliding fracture

(Gt): tearing fracture

***(H(x))*:** Jump function

(α_I = a_I): Nodal enriched degree of freedom vector

($N_I(x)$ $N_I(x)$): Shape function

($f_\alpha(x)$ $f_\alpha(x)$): Asymptotic crack-tip functions

(b_I^α): Nodal enriched degree of freedom vector

(e): Eccentricity parameter

(ν): Viscosity setting

(τ_u): ultimate shear strength

(δ_u): Maximum shear deformation

(δ_e): elastic shear deformation

(μ): ductility

(δ_u): displacement at ultimate load

(δ_y): displacement at the load causing yield condition

(MT): control panels

(MTA): control panels constructed with mortar type A

(MTB): control panels constructed with mortar type B

(μ_u/μ_o): improvement between unreinforced and reinforced masonry walls

fibers (%): percentage occupation of the surface walls by carbon fiber band

(d_c): the compressive damaged parameter

(d_t): the tensile Damaged parameter

Chapter 1

Introduction

1. 1 Background

Masonry has been the most common building material for centuries and is still one of the oldest building materials used in modern construction. Masonry is a combination of units bonded together with mortar; but these units can be made from different materials and have different mechanical properties. The combination and configuration of these constituent materials result in a complex and diverse construction material. The structural response of brick masonry depends on the mechanical properties of its components (unit and mortar) and the bonding properties of the unit-mortar interface.

Around the world, there are many old unreinforced masonry (URM) structures such as historical cultural monuments and bridges, etc. which are deteriorated or damaged during earthquake events. In order to extend the life of such structures, strengthening or repairing by implementing new techniques have been developed. Many of these strengthening techniques including the use of fiber reinforced polymer (FRP) composites have been used to reinforce masonry structures. The use of this technique offers several advantages such as increasing strength and ductility of walls subjected to out-of-plane or in-plane lateral loading. FRP is high strength fibers incorporated into a polymeric matrix (epoxy, polyester, etc), These composites are manufactured in different characteristics depending on the fiber material type such as carbon (CFRP), glass (GFRP), and Aramid (AFRP). FRP strips offer the possibility of application by gluing on the outside surface EB (externally bonded) or inserting inside a groove of element by the NSM technique. Experimental studies have evaluated the effect of different variables for example, the effect of retrofitting configuration of FRP composite, type of FRP composites and the type of masonry components, through small-scale testing such as triplets test, and by full scale testing. Many authors have studied the rehabilitation and retrofit of masonry walls by using externally bonded fiber reinforced polymer (FRP) strip (Haroun et al., [1], Tumialam et al., [2], Hamid et al., [3] and Li et al., [4]) The authors have shown that, FRP composites can improve the shear capacities of URM walls significantly. All of these experimental studies have proved that, the use of FRP strengthening technique can ensure an adequate increase in seismic

capacity, stiffness and ductility of masonry wall subjected to in-plane lateral loading [5] or out-of-plane loading [6].The NSM technique has been studied by several authors Seracino and Wylie.,[7], Valluzzi et al.,[8], Petersen et al., [9]. and Dizhur et al.,[10]. The effect of different parameters including the groove size, the dimensions and shape of CFRP, the adhesive type on NSM-strengthened brick masonry has been assessed by Maljaee et al.,[11]. However, the effect of mortar type and combined stresses on the strength and ductility of the reinforced masonry wall is not widely investigated in the literature.

The experimental test of compressive strength, ultimate shear strength, and failure modes for unreinforced and reinforced masonry walls take a lot of time and effort. This drawback can be overcome by effective and reliable computer simulation of the masonry assemblages test. For this reason, many research studies have focused on interpreting the in-plane failure modes obtained in the experimental tests of these structural members. However, this recent advent of sophisticated numerical methods has produced various techniques for simulating the behaviour of masonry structures. In this context, a combination of experimental and numerical modeling is needed to consolidate the existing knowledge and to better understand the complex behaviour of masonry under in- plane loading.

Two major approaches have been developed for masonry walls modeling, namely heterogeneous and homogeneous modeling. In the first one, the unit bricks and mortar are considered separately. In the second one, the unit bricks, mortar and interface are assumed as an isotropic or anisotropic composite material. According to the classification of Lourenco, there are two main modeling approaches: macro-modeling and micro-modeling. The micro-modeling itself is divided into two techniques: detailed micro-modeling (DMM) and simplified micro-modeling (SMM) [12, 13]. The DMM introduces the simulation of each component (Units, mortar) separately with a unit-mortar interface as shown in Figure 1.1.a ; there is no difference is made between individual brick units and joints, and thus they are treated as a homogeneous material. The brick units and mortar are modeled as continuum elements in order to reduce the time taken by the computer processing unit (CPU) as well as the material parameters and computational effort [14], which are consumed when solid or shell element is used. However, the detailed failure modes and cracking patterns in the mortar cannot be captured, because the contact between the brick and mortar joints is ignored. Therefore, it is adopted to e analyze the global behavior of complex masonry structures. The literature has clearly emphasized the importance of introducing all masonry failure mechanisms in the numerical simulation to understand its behavior in terms of ultimate load and ductility. The damage is usually found concentrated in the mortar joints interface.

In microscopic modeling, only a tensile failure of the bricks is taken into account, relying on a linear elastic behavior of the bricks. In these models, the authors recognize the need to incorporate the post-peak softening behavior of the mortar. The progressive cracking of brick units and mortar must be represented by the softening in tension, weakening of the cohesion and that in compression, which leads to the breaking of the masonry walls. The softening behavior laws, which are thus essential for modeling, however, relying on the definition of many parameters, whose values are difficult to appreciate a priori. Therefore, this modeling is only feasible if it is coupled with several experimental tests for the best representation of the materials and their interactions.

More complex numerical tools have been presented that are able to predict the behavior of structure from the linear stage, throughout cracking and degradation up to complete failure. Nonlinear analysis is needed to evaluate vulnerability and to propose adequate seismic retrofit schemes for traditional masonry structures. The availability of a suitable nonlinear model for the seismic estimation of masonry structural wall is therefore a significant requirement. This goal can be only achieved implementing an accurate and robust constitutive model using advanced solution methods of equations system, which results from the finite element method. The detailed micro-modelling technique provides the most reliable results, although it is computationally intensive due to the detailed level of refinement. Therefore, this study adopted the detailed micro-modelling technique to perform a numerical simulation of the masonry specimen. The calibration and validation of the FE model were performed using the experimental results and failure modes observed. In order to simulate the initiation and propagation of cracks in the specimens, the Extended Finite Element Method noted (XFEM) is used to model the cracking propagation in the mortar without requiring an initial representation of the crack location. This method has proven to be a very efficient tool for the numerical modeling of cracks propagation, so that during analysis, the crack can propagate randomly and be used for the modeling of multiple continuous cracks.

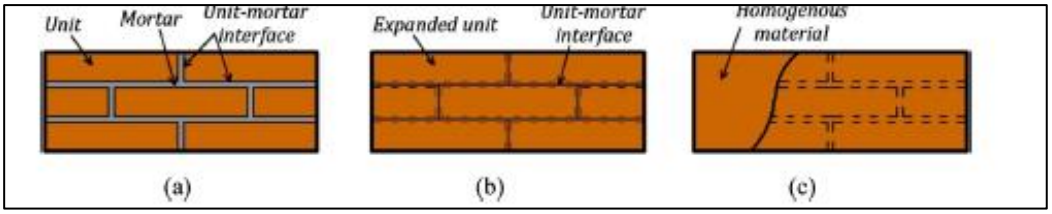

Figure 1.1 Modeling strategies for masonry structures [11]:(a) detailed Micro-model; (b) simplified Micro-model; (c) Macro-model

1.2 Aim and objectives

The objective of this research was to present laboratory experiments and a numerical investigation on the masonry assemblages in order to understand the behavior of CFRP reinforced brick masonry wall structure under in-plane loading and to develop an advanced model that adopts the detailed micro-modeling (DMM) approach that can be used for modeling FRP reinforced masonry wall. The main goals of this thesis can be summarized as follows:

- Obtaining accurate interfacial mechanical properties of the unit-mortar interface required for the development of a detailed micro-modelling of masonry assemblage.
- Conducting experimental studies of unreinforced and FRP reinforced brick masonry assemblages in different scale laboratory tests.
- Developing an advanced numerical model to reproduce the in-plane behavior of the strengthened brick masonry walls.
- Providing an adequate nonlinear model for the estimation of masonry structural walls. This goal can be achieved only using an accurate and robust constitutive model by introducing a constitutive law that includes anisotropic inelastic behavior. The inelastic behavior includes tensile strength softening, cohesion softening, compressive strength hardening and softening.
- Incorporating the Knowledge of nonlinear fracture mechanics used in crack propagation problems by using The XFEM method in simulating crack propagation within mortar without an initial definition of crack location.
- Calibration and validation of the FE model were done using the experimental results and observed failure modes.

1.3 Layout of the thesis

This thesis is divided into six chapters:

- Chapter 1 gives a general overview and the main aims of the present research.
- Chapter 2 presents some fundamental aspects concerning the behavior of unreinforced masonry as a structural material and its constituents. A brief review of the types of masonry, types of failure, and state of the art in masonry for unreinforced and FRP strengthened masonry under in-plane loads is also given. A general description of the different types of models and proposals for the analysis of the behavior of unreinforced and FRP strengthened masonry wall is provided in

this chapter. The out of plane behavior of masonry will not be mentioned here because it is out of the scope of the present thesis.

- Chapter 3 describes the details of the experimental investigation of the brick masonry assemblages retrofitted with CFRP under in-plane loading on the small-scale models. Mechanical properties such as compressive strength, shear bond strength, and interface behaviour of masonry specimens were evaluated. the influence of the type of joint mortar and location of the CFRP composites in the strengthened wallette externally bonded with carbon fiber-reinforced polymer (EB-CFRP) is evaluated by experimental tests using a diagonal compression test. the influence of the orientation of the applied loads to the joints, the efficiency of NSM-FRP technique, and the position of the CFRP strips to improve the shear strength and ductility of the reinforced masonry wallette are investigated in this chapter.
- In chapter 4 a FE model based on DMM approach was developed using FE software ABAQUS to modelling the behavior and the failure mechanisms of the brick masonry assemblages retrofitted with CFRP under in-plane loading. Different constitutive laws were selected for each component of masonry. These constitutive models include surface-based cohesive behavior to capture the elastic / plastic behaviour of unit- mortar interface and concrete damage plasticity model (CDP) to simulate the cracking and crushing of masonry units and mortar. The Extended Finite Element Method (XFEM)-based cohesive zone approach was employed to simulate the random cracks initiation and propagation in mortar without an initial definition of crack location. The Validation of the model is performed via a comparison between the obtained numerical results and experimental results.

Chapter 7 summarizes the main conclusions from the present study and proposes future research

Chapter **2**

Literature review

2.1 Introduction

Masonry is not a building material like wood or steel, but it is built up of two different materials each of which has a wide range of property values. the unit is shaped of bricks, stones, marbles, granites, concrete blocks, tiles, etc, as for the Mortar is a blend of binding material with sand. Binding materials can be cement, lime, soil or any other. There are different types of masonry walls employed in building construction. All of this type represents an important part of the building stock that is highly vulnerable to earthquakes. The durability and strength of masonry wall construction depend on the type and quality of material used and workmanship. Masonry is used primarily for constructing walls, as a load-bearing or partitioning wall, as a coating to protect, or as infilling between columns and beams. Its are classified according to the material used, load-bearing condition and applied location (see Figure 2.1).

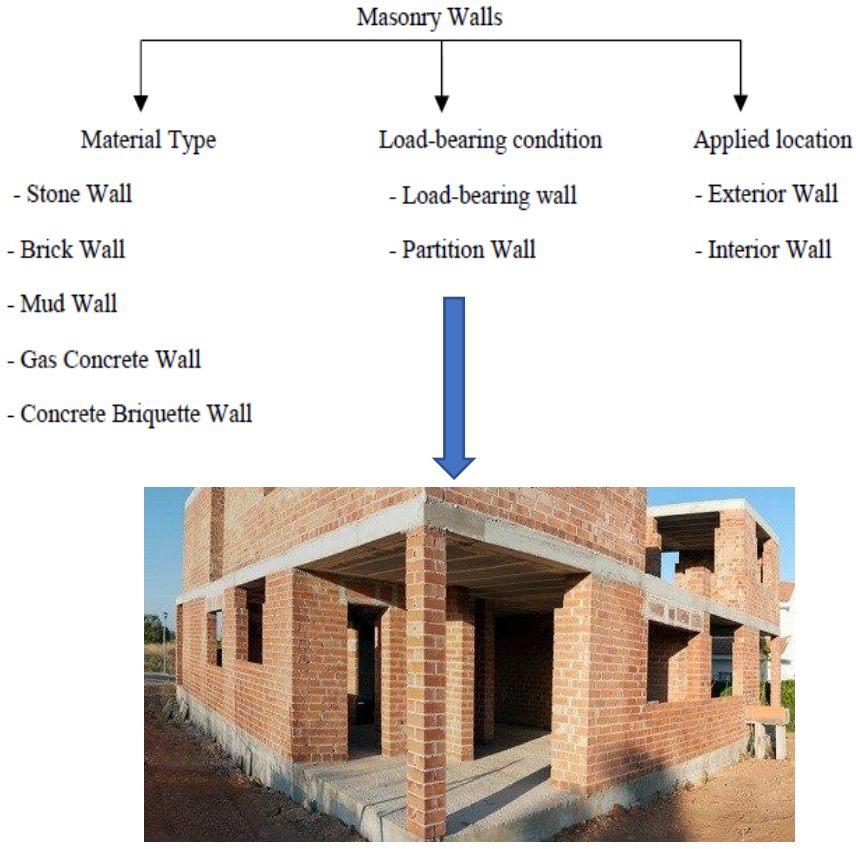

Figure 2.1 classification of masonry walls

2.2 Masonry structures

The most important parameters affecting the behavior of masonry structures against earthquakes loads are the individual properties of masonry unit and joint mortar. If these parameters are determined, the behavior of masonry structures can also be estimated. Many experimental techniques have been developed for the determination of material properties. The purpose of these experiments is to control the homogeneity of structural elements and to determine the material properties such as compressive, tensile and shear strength, poison ratios, deformation properties and elasticity modulus of materials of masonry unit and mortar.

2.2.1 Constituent materials of masonry

2.2.1.1 Brick elements

The first component of masonry wall is the brick element. This element can be classified according to the type of material (stone, raw or cooked earth, concrete, etc.), or according to its geometry (brick full, cellular, hollow, etc.). Bricks have been used frequently in the structure sector since ancient times. It is very useful due to its cheap and easy production, superior properties such as sound insulation and thermal insulation. It is produced by the factories in different geometries including hollow unit, frogged unit and solid unit. These bricks are divided into two type according to unit volume mass TS EN 771-1: 2011 + A1 standard[15]. The masonry units with low unit volume mass are called LD and the masonry units with high unit volume mass are called HD. Brick samples for LD and HD units are given in Figure 2.2.

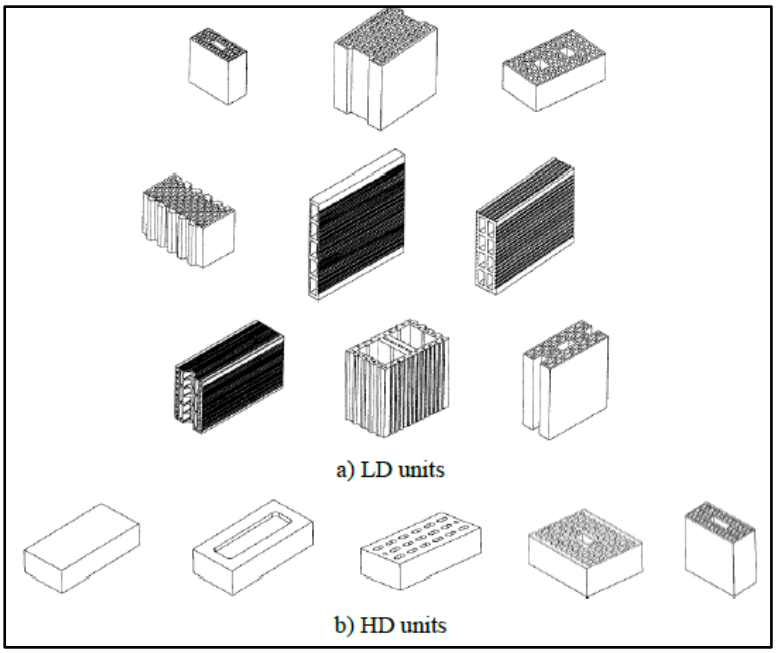

Figure 2.2 Examples for LD and HD units

To determine the compressive strength, uniaxial compression type tests according to European standards or French standards are used (NF EN 771)[2]. The tensile strength is generally deduced from the flexural strength of the elements.

The Young's modulus and the Poisson's ratio of the brick can be determined from uni-axial compression tests on masonry walls according to the recommendations ASTM E474[16] or EN1052-1[17]. In principle, the Young's modulus is determined from the stress vs vertical deformation curves in the elastic phase between 5% and 30% of the maximum resistance, while the Poisson's ratio is determined from the vertical vs horizontal deformation curves brick.

Table.2.1 summarizes some mechanical properties of the brick unit of the usual elements.

Table.2.1 propriétés mécaniques des briques d'après[18]

Properties	Density (kg/m3)	Young's modulus (MPa)	Poisson coefficient	Compressive Strength (MPa)	Tensile Strength (MPa)
Granit	2600	50000	0,3	170	-
Limestone	2000-2600	45000	0,2	5-25	2,5
Concrete	2400	40000	0,3	10-40	4
Hollow brick	3000	5000	0,3	20	8
Solid brick	3000	15000	0,2	40	4

To estimate the elasticity module (Eb) of clay bricks, (Kaushik, Rai, & Jain, 2007) recommends a range of values depending on the compressive strength of the brick (fb). These values are:
$150 \cdot fb \leq Eb \leq 500 \cdot fb$
This relationship is graphically showed in Figure 2.3

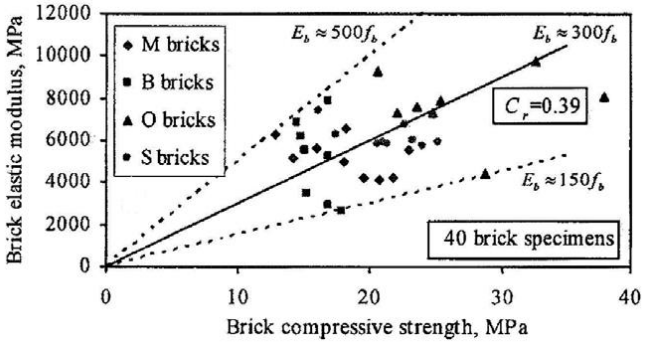

Figure 2.3 Relationship between compressive strength an elasticity module for bricks (Kaushik, Rai, & Jain, 2007)

2.2.1.2 Mortar elements

Although mortar accounts for as little as 7% of the total volume of masonry, its influence on the masonry assemblage is far more than this proportion indicates. The mortar is partly responsible for the strength characteristics of the masonry. Mortar joints also contribute to aesthetic features such as color and texture. The critical characteristics of the hardened mortar are bond strength, resistance to rain penetration, durability, and compressive strength.

The most commonly used cement in mortar is ordinary Portland cement, it has become the major binding ingredient of masonry mortar. Sometimes, it is used with sand and water in what is called a straight cement mortar. Such a mix in proportions 1 cement: 3part sand by volume gives a mortar which hardens quickly and consistently, exhibits high strength and poor bond.

The use of such cement mortar is therefore restricted to special situations where its favorable properties over-ride its disadvantages. The mortars used nowadays are cement based and have a cement: lime :sand volume ration of 1:1:6 or 1:1:5. in this type of mix, the cement contributes durability, high early strength, a consistent hardening rate and high compressive strength; lime adds workability, water retention and bonding properties and elasticity. Cement: lime mixes usually produce highly satisfactory mortars with a good overall performance.

The main types of mortar are:

1- Cement mortar
2- Cement-lime mortar
3- Lime mortar
4- Lime-pozzolan mortar

Cement-lime mortars are mixed to meet minimum physical requirements. they are produced by blending lime-sand mortar with Portland cement. A lime-sand mortar possesses excellent workability and high-water retention, while Portland cement increases setting time and provides additional strength. these mortars are further subclassified in various types (see Table 3). The table above gives an overview of the mechanical properties of mortars.

There is no single mortar mix that is uniquely suitable for all applications. No one mortar type rates the highest in all areas of applications. No single mortar property defines mortar quality. Therefore, it is very important to understand the selection of the right type of mortar as it influences both the construction process and the quality of finished product. ASTM Standard[16] specifications provide a means for specifications to identify acceptable materials and products without limiting those items to specific brands of manufacturers.

Compressive strength, tensile strength and elastic properties are important mechanical properties of mortar. The compressive strength of the mortar is sometimes considered the main criterion for choosing the type of mortar, since it is relatively easy to measure. This resistance largely depends on the formulation of the mortar and the water / cement ratio. For example, the W / C ratio is equal to 0.5 for a normal type mortar (EN 196-1)[19].The influence of the cement /water ratio on the compressive strength of the mortar depends on its class, this influence is the most important for class I mortar and is reduced with the mortar of classes II and III.

Durability and load bearing ability require that mortar develop early strength as it hardens to allow building to proceed without unnecessary delay. However, a final compressive strength of 2-5N/mm^2 when mortar is fully cured is adequate for most low-rise masonry structures. Mortar within this strength range will have the ability to accommodate small movements and any cracking in the masonry will usually be distributed as hair cracks in the joints where they are not easily seen and do not influence the wall stability. However, weaker mortars will not be durable under severe conditions but using unnecessarily strong mortars will concentrate the effects of movement in fewer and wider cracks in the wall unless adequate movement joints are provided.

To estimate the elasticity module (Em) of mortar, (Kaushik, Rai, & Jain, 2007) recommends a range of values depending on the compression strength of the mortar (fm). These values are:

$100 \cdot fm \leq Em \leq 400 \cdot fm.$

This relationship is graphically showed in Figure 2.4.

A typical stress-strain curve for compression in mortar is shown in Figure 2.5

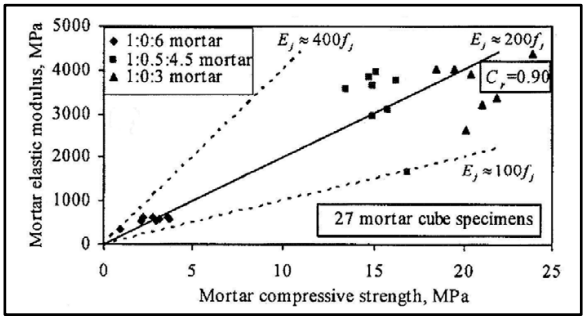

Figure 2.4 Relationship between compressive strength an elasticity module for mortar(Kaushik,rai, , & Jain, 2007).

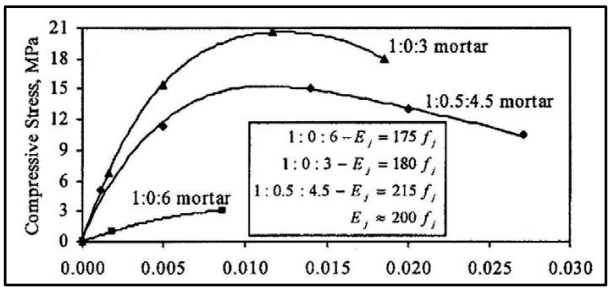

Figure 2.5 Typical stress-strain curve for compression in mortar (Kaushik,Rai,and jain,2007).

Table. 3 Guide for selection of Masonry Mortars (ASTMC270-05a)

Location	Building segment	Mortar type	
		Recommended	Alternative
Exterior, above grade	Load-bearing walls,	N	S or M
	Non-load-bearing walls	O*	N or S
	Parapet walls	N	S
		S†	M or N†
Exterior, at or below grade	Foundation walls, retaining walls, manholes, sewers, pavements, walks, and patios	N	S or M
Interior	Non-load-bearing partitions	O	N

2.3 Behavior of unreinforced masonry

Understanding the behavior of masonry on different scales under different loading conditions is necessary in order, on the one hand, to identify the elements where structural disorders and cracks will be initiated in the event of earthquakes and on the other hand to improve the methods of calculation and modeling of masonry, always delicate because of the high heterogeneity (intrinsic and induced) of the material.

Masonry is a composite material with an overall anisotropic behaviour. Such an anisotropy arises from the geometrical arrangements of units and mortar, even if the properties of these constituents are isotropic. Moreover, the constituents are arranged in such a way that the horizontal and vertical directions are obviously not equivalent. The mortar joints act as planes of weakness. Therefore, structural response is strongly dependent on the orientations of the bed joints (show Figure 2.6) .

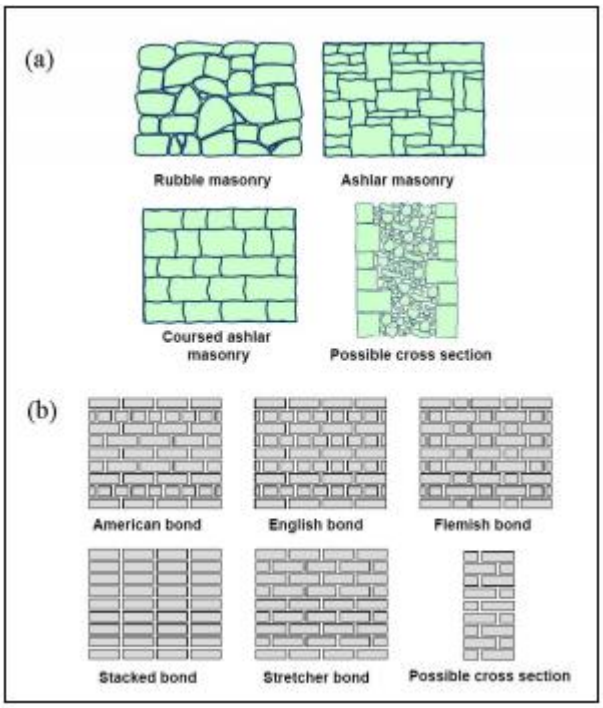

Figure 2.6 variability of masonry: stone masonry(a), brick masonry(b)

2.3.1 Uni-axial Compression

Hilsdorf (1969) demonstrated that the difference in elastic properties of the unit and mortar is the precursor of failure. In fact, units are normally stiffer than mortar and the difference is more pronounced in ancient masonry, built with lime mortar. Uniaxial compression of masonry in direction perpendicular to bed joints leads to a state of triaxial compression in the mortar and compression/biaxial tension in the unit, see Figure 2.8. In practice, the unit confines the mortar and avoids its lateral extension. As a consequence, vertical cracks appear in the units. Upon increasing deformation, additional vertical cracks appear, until the failure. The uni-axial compression of the masonry leads to a triaxial compression state in the mortar and to a bi-axial compression and traction in the brick elements. The strength and the failure mode change when different inclinations of bed joints are considered (Page[20, 21]; Samarasinghe and Hendry[22]) Page[20] notes that the rupture in uniaxial compression generally takes place in a plane normal to the panel tested. According to the orientation of the horizontal joint with respect to the constraints applied, failure occurs by cracking and sliding in the horizontal and / or vertical joints; or by a mechanism combining both the breaking of the brick and the mortar (see Figure 2.7).

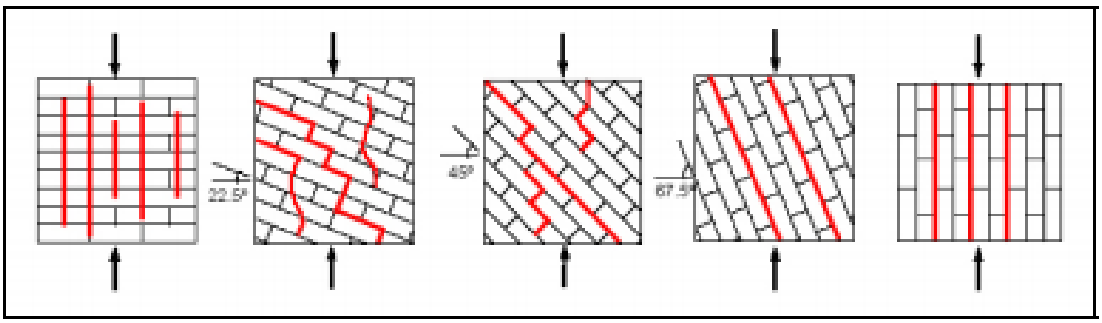

Figure 2.7 Modes of failure of solid clay units masonry under uniaxial compression, from page[8,9]

Most standards advise the determination of the compressive strength from tests on simple masonry prisms, composed of 3, 4 or 5 elements, subjected to uniaxial compression. In general, experience Page[23] has shown that the resistance of the prism is greater than that of the mortar and less than that of the insulated masonry unit (Figure 2.10).

The compressive strength perpendicular to the joints is considered an important parameter for the characterization of masonry. The rupture occurs by sliding or cracking of the joint and accompanied by cracking of the stone parallel to the axis of loading.

The compressive strength of masonry is influenced by the mechanical properties of the block and mortar, as well as the proportion of joint and the age of the structure. EN 96 considers that the factors which influence the compressive strength are; the number of layers of mortar, the compressive strength of the mortar, the tensile strength of the block, and the dimension of the prism of the masonry tested .The compression behavior of masonry is studied with Zucchini et al. 2006 [24] in a simplified homogenization model for mortar and block behaviors. they consider that the behavior of compressed masonry depends essentially on the compressive and tensile strength of blocks. Moreover, for a mortar of weak resistance, the stone is subjected, at the level of joints, to a bi-axial traction which accompanies the vertical compression of the stone. On the other hand, if the mortar is much more resistant and rigid, the stone is subjected to a state of triaxial compression.

In addition, increasing the compressive strength of mortar increases the strength of the masonry and reduces vertical displacement. This result is obtained with Binda et al. 1988 for solid earth brick masonry [25]. Yet Fishburn. 1961[26] notes that the influence of mortar strength on the strength of masonry is limited. Indeed, a 130% increase in the mortar strength produces a 10% increase in the compressive strength of the masonry. And similarly, a 160% increase in the mortar strength increases the compressive strength of masonry by 25%. The standards define two types of specimens for the uni-axial compression test, presented in Figure 2.9. The RILEM recommendations [27] impose the use of specimens whose geometry is shown in Figure 2.9.b. The use of this geometry requires higher loads than the loads applied to the prismatic specimen.

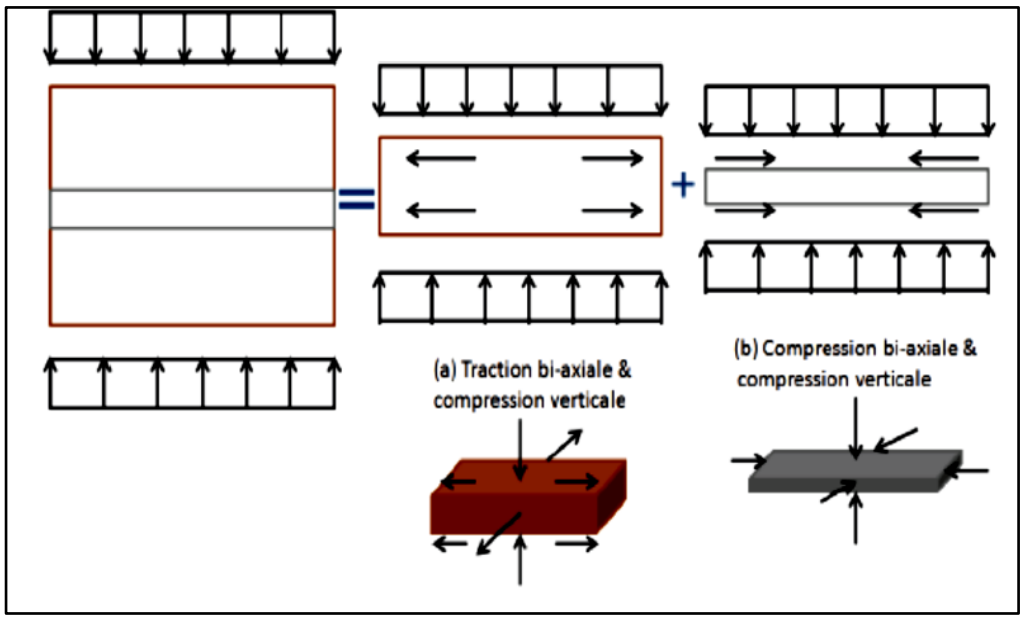

Figure 2.8 State of stress in a prismatic test specimen of masonry, (a) in brick (b) in mortar.

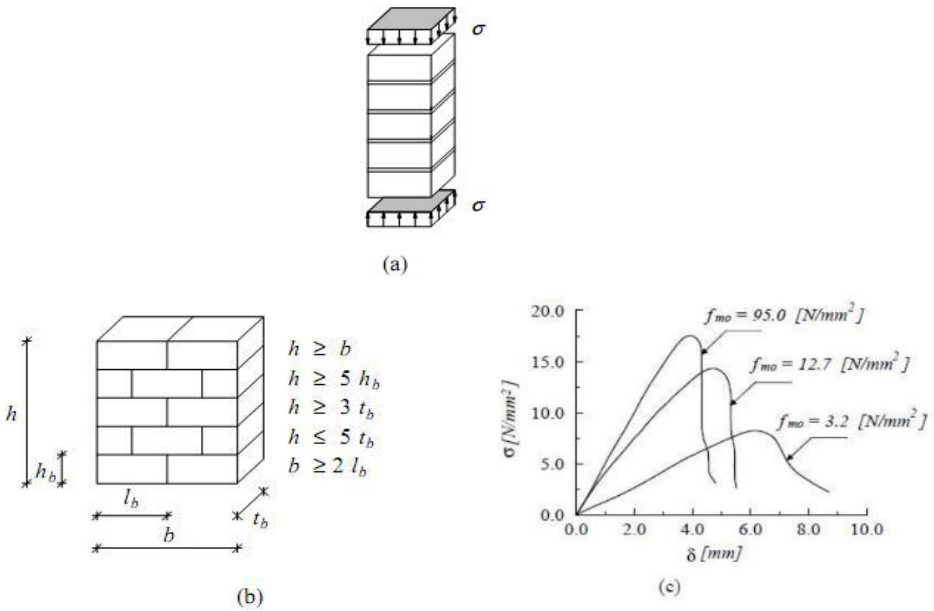

Figure 2.9 Behavior of masonry under the effect of a normal force at horizontal joints

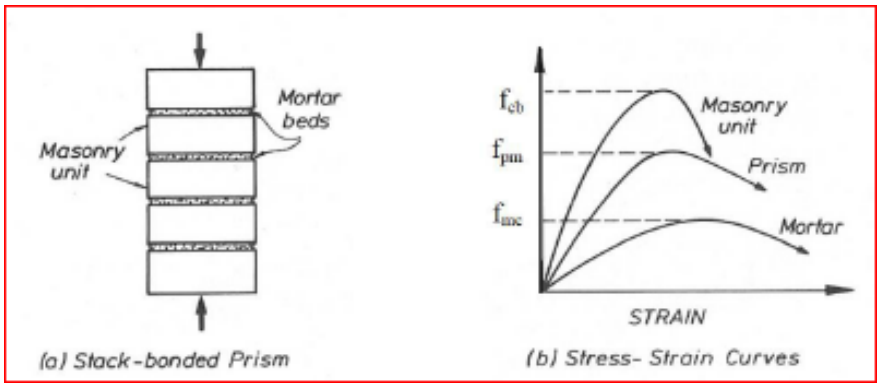

Figure 2.10 behavior of prisms in compression

In absence of proper compressive test results, the Eurocode 6 [28] gives a formula for the estimation of masonry compressive strength (f_k), obtained from the characteristic resistance of the brick unit and mortar as follows:

$$f_k = K * f_b^{\alpha} * f_m^{\beta} \quad (2.1)$$

where f_b is the normalised mean compressive strength of the units, f_m is the average resistance of the mortar joint, and K is a coefficient which depends on the type of blocks and mortar assembled. The coefficients α and β are taken equal to 0.7 and 0.3 respectively, in the case of an installation with ordinary mortar with a thick joint (> 3mm). The coefficient α is greater than β, because the compressive strength of the masonry is assumed to be more influenced by the resistance of the blocks than by the resistance of the mortar. Kaushik and. al [18] studied the conformity of this equation with experimental results. The Eurocode 6 equation would be appropriate in the case of masonry consisting of bricks with high resistance, but the error increases when we consider bricks with lower resistance. For bricks of low to medium strength, the authors propose coefficients α = 0.49 and β = 0.32, adjusted with respect to their experimental campaign, which better predicted the compressive strength of the masonry in these cases.

2.3.2 Uni-axial traction

The masonry tensile strength can be equated to the tensile bond strength between the joint and the unit when the bricks are much stiffer than mortar, and equal to the tensile strength of bricks when bricks are softer and high-strength mortar is used. For tensile loading parallel to the bed

joints a complete test program was set-up by Backes[29]. The author tested masonry wallets under direct tension and he found that tension failure was affected by the type of the mortar and the masonry units. For stronger mortar and weaker masonry units, the tension cracks passed along the head mortar joints and through the center of the bricks at the intervening courses. For weaker mortar joints and stronger masonry units, the tension crack passed along the head joints of the masonry units and the length of bed joints between staggered head joints.

Figure 2.11 shows different modes of failure observed by Page [21] on solid clay units masonry walls subjected to uniaxial tension. As can be seen, for intermediate inclinations of the bed joints, the failure is concentrated on joints. For a masonry structure subjected to a tensile load in the direction perpendicular to the horizontal joints, the rupture is generally caused by the separation between the bricks and the mortar. The tensile behavior can be characterized by the adhesion resistance between the brick and the mortar joint, therefore by the tensile strength of the element / mortar interface.

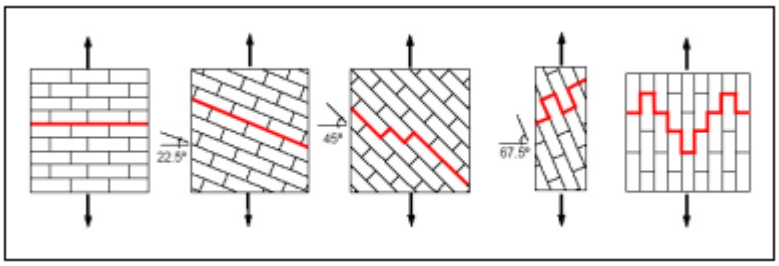

Figure 2.11 Modes of failure of solid clay units masonry under uniaxial tension, from page [21]

2.3.3 Behavior under biaxial tension-compression

The anisotropy of a masonry element generated by the weakness of the joints compared to bricks and / or blocks requires the analysis of the behavior under bi-axial loading. The behavior must be described by a complete stress tensor, that is to say taking into account the anisotropy of the masonry material, which implies different behaviors along the material axes.

The constitutive behaviour of masonry under biaxial states of stress cannot be completely described from the constitutive behaviour under uniaxial loading conditions. The most complete set of experimental data of masonry subjected to proportional biaxial loading was provided by Page [20, 21]. The tests were carried out with half scale solid clay units. Both the orientation of the principal stresses with regard to the material axes and the principal stress ratio considerably influence the failure mode and strength. In tension-compression the failure occurs

either by cracking and sliding of the joints or in a combined mechanism involving both units and joints, see Figure 2.12.

In biaxial compression failure typically occurs by splitting of the specimen at mid thickness, in a plane parallel to its free surface, regardless of the orientation of the principal stresses, see Figure 2.13.b. In this case, failure occurs in a combined mechanism involving both joint failure and lateral splitting. Comprehensive programs to characterize the biaxial strength of different masonry types were carried using full scale specimens, see Ganz and Thürlimann [30] for hollow clay units masonry, Guggisberg and Thürlimann [31] for clay and calcium-silicate units masonry and Lurati et al. [32] for concrete units masonry.

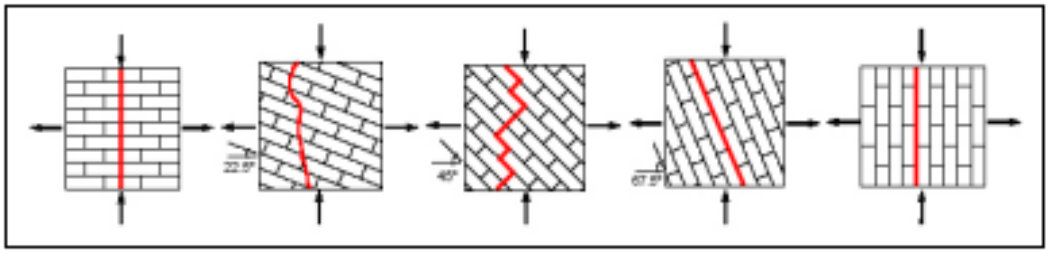

Figure 2.12 Modes of failure of solid clay units masonry under biaxial tension-compression, from page[22].

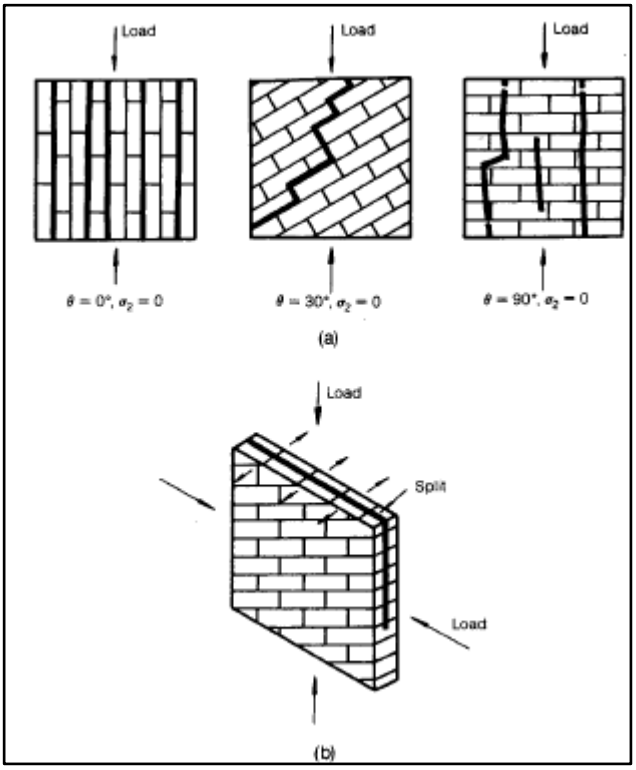

Figure 2.13 Failure modes of biaxial compression tests on brickwork: (a) uniaxial compression; (b) biaxial compression[21]

2.3.4 Shear behavior

Masonry walls can be subjected to horizontal forces, such as wind, earth surges and earthquakes, in their planes and also along the plane perpendicular to the walls. The evaluation of the resistance of masonry due to shear forces makes it possible to predict and estimate the stability and reliability of the structure. In the case of in-plane shearing, the wall is subjected to horizontal forces, in addition to vertical loading in the wall plane.

- ***Diagonal compression test (Direct shear tests)***

To measure the shear strength of masonry assemblies, the American standard ASTM [33]recommends the test in diagonal compression. A square masonry panel is subjected to a compressive force along its diagonal. The failure of the panel is generally associated with a rupture in diagonal tension. The cracks develop from the center of the specimen and spread to the upper and lower corners. The diagonal compression test can have several interpretations. In the standard interpretation of the test (ASTM standard [33]), it is considered that this test generates a state of uniform pure shear stress within the panel (see Figure 2.14)

$$\tau_u = \frac{0.707.p_d}{\mathrm{A}} \qquad (2.2)$$

where p_d is the maximum value of the force imposed and A is the net area of the panel.

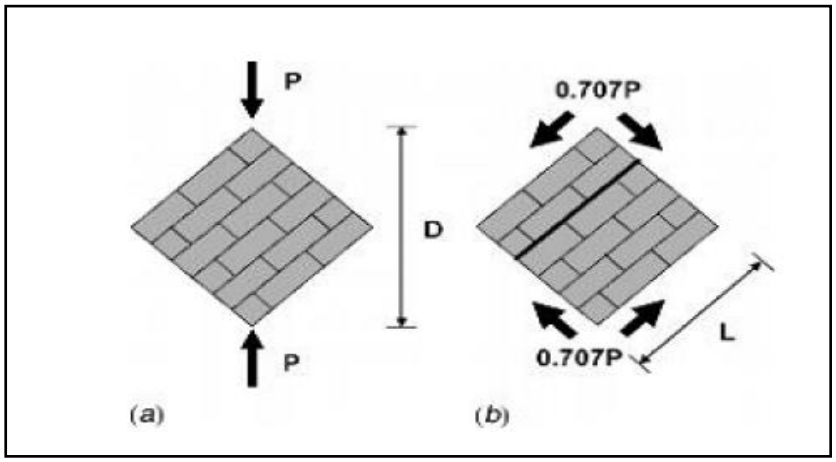

Figure 2.14 Test setup (ASTM E 519-02, 2012). (a) Test according to ASTM E 519; (b) Potential rupture plan following the joint bed.

2.3.4.1 Types of Failure

The typical failure modes of load-bearing masonry shear walls include: sliding, diagonal cracking and rocking (Figure 2.15). The mechanisms depend primarily on the geometry of the wall (height/length ratio), on the boundary conditions and on the magnitude of vertical loads,

and then on the masonry properties (Magenes and Calvi,[34]; Tomaževi˘c,[35]; ElGawady et al.,[36]).Masonry walls resisting in-plane loads usually exhibit the following three modes of failure:

- **Sliding failure**

This failure mode can occur for low vertical load levels or for low friction coefficients of the joints. where horizontal cracks appear at the level of the horizontal mortar. Thus, sliding planes are formed along these cracks. (Figure 2.15.a).

- **Shear failure**

Shear failure is exhibited when a wall is loaded with significant vertical as well as horizontal forces and low aspect ratios (height/length). diagonally inclined stepped pattern may occur through the horizontal and vertical mortar joints in the form of staircase shape (show Figure 2.15.c), it can also through the brick units depending on their relative strengths noted diagonal cracking (the failure occurs by tensile strength). Ultimate strength is governed by the formation and development of diagonal cracks. It can also induce through both, units and joints due to an exceeding of the tensile strength (see Figure 2.16).

- **Bending failure**

This failure mode is based on the compressive strength of the compressed corner. this rupture occurs by a bending moment in the plane of the wall when the load or the horizontal displacement increases. This failure is characterized by a toe-crushing on the lower side of the wall (compressed area) and/or an opening on the other side. The formation of horizontal cracking and top rotation is due to the low vertical loading, poor mortar and wall slenderness (Figure 2.15.b).

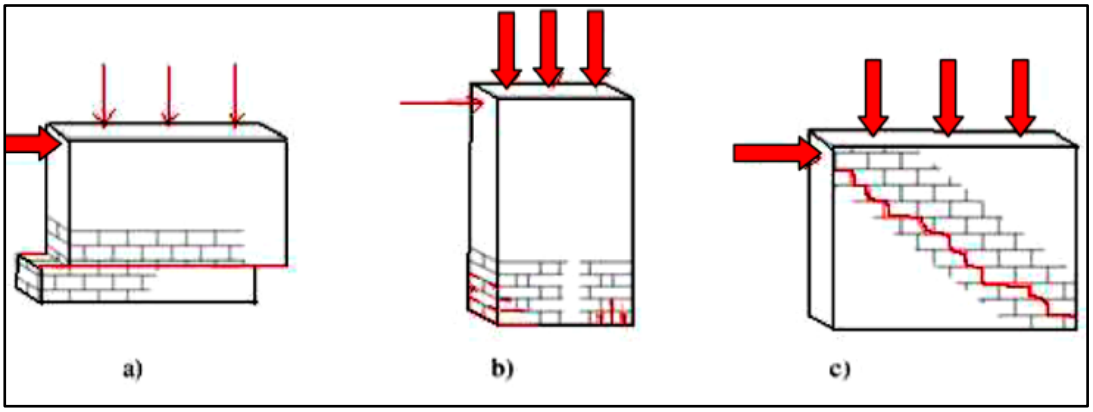

Figure 2.15 Failure modes of URM shear wall: (a) sliding; (b) rocking (with toe crushing) ;(c) diagonal cracking (through brick unit and mortar joints)

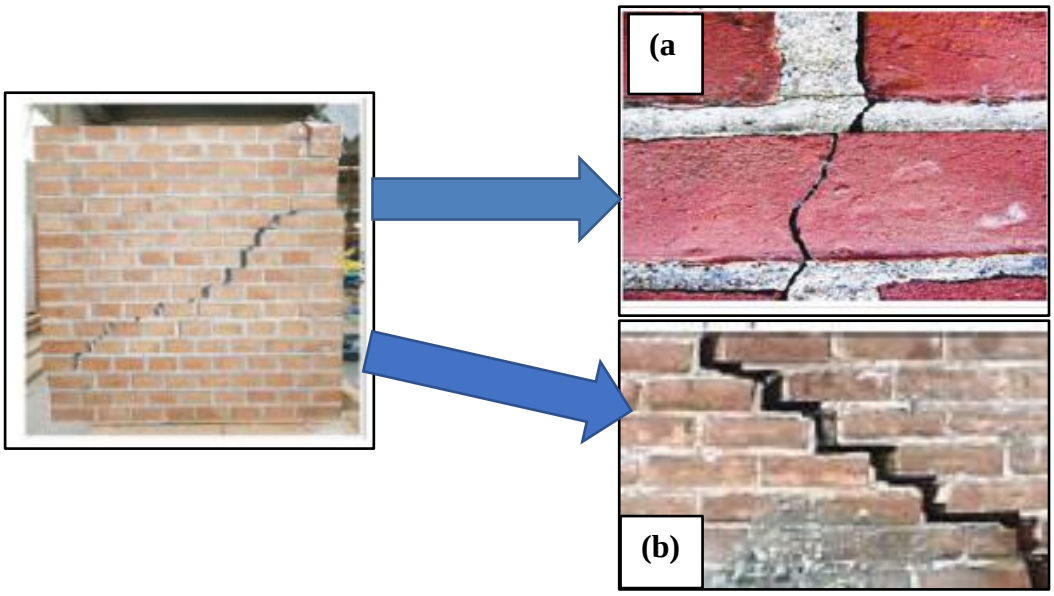

Figure 2.16 real photo of shear failure of URM wall:(a) diagonal cracking;(b) stepped cracking

2.4 properties of unit-mortar interface

Masonry has a very complex mechanical behavior seen its heterogeneity. Its behavior varies according to the mechanical characteristics of the bricks and the mortar which composes it, as well as with the interaction of the latter. It also varies with the applied stress and the condition of implementation. In the majority of studies, calculations on masonry have was performed in isotropic linear elasticity. Masonry was considered a homogeneous isotropic material, with average mechanical characteristics. Such an approach did not take into account the heterogeneities of the structure induced by the mortar joints. when analyzing masonry, A prominent feature of masonry to be considered is the softening behaviour, which is typical of quasi-brittle materials. Softening is a gradual decrease of mechanical resistance under a continuous increase of deformation and it is due to a process of progressive internal crack growth. Such mechanical behaviour is commonly attributed to the heterogeneity of the material, due to the presence of different phases and material defects, like flaws and voids. usually, the bond between brick unit and mortar is considered to be the weakest part in masonry assemblage, the nonlinear response of the mortar joints is associated with two types of failure modes: tensile failure (mode I) and shear failure (mode II).

- ***Indirect shear tests: (EN 1052-3)***

the shear test consists in applying lateral forces at the joints in assemblies composed of two, three or four stones. Therefore, one or two mortar joints are sheared with or without an orthogonal joint to the sheared joints in the test. To determine the tensile behaviour of the interface between brick and mortar from laboratory tests, the "tensile bond test" may be used (see Figure 2.19). On the other hand, the estimation of the shear-behaviour of the interface between brick and mortar is made using the "shear bond test" (see Figure 2.18). In this test the failure can occur either on the interface or in the mortar. The main result of both tests is the maximum strength (tensile or shear). All these tests are also widely and clearly described in literature.

Figure 2.17.b represents a shear test on couplets, this case was adopted by Pluijm Rvd [37] and Abdou et al [38]. Figure 2.17.d,e is the standard shear test on triplets designed according to standard NF EN 1052-3 [39]; be aware that this test is most often used. The shear test shown in Figure 2.17.c used by Calderini [40] and Gabor [41] and which are designed according to the RILEM standard[42].

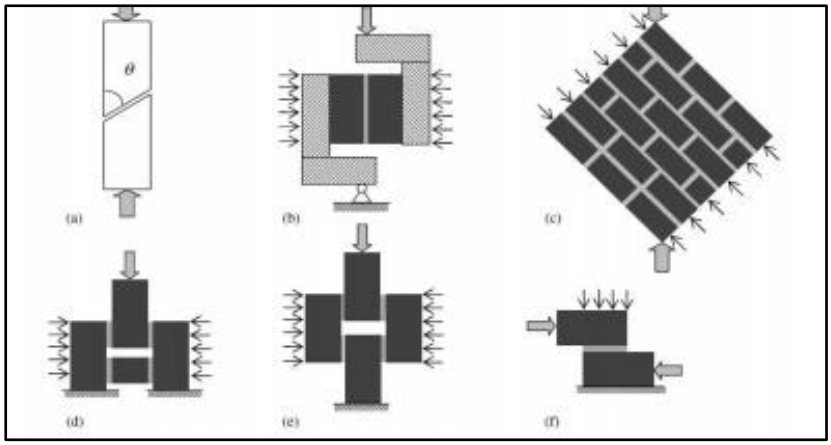

Figure 2.17 different types of shear test specimens (a)Nuss Shear Test,(b) Van der Pluijm Test,(c) Diagonal tension Test,(d) Triplet Test,(e) Meli Test,(f) Direct Shear Test

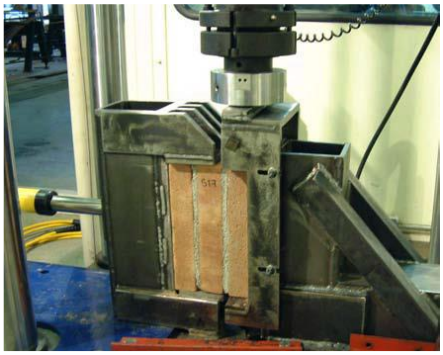

Figure 2.18 Shear bond test for the brick- mortar interface (Charry, 2010).

Figure 2.19 Tensile bond test for the brick-mortar interface (Grabowski, 2005a).

Figure 2.20 shows characteristic stress-displacement diagrams for quasi-brittle materials in uniaxial tension, uniaxial compression and pure shear[43]. The integral of the σ−δ diagram is the fracture energy, denoted by G_f and G_c, for tension and compression, respectively (Figure 2.20.a,b). In case of mode II failure mechanism, i.e. slip of the unit-mortar interface under shear loading, the inelastic behaviour in shear can be described by the mode II fracture energy $G_{II,f}$, defined by the integral of the τ−δ diagram(show Figure 2.20.c). The value of the fracture energy depends on the level of the confining stress. Shear failure is a salient feature of masonry behaviour which must be incorporated in a micro-modelling strategy. However, for continuum macro-models, this failure cannot be directly included because the unit and mortar geometries are not discretized. Shear failure is then associated with tension and compression modes in a principal stress space.

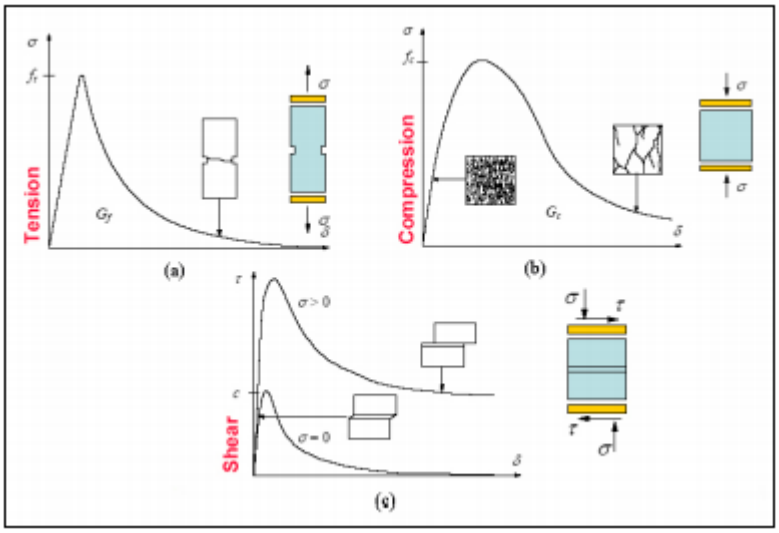

Figure 2.20 typical behavior of quasi-brittle materials and definition of fracture energy: uniaxial tensile loading(a); uniaxial compressive loading(b); pure shear(c)[33]

2.5 Modern Strengthening techniques

The development of new materials and techniques came as a consequence of the need to surmount the limitations of traditional strengthening systems. Many of those disadvantages could be repressed by using modern techniques for retrofitting. The polymer reinforced polymers are an efficient alternative, as they improve the behavior of masonry elements under monotonic, seismic and explosive loads. Additionally, since the added mass and stiffness are negligible, the dynamic properties of the reinforced structure will not be altered.

2.5.1 TRM (Textile reinforced mortar)

It is a technique that combines the essential properties of both conventional and modern materials by using textile grids externally embedded in mortars. The grid is made of long fiber rovings (made of carbon, glass or aramid) arranged in two orthogonal directions. Instead of polymer resins, cement or lime-based mortars are used. The composite action of TRM is achieved through the mechanical interlock of the grid structure and the mortar. It increases shear strength, stiffness, and ductility.

2.5.2 *Fiber Reinforced Mortar (FRM)*

It is a reinforcing technique that consists of microfibers made of steel, glass, synthetic fibers (acrylic, aramid, carbon, nylon, polyester, polyethylene and polypropylene) and natural fibers (straw, coconut, bamboo, etc.) embedded in mortar.

2.5.3 Strengthened masonry structure with fiber reinforced polymers (*FRP)*

The aim of a strengthening technique is to increase the capacity of the structure to absorb inelastic deformation. There is more technique for strengthening or repairing the unreinforced masonry wall (URM), many of these strengthening techniques including the use of fiber reinforced polymer (FRP) materials. The use of fiber-reinforced polymer (FRP) material for masonry is an innovative technique that can enhance the structure's load-carrying capacity and integrity. A fiber reinforced polymer (FRP) system consists of two main materials: resin and fibers impregnated with polymeric matrix such as (polyester, epoxy, mortar mix) with high tensile strength, lightness and corrosion resistance. the fibers are the main load-carrying components in FRP while the resins protect the fiber and transfer stress from fiber to fiber.

For the all assemblage studied in this project, carbon fibers were chosen. The mechanical properties of carbon fibers are shown in Table. 2.4. Their stress-strain relationship up to failure

is linear. The typical mechanical properties of the most common types of fibers are given in Table. 2.2.

Resins are used in the FRP strips to create the matrix in which the fiber reinforcement will be embedded. For the FRP systems. The most common types of resins used in the FRP materials are epoxies, vinylesters, phenolics and unsaturated polyester. Epoxies have good strength, bond, creep properties and chemical resistance. The typical mechanical properties of the most common types of thermosetting resins are given in Table. 2.3.

FRP has high tensile strength, stiffness, corrosion resistance and are lightweight. However, some of the disadvantages include high cost, low impact resistance, and high electrical conductivity. these composites are manufactured in different features depending on the fiber material type like Carbon Fiber (CFRP), Glass (GFRP), and Aramid (AFRP).

The FRP reinforcement is designed to provide tensile to a masonry wall and restore capacity of cracked masonry. In strengthening masonry structure, FRP shows its great advantages when corrosion, traffic management costs, and length of the required strengthening should be taken into account. These advantages are:

- FRP materials are easy to transport and handle, which may be used in areas with difficult access due to their lightweight.
- The fibers can be introduced in a certain position, volume fraction and direction in the matrix to obtain maximum efficiency.
- FRP materials are noncorrosive and exhibit high tensile strength.

The main disadvantage with using FRP for reinforcement is that has brittle failure modes, debonding of FRP occurs if no mechanical anchorage is provided when the shear strength of the adhesive or the superficial layer of brick is exceeded because the tensile force in the FRP material is transferred through the adhesive(epoxy).

Retrofitting of URM wall with FRP is a promising technique as it was observed that FRP improves the in-plane lateral resistance by 1 - 3 times and the out-of-plane resistance by more than 7 times. Triantafillou proposed that the shear resistance of the FRP retrofitted URM is equal to the shear resistance of the FRP material itself, plus the shear resistance of the URM [44].

$$F_{FRP} = \rho_h \cdot E_{FRP} \cdot \varepsilon_{tu} \cdot k \cdot t \cdot L$$

where:

F_{FRP}: the contribution of the FRP in the lateral resistance of URM specimen; ρh: the reinforcement ratio of FRP in the horizontal direction; E_{FRP}: modulus of elasticity of FRP; ε_{tu}: the ultimate strain of FRP; k: efficiency factor; t: wall thickness; L: wall length.

Nanni and Tumialan,[45] , proposed a value of k as 0.3, whereas Zhao et al.,[46] proposed a value of 0.2 for pre-cracked specimens and 0.3 for uncracked specimens.

The main types of in-plane failure of URM-FRP walls are:

a) shear failure: step-like cracks that pass through either head or bed joint;

b) sliding failure: complete separation at bed joints with a fracture of fiber material;

c) flexural failure: complete separation at bed joints with a fracture of fiber material;

Table. 2.2 Typical properties of glass, carbon and aramid fibers (from Holloway et al. 2001).

Material	Elastic Modulus GPa (ksi)	Tensile Strength MPa (ksi)	Ultimate Strain %
Glass	70-85 (10150-12500)	2500-4500 (362-650)	3.5-6
Aramid	80-125 (11000-18000)	2750 (399)	2.5-4
carbon	220-240 (32000-34800)	3790-4820 (550-700)	1.4-1.5

Table. 2.3 Typical properties of thermosetting resins (from Holloway et al. (2001).

Material	Elastic Modulus GPa (10^3 ksi)	Tensile Strength MPa (ksi)	Ultimate Strain %
Polyester	2.5-4 (362-580)	45-90 (6.5-13)	1.0-6.5
Vinylester	4 (580)	90 (13)	-
Epoxy	3.5-7 (507-1015)	90-110 (13-16)	1.5-9

Table. 2.4 Carbon fiber properties from manufacturer's data (Sika, Version 3.0).

	Density g/cm^3	Elastic Modulus GPa (10^3ksi)	Tensile Strength MPa (ksi)	Elongation %
Carbon	1.8 (0.065	220-240 (32-34)	3790-4820 (550-700)	1.4-1.5

A general classification of FRP systems models can be made with how they are delivered and installed:

• **Externally bonded technique (EB-FRP):** The strip is adhesively bonded to the masonry surface by means of epoxy adhesive.

• **Near surface mounted technique (NSM-FRP)**: The strips are placed in a groove made on the masonry surface. The two techniques are explained in the following sections.

2.5.1.1 Externally bonded reinforcement(strips/sheets/Fabric):

In this technique, performed FRP strips or FRP fabric sheets are bonded to the external surface of a wall typically using a two-part epoxy adhesive. The fabric sheets may first be impregnated with a layer of epoxy and allowed to cure before being bonded to the wall, alternatively, the fabric sheets can be bonded to the wall using the wet lay-up technique in this technique the composite are first pressed into a layer of epoxy painted onto the surface of the wall and are then covered with another layer of epoxy, the wet-lay-up technique is described in greater detail by (Stratford [47]). to improve the in plane-shear resistance of masonry wall, the application of EB-FRP technique to strengthen and repaired masonry wall has been studied by several authors .different experimental studied to evaluate the effect of different parameter for example, the effect of retrofitting configuration of FRP composite, type of FRP composites and the type of masonry components, through small-scale testing such as triplets test, Wallette and by full scale testing.

Mahmood and Ingham [48] conducted a series of experimental test on URM walls (see Figure 2.23), they illustrated the effectiveness of FRP retrofitting system in improving the shear strength of unreinforced masonry with a factor of 3.25 (see Figure 2.24 and Figure 2.25) . Several researchers such as Haroun et al [1], Tumialam et al [2], Hamid et al [3] and Li et al [4] have shown that FRP composites can improve the shear capacities of URM walls significantly. All these experimental studies have shown that the use of FRP strengthening technique can ensure adequate increase of seismic capacity, stiffness and ductility of masonry wall in the in plane lateral loading or out-of-plane. Most of these researchers have used EB-FRP strips and sheets to strengthen against diagonal-cracking, and against sliding along a single bed joint [49].these researchers have aligned the FRP strips/sheets in diagonal patterns, horizontal patterns, vertical patterns, and orthogonal or X type patterns.

The results from these tests have shown that EB-FRP strips/ sheets are effective at the opening of the diagonal crack restrains sliding of bed joint and increasing the shear strength of the wall. there is two common failure modes: debonding of FRP composite from the wall(FRP composite rupture) or failure of the wall either by crushing (Marcani [50]) or by separation of masonry leaves in a double- leaf masonry wall (see Figure 2.26 and Figure 2.27).In some case the failure

caused by cracking outside of FRP composite. A number of researchers have also investigated the effect of single-sided (or non-symmetric) strengthening, valluzzi and al [8] tested a series of unreinforced brick masonry panels strengthened by different materials (GFRP, CFRP and PVAFRP of different configuration. All tested specimens were subjected to a diagonal compression test (see Figure 2.22). the results showed that the application of FRP at one side of the wall only produces a significant out-of-plane deformation, and the failure mode of the out-of-plane displacement exaggerated by the little restraint at the top and bottom corners of the wall.in several other tests, however, where the walls had some form of the non-symmetric reinforcement was not as severe this is confirmed by both Marshall and sweeny [49] and chuang and al [51].

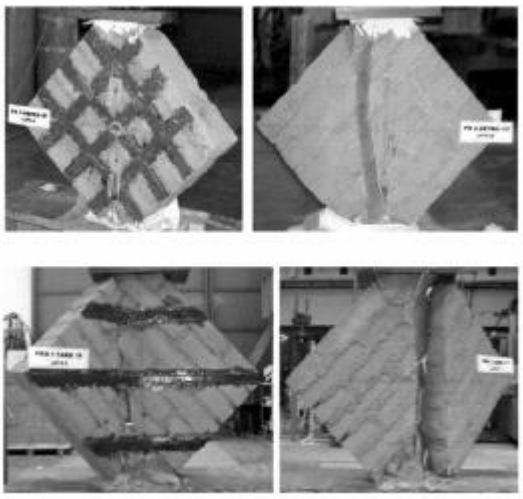

Figure 2.21 single-side reinforced panel failure mode: diagonal splitting with a single large crack on the unreinforced side. Notice the bending along the free diagonal [8]

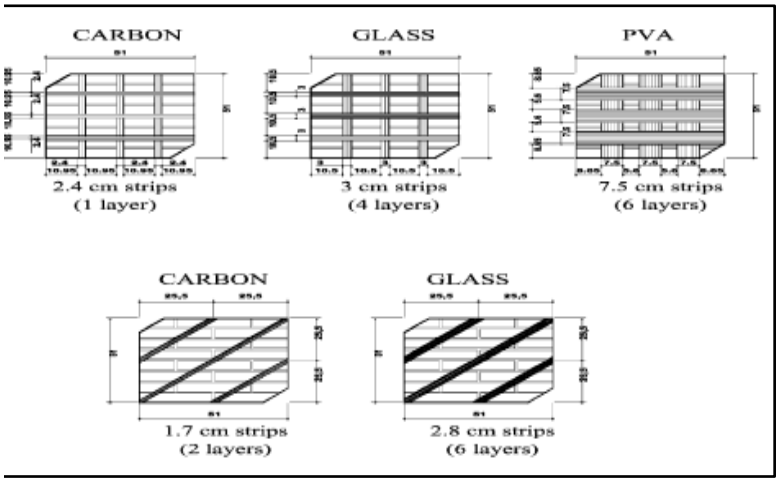

Figure 2.22 single-side strengthening patterns [8]

Jan Kubica and I.Galman[52] study the effectiveness of strengthening wall made with AAC blocks with carbon fibers strips in different assembly configurations. All specimens were subjected to diagonal compressive loading according to RILEM LUMB6 recommendation, they observed an increase in the shear capacity of both types of strengthening in comparison to the unreinforced wall. It is found that the location and the number of CFRP strips as well as orientation with respect to the bed joint are affect the behavior of the wall (see Figure 2.28).

Externally bonded FRP strips/sheets have the following disadvantages: they have a large impact on the aesthetics of a wall, highly susceptible to debonding failure modes, buckle from the surface of the wall in compression, and they are exposed to act of vandalism or fire.

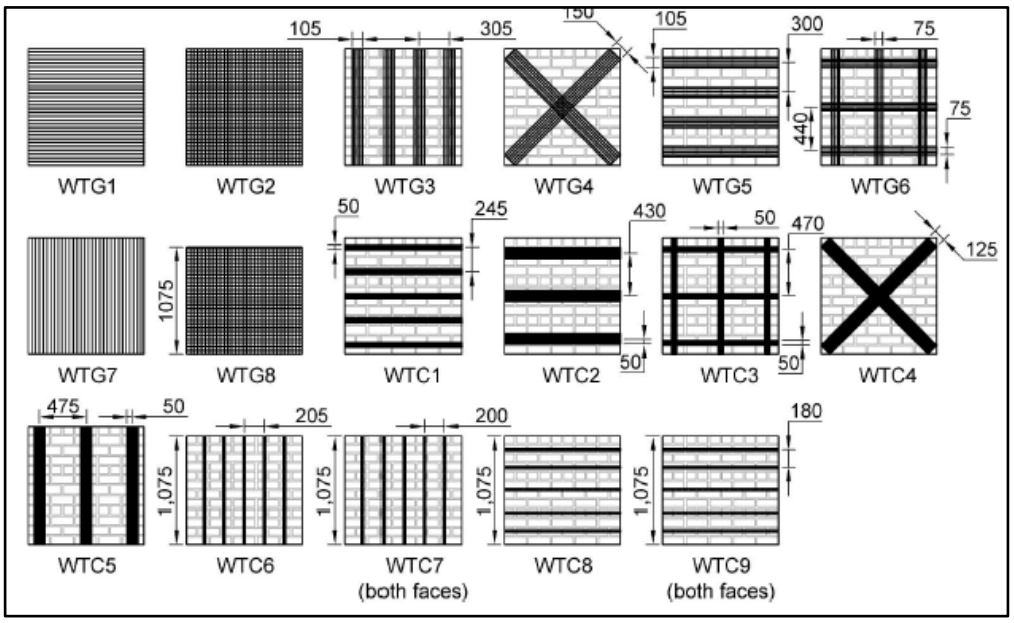

Figure 2.23 FRP retrofit details (all dimension in mm); Wallette height is 1.170mm unless otherwise noted [51]

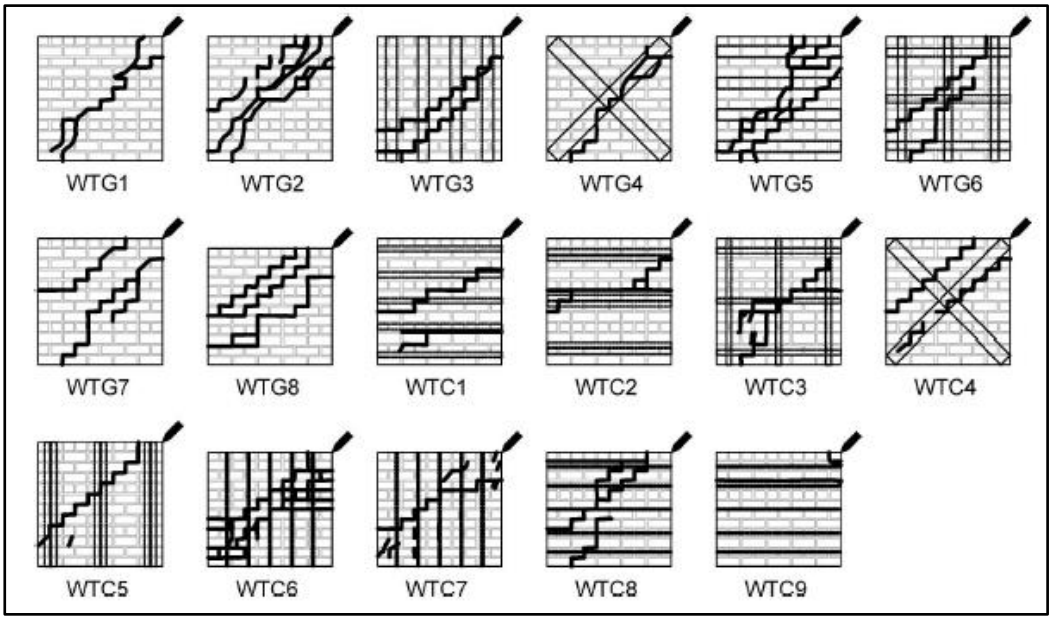

Figure 2.24 cracking patterns of FRP-retrofitted walls [51]

Figure 2.25 diagonal crack in a Wallette and debonding of CFRP plate [51]

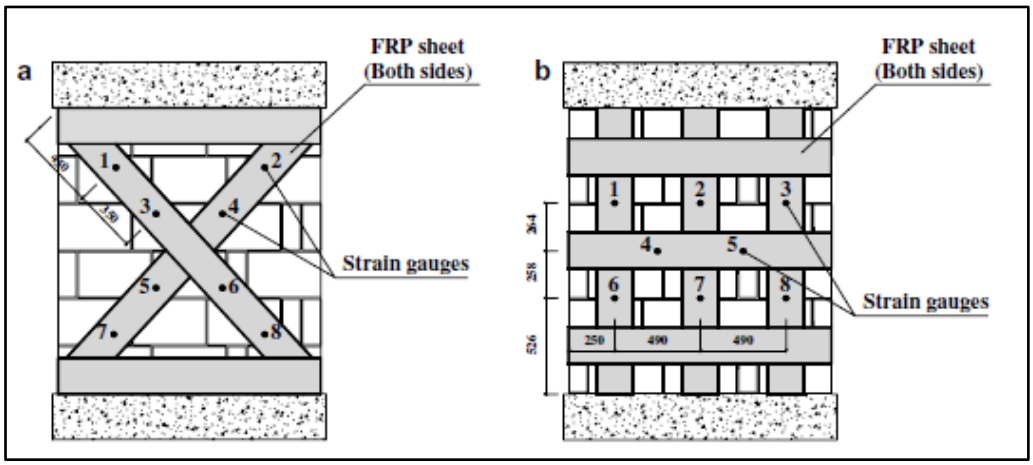

Figure 2.26 reinforcement layout :(a) cross layout and (b) grid layout [53]

(a

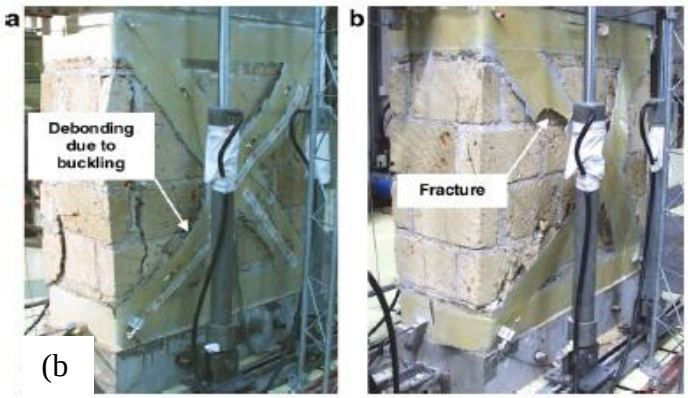

(b

Figure 2.27 (a) Damage of panels strengthened with grid pattern; (b) Typical photographs of the panels strengthened with cross layout [53]

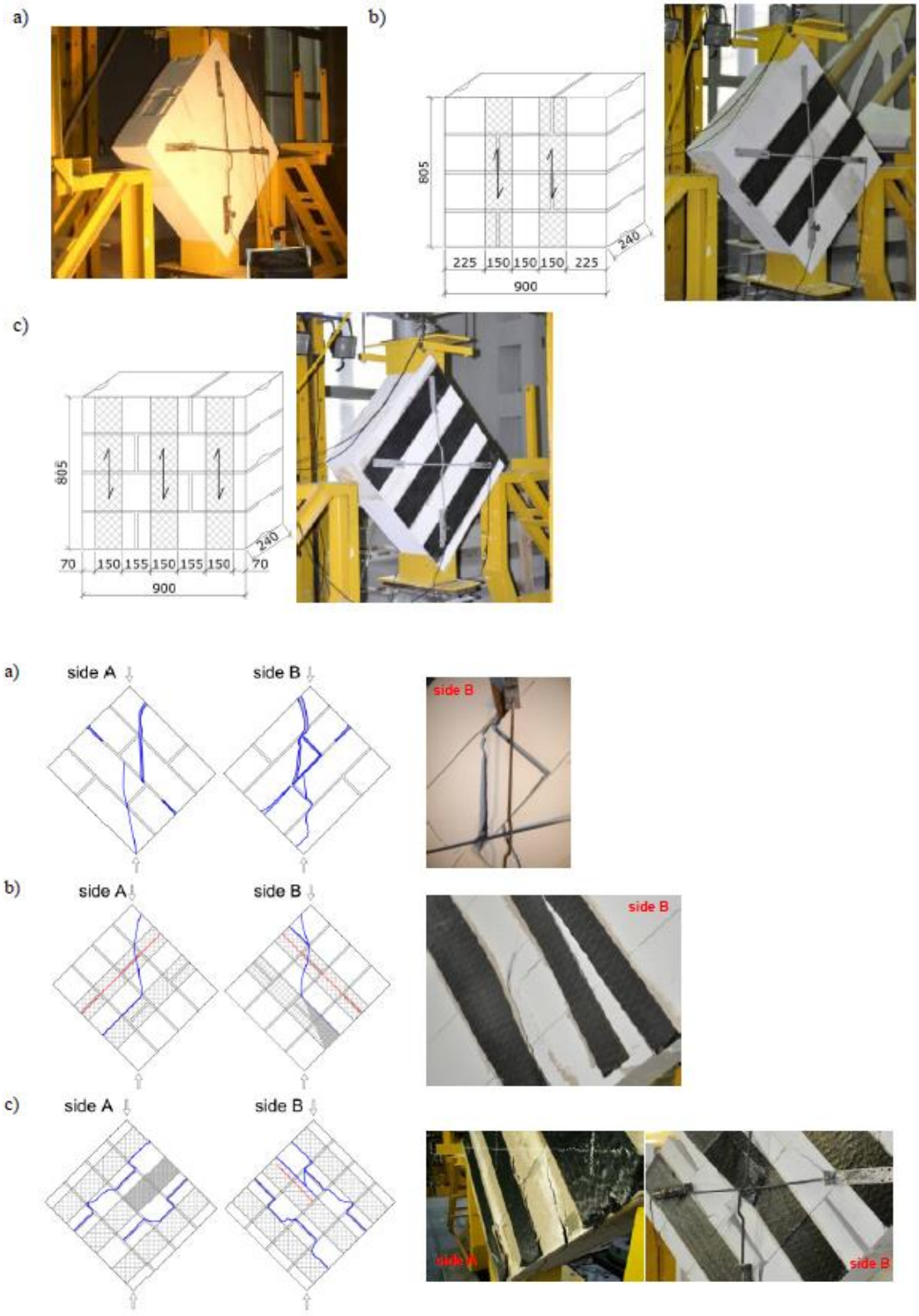

Figure 2.28 Typical modes of failure for specimens: a) a)NS-3 ;b)IIc-5;c)IIIc-5 [55]

2.5.2.2 Near-surface mounting

NSM-FRP is a relatively new reinforcement technique compared to other FRP reinforcement techniques, and can be used as an alternative to EB-FRP strips or sheets. This technique involves inserting FRP bars or strips into grooves cut into the surface of a masonry wall. The method consists of cutting grooves or slots having a diameter of one and a half times the bar diameter in joints or unit, where the grooves are cut with a circular saw fitted with a brick cutting blade. the FRP composite is then bonded into the groove using a two-part epoxy or cement-based mortar.

Petersen and al [9] conducted pull out tests to investigate the bond behavior of solid clay brick masonry prisms strengthened with vertical strips (CFRP perpendicular to bed joints) and horizontally strips (CFRP parallel to bed joints). They used CFRP strips with a rectangular shape to maximize the confinement from surrounding concrete. Tests showed that the main failure mode was the debonding of FRP from masonry for both orientations of CFRP strips. For prisms with horizontally aligned CFRP strips, a compression load applied perpendicular to the strip to simulate a vertical compression in masonry structures. For solid bricks with vertical NSM-CFRP strips inserted into brick only, they found that the bond strength was decreased by 8%. If the vertical NSM-CFRP strips passed through mortar head joint, a reduction in the bond strength of 11% was observed. A larger decrease (31%) in bond strength was recorded when the FRP was aligned horizontally.

Petersen [53] studied the in-plane shear behavior of masonry panels strengthened with NSM CFRP using different reinforcement orientations including vertical, horizontal, and a combination of both. It was found that the use of vertical NSM-FRP strips resulted in a 28% increase in load capacity when the strips were applied only to one side, and 46% increase when they are applied to both front and back sides of the URM walls. It was referred that the vertical strips also proved to be effective in preventing sliding URM failure, and indicate that the strips resisted opening of the sliding cracks. In addition, when both horizontal and vertical NSM strips were employed, the horizontal strips prevented opening of diagonal cracks while the vertical strips prevented sliding failure.

Dizhur and al [10] performed several tests with various NSM-CRFP retrofitting and repair schemes on URM walls loaded in diagonal compression(see Figure 2.29). They reported that retrofitted walls showed an increase in the maximum shear strength ranging from 1.3 to 2.6 times, and 1.3 to 3.7 times for repaired walls, as compared to the URM masonry wall. Also, for

ductility, they observed substantially an increase of 2.6 times for walls retrofitted on one side to 25.5 times for the walls with retrofit on both sides (see Figure 2.30). The effect of different parameters including the groove dimensions, the dimensions, and shape of CFRP, the adhesive type has been investigated in NSM-strengthened brick masonry by **Maljaee and al** [11] (see Figure 2.31).

Mahmoud et al [48] conducted a series of diagonal compression experimental tests on URM walls using a NSM-CFRP pultruded bars and EB-CFRP/GFRP plates, they illustrated the effectiveness of FRP retrofitting system in improving the shear strength of unreinforced masonry with a factor of 3.25.it was noted that the ductility and the shear strength of wall improved when both sides of the wall were strengthened with the NSM technique. the vertical or diagonal FRP strips were able to prevent the sliding failure mode.

To study the parameters who affect the bond behavior of reinforced masonry wall, **Willis and al**.[54] performed a series of pull tests using both EB-CFRP and NSM-CFRP to retrofit unreinforced modern clay brick masonry walls, to understand the influence of various parameters such as geometric properties, surface preparation, location of FRP relative to core and bed joints and bonding agent of bed joints. they indicate that for NSM-CFRP, increasing the embedment of the strip in the groove improves the bond strength provided that the embedment depth cannot exceed the depth of the brick core(see Figure 2.33). They noted that the placing of NSM-FRP strips through the head joints resulted in a reduction of bond strength by 10% and is not is not suggested. The bond-slip curves indicated that NSM-CFRP provided significantly higher bond strength and ductility. Also improved the shear stress by double when compared to EB-CFRP.

Konthesingha and al [55] investigated the use of NSM CFRP laminate on damaged masonry walls. they applied three different configurations; horizontal reinforcement on one side, horizontal reinforcement on two sides and horizontal and vertical reinforcement on both sides of the wall (see Figure 2.34). The results show that the reinforcement of the wall with horizontal and vertical form improves the resistance, deformation and dissipation of energy (Figure 2.35). In terms of NSM FRP bond, the variables that affect the bond behaviour include the: unit strength; bond length; FRP reinforcement cross-section dimensions; material properties of the FRP reinforcement; strength of the adhesive; distance between the FRP reinforcement and unit edge and distance between multiple parallel FRP reinforcement.

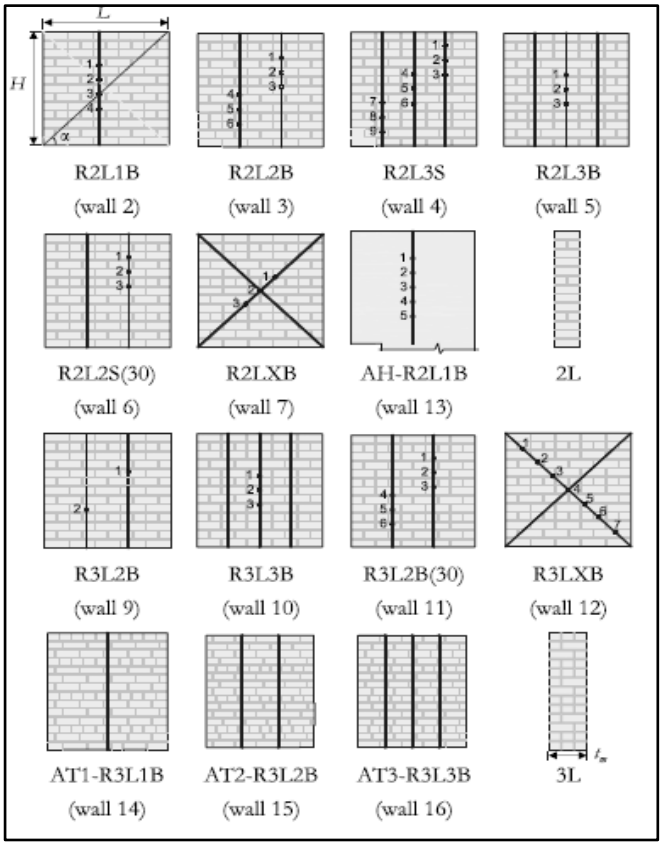

Figure 2.29 Wall panel retrofit details showing location of strains gauges [10]

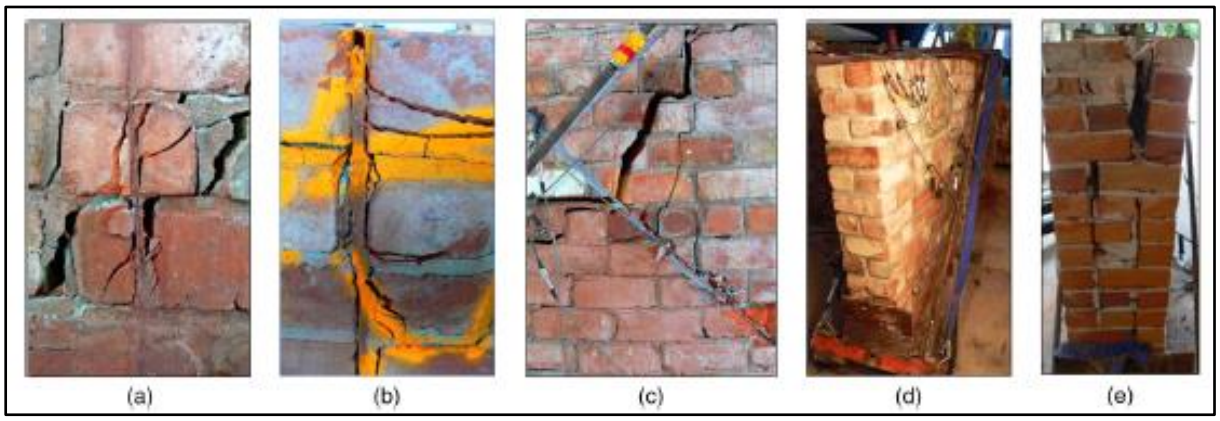

Figure 2.30 Observed wall deformation and crack patterns: (a) localized cracking R2L2B(wall 3); (b) CFRP strip pull-out R3L2B(wall 9);(c)IC debonding of CFRP strip R2LXB(wall 7);(d) out-of-plane deformation,R2L3S(wall 4);(e) separation of individual leafs,AT2-R3L2B(wall 15)[10]

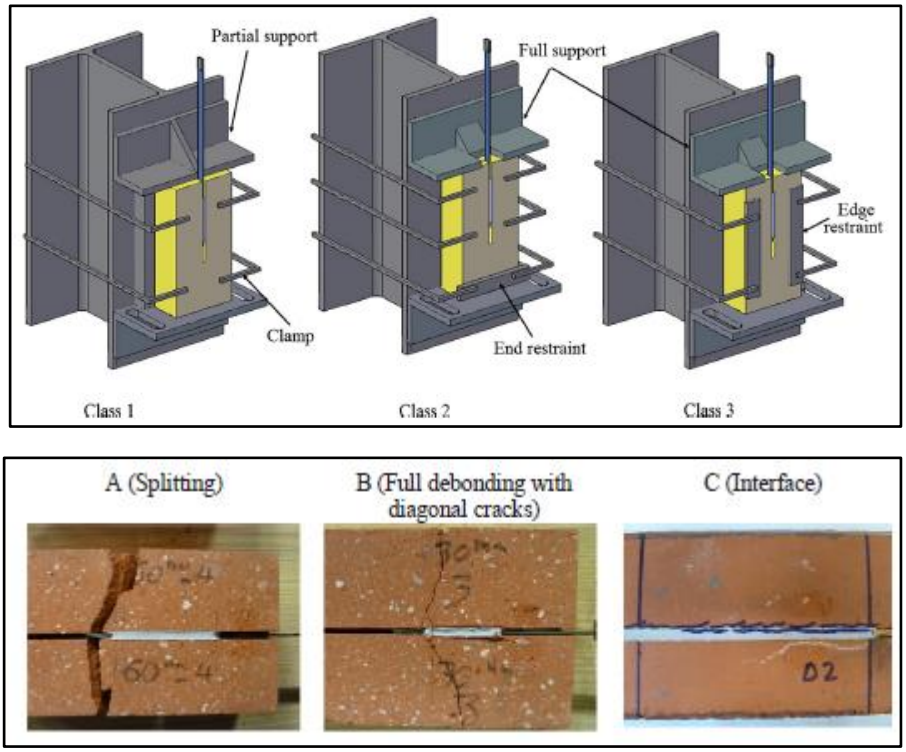

Figure 2.31 Test setup improvements and Typical failure modes. [11]

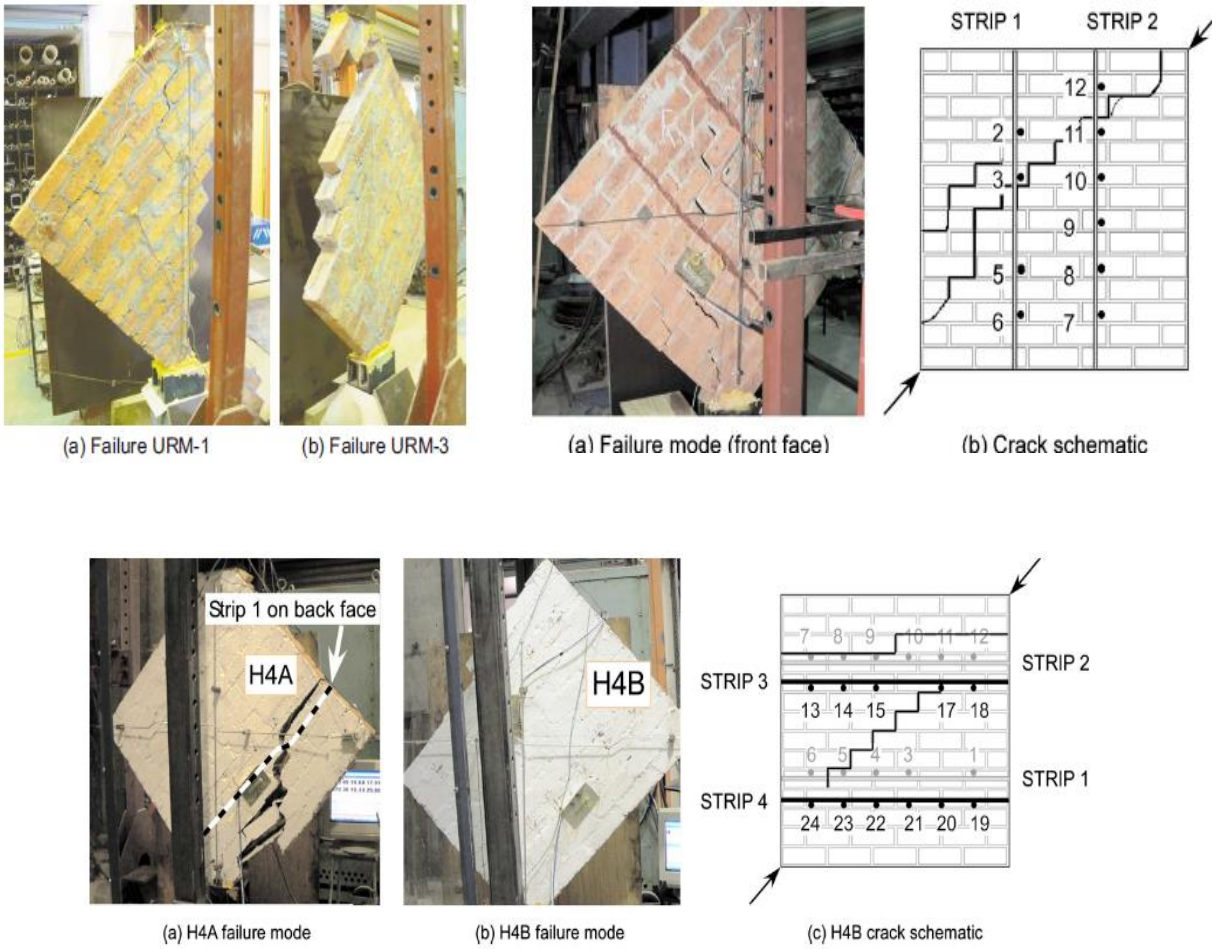

Figure 2.32Typical failure modes of URM specimens [55]

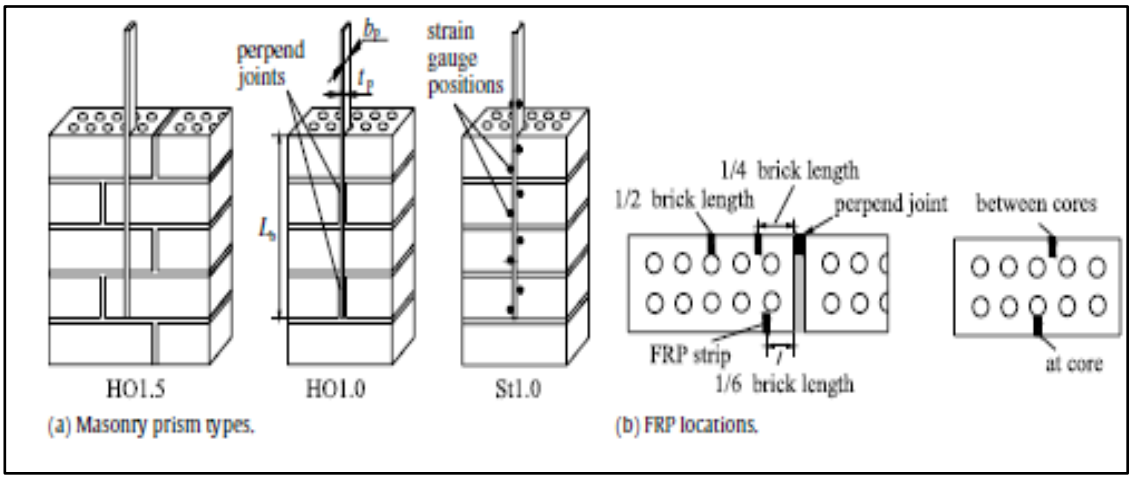

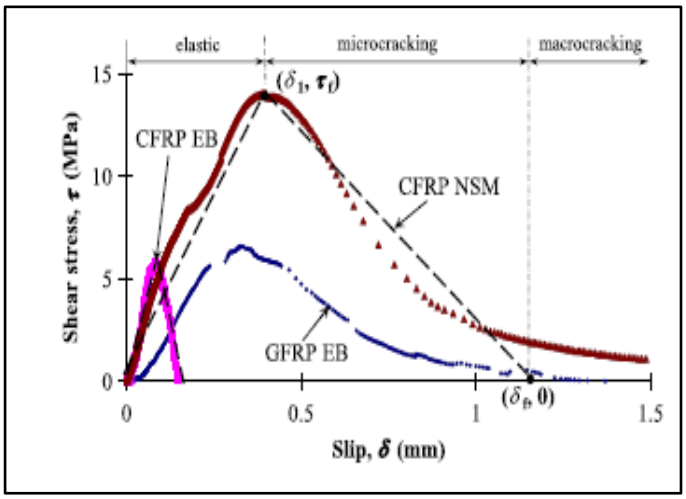

Figure 2.33 NSM specimen configurations and Typical local bond-slip responses [57].

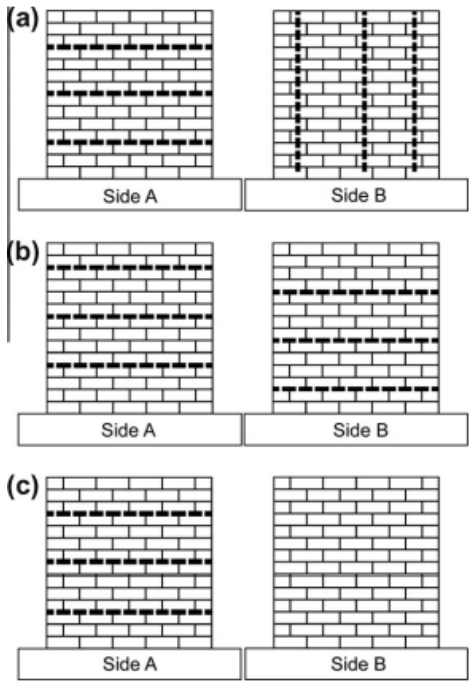

Figure 2.34 CFRP retrofitting schemes [58]

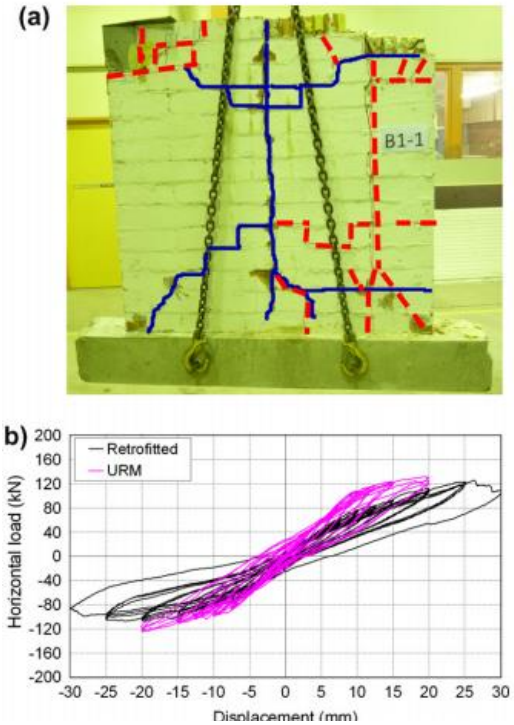

Figure 2.35 Specimen B1-1 (a) crack pattern :solid lines show cracking after the URM (2.0 MPa); (b) load displacement diagrams [58]

2.6 FRP strengthened masonry triplets

Other tests on FRP strengthened masonry assemblages have been used to characterise the composite behaviour between FRP and masonry.

Ehsani and al [56] investigated the effect of externally bonded FRP sheets to the shear strength, They conducted thirty-seven direct shear tests on clay brick specimens triplet strengthened with bidirectional GFRP sheets (see Figure 2.38). They varied several parameters, as well as length fiber, fiber orientation and FRP materials with different glass fiber densities. The fibers were oriented at each 0°; 45°; 90°;135°, with respect to the loading direction. They observed two failure modes: shear failure (of the GFRP) along the bed joint, debonding of the GFRP laminate in the middle-brick region of the fabric edges. It was observed that the type of failure was influenced by the strength and bonded length of the GFRP laminate. For strong GFRP sheets debonding typically occurred, whereas for weak GFRP laminate, shear failure occurred. Weak GFRP laminate with a short-bonded length failed in a combination of shear and debonding. The fiber orientation was shown to have an effect on the strength and stiffness of the specimens.

When the fibers were aligned at 45° and 135° a stiffer response was observed with a higher load. When the fibers were aligned at 0° and 90° a more ductile response was observed (see Figure 2.39).

Hamid and al [3] carried out different tests under different stress conditions to study the in-plane behavior of unreinforced wall strengthened with FRP laminates. The tests involved diagonal tension specimens, and prisms loaded in compression, with different bed joint orientations (on/off-axis compression), and specimens loaded under joint shear. The masonry wall was assembled using face shell bedded hollow concrete blocks. The specimens were strengthened by covering the full surface on both sides with EB- GFRP sheets. they noticed that the wall failed by shear sliding (specimens tested in direct shear, diagonal tension and 30°/ 45° degrees off-axis compression), this mode significantly enhanced with FRP strengthening. Rather than brittle shear sliding, the strengthened specimens failed by crushing or web splitting of the masonry units. The highest increase in strength was found in the direct joint shear specimens. The FRP laminates did, however, give stability to the shells of the masonry units after the webs had split(see Figure 2.36 and Figure 2.37). Similar researches have been conducted by **El-Dakhakhni and al** [57] and **Campanaro and al** [58].

G. S. Pavan and al [59] studied the enhancement of the brick–mortar interface characteristics through the application of FRP composites in masonry with brick of lower modulus of elasticity than mortar (Figure 2.40 and Figure 2.41). The main aims were to studied the effect of different variables like type and grade of FRP composite on the interface characteristic of masonry such as ultimate displacement also shear strength. it was observed debonding of FRP reinforcement, these modes were influenced by the bond strength of FRP with masonry (Figure 2.42).

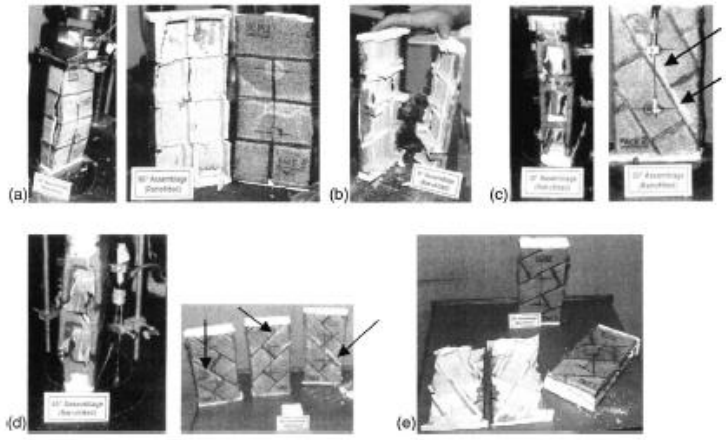

Figure 2.36 Failure modes of retrofitted on/off-axis compression assemblages:(a) series 90R,(b) series 00R,(c) series 30R,(d)series 45R and (e) series 60R [3]

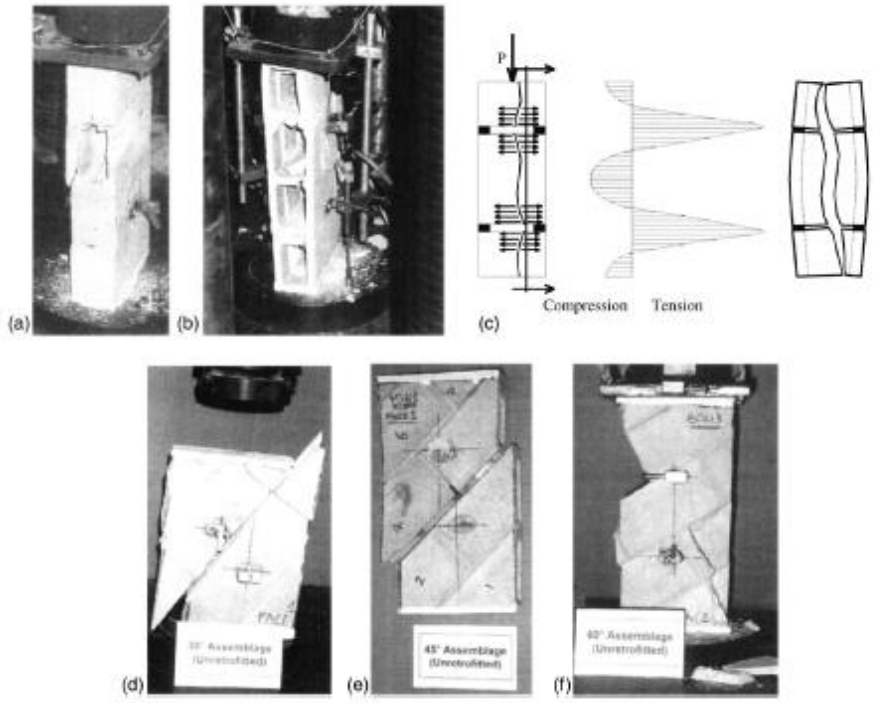

Figure 2.37 Failure modes of unretrofitted on/off-axis compression assemblages:(a) series 90U, (b) series 00U, (c)web splitting mechanism of face shell mortar bedded masonry ;(d) series 30U;(e) series 45U and (f) series 60U [3]

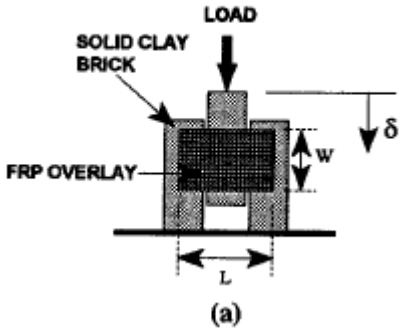

Figure 2.38 test specimen (retrofitted triplet)[60]

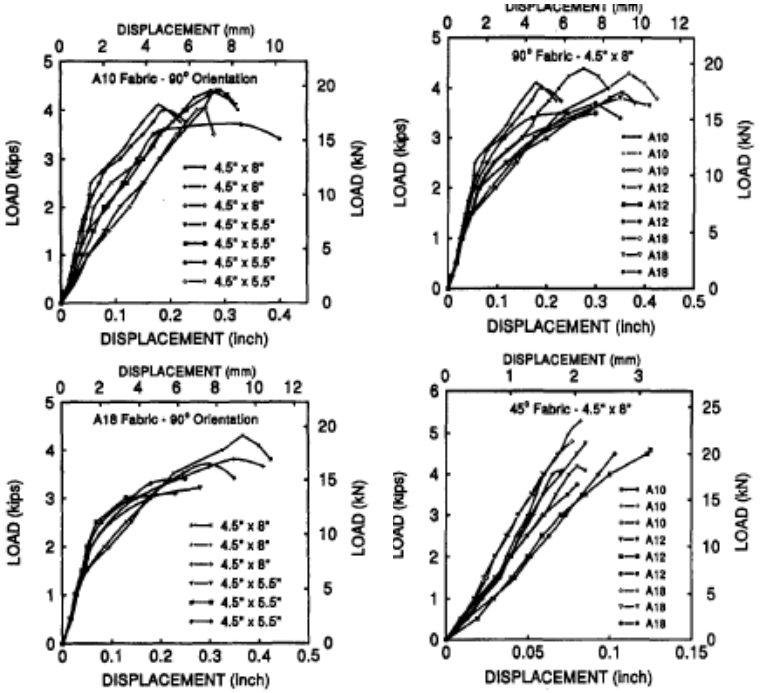

Figure 2.39 Effect of Fabric density and of fabric length on ultimate Load [60]

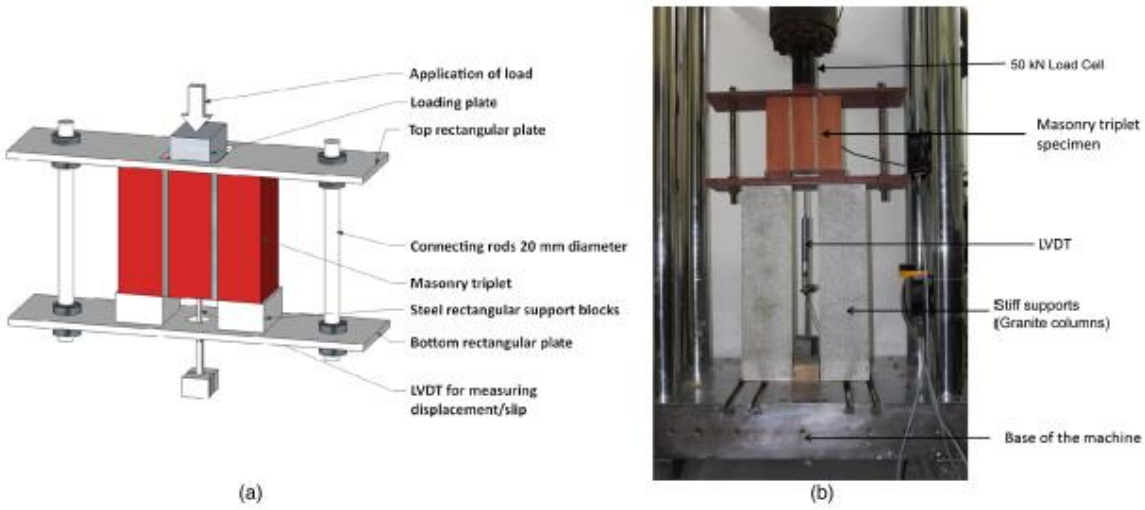

Figure 2.40 Experimental set-up for testing of masonry triplets: (a)schematic diagram of the experimental set-up for triplet specimens;(b) testing of T-co masonry triplet [62]

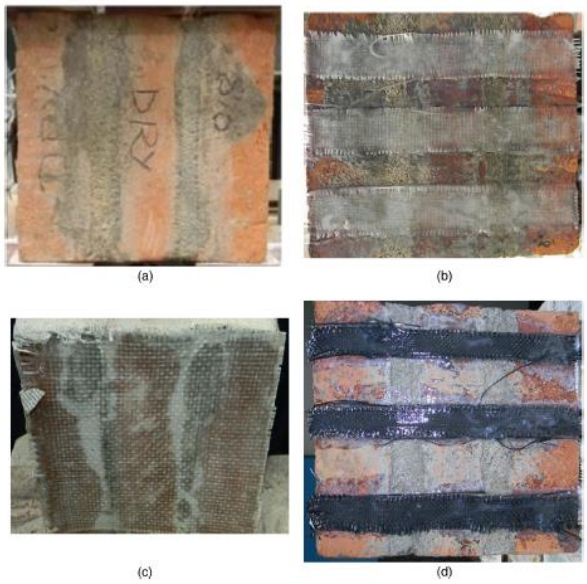

Figure 2.41 Masonry triplets reinforced with CFRP composite [62]

Figure 2.42 Failure patterns of triplet specimen with CFRP composite:(a) and (b) debonding failure, (c) tensile rupture failure [62]

2.7 Numerical Modeling Approaches for Structural Masonry Analysis

Numerical modeling of structural masonry is one of the most complicated problems in structural engineering research and practice. This complexity is attributed to the large number of factors, such as material properties of both brick and mortar anisotropy and dimension of bricks, arrangement and joint width of joints, and quality of workmanship.

In this section a brief explanation of the different types of models used to analyze the in-plane behavior of masonry is showed. Additionally, some other proposals to analysis the structural behavior of reinforced masonry is presented.

2.7.2 Modeling of masonry

There are various numerical modeling approaches with different accuracy for the analysis of masonry structures in the literature, as shown in Figure 2.43. according to the classification of Lourenco [60], Asteris et al [61], depending on the level of simplicity and accuracy desired. the

different analytical methods could be summarized in three different approaches are used for masonry models:

2.7.2.1 Macro-modeling (Modeling masonry as one-phase material).

- **Continuum Approaches:** In the macro-modelling approach all of the components of the masonry (the units, mortar joints, unit/mortar interface) are smeared into a homogeneous continuum element. The continuum medium is commonly modelled with isotropic or anisotropic material behaviour to account for the directional properties of masonry. The material stress-strain behaviours are determined from experimental tests on masonry assemblages (for example the biaxial tests of Page 1983), or using a process known as homogenization (see Figure 2.44.b). A review of homogenisation techniques is provided in Lourenço [13].
- **Discontinuum Approaches:** Calio and al [62] proposed an innovative so-called discrete-element model to simulate the nonlinear seismic behavior of masonry buildings. To this end, the in-plane nonlinear response of masonry walls was approximated by an equivalent discrete element using the concept of macro-element discretization. The equivalent macro-element is modeled by the use of an articulated quadrilateral with surrounding rigid edges and to simulate the shear behavior of masonry, two internal diagonal springs are utilized. The advantage of the model is that it requires low computational resources for investigating the nonlinear behavior of Unreinforced Masonry (URM) buildings. The elastic characteristics of the springs are defined by a specific procedure of identification with the objective to transfer some characteristics of the internal texture to the macro-scale model.

The macro-modelling technique is unable to model local failure modes (unlike the micro-modelling technique). however, it is suitable for modelling large scale of masonry, where only a simplified representation of composite behaviour is required, and local failure modes are not so important. it is not suitable for the detailed stress analysis of a small masonry panel, due to the difficulty of capturing all its expected failure modes. The influence of existing mortar joints as the major source of weakness and nonlinearity cannot be addressed using this strategy.

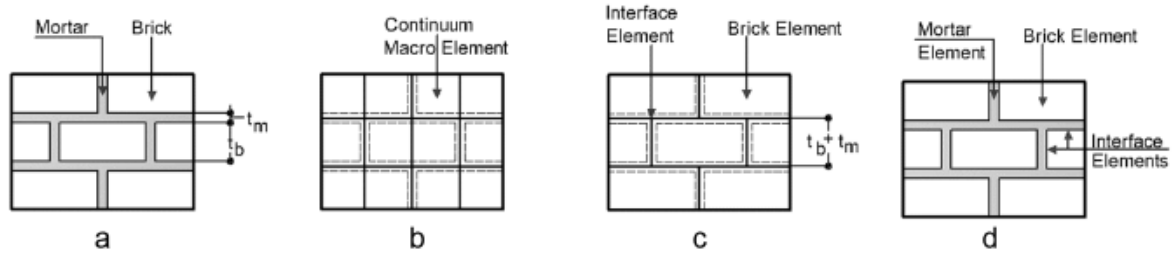

Figure 2.43 Masonry modeling strategies :(a) Masonry sample;(b) one-phase macro-modeling;(c) Two-phase micro-modeling;(d) Tree-phase micro modeling[13]

2.7.2.2 Simplified micro-modeling (Modeling masonry as two-phase material):

In this approach, the bricks are represented as fictitious expanded bricks by continuum elements with the same size as the original bricks dimensions plus the real joint thickness. The mortar joint is also modeled as an interface with zero thickness as shown in Figure 2.43.c and Figure 2.47.b. The interfaces stiffness is deduced from the stiffness of the real joints. According to this procedure, the properties of the mortar and the unit/mortar interface are lumped into a common element, while expanded elements are used to represent the brick units. Zero-thickness interface elements (a type of discontinuum element) are normally used for the interfaces. Interface elements relate the interface stresses (normal stress and shear stress) to the relative displacements across the interface (normal displacement and shear displacement). Contact elements, which are a special kind of interface element, have also been used to model the interfaces[13].

Micro-models that incorporate these failure mechanisms (with post peak softening included) are able to reproduce crack patterns and the complete load-displacement path of a masonry structure up to and beyond the peak load. The material properties required for the micro-model are determined from experimental tests on masonry joints and assemblages. A detailed description on the types of tests used to determine the material properties is provided in Rots [63]. This approach is suited for small structural elements with particular interest in strongly heterogeneous states of stress and strain. The primary aim of micro-modeling is to closely represent masonry from the knowledge of the properties of each constituent and the interface. The necessary experimental data must be obtained from laboratory tests in the constituents and

small masonry samples. This approach leads to the reduction of the computational effort and yields a model that is applicable to a wider range of structures.

- **Discontinuum Finite Element Models (D-FEMs)**

in the modeling of masonry, the mortar joints are represented as discontinuities where a potential crack, slip or crushing failure can occur, the unit-mortar interface can be modeled using interface elements that are zero-thickness finite elements (FE) characterized by two surfaces connected to each other that separate in the deformed shape (Oliveira[64]). The function of these elements is to represent the interaction between deformable structures, along surfaces where separation and sliding may occur. The modeling of these boundary conditions is one of the main tasks for all the modeling techniques for masonry structures. Many researchers, Among them Mohebkhah and al [65]; Kouris and Kappos [66], proposed spring elements to connect the boundary nodes of the infill panel and the around frame. These elements enable two adjacent nodes to be tied together or released suit to specified conditions. Each node of the element has two translational DDL. The element is able to transfer compressive and adherence forces but is unsuited of resisting tensile forces. when the link is active, great values of the normal and tangential stiffnesses were adopted. Conversely, the link is released by replacing these values to zero. In software packages, the behavior of interface elements in a model can be run by a discrete crack model, a Coulomb friction model, or a model proposed by Lourenco [67] and Van Zijl [68], which combines Coulomb friction, tension cut-off, and a compression cap. (see Figure 2.44).

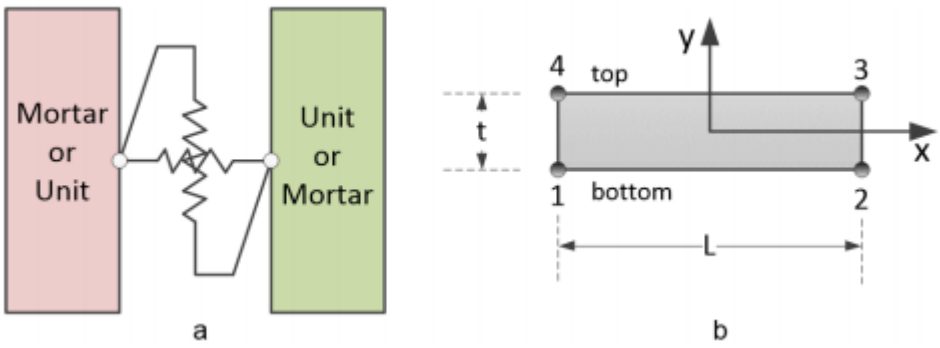

Figure 2.44 Models for mortar-unit interface: (a) Spring elements;(b) Interface element [71]

- **Discrete Element (DE) Models**

The method discrete elements were initiated and developed by Cundall [69] for the study of joints and massive rock fractures, Otto Strack and Peter[70], they applied this new approach to the investigation of solids . After then, the method has been significantly updated and developed [71, 72].DEM method is particularly suitable for represent or approximate a continuum body into a series of discrete elements and aims to simulate and analyze its micro and macro behavior. In discrete micro-mechanical models, masonry wall is considered as a set of elements attached to each other by contact laws assuming the deformation of the joint., the blocks are modeled by rigid or deformable solids linked together by regular laws of contact and whose movement is described by the Newton-Euler equations which aims to simulate the behavior of the mortar joint.; the problem is then resolved by explicit diagrams. Bui, and al [73] explained that due to the heterogeneity of masonry walls (bricks, joints, and interfaces), the discrete element method (DEM) is the best-adapted tool available now to analyze this type of structures, mainly to reproduce the nonlinear behavior that seems beyond the elastic phase. Whatever the strategies concerning DEM simulations. among the most famous approaches that have been employed to the modeling of masonry structures there are:

- FEM-DEM coupling approach
- Discontinues Deformation Analysis (DDA)
- Distinct Element Method
- DEM Particle flow approach (PFC)

In the literature, discrete element methods divided into two categories: " smooth DEM " and "non- smooth DEM ". In the smooth DEM methods, the laws of interaction between the blocks are continuous and differentiable functions and an explicit integrator intervenes in the management of the dynamic evolution of the medium. non-smooth DEM has an implicit algorithm to solve the dynamic equations. In these methods, the interaction laws between blocks are non-regular contact laws such as Signorini conditions or Coulomb dry friction. These two types of the method have shown their effectiveness in modeling the quasi-static behavior of masonry.

- **Boundary Element Models**

In the literature, there is fewer studies deal with the application of the Boundary Element Method (BEM) in the modeling of masonry structures. Rashed et al [74] applied the BEM to model the non-linear behavior of the masonry structure. Cracking, debonding and crushing

failure modes were considered, while the material non-linearity was ignored. First stresses, based on a developed algorithm, were used to describe the failure modes. The model used an incremental iterative solution procedure to follow the failure at each loading step.

- **Discrete Limit Analysis Models (D-LAM)**

Based on the work of Heyman [75], Livesley [76] developed the limit analysis method for simulating discretized behavior in masonry structures. Several other researchers have used the limit analysis for the evaluation of masonry structures (Gilbert[77]; Orduña and Lourenço [78]).

The following hypotheses are usually adopted:

- The masonry units are infinitely rigid;
- The masonry units are infinitely strong;
- The masonry units do not slide at the joints;
- The joints transmit no tension.

2.7.2.3 Detailed micro-modeling (Modeling masonry as a three-phase material)

In this strategy, units and mortar in the joints are represented by continuum elements whereas the unit–mortar interface is represented by discontinuum elements (Figure 2.47.d and Figure 2.46). While this modeling leads to more accurate results, the level of refinement means that the corresponding analysis is computationally intensive, limiting its application to small scale laboratory specimens and structural details. Detailed micro-modelling is able to represent the real behavior of each component of masonry. In this approach, both the elastic and inelastic properties of both the units and the mortar can be realistically taken into account. A suitable constitutive law is introduced in order to reproduce not only the behavior of the masonry units and mortar, but also their interaction. A complete micro-model needs to include all of the failure mechanisms of masonry including: joint cracking in tension; joint sliding; cracking of the units; and crushing of the masonry. The major drawback of the method is that requires large computational effort to analyze. Today, this method is used mainly to simulate tests on small specimens in order to determine accurately the stress distribution in the masonry materials [79].

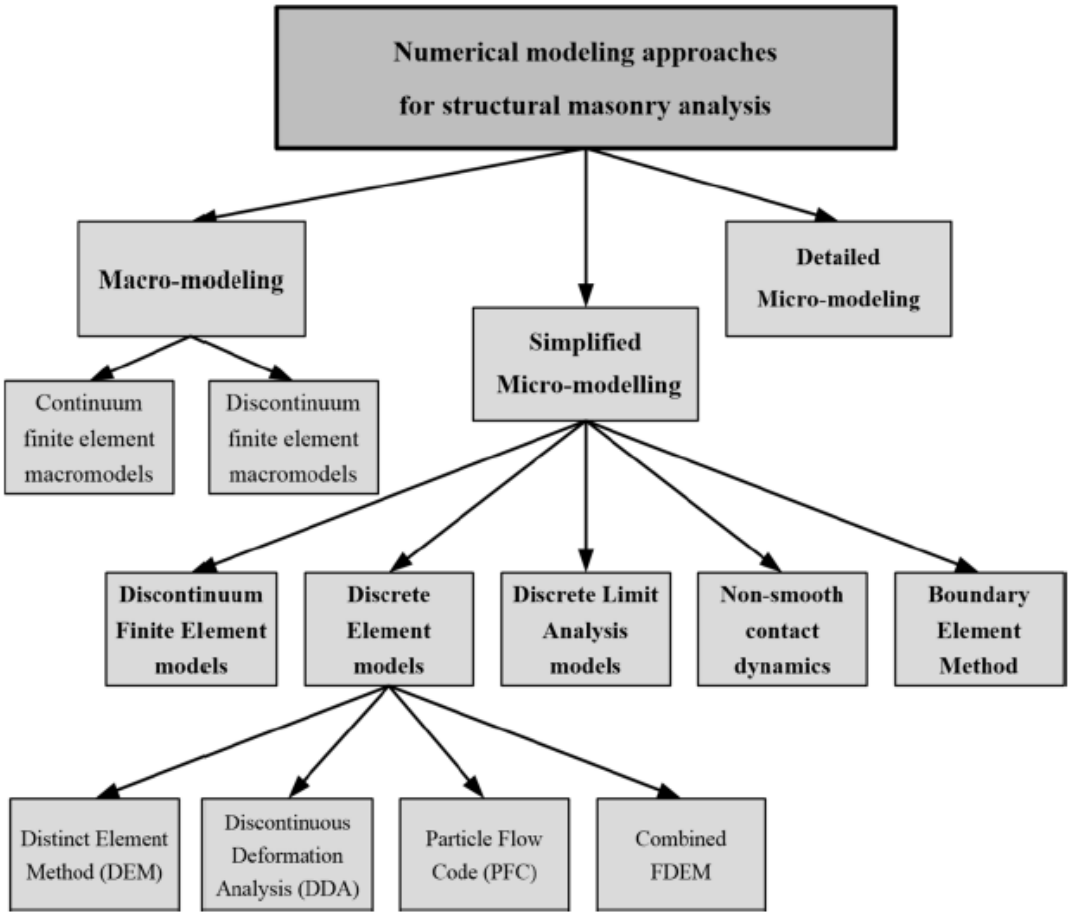

Figure 2.45 Different numerical modeling approaches for structural masonry analysis

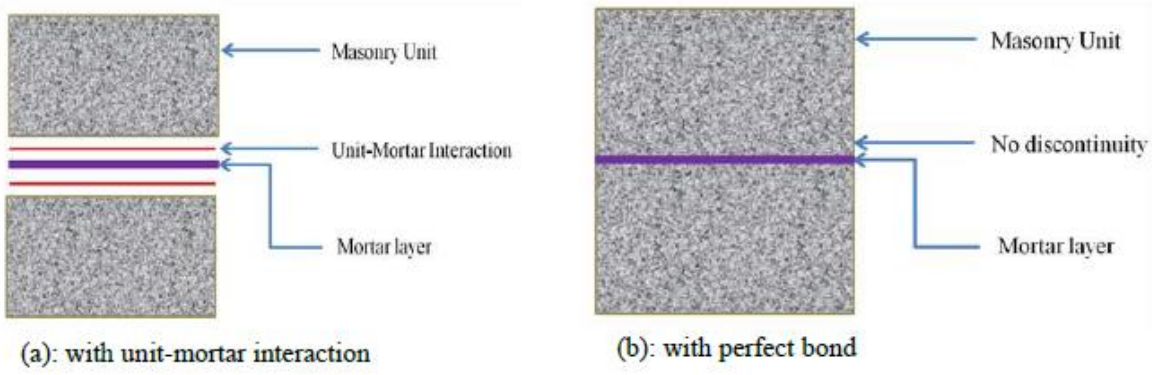

Figure 2.46 Detailed masonry micro-modeling[67]

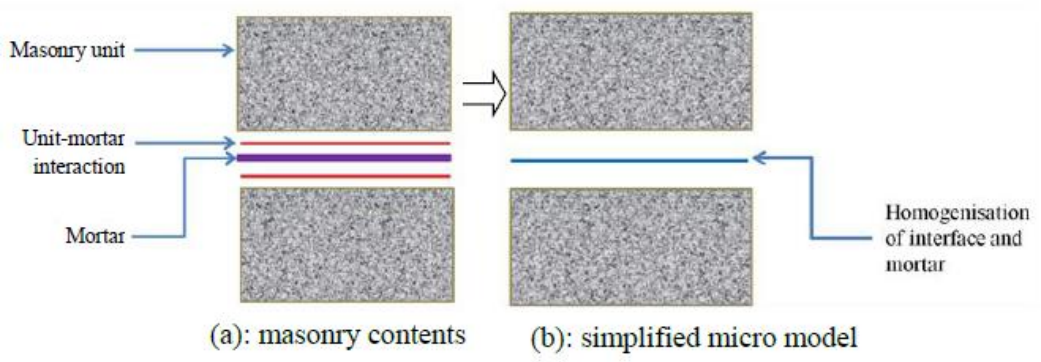

Figure 2.47 simplified masonry micro-modeling[67]

2.7.3 Constitutive law material models of masonry

The researches relating to the microscopic modeling by finite elements of the masonry structures agree on the fact that the effectiveness of the model is related to its capacity to reproduce the various modes of rupture of the masonry. Lourenço identifies two different phenomena at the origin of the rupture of the brick / mortar interface: one is associated with a rupture by traction (mode I), the other with a rupture in shear (mode II). To these two potential failure modes can be added a last mode relating to a compression failure of the masonry. The different models present in the literature differ by the failure modes taken into account and by the modeling strategies adopted for each failure mode considered.

2.7.3.1 Modélisation en élasto-plasticité (loi de Drucker-Prager) :

The plastic modelling of masonry structures can be carried out with the Drucker-Prager surface, which is generally used to characterize the stress-strain behaviour of tension/compression asymmetric materials (see Figure 2.48). The Drucker-Prager yield criterion can be used with a non-associated flow rule typical of masonry and the yield surface does not change with progressive yielding, hence there is no hardening rule and the material is elastic-perfectly plastic. This plastic model from Drucker Prager was used in Aron Gabor's study [41, 80].
The other parameters of the model are defined by c and φ:

$$\alpha . I_1 = +\sqrt{J_2} - k \leq 0 \qquad (2.3)$$

Or

$$I_1 = \frac{1}{3}(\sigma_1 + \sigma_2 + \sigma_3) \quad (2.4)$$

$$J_2 = \frac{1}{6}((\sigma_1 - \sigma_2)^2(\sigma_3 - \sigma_2)^2(\sigma_1 - \sigma_3)^2) \quad (2.5)$$

k et α are two constants of the material:

C = H tan φ $\rightarrow$ $\alpha H = 2\sqrt{3}\frac{\cos\varphi}{3-\sin\varphi}$ (2.6)

$$\alpha = \frac{2.\sin\varphi}{\sqrt{3}(3-\sin\varphi)} \qquad k = \frac{6c.\sin\varphi}{\sqrt{3}(3-\sin\varphi)} \quad (2.7)$$

Or

$I1$: The first invariant of stress tensor,

$J2$: The second invariant of the Deviatoric stress tensor,

φ : The internal friction angles.

c: cohesion value

In particular the parameter α is evaluated using the angle of internal friction value, the angle of dilatance Ψ which describes the potential flow (inelastic voluminal deformation), in the case of a material with a non-associate flow rule, assumes a value between 0 and the value of internal friction angle. When Ψ ≠ Φ, the flow law is associated, in this case the plastic deformation occurs perpendicular to the threshold surface and there is a volumetric expansion of the material with plastic deformation. If Ψ = Φ there is less volumetric expansion and if Ψ =0°, there is no volumetric expansion. In the specific case of masonry ψ usually takes a value between 1/3 and 2/3 of ϕ. As is well known the limit surface corresponding to that plastic model is represented by a cone in the space of principal stress whose intersection with the plane of principal stress defines generally in the case of masonry a parable or a hyperbole whose intersections with the principal axes Fc and Ft are given respectively by the following expressions[81]:

$$F_c = \frac{2k\alpha\sqrt{3}}{2\alpha^2\sqrt{3}-2\alpha} \quad ; \quad F_t = \frac{F_c(\alpha\sqrt{3}-1}{2\alpha^2\sqrt{3}-2\alpha} \quad (2.8)$$

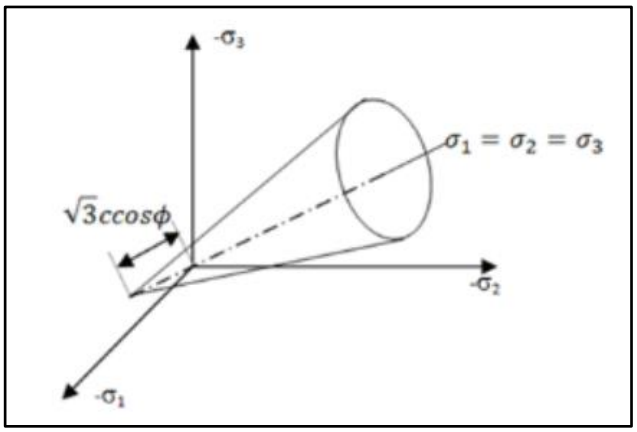

Figure 2.48 Drucker-Prager yield surface in the main stress space [84]

2.7.3.2 Modeling in elastoplasticity with softening:

Lourenço et al have developed a model with a powerful representation of orthotropic plasticity with different hardening softening behavior for masonry: Masonry is considered as a homogeneous continuous and orthotropic material under the hypothesis of plane stresses. (see Figure 2.49). the combination of a Rankine-like modified model in tension and the model of Hill-like in compression are proposed by [82, 83] to simulate the masonry behavior by means of the tension-compression multi-surfaces criterion. in this model, the anisotropy and the variation of the shear stress of the masonry are considered, the tension stress and compression vary in both directions. The application of the model in structural modeling of masonry structures leads to excellent results, both in terms of collapse loads and in terms of reproduced behaviour. See Figure 2.50.

Abdou (2005) implemented this model combined with damage criterion to evaluate the masonry wall behavior, which results were acceptable. A detail discussion of the numerical results has been presented in[84] .

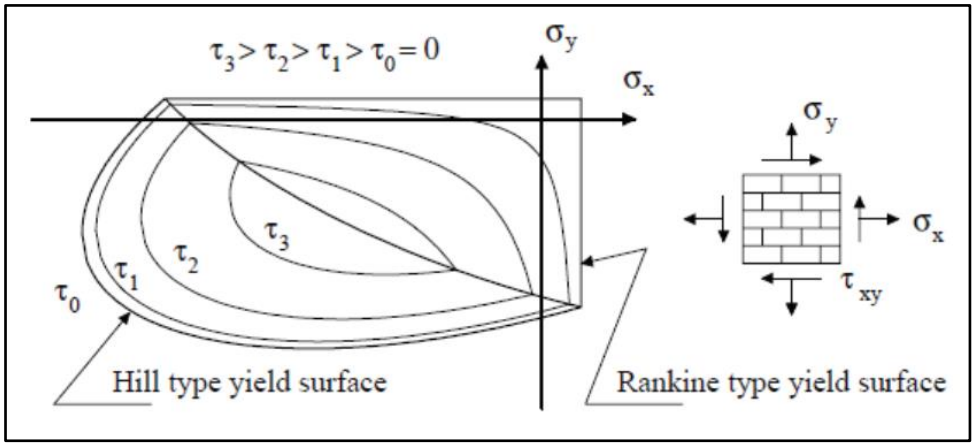

Figure 2.49 Continuum failure surface for masonry (plane stress representation). [85]

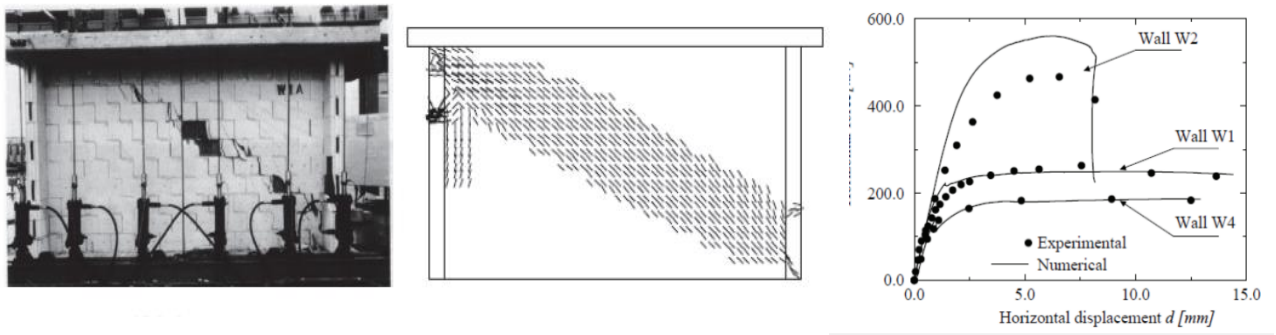

Figure 2.50 validation of the orthotropic plasticity model by a comparison of the numerical and experimental results [86].

2.7.3.3 Damage modeling with the "concrete" model:

The concrete model considers a linear elastic behavior of the material delimited by a failure surface for brittle materials proposed by William and Warnke [85]. The solid element is capable to take into account both cracking and crushing failure modes, in tension and in compression, respectively. In particular [86], in three orthogonal directions for each integration point, the failure surface is represented on the principal stress plane by a limit domain that is associated respectively a smeared cracking behavior for the tensile principal stress quadrant and a cracking/crushing behavior for the other quadrants. The concrete failure criterion due to a multiaxial stress state can be represented in the following form:

$$\frac{F}{F_c} - S \geq 0 \qquad (2.9)$$

Where

F: function of the principal stress state,

S: the failure surface expressed in terms of principal stresses and five input parameters ft, fc, fcb, $f1$ and $f2$.

ft: the uniaxial tensile strength; fc: the ultimate uniaxial compressive strength; fcb : the ultimate biaxial compressive strength; $f1$: the ultimate compressive strength for a state of biaxial compression superimposed on hydrostatic stress state failure surface proposed by William and Warnke in principal stress space

$f_t < F_t \; ; \; f_c < F_c$

$fcb = 1{,}2\, fc \qquad f1 = 1{,}45\, fc \qquad f2 = 1{,}725\, fc$

If the failure criterion is satisfied in a direction, cracking or crushing occurs. In particular, the material cracks occur when the tensile stress exceeds the limit value ft (Rankine criterion), the crushing occurs while all the principal stresses exceed the compression limit value(see Figure 2.51). In the study of Avossa and Malangone [81] the numerical result achieved by using this model demonstrated that this model cannot be captured the real ductility of the masonry structures. but only is capable of restoring the maximum experimental resistance value.

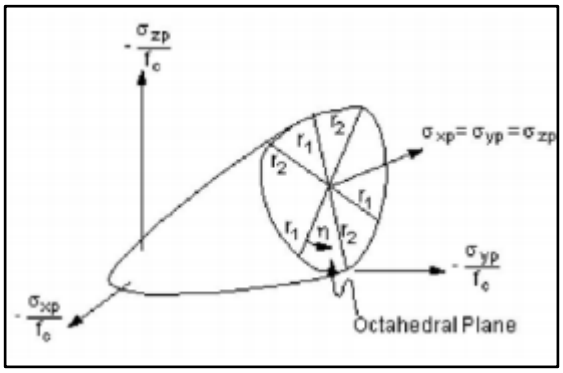

Figure 2.51 Failure surface proposed by William & Warnke in principal stress space [88]

2.7.3.4 Elastoplasticity modeling coupled with damage:

The use of Drucker-Prager model, which defines an elastic-perfectly plastic behavior for the material, does not allow to better simulate the stress distribution into the structural element neglecting besides the cracking. Such observations give evidence that an appropriate

combination of plasticity criterion, crushing surface in compression and cracking surface in tension allows to reproduce all the crises of the material. The only recourse to the theory of plasticity finds its limits for the modeling of the cyclic stresses of the masonry insofar as in plasticity. Certain authors thus coupled the theory of plasticity with that of the damage because the theory of plasticity reflects the irreversible deformations of the masonry while that of the damage accounts for the mechanism of propagation of the cracks and the loss of rigidity associated with it.

Papa and Nappi[87] have developed a model that combines plasticity and fragile damage in traction of masonry. They consider masonry to be an orthotropic material in a state of plane stresses. In Figure 2.52, the predictions of this model are compared to the experimental results obtained on a reduced model of a masonry structure. The masonry structure is a two-level wall, with openings, subjected to concentrated lateral forces at the height of the floors. Following the authors' conclusions, the model gives a good approximation of the ultimate load that the wall resists as well as the most damaged areas. On the other hand, the model turns out to be more rigid, with less significant displacements of the order of 10 to 15%.

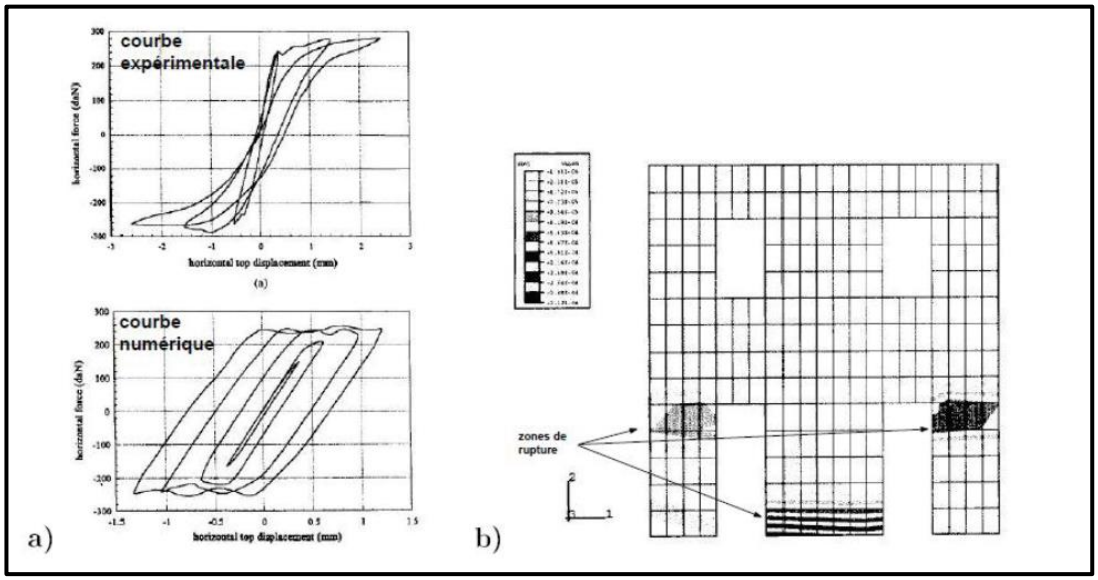

Figure 2.52 A validation of the model: a- force-displacement curves; b- survey of damaged areas. [90]

M. Avossa and P.Malangone [81] have developed a new CoDIC (Concrete Drucker Prager - Ideal Spherical Compression Cap) model which is a combination of two Concrete and Drucker-Prager models (see Figure 2.53). This model is defined through an appropriate intersection of a modified concrete model domain with the plasticity Drucker Prager domain and by means of

the definition of a new compression failure surface. Particularly, the smeared crack behavior of the concrete model, valid in the field of positive principal positive stress (tension), is extended to mixed tension-compression zones also neglecting the stress limit in compression.

The intersection with the Drucker-Prager model is governed by conditions that the parameters of the two different models should follow. In particular, the relationship between the uni-axial tensile strength f_t and the compression f_c defined for the concrete model with the corresponding uni-axial resistances F_t et F_c of the Drucker-Prager model must verify the following relationship: $f_t < F_t$; $f_c < F_c$

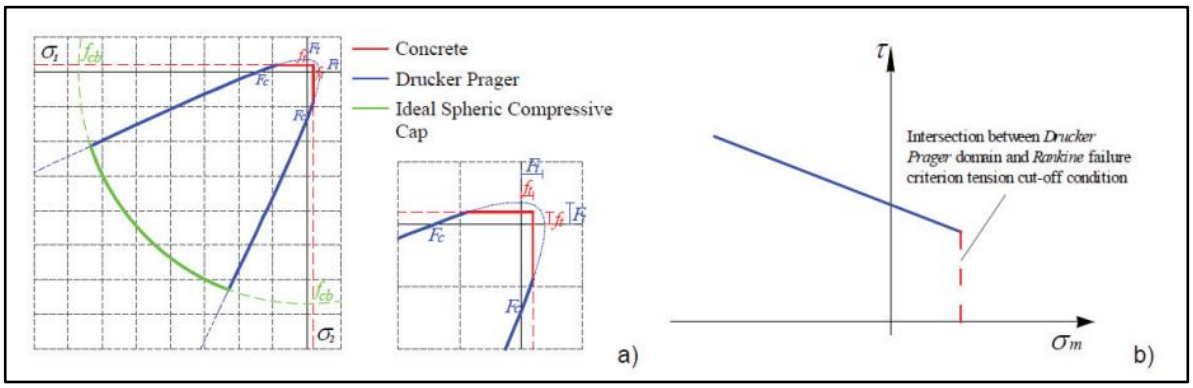

Figure 2.53: a) CoDIC domain in the main stress plane; b) "cut-off" traction condition for traction behavior. [84]

The authors validated this model by comparison with the experimental results available in the literature [82]. From the results obtained, the authors mentioned that there is a great correlation between the numerical and experimental results in terms of maximum load and maximum displacement. In addition, they concluded that the use of the new CoDIC model makes it possible to exceed the above limits of single-use of either the concrete model or of the Drucker-Prager model). Consequently, this new CoDIC model is suitable to account for the behavior of masonry by taking into account both the cracking and the plasticity of the material in the compression zones.

2.7.3.5 composite interface model of Lourenço

One of the most sophisticated simplified microscopic models was presented by Lourenço [63]. It is a "multi-surface" plasticity model which takes into account five forms of the failure modes of mortar joints by tension, shear and compression. The plasticity model of the joints is able to

reproduce three different types of failure mechanisms: tension cut-off (Mode I), Coulomb friction model and compression (considering an ellipsoidal surface cap) and combined shear-compression failure. The model was successful recommended for the study of small structures and structural details. The interface cap model used by Lourenço is shown in Figure 2.54.

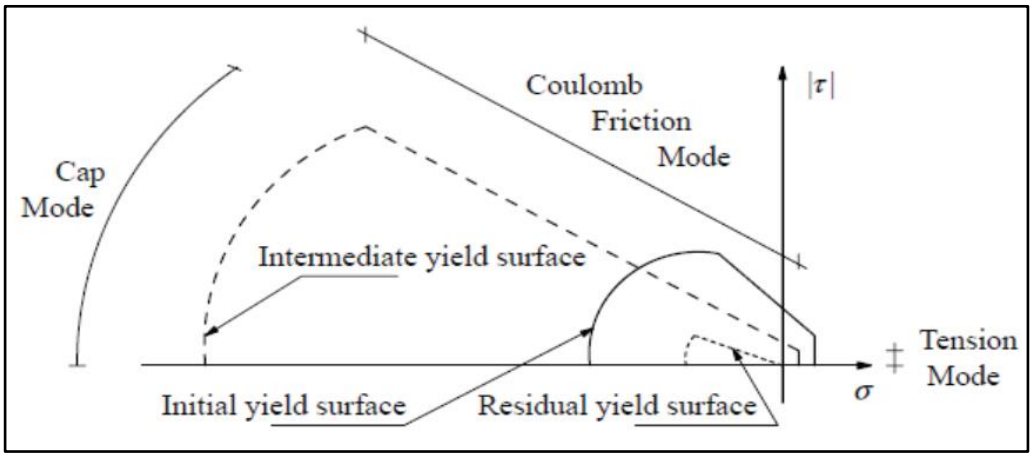

Figure 2.54 interface cap model [66]

These three modes are governed by different criteria: a criterion of maximum normal stress (Rankine) in traction (cut-off), a linear Mohr-Coulomb criterion in shear and a compression criterion of type " cap model "to close the set. Boundary surfaces evolve with softening laws. In addition, potential cracks in bricks are considered by the Rankine criterion. Indeed, in this approach, the interface elements are not only between the bricks, where they represent mortar joints, but they also appear within the bricks, in the middle (Figure 2.55). According to [63], the cracking in the bricks must be taken into account otherwise the simulations lead to overestimates of the wall strengths which also have a stiffness greater than that observed experimentally. The brick / brick interface is characterized by tensile strength and softening behavior in the post-peak phase.

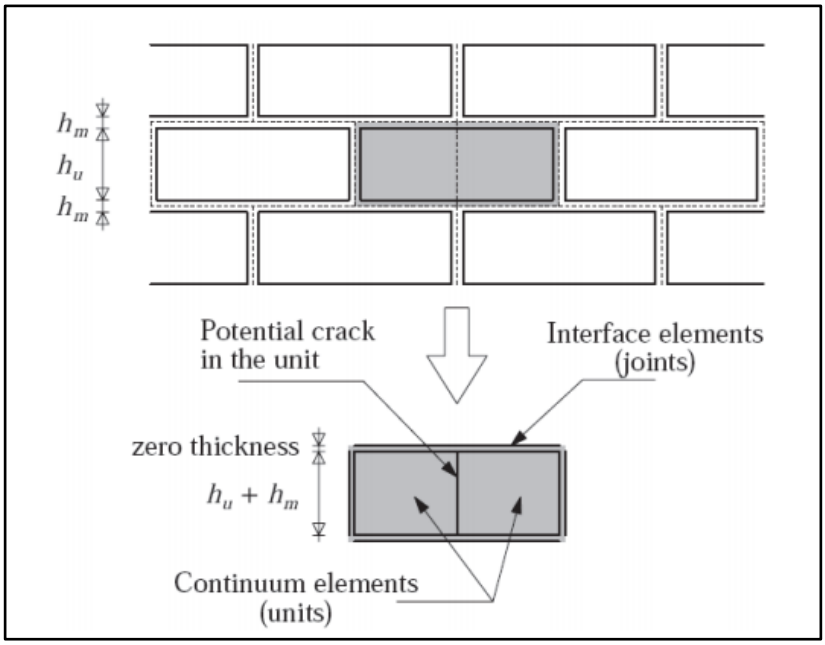

Figure 2.55 Suggested modeling strategy. Units (u), which are expanded in both directions by the mortar thickness, are modeled with continuum elements. Mortar joints (m) and potential cracks in the units are modeled with zero-thickness interface elements. [66]

Lourenço validated this model to analyses solid and hollow masonry shear-walls to predicted the experimental collapse load by a comparison with experimental results available in the literature (Raijmakers and Vermeltfoort)[88]. This model is very adequate for the prediction of the zones of rupture and maximum deformation (see Figure 2.56). shows a very good agreement and provides additional knowledge about the behaviour of such structures. The model is able to reproduce the complete path of the structures until total degradation without numerical difficulties.

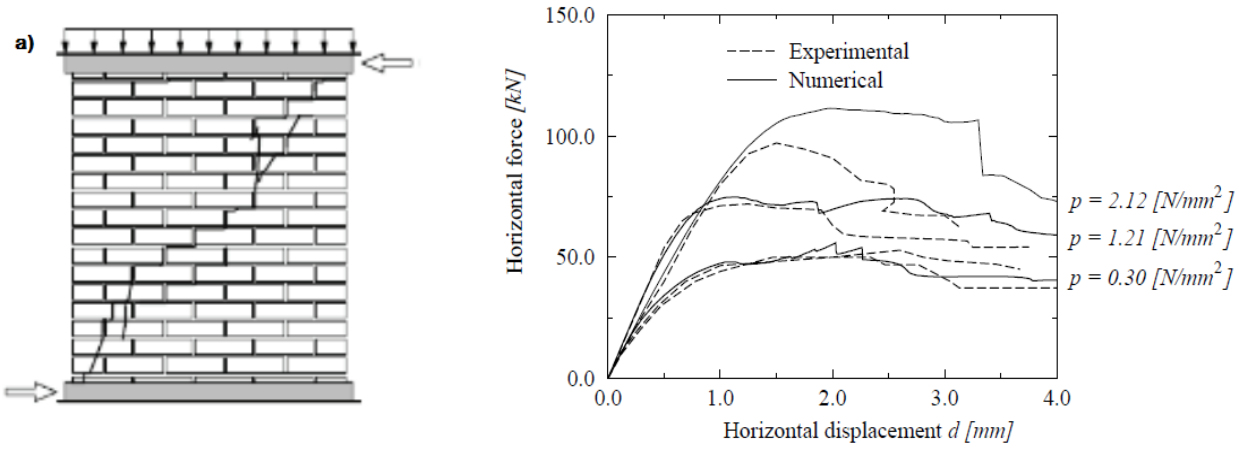

Figure 2.56 Validation of the model: a) loading configuration, b) Load - displacement curves [66]

2.7.3.6 Simplified Micro-modelling of Giambanco

The author proposed a model shares most of the characteristics of the Lourenço model, except that it does not consider the mode of rupture by compression or the crashing of the bricks. Its contribution lies in the introduction of an "adherent/ friction interface" model which makes it possible to account for the influences of the roughness of the fracture surface on post-peak behavior. This roughness is introduced into the model by an angle $\emptyset$ which is added to the friction angle in the threshold shear function.

$$f(\tau, \alpha) = |\tau| - \sigma \tan(\emptyset + \alpha) \leq 0 \qquad (2.12)$$

This angle depends on the configuration of the contact surface and on the loss of cohesion following sliding.

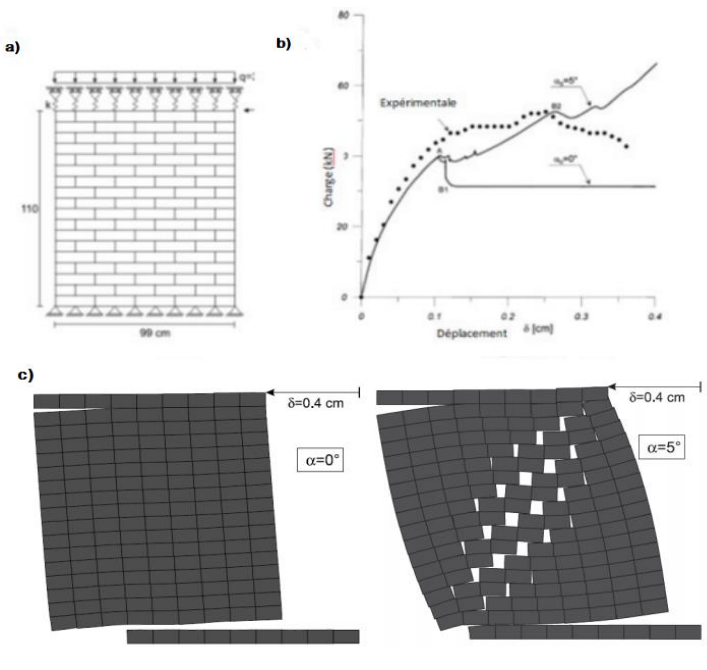

Figure 2.57 Numerical example at structure scale: a) specimen and loadings; b) stress-lateral displacement curve; c) failure modes in two cases with and without roughness. [92]

Figure 2.57 present the numerical failure modes into cases with and without roughness. It appears that taking roughness into account strongly influences the failure mode and the post-peak behavior of the wall considered. In the absence of roughness, the model reproduces a located rupture at the bottom and at the top of the wall with a decrease in load after the peak, which is not in agreement with the experimental results. On the other hand, the addition of an asperities makes it possible to pass to a rupture according to the diagonal of the wall with a positive hardening in the global behavior law, in this case, the model showed good agreement with experimental results [89].

K. F. Abdulla and al [90] proposed a model to simulate the behavior of masonry walls using a simplified micro-model approach. It work aims to see the response of the masonry under loading in the plan: The data and the results of the masonry shear walls tested experimentally undertaken and reported in [28] was adopted to validate the numerical model under loading in the plan(show Figure 2.58).

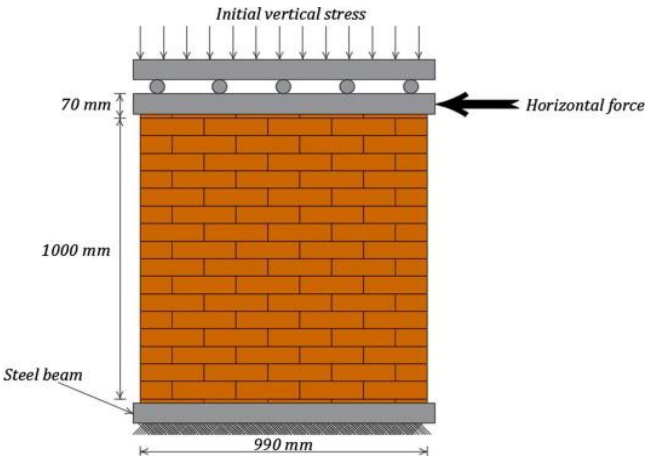

Figure 2.58 experimental testing setup to assess the shear strength of a masonry wall [93].

The numerical results show a good agreement with the experimental results in terms of load-displacement relationships. In addition, the failure modes obtained from numerically were consistent with this experimentally (Figure 2.59).

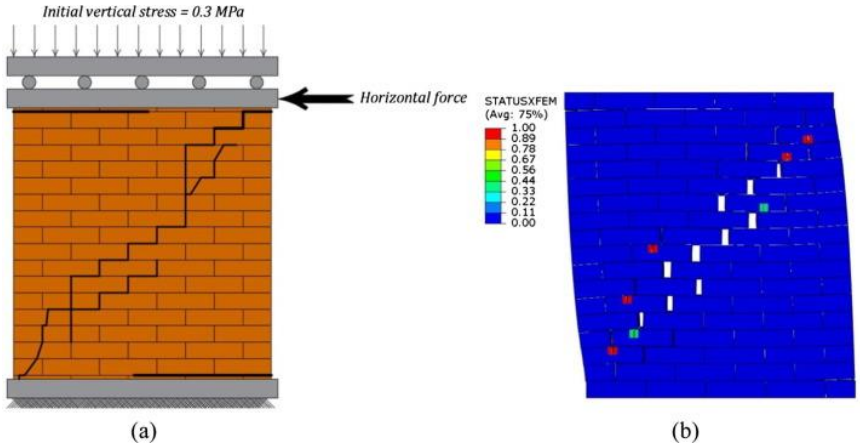

Figure 2.59 Comparaison of Failure modes: (a) experimental rupture models ; (b) numerical rupture models (facteur d'échelle = 20)[93].

Lourenco [91] proposed a polygonal particle-based model approach to represent the microstructure of units and mortars for the analysis of masonry assemblages under compression. The masonry components are composed by linear elastic particles of polygonal shape separated by non-liner interface elements. In this case, inelastic phenomena were able to occur in the interfaces while the process of fracturing consists of progressive bond-breakage. Typical numerical results together with experimental results are shown in Figure 2.60. Results are also compared with a continuum model (CM). The experimental results seem to be over-estimated with the continuum model, although a much better agreement observed with the experimental strength and peak strain with the particle model (PM).

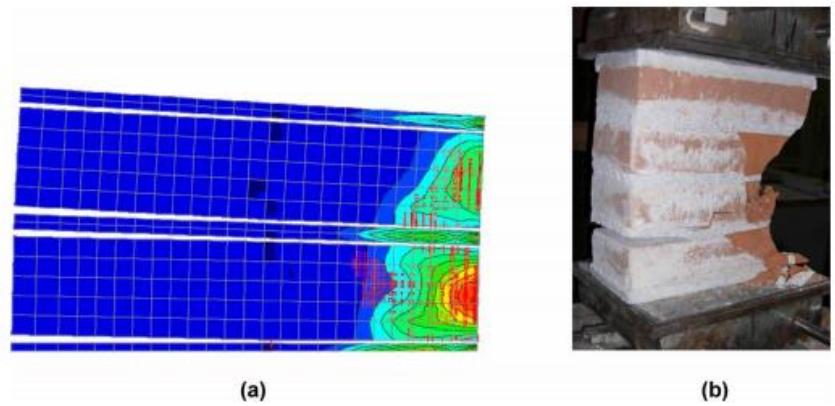

Figure 2.60 Comparison between experimental and FEM failure patterns: (a) computational crack pattern;(b) Experimental crack pattern[94]

2.7.4 Other reviewed proposals

There are many other proposals to represent the nonlinear structural behavior of masonry. These proposals require different parameters as input, considering more or less detail in the information related to geometry, quality of brick, mortar or the contact zone between them. They also have different ways to define the models, considering finite elements, non-linear springs, especially defined elements, etc. Moreover, they consider the non-linearity of the model in a variety of forms, distributed in the elements, concentrated in some of them, etc. These proposals include different types of modeling strategies and are oriented to different types of masonry. Some of these proposals are the model of (Chen and al [92]), the macro model for confined masonry walls of (Annecchiarico and al [93]),The micro-modeling model of (Drougkas and all [94]).this approach was investigated according to different geometrical conditions, including 2D models in plane stress and plane strain and 3D models. In addition, a limited digression in the modeling approach was made in order to investigate the compression of masonry using meso-models, consisting of detailed micro-models with perfect bond between the units and the mortar Certainly, the simplified micro model of [95].also there are many other proposals in literature considering other masonry types with different modeling strategies.

2.7.5 Modelling of FRP strengthened Masonry

Luccioni.B and V. Rougier [96, 97] proposed two different approaches to analyze the in-plane mechanical behaviour of unreinforced and carbon fibre reinforced polymer (CFRP) retrofitted masonry walls. A diagonal compression test of unreinforced and CFRP reinforced are simulated with a micromodel in which bricks and mortar are separately modeled. An anisotropic plastic damage model was used to simulate the behaviour of bricks, mortar and CFRP reinforcement. In this way, the behaviour under monotonic and cyclic loads characterized by permanent deformations and stiffness degradation can be accurately reproduced. The interfaces between the different constituents are not explicitly modeled but are indirectly taken into account in the constitutive laws of the materials with a consequent reduction in computational cost. a reasonable agreement between experimental and numerical results was obtained showing that an equivalent homogeneous anisotropic damage model can be used to model actual masonry elements with a great save of computational cost. In both approaches, FRP reinforcement is simulated without explicitly modeling reinforcement elements but with a generalization of the classic mixture theory. In this way, FRP reinforced bricks or FRP reinforced mortar in the micro-approach or FRP reinforced masonry in the homogenized approach are considered as

composite materials made of bricks, mortar or masonry, and FRP composite respectively. The mixture theory was applied to these composites and the modified mixture theory was used for the FRP composite itself. The comparison of numerical and experimental results shows the models ability to simulate the in-plane behaviour of masonry elements retrofitted with CFRP (see Figure 2.61).

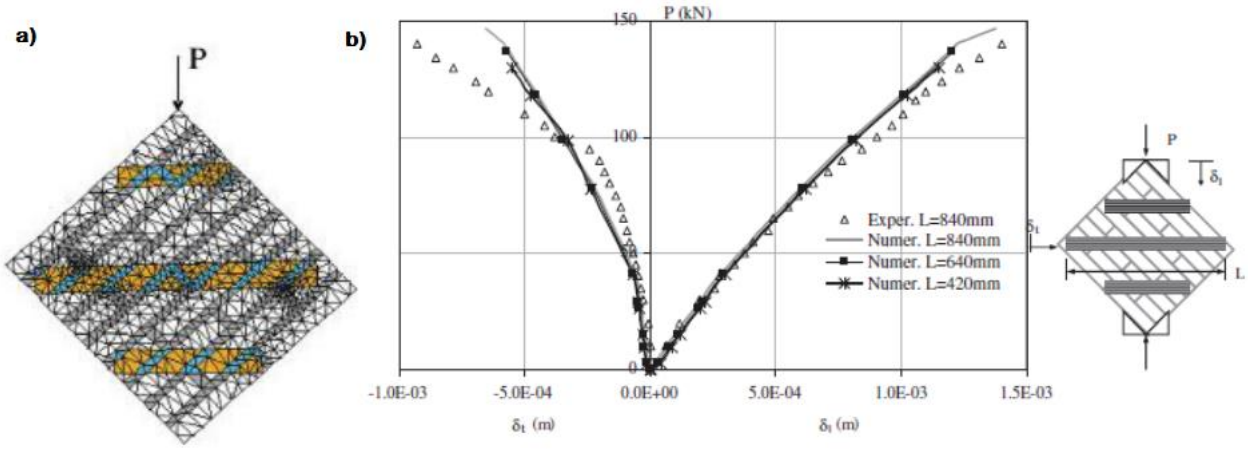

Figure 2.61 (a) Finite element model (b): comparison between numerical and experimental results of FRP reinforced walls in diagonal compression test. [99]

Kabir and Kalali [98] presented a finite element modeling approach to analysis the behaviour of unreinforced and FRP strengthened perforated brick shear walls under combined compression-shear loading. This modeling was done in 3D using ANSYS program. where the "concrete" damage model has been used with the failure surface proposed by William and Warnke which allows to simulate cracking in tension and crushing in compression. the FRP reinforcement modeled as an orthotropic elastic linear material that is perfectly connected to the masonry elements. effects of different strengthening configurations with FRP on the in-plane cyclic performance of brick walls with openings (e.g. door, window) having different aspect ratios and positions were investigated. The results of the numerical simulation were compared with the experimental results and the validity of the model was proved (see Figure 2.62).

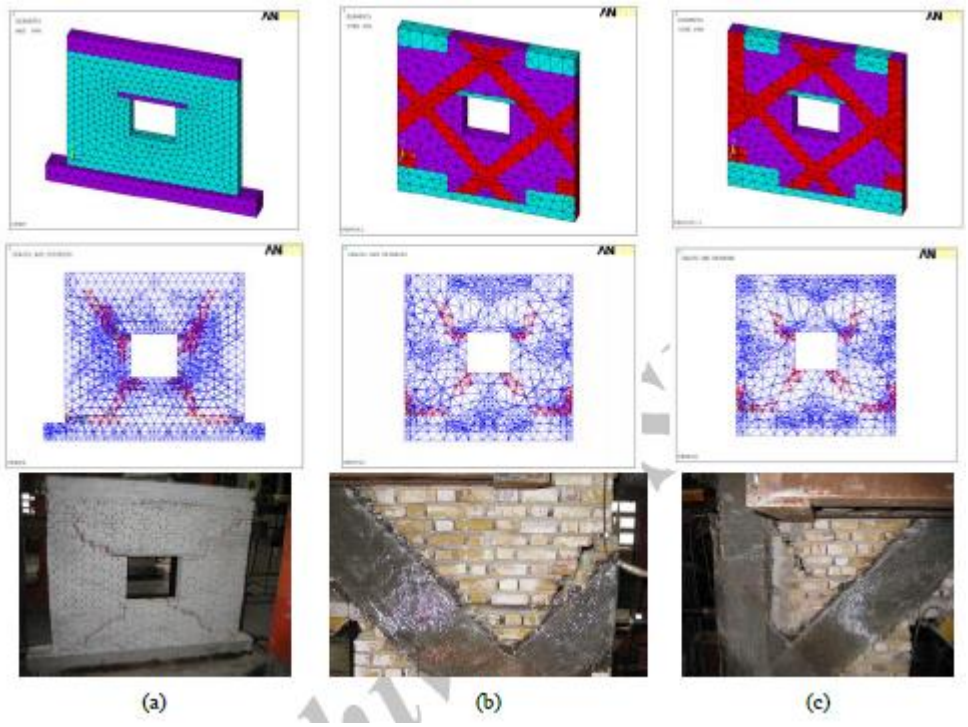

Figure 2.62 Finite element model and cracking pattern of the test walls in two cases of numerical and experimental: (a) URBW;(b)RBW-X-S1;(c)RBW-X-S2[101]

Gabor et al [99] presented three different finite element approaches developed with a commercial software for the analysis of unreinforced and FRP retrofitted hollow brick masonry walls subjected to in plane loading. A validation was performed in the case of panels submitted to diagonal compression test. The micro-modelling approach was used in this model considers the real configuration of the masonry panels (bricks, mortar, interface joint) and the composite reinforcement. This modelling was applied in both cases unreinforced and strengthened masonry panels. They modelled both the brick, units and the mortar joints separately, with continuum elements. the bricks as fully elastic and used an elastic plastic model in the mortar joint to represent the non-linear behaviour of the brick/mortar interface in shear. For the simplified model, considering the experimentally measured global mechanical parameters of the masonry panels, based on homogenisation theory, where bricks and mortar were replaced by an equivalent continuum, were used for the analysis of unreinforced masonry. They

concluded that the finite element modelling can be a useful tool for the design of FRP reinforcement. They did not include debonding of the FRP in their models, but this did not affect their results because debonding was not observed in the experimental tests that they used to verify their models. In this case FRP elements mechanically directly fixed to the masonry area (perfect bond). A good correlation between experimental results and numerical results using homogenisation models for unreinforced masonry was found. Since detailed models used for retrofitted masonry required a high computational cost. (see Figure 2.63)

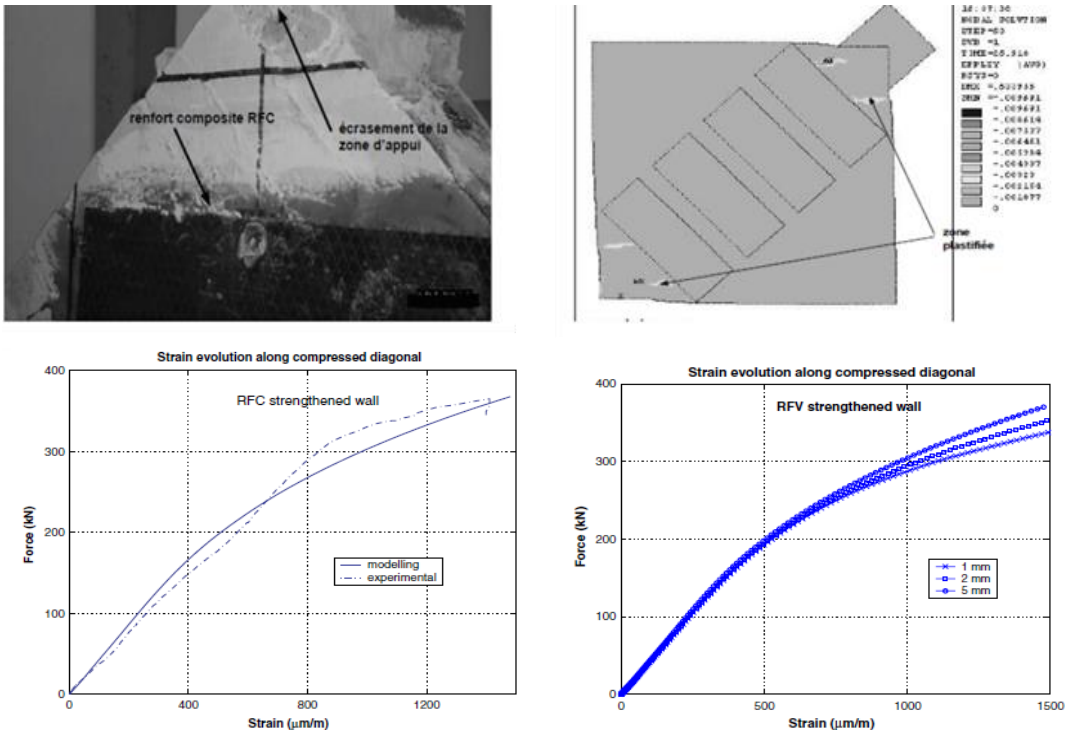

Figure 2.63 Confrontation between experimental and numerical results of unreinforced and FRP retrofitted masonry walls [44]

Grande et al [100] proposed two different suitable mechanical models able to model the behaviour of unreinforced and reinforced masonry structures. The first one was based on a micro-mechanical and multi-scale analysis combined with the use of the kinematic and static theorems of the limit analysis. FRP masonry interaction was simulated with a rigid-perfectly plastic constitutive relationship. The second approach was based on a macroscopic model. A smeared crack approach was used for masonry to accounting the damage and softening effect.

Furthermore, different modelling approaches and constitutive laws were adopted for the FRP-reinforcement taking into account the delamination phenomenon. FRP strips were modelled using truss elements directly connected perfectly to the corresponding nodes of the masonry panels. To account for debonding of the FRP from the masonry they treated the FRP truss elements as an elastic-brittle material. Both experimental failure loads and load–displacement curves were satisfactorily reproduced with all the adopted models (see Figure 2.64). However, the post-peak behavior was captured well only when brittle phenomena were taken into account. the simplified approach proposed to take into account the contribution of the reinforcement was capable to reproduce the delamination process of the FRP strengthening when the strips are not mechanically fixed to the masonry area, and the delamination failure started from the free edges of the strips.

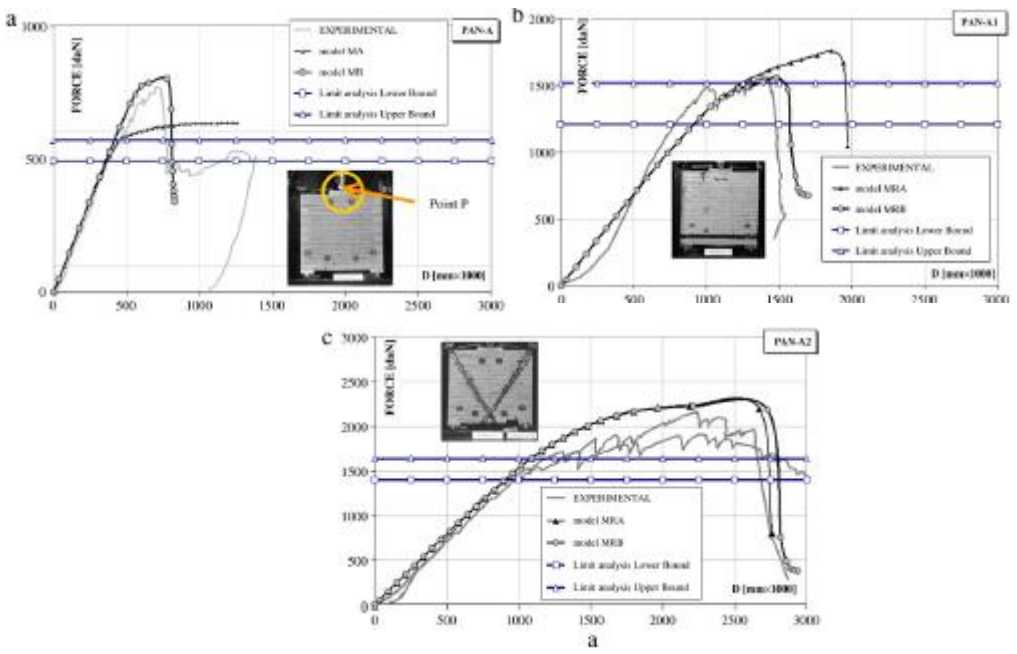

Figure 2.64 Confrontation between experimental and numerical results of unreinforced and FRP retrofitted masonry walls [102]

Zhang et al [101] presented a Finite Element (FE) model for the study of the behaviour of unreinforced and externally reinforced masonry walls under in-plane seismic loading. the model was validated against experimental tests, the element-based cohesive element with zero thickness was used for modeling the behaviour of mortar joints in masonry wall subjected to

both monotonic and cyclic loading. FRP strips are simulated by shell elements. a full adhesion between the surface of the masonry and the FRP was assumed, the FRP strips in the model are considered to be tied directly to the masonry. The concrete damage plasticity (CDP) model was selected to simulate the non-linear behaviour of the masonry units. The FRP was assumed to be orthotropic and was characterized by the behavior of lamina which was assumed to remain elastic. No Fracture and debonding failure of the FRP was considered in this research. they concluded that the models have the potential to be used in practice to predict damage progression in the unreinforced and FRP reinforced masonry walls under in-plane cyclic loading (see Figure 2.65), even it can predict the propagation of cracks under the BFRP reinforcement **.**

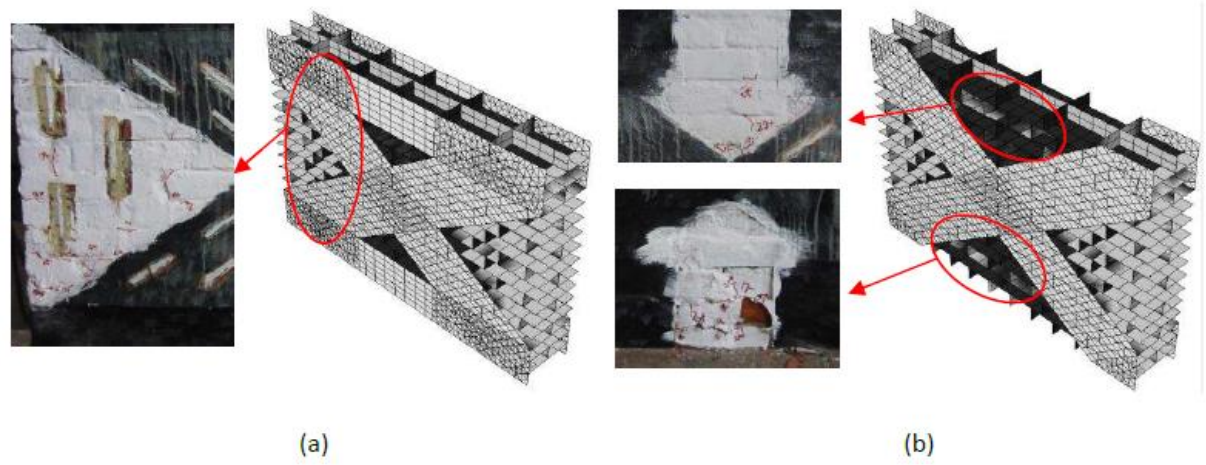

Figure 2.65 cracking pattern of the BFRP-reinforced masonry: (a) with horizontal reinforcement;(b) without horizontal reinforcement;(insert zoomed-in images from experiment for comparisons[103].

FRP reinforcement can be modeled with tension elements only (such as truss elements for thin reinforcements), or other continuum elements (such as typical quadrilateral elements) for fabric sheets. To model the debonding of the FRP from the masonry, a discontinuous element (such as an interface element) was modeled between them. Some authors have used finite element models and the discrete element method to predict the in-plane behavior of FRP strengthened masonry walls. Debonding of the FRP from the masonry was considered in only a few of these models[100, 102-104]. Both Zhuge [104] and Grande et al [104] verified their models with experiments where debonding was a failure mode. The model results did, however, highlight the importance of the bond strength between the FRP and the masonry. On the other hand, Van

Zijl and DeVries [105] did verify their model with experimental results, but in both the experiment and the model debonding was not observed.

2.8 Commercial Software

There are a number of general-purpose finite element and discrete element commercial software packages available for numerical modeling and analysis of different types of structures. These packages are capable of performing two or three dimensional nonlinear static or dynamic analyses. Most of the packages developed based on the finite element method (e.g. ANSYS, ABAQUS, ADINA, DIANA, LUSAS, NASTRAN) include different kinds of elements, solution strategies and material behavioral modes and hence, have been used for the analysis of brittle materials, such as masonry.

2.9 Conclusion

masonry walls are an important part of a structure. Masonry walls are distinguished by the construction materials as well as by the structure of the wall. These features require an analysis of the mechanical behavior on several scales, the objectives of which will be to observe the phenomena manifested at the level of the constituent materials (block, mortar) and their interactions at the level of the block / mortar interface. In addition, the complex and multiaxial state of stress will require an experimental analysis using different elementary tests (tension, compression, shear). The quantification of physical and mechanical quantities on the scale of the material (local), transposed to the real (global) scale are supposed to release information which will allow a complete analysis of a structural element of masonry under stresses in the plan and out of plan Consequently, the mechanical behavior of unreinforced masonry walls will be studied on two scales; locally on small test specimen made up of two or three blocks, and on a global scale on walls made up of several rows of block.

The purpose of carrying out tests on small test specimen is to determine mechanical parameters such as compressive, tensile and shear strength, elasticity modulus, coefficient of friction, shear modulus and energy shear failure. In the other hand, the tests carried out on unreinforced masonry walls make it possible to define failure modes corresponding to the loads (compression, shear, bending), as well as global parameters of resistance and rigidity of the walls.

This chapter is a review of existing knowledge relevant to URM masonry structures and FRP strengthened masonry walls.

The knowledge of masonry wall has been reviewed to create a solid background about the material properties and behaviour of masonry walls under in plane loading, which is needed to be used in Chapter 3 to conduct a well-designed experimental study.

After reviewing the existing numerical studies on the masonry structures, it is clearly that the choice of the method to choose depends on the level of information available, accuracy and simplicity desired. Detailed Micro-Modeling is the most accurate approach to simulate the real behavior of structural masonry as both the masonry units and the mortar are discretized and modeled with continuum elements while the unit/mortar interface is represented by discontinuous elements accounting for potential crack or slip planes. However, due to the large computational effort required by detailed micro-modeling, it is used mainly to simulate the behavior of small-scale masonry specimens and for research purposes. wherefore, this study adopts the detailed micro-modelling technique to perform a numeric simulation of the brick masonry specimen. This modeling can therefore only be envisaged if it is coupled with a large-scale experimental campaign for the finest possible characterization of the materials and their interactions. The micro-modelling approach was adopted in this work for the following reasons:

- it is able to reproduce crack patterns and the complete load displacement path of a masonry assemblage, and is therefore well suited for understanding experimental results
- it is considered more suitable (than the macro-model approach) for modelling FRP strengthened structures.

A numerical study onto the unreinforced and reinforced masonry assemblages is thus presented in the Chapter 4.

Chapter 3

Experimental study for analysis the behavior of FRP strengthened masonry assemblages under in-plane loading

3.1 Introduction

Masonry is an anisotropic material. Also considering only plane homogenous stress states (show Figure 3.1), it is characterized by many different failure modes and strengths [106],[107].This property strongly affects the response of masonry wall subjected to in-plane loading.

From the uniaxial compressive load tests on masonry panels whose bed joints are oriented at different angles to the direction of the applied load, the combined shear–compression behaviour of masonry have also been reported by some researchers ([108],[109]). The failure of masonry under uniaxial compression combined shear and compression has been extensively studied in the past by many researches [110]. These failures represent particular points on the general failure surface. the influence of the orientation of the applied stresses to the joints has also been noted in a number of investigations into shear wall behaviour[20].

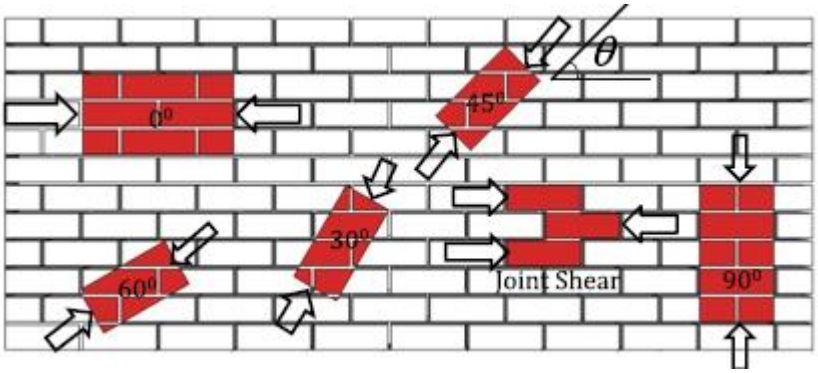

Figure 3.1 States of stress present in various regions of a masonry wall under in plane horizontal and vertical loads(adapted from Hamid et al)

There is significant potential for the application of FRP in the masonry industry, both in the construction and rehabilitation of older structures. The use of composite materials for the reinforcement of URM structures has been studied by several researchers. Many of these strengthening techniques including the use of fiber reinforced polymer (FRP) composites were used to reinforce masonry structures. FRP strips offer the possibility of application by gluing on the outside surface EB (externally bonded) or inserting inside the groove of element by the near-surface mounted (NSM)technique.

In the first this chapter presents an experimental characterization of unreinforced perforated brick masonry components. The focus is to obtain accurate mechanical properties of the unit, mortar and the interfacial properties of the unit-mortar joint that is necessary to produce a detailed micro-modelling of masonry structures. The experiments were carried out on brick masonry prisms under axial compression, unreinforced and reinforced shear triplet test, diagonal tension test for unreinforced and reinforced masonry wallettes externally bonded with carbon fiber-reinforced polymer (EB-CFRP) sheets, and masonry Wallettes Strengthened by NSM FRP Strips Subjected to Combined Forces.

3.2 Experimental program

3.2.1 Material properties test

3.2.1.1 Brick Units

The perforated brick used was manufactured by the brickyard of Setif. The brick is rectangular, based on clay (clay is often degreased with sand). The dimensions (Length x Width x Height) are given as follows: 220 x 105 x 55 mm^3 (show Figure 3.2). Five test series has been studied to obtain the average values of compressive strength and the elastic modulus (see Table *3.2* and Table 3.4). The tests were carried out using a hydraulic press according to the EN 771-1[111]. The average compressive stress-strain response of brick is shown in Figure 3.4. according to Vasconcelos and Lourenço [112]. the E_b is calculated by considering values between 30% and

60% of the maximum stress. Also, Poisson's ratio (ν_b) is calculated by plotting the lateral strains Vs longitudinal strains of each brick. The best line of fit is then plotted to determine the relationship between the lateral and longitudinal strain. E_b and ν_b were only determined for bricks loaded in bed face because the masonry specimens tested in section were constructed

with brick placed in bed face. The compressive strength as a function of the arrangement of the bricks is given in the

Table 3.*2*.

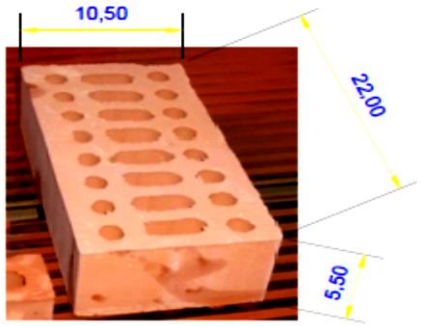

Figure 3.2 perforated bricks

Table 3.1 Physical characteristic of the perforated clay bricks.

No.	M(g)	V(cm^3)	ρ(g/cm^3)	ρ_{moy}(kg/m^3)
1	1589,2	877	1,81	1800
2	1592,4	880	1,81	
3	1588,7	895	1,78	

Table 3.2 Results of brick compression test

Direction 1	Direction 2	Direction 3
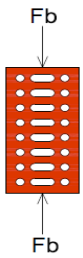	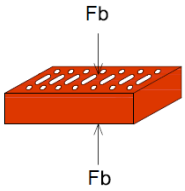	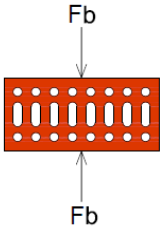
3.76(MPa)	14.53(MPa)	5.66(MPa)

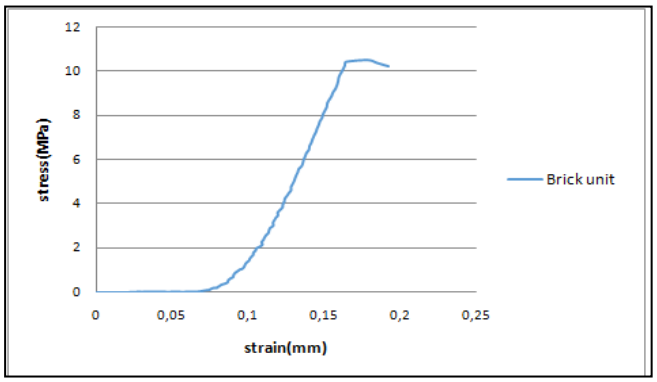

Figure 3.4 compressive stress-strain relationship of Brick

3.2.1.2 Mortar

The Cement-lime mortars are commonly adopted, because these mortars have the good properties of cement as well as lime mortars, that is, medium strength along with good water retentively, good workability and to some extent freedom from cracks. Therefore, this type of mortar has been adopted.

Two mixes consisting of cement: lime: sand proportions (1:1:3 and 1:1:5) were prepared using an electrical mixer by weight batching (see Figure 3.5). Water was added and the mixture was remixed to achieve a workable consistency. In order to measure the mechanical properties of these mortars, the prepared mixtures were cast into standard molds and then maintained in the standard curing (show Figure 3.6).

The mechanical properties of mortars were determined at the age of 3, 7, 14 and 28 days after de-molding. Flexural and compressive strength tests were measured according to EN1015-11[113]. By using the universal testing machine, the flexural strength has been tested on specimens in the shape of a prism ($40\times40\times160$ mm^3). Afterward, the two half-prisms obtained after breaking into two parts from the specimen during the flexural test were subjected to the uniaxial compressive test (results are shown in Table *3.3*). The compressive stress-strain relationship of these mortars is shown in Figure 3.7. Six specimens of each mix are tested to have the average value of the response. The secant modulus of elasticity is found to vary between 500 and 510 times of compressive strength of the mortar. The average values of the

brick compressive strength, the mortars compressive strength and secant modulus of elasticity are reported in Table 3.4.

Figure 3.5 The cement-lime-sand dosage for the preparation of mortar

Figure 3.6 Preparation and storage of prismatic test pieces of dimensions 40x40x160 mm

Table 3.3 Flexural and compressive strength tests for mortars

Type Mortar	NS	Mean value of fc, mortar [N/mm2]	COV [%]	Mean value of ft, mortar [N/mm2]	COV [%]	Young's modulus E(MPa)
Mortar A (1:1:3)	6	7.187	5	3.341	5	3639,24
Mortar B (1:1:5)		3.643		1.453		1821.87

Figure 3.7 Test Mortar and Compressive stress-strain response of different type of mortar

Table 3.4 Compressive strength and young modulus of mortar and brick

Material	Stress (MPa)	Young's modulus E(MPa)
Brick	10.53	9839.13
Mortar A (1:1:3)	7.187	3639,24
Mortar B (1:1:5)	3.643	1821.87

3.2.1.3 Composite Materials

In this study, two type of uni-directional carbon fiber (Sika Wrap carbon fiber fabric) were used, these CFRP reinforcing system are presented in Table 3.5 and Table 3.6

Table 3.5 Mechanical properties of the CFRP reinforcing system CFRP sheet (nominal values reported by the manufacturer

Property	Value
CFRP width	300 / 600 mm
CFRP length / roll	≥ 50 m
Poids	235 g/m² ± 10 g/m²
Thickness	0,129 mm (based on fiber content)
Density (Fiber)	1,82 g/cm³
E_{CFRP}	230 kN/mm²
Ft_{CFRP}	4000 N/mm²
Rupture strain	1,70%

Table 3.6 Mechanical properties of the reinforcing system CFRP strips

Property and unit	Value
Width CFRP (mm)	15
Thicknes (mm)	2.5
E_{CFRP} (MPa)	165 000
F_{tCFRP} (MPa)	3 100
Rupture strain (%)	1.7

3.2.2 Axial compression tests

3.2.2.1 Test setup and loading procedure

Three perforated bricks were laid in the horizontal face with mortar and then tested under axial compression according to the RILEM technical recommendation [114]. The triplet brick prisms were cast using one type of mortar (1:1:5) with a thickness of 10 mm and perforated brick. The specimens were tested after 28 days of curing using the 500 KN universal testing machine. Steel plates were placed at the top and the bottom of the specimen in order to ensure a similar distribution of load. The specimen was aligned carefully between the platens of the testing machine to avoid any accidental eccentricity for the concentrically loaded combinations. Furthermore, to reduce the platen restrain effect between loading steel plate and masonry, 5 mm plywood capping was placed on the top and bottom bed faces of the specimen. In order to get the complete stress-strain curve, the tests occurred under displacement control. The test as shown in Figure 3.8.

3.2.2.2 Test results

The result of compressive test of three test specimen and value of elastic modulus are given in Table 3.7.

Figure 3.8 test arrangement and crack pattern of masonry prism

The failure mode of the prisms was characterized by the development of tension cracks parallel to the axis loading; they began at the level of face shells of the top brick and propagated to the bottom units. This pattern of failure commencing with cracks beginning at the middle web has also been reported by other researchers[96].

Table 3.7 Experimental results of masonry prism under compression

Specimen No	Load at failure (KN)	Compressive strength (MPa)	Tensile Strength* (MPa)	Young's modulus E(MPa)
1	100	2.16	0.219	1392
2	103.026	2.23		
3	100.72	2.18		
Average value of compressive strength (MPa)	2.19			

*Tensile strength of masonry prism represents 10% of its measured compressive strength (Kyriakides et al., 2012).

3.2.3 Shear triplet externally bonded with carbon fiber-reinforced polymer (EB-CFRP) strips

3.2.3.1 Test setup and loading procedure

To assess the frictional parameters shear (initial strength and friction angle of the unit-mortar interface), four different compressive normal stress levels (0, 0.2, 0.6 and 1.0) MPa were adopted according to the BS EN1052-3[115]. For each pre-compression stress level, three specimens were tested. Each specimen consists of three perforated bricks of size (210 mm × 105 mm × 55 mm) bonded by mortar joints of a thickness of 10 mm. The specimens were centered in a vertical position in a hydraulic compression testing machine and the shearing load was gradually applied (see Figure 3.9.a). A test setup was fabricated for applicate a different pre-compressive normal stress levels at the shear triplet specimens.it consist of top and bottom steel plates connected by bolts at the end. The pre-compressive normal stress was applied first and remained constant through the test. To study the behavior of reinforced shear triplets, shear strength was calculated by finding the ratio between load and area parallel to the mortar joint as follows:

$$\tau = \frac{P_{max}}{2A} \tag{3.1}$$

P_{max}: the shear load at failure and A is the total cross-sectional contact area between two bricks. The failure behavior of the unit-mortar interface of masonry under shear can be characterized by the Coulomb friction criterion, for lower level of normal compressive stresses to the joint (2MPa).

$$\tau_u = c + \mu * \sigma_n \tag{3.2}$$

$\mu = tan\,\varphi$: frictional coefficient between the unit and the mortar

$C = \tau_0$: the shear strength under zero compression loads and represents the cohesion (bond shear stress).

$\sigma_n = \sigma_0$: the normal stress

3.2.3.2 Test results

- ***Unreinforced shear triplets***

One of the important results of the shear tests is the relationship between shear strength and compressive normal stress. The shear stress-strain response of the specimen triplet test shown in Figure 3.10. These curves represent the behavior of stress-shear deformation for four levels of compressive normal stresses applied initially. From this figure, it is noticed that the value of maximum vertical load (shearing force) increases with increasing of compressive normal stress. Figure 3.11 shows the relationship between the shear strength and the normal stress for all series of specimens. The results give almost a linear relationship between shear and normal stresses (σ-τ) which was represented by the linear relationships:

$$\tau = 1.04 * \sigma + 0.435 \quad (3.3)$$

According to this formulation, the value of cohesion (c) equals 0.435 MPa and the friction coefficient (μ) equals 1.04. Similar results of Paulay and Priestley [116] proposed an average cohesion value equal to 3% of the compressive strength, and value of 0.3-1.2 for the coefficient of friction of the masonry.

During testing under pure shear loading, cracks began to develop along the bed joint after the shearing strain reached 0.012. The masonry walls exhibited failure brick and mortar joint began to slide at very low displacements, as shown in Figure 3.9.c. This may be attributed to the lack of frictional resistance due to the absence of compressive stress normal to the bed joint during the shearing stage. Prakash, 2005, found a similar result.

Figure 3.9 shows differences in the failure mode obtained, albeit three failure modes were found during the shear tests, i.e.:

- Sliding at the brick-mortar interfaces (Figure 3.9.b).
- Sliding at the brick-mortar interfaces accompanied by a diagonal shear crack at mortar joint (Figure 3.9.c).
- Shear crack at mortar joint accompanied by splitting cracks followed by brick crushing (Figure 3.9.d).

The most important characteristic that governs the behaviour of a brick masonry wall is the brick-mortar interface because it habitually acts as a plane of weakness. Two failure modes can occur in the brick-mortar interface: tensile failure (mode I) and shear failure (mode II).

Figure 3.12 shows that the fracture energy (mode II) increased linearly with the confining stress to give the following relationship G_{II}^{f}= 0.134X+0.128, so the value of G_{II}^{f} was 0.1 N/mm at zero

confining stress; this agrees with the value obtained by Zinjl (2004). Moreover, for brick masonry, Vander Pluijm,1993[37] found that the fracture energy (Mode II) varied between 0.01 and 0.25 N/mm when the initial cohesion ranged from 0.1 to 1.8 N/mm.

(a) test setup

(b) sliding along bed joint and diagonal shear

(c) sliding a long bed joint

(d) Diagonal shear crack at mortar on the left and the right side

Figure 3.9 test arrangement and failure mode of brick triplet

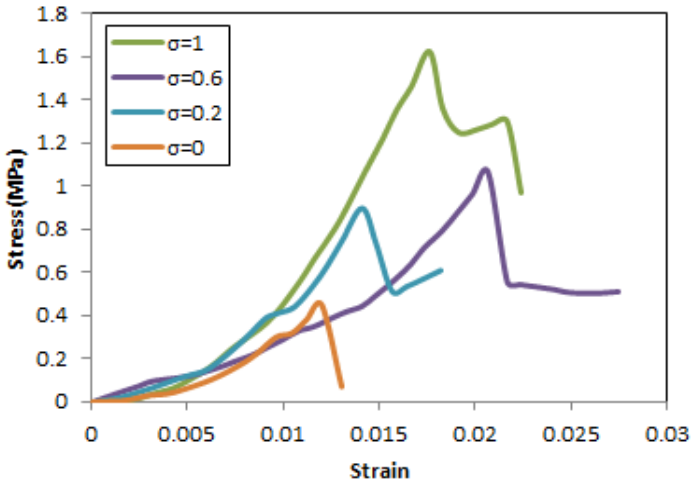

Figure 3.10 Stress-strain curves for various pre-compression

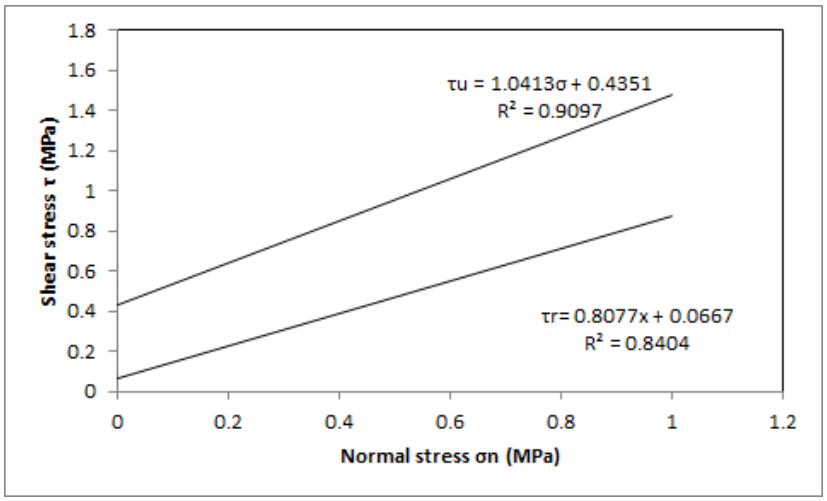

Figure 3.11 maximum shear stress versus normal stress for shear triplet test

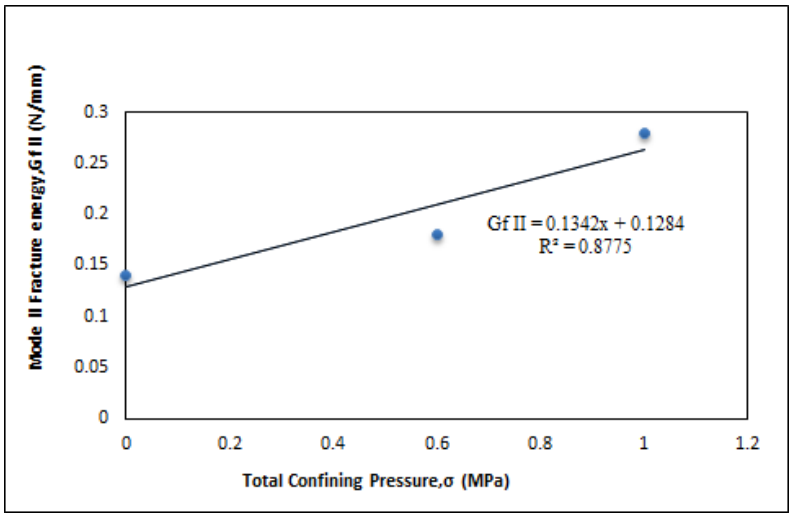

Figure 3.12 Evolution Mode II fracture energy as a function of normal compressive stress

Table 3.8 Ultimate shear strength of unreinforced triplets under different values of compression stresses

Specimens	Size(lxbxh)(mm)	Horizontal stress σn (N/mm2)	Failure load (KN)	Ultimate Shear srength τ (MPa)
ST1	220x55x105	0 N/mm2	10.17	0.44
ST2		0.4 N/mm2	20.8	0.9
ST3		0.8N/mm2	24.49	1.06
ST4		1 N/mm2	37.42	1.62

- ***CFRP reinforced shear triplets***

In the same manner, the reinforced shear triplet was subjected to pure shear loading. The test results of reinforced specimens are shown in Table 3.9. This table illustrates the effects of CFRP on masonry walls behavior in terms of shear strength. These specimens were given symbols to indicate the configuration of CFRP strengthening. (ST) refers to the control triplet specimen, (SRV) denotes a masonry wall specimen with vertical FRP, (SRX) indicates an X pattern of FRP reinforcement applied to one side of the masonry wall specimen, and (SR2X) indicates the specimen reinforced with FRP on two sides. The table indicates that all the reinforced specimens revealed a significant improvement in ductility compared to the corresponding control specimen. Similar results were also reported in the literature by Saghafi et al [117]

The curves in Figure 3.14 reveal remarkable differences in the ultimate shear stress when maximum stress was reached. The reinforced specimen, unlike the corresponding control specimen, became softer and began to slide at the brick-mortar interface. The results obtained from these investigations are was clear that the reinforcement with CFRP strips parallel to the joint (vertical) improved the shear strength by almost13.6% whereas CFRP reinforcement on both sides in an X pattern increased the strength by almost 150 %; ductile behaviour was also obtained and the deformation capacity of the specimens increased.

The specimen reinforced (SRV) by two CFRP strips extended along the mortar joint. Figure 3.13 showed a brittle failure with a sudden loss of strength while the specimen noted (SRX) reinforced using diagonal CFRP strips on one side revealed less brittle failure mode with larger deformation. The specimen reinforced using horizontal CFRP as shown in Figure 3.13 failed by sliding at the interface between brick and mortar and shear cracks along the mortar joint. The specimen reinforced with diagonal CFRP strips on both sides was more ductile than the

control specimen, but it failed due to shear cracks along the mortar. The CFRP strips also deboned when this specimen failed completely (Figure 3.13.b, c).

Figure 3.13 Different reinforcing patterns of the masonry walls by CFRP strips

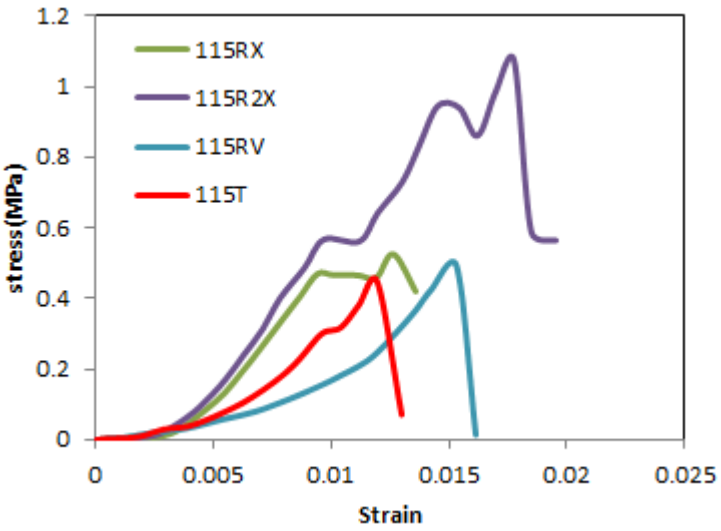

Figure 3.14 Stress-strain curve for unreinforced and reinforced triplets with different disposition of CFRP strips

Table 3.9 Ultimate shear strength and strain of unreinforced and reinforced shear triplets test

Specimens type	ultimate shear strength (MPa)	Maximum shear strain	Percentage of improvement %
ST	0.44	0.012	---
SRV	0.5	0.014	14
SRX	0.6	0.017	36
SR2X	1.1	0.019	150

3.2.4 Diagonal compression test of masonry wall reinforced with (EB-CFRP) sheets.

In this section, the influence of the type of mortar joint and location of the CFRP composites in the strengthened brick masonry wallette subjected to shear loads is evaluated by diagonal compression test.

3.2.4.1 Test setup and loading procedure

The test specimens were made according to the instructions given in RILEM technical recommendation [42]. A series of ten masonry wallettes were constructed from perforated brick with dimensions 220x105x55 mm and mortar joint with 10mm of thickness. Two types of mortar (type A, type B) were used in the construction of the panels having mix ratio of 1:1:3 and 1:1:5 of (Portland cement: hydrated lime: sand). The test involves subjecting a square section of masonry, with global dimensions 400x400x105mm^3, to a compressive load applied along the diagonal. the experimental setup for the diagonal compression test is presented in Figure 3.17.

The walls are placed and centered diagonally between the two plates of the press with the help of the metal shoes. These allow the transmission of the load to the wall in the vertical direction. The load is applied using the hydraulic cylinder which is placed below the load cell. The measurement of displacements is carried out using two displacement sensors which are installed on the diagonal of the wall. All data, forces and displacements, are automatically recorded by a data acquisition system, and given automatically by the system. The loading is applied by a machine of capacity 500KN. The loading speed is 5mm / min. The tests were performed under displacement control in order to obtain the complete stress-strain curve of the

panels. All tested wall panels were of similar dimensions in order to permit direct comparison of their failure loads (see Figure 3.15).

The test consists of testing four unreinforced walls (control panels noted MT) and six walls reinforced with CFRP composites in order to evaluate the reinforcement efficiency and the mode of rupture that each case reinforcement. The reinforced panels were strengthened by sika Warp carbon fiber CFRP composites of 50 mm wide. The FRP reinforcement was glued, using two-part epoxy adhesive. Three configurations of the retrofit system were investigated. The reinforcement schemes (MI, MH,MX) used for the strengthening of wall panels are summarized in Figure 3.16.

The shear strength is calculated according to the state of stress in the center of the wall; isotropic or anisotropic. The calculation of the shear stress τ_{dt} is made according to ASTM 519 – 02 [33]. considering a state of isotropic stress in the center of the wall.

$$\tau_{dt} = \frac{P_{max}}{\sqrt{2} \times A} \quad (3.4)$$

The lateral surface A is subjected to a maximum load P_{max}. Area A is calculated with Equation (3.5)

by considering w width, h height and t wall thickness.

$$A = \frac{w+h}{2} \times t \quad (3.5)$$

The displacement ductility factor (μ) is defined as the ratio between the ultimate displacement to the yield displacement. Or:

$$\mu = \frac{\delta_u}{\delta_y} \quad (3.6)$$

Where,

δ_u = displacement at ultimate load

δ_y = displacement at the load causing yield condition

The shear modulus G is calculated in the zone of elastic stress $\Delta\tau_e$ with Equation (3.7)

$$G = \frac{\Delta\tau_e}{\Delta\gamma_e} \quad (3.7)$$

$\Delta\tau_e$ and $\Delta\gamma_e$represent stress and elastic strain, respectively.

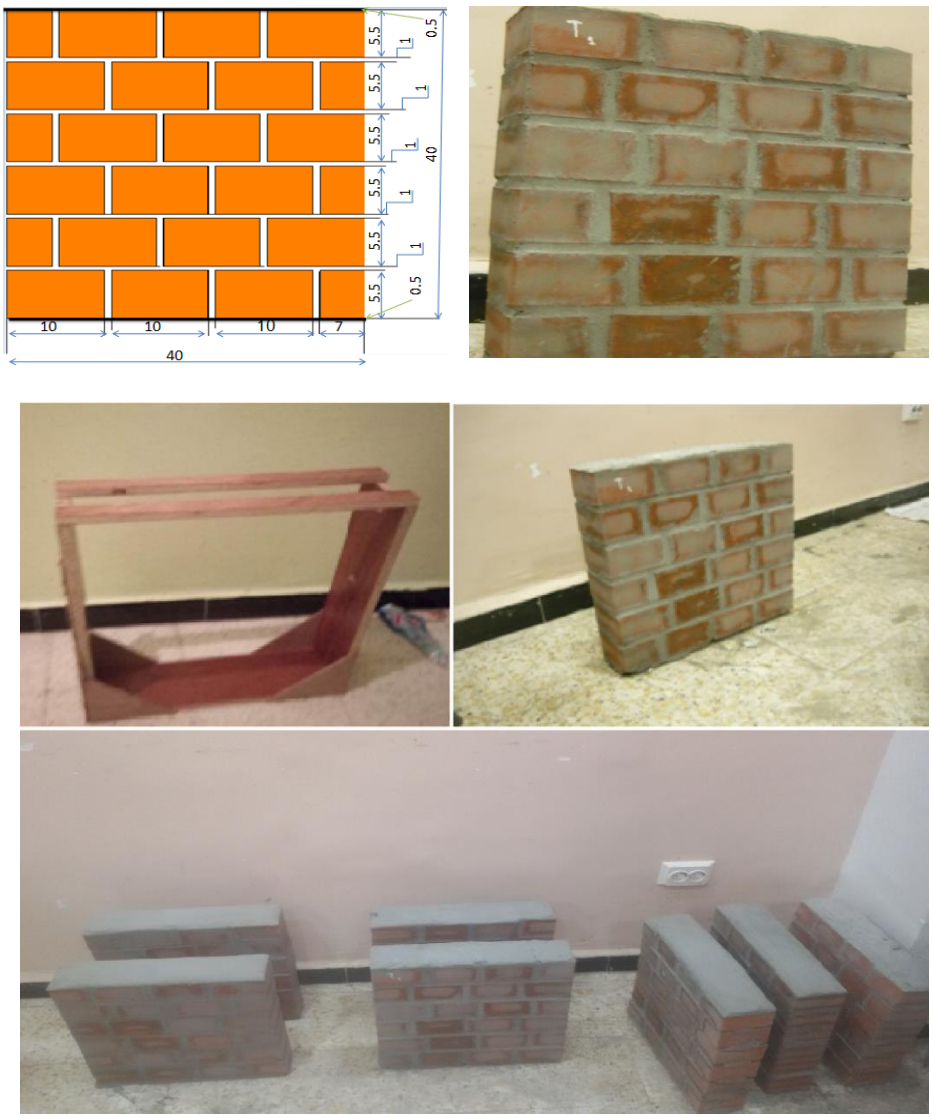

Figure 3.15 Specimen preparations of unreinforced masonry panels

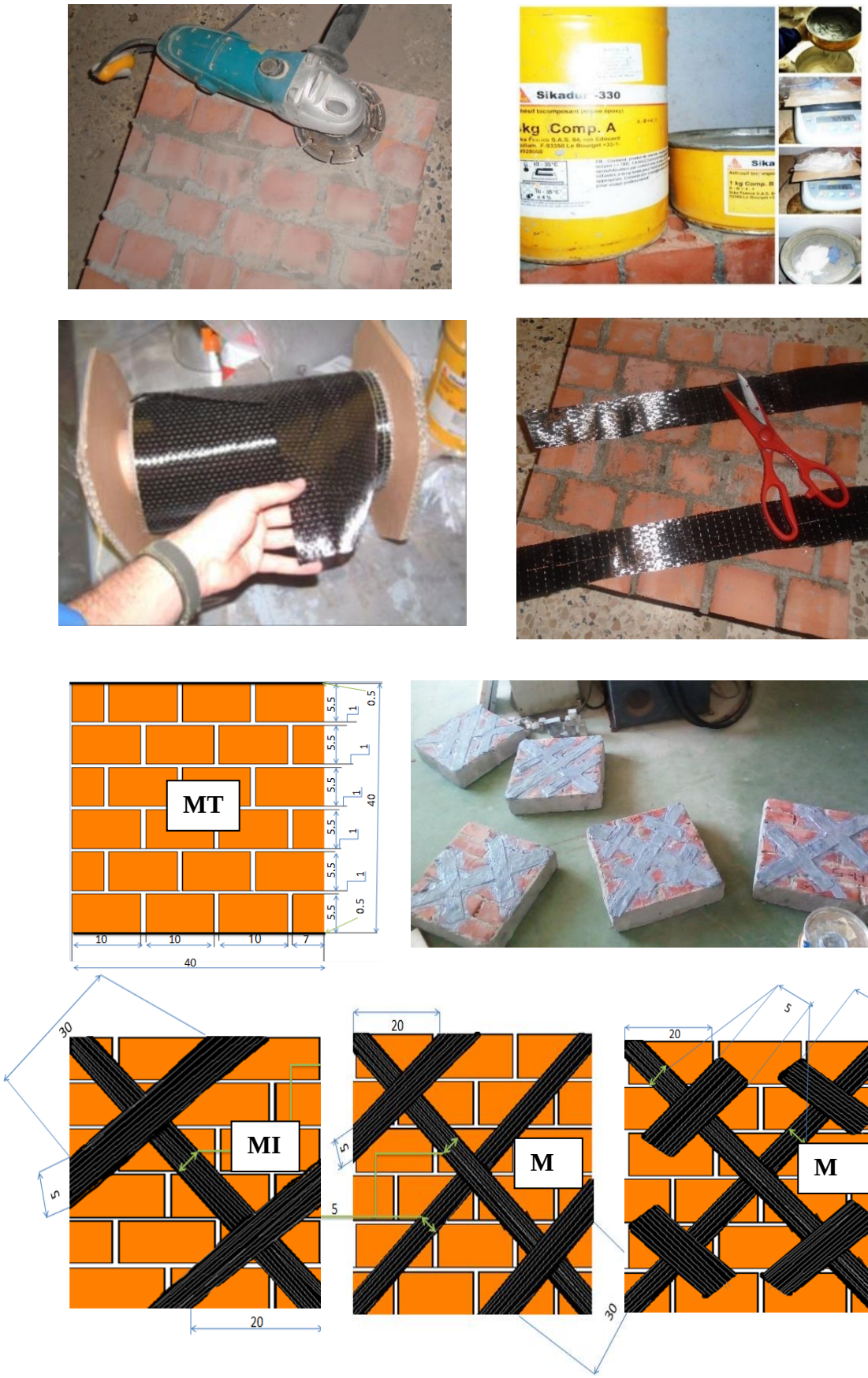

Figure 3.16 Specimen preparations and configuration of reinforcing for masonry panels

Figure 3.17 Experimental setup of unreinforced masonry panels tested in diagonal compression

3.2.4.2 Experimental results and discussion

- **Behavior of control walls**

In wall panels MTA and MTB cracking occurred predominately through the mortar joints in a diagonal, followed by a rapid decrease in load capacity. With load increasing, the wall exhibited a gradual increase in the width of predominately diagonally oriented crack, with further increase in load multiple cracks were observed in the panel before failure as shown in Figure 3.18.
The MTA control wall has a maximum shear strength of 0.5 MPa corresponding to a maximum force of 33.66 KN. In addition, the MTB wall has a breaking force of 35.06 kN, which produces in this wall a maximum shear stress of 0.56MPa (see

Table 3.10). The shear stress-strain response of the tested unreinforced wall panels (MTA and MTB) is summarized in Figure 3.20. For a comparison between the two responses, the wall panel constructed with mortar A failed at lower load compared to the wall panel type B, but with a slight difference. Both MTA and MTB wall panels exhibited an approximately linear shear stress-strain response until cracking, for the wall MTA followed by rapid degradation of

shear strength once cracking propagated, but for wall MTB followed by a slight increase in shear strength and deformation capacity before the rupture.

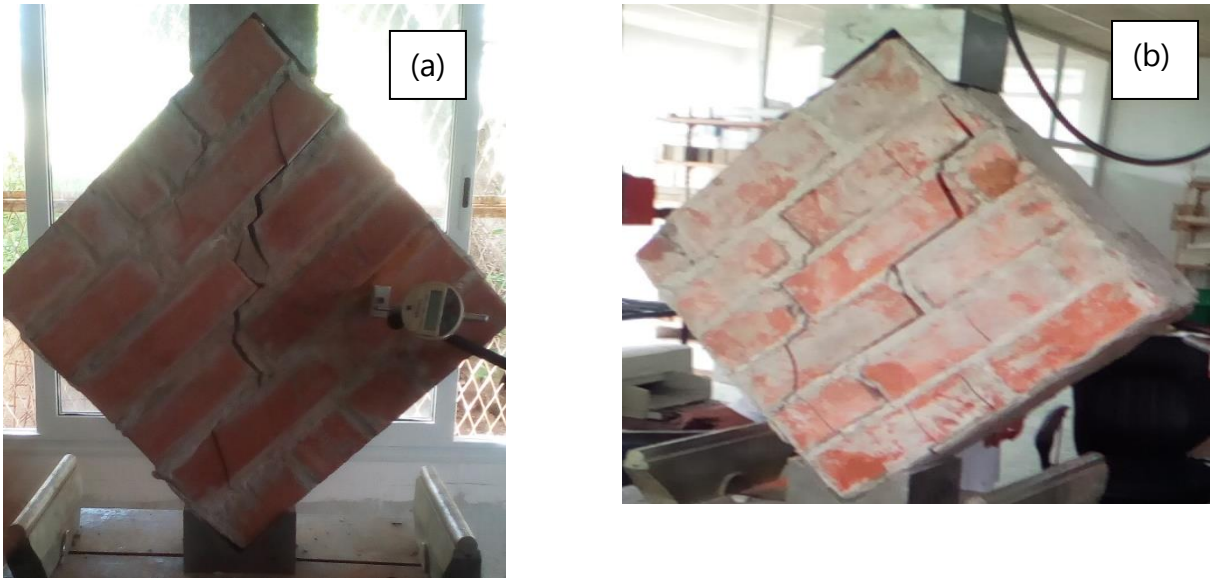

Figure 3.18 Failure modes of control masonry panels: (a) MTA, (b) MTB

- **Reinforced masonry panels**

In unreinforced walls, the tensile stress causes an appearance of cracks leading to a complete destruction. However, in the case of walls strengthened with CFRP composites, the tensile stresses are transferred to these strips results in a significant reduction of stress in the masonry wall.

Regarding the overall response of the walls, the results obtained revealed a significant increase in shear stress from 65% to 270% compared to unreinforced walls. Likewise, it was found that the improvement in ductility for strengthened wall panels type A ranged from 74% to 80% ,whereas for wall panels type B it ranged between 80% to 88% (see

Table 3.10).

The CFRP reinforced panel failed suddenly due to a cracking along the compressed diagonal at the ends of the composite strips (see Figure 3.19).

The MRX and MRH walls has a maximum force of 55.27 KN and 57.58KN respectively, which is a value of 1.82 MPa,1.85 MPa for shear strength. exhibits better shear behavior with increase of 200%. This reinforcement allowed to increase the ductility μ up to 88%. Thus, when the joint of the mortar cracks, there is a redistribution of the force towards the part of the reinforcement which is in the vicinity of the crack. Therefore, the arrangement of the reinforcing composites has a very important effect on the local behavior of the structure, due to the stress distribution and the deformation of the structure.

an application of CFRP composite on a 24% wall surface sufficient to increase wall ductility, and give almost the same results as that recorded when the fabric covers an area of 54 and 56%.

The first conclusion, which can be obtained from the experimental results, is that the Wall panels reinforced by CFRP composite technique presented more ductile behavior compared with the control wall panels for each type of mortar (see Figure 3.20).Moreover, the shear strength of reinforced wall panels is dependent on the mortar resistance.

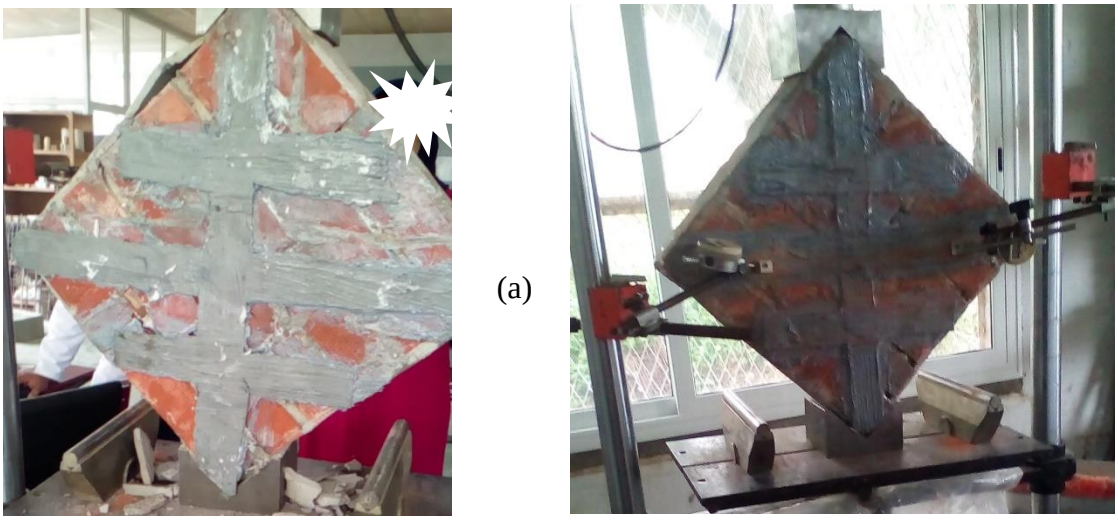

(a)

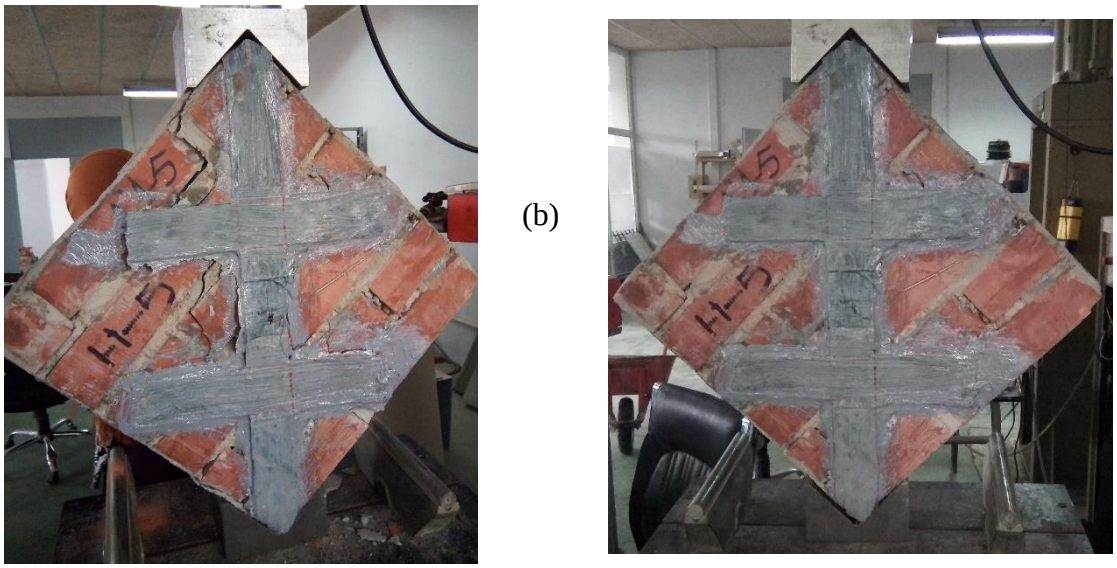

(b)

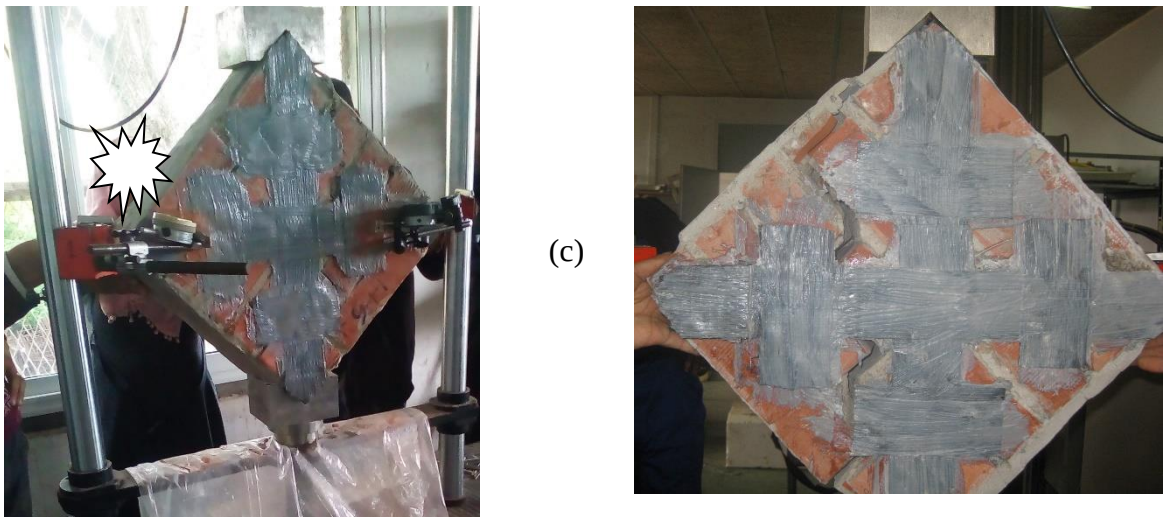

(c)

Figure 3.19 Failure modes of all strengthened masonry panels :(a) MHA and MHB, :(b) MIA and MIB, :(c) MXA and MXB

Table 3.10 ultimate shear strength and ductility factors for experimental tests of unreinforced and reinforced wall

panels	type	fibers ٪	F_{max}(KN)	τ(MPA)	G (MPa)	γ_e	γ_u	μ	(μ_u/μ_o)
MT	A		33.66	0.50	77	0.023	0.027	1.16	
	B		35.063	0.56	78	0.029	0.031	0.94	
MRH	A	54.68٪	54.958	1.76	92	0.056	0.111	2.02	73.98
	B	54.68٪	57.583	1.85	80	0.0334	0.058	1.74	85.06
MRX	A	54.06٪	50.815	1.61	117	0.027	0.057	2.1	80.87
	B	54.06٪	55.274	1.82	128	0.028	0.049	1.78	88.83
MRI	A	22.91٪	50.455	1.59	113	0.021	0.039	1.90	64.09
	B	22.91٪	45.607	1.45	103	0.021	0.036	1.80	80.00

γ_e : Elastic deformation

γ_u : Maximum deformation at ultimate load

μ : ductility factor

(μ_u/μ_o): improvement between unreinforced and reinforced masonry walls

fibers (٪): percentage occupation of the surface walls by carbon fiber band

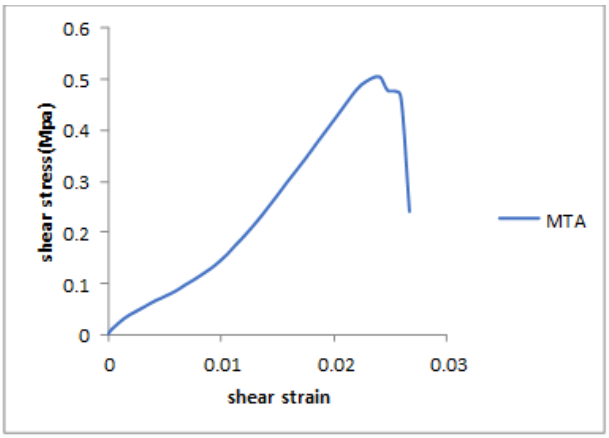
shear stress(Mpa)
shear strain
MTA

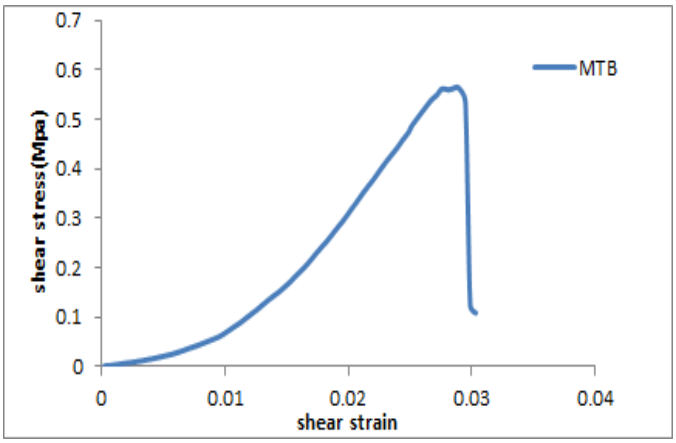
shear stress(Mpa)
shear strain
MTB

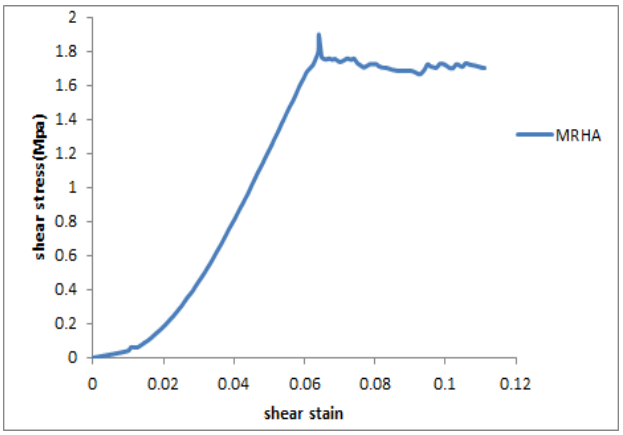
shear stress(Mpa)
shear stain
MRHA

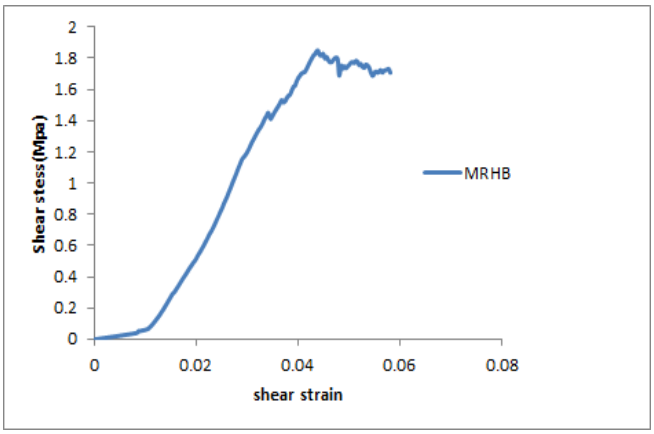
Shear stess(Mpa)
shear strain
MRHB

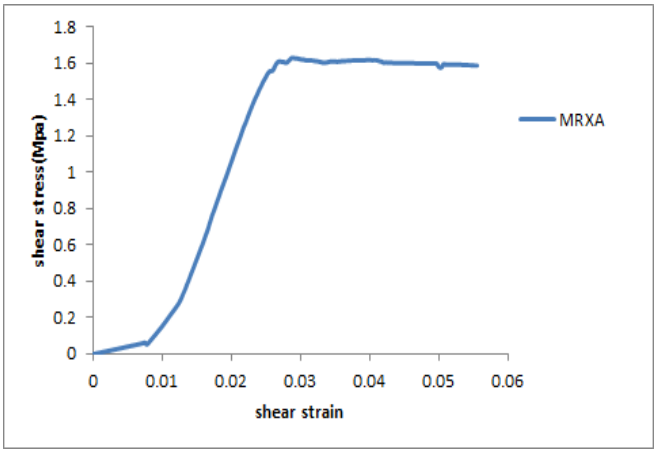
shear stress(Mpa)
shear strain
MRXA

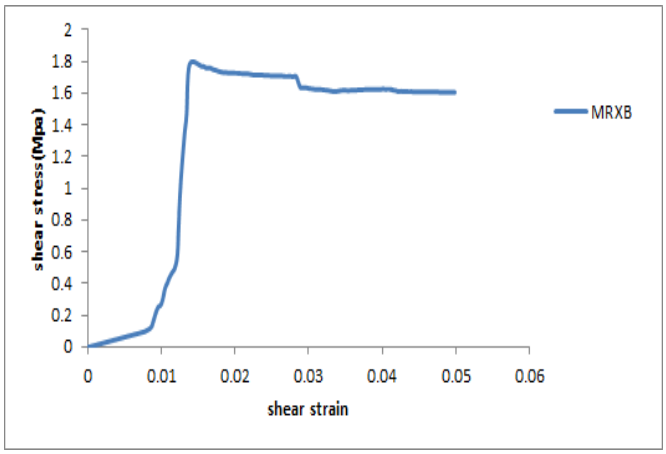
shear stress(Mpa)
shear strain
MRXB

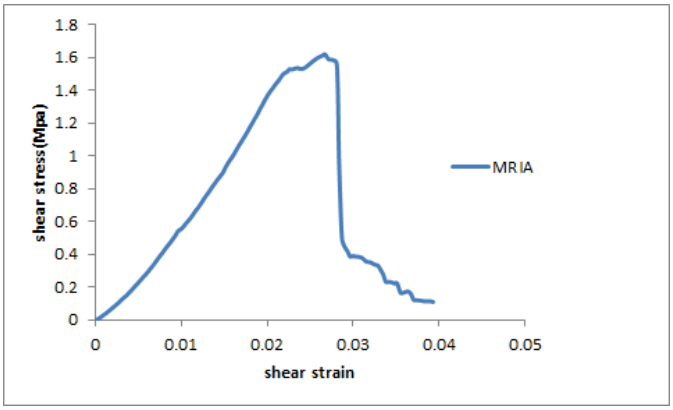

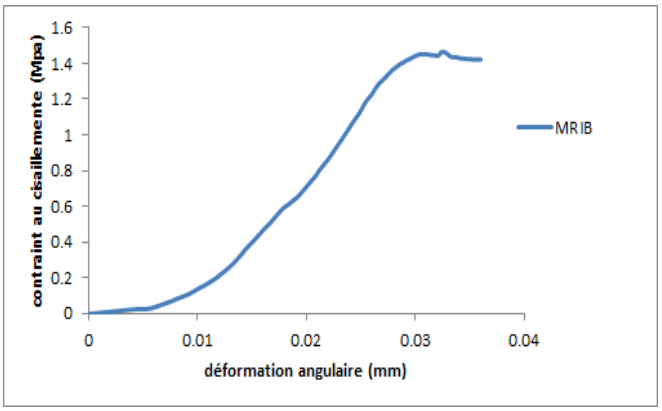

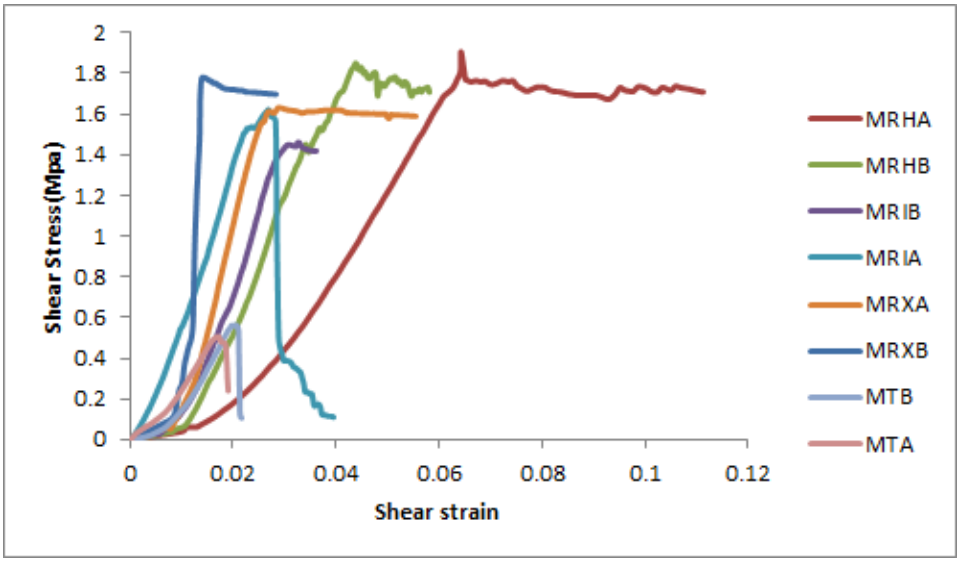

Figure 3.20 shear stress-strain relationship for unreinforced and reinforced masonry panels

3.2.5 Masonry Wallettes Strengthened by NSM FRP Strips Subjected to Combined Forces.

3.2.5.1 Experimental Testing Program

Twenty masonry panels with two bed joint orientations (45°,90°) were constructed and tested under vertical compression to generate a wide range of compression to shear ratios from one to infinity at each of the bed joints of the panels. The effect of the orientation of mortar joint, the efficiency of NSM-FRP technique and the position of the CFRP strips for improving the shear strength and ductility of the reinforced wall is discussed in this section.

The test specimens were made according to the instructions given in RILEM technical recommendation which illustrate the determination of masonry strength under compression RILEM. LUMB1[114]. The specimen, was a masonry panel made of perforated brick with dimensions 220x105x55 mm. Two types of mortar were used in the construction of the panels having mix ratio of 1:1:3 and 1:1:5 of (Portland cement: hydrated lime: sand). The specimens were tested under uniaxial loading with different orientations of the bed joints. The varied inclinations were 90° and 45° (see Figure 3.21.b). The tests were performed under displacement control in order to obtain the complete stress-strain curve of the panels (see Figure 3.21.a). All tested wall panels were of similar dimensions in order to permit direct comparison of their failure loads. The reinforced panels were strengthened by CFRP strips 15mm wide and 2.5mm thick. The FRP reinforcement was glued, using two-part epoxy adhesive, into rectangular grooves cut in the surface of the masonry with a circular saw. Full view of the fabrication of specimens and installation of CFRP is shown in Figure 3.21.d.

The masonry panels are categorized into two series, in the first series, the comportment of compression is defined on panel subjected to uniaxial compression perpendicular to bed joint θ=90° with two different types of mortar (A and B). In the second series of tests, the shear comportment of unstrengthened and strengthened masonry (θ=45°) has been studied with same types of mortar.

The experimental program consisted of a total of twenty tests, six unstrengthened masonry panels as control specimens (MCA, MCB) with θ=90° and (MTA, MTB) with θ=45°, and twelve strengthened panels. Four of the strengthened panels have only horizontal NSM CFRP strips (parallel to bed joints) with both types of mortar (MRHA, MRHB), and four have only vertical NSM CFRP strips (perpendicular to bed joints) with both types of mortar (MRVA, MRVB). The remaining four panels were reinforced with two vertical strips on one side of the panels and two horizontal strips on the other side MR2A and MR2B (see Figure 3.21.c). all detail of experimental tests is reported in Table 3.11.

The CFRP strip has an elastic modulus equal to approximately 165000 MPa, and a rupture strain equal to 1.7 %. The properties of composite materials of CFRP applied in the reinforcement of masonry wall panels are presented in Table 3.6.

(a) Test setup

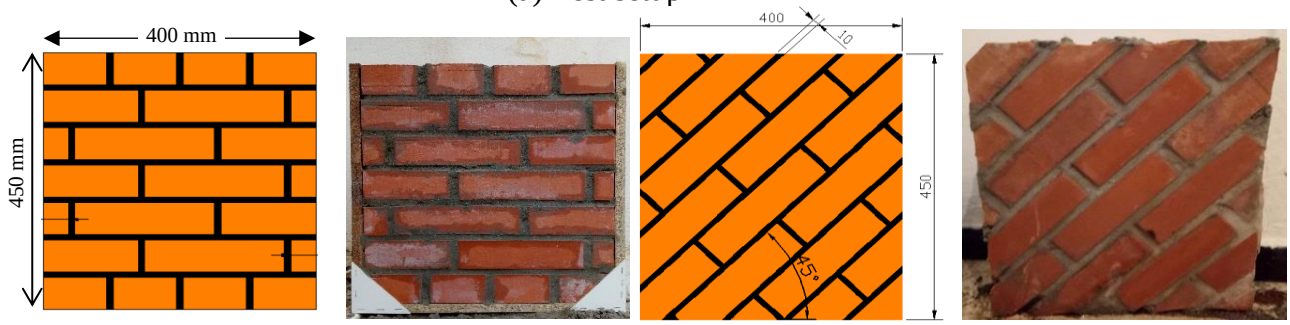

(b) Unreinforced masonry panel (θ=90° and θ=45°)

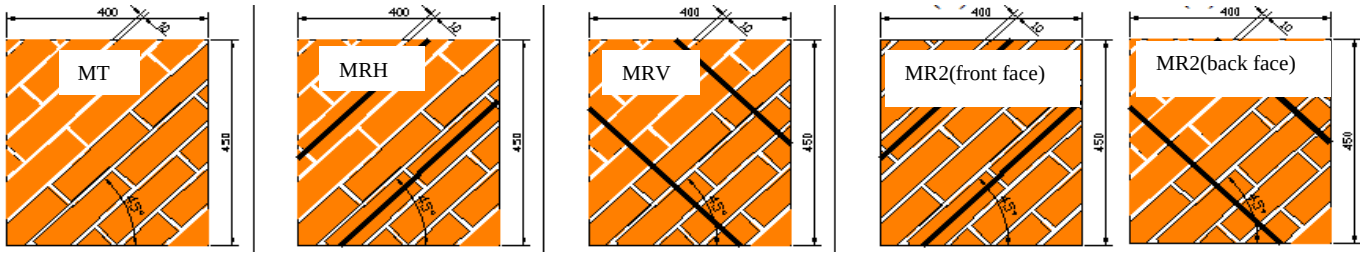

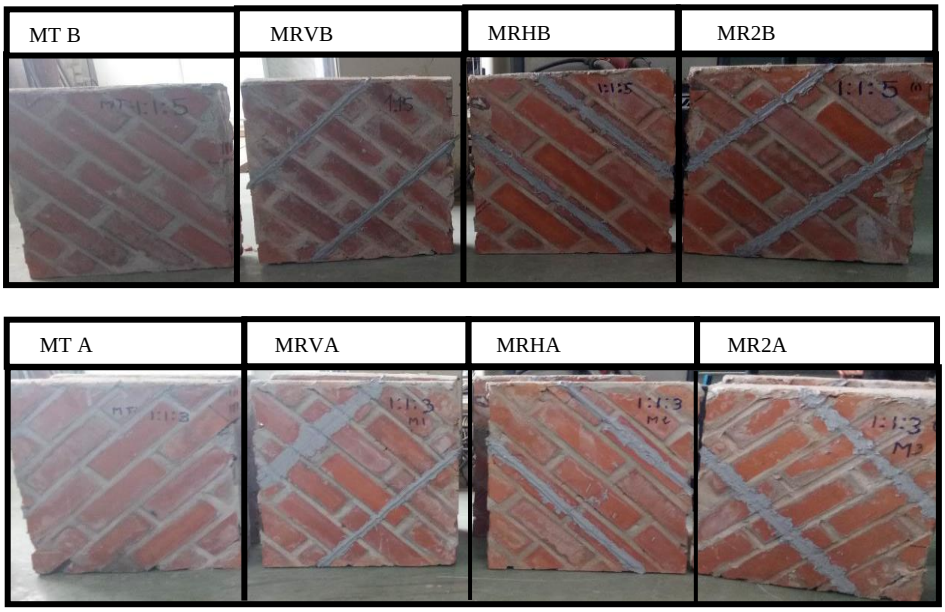

(c) Reinforced masonry panel (θ=45°)

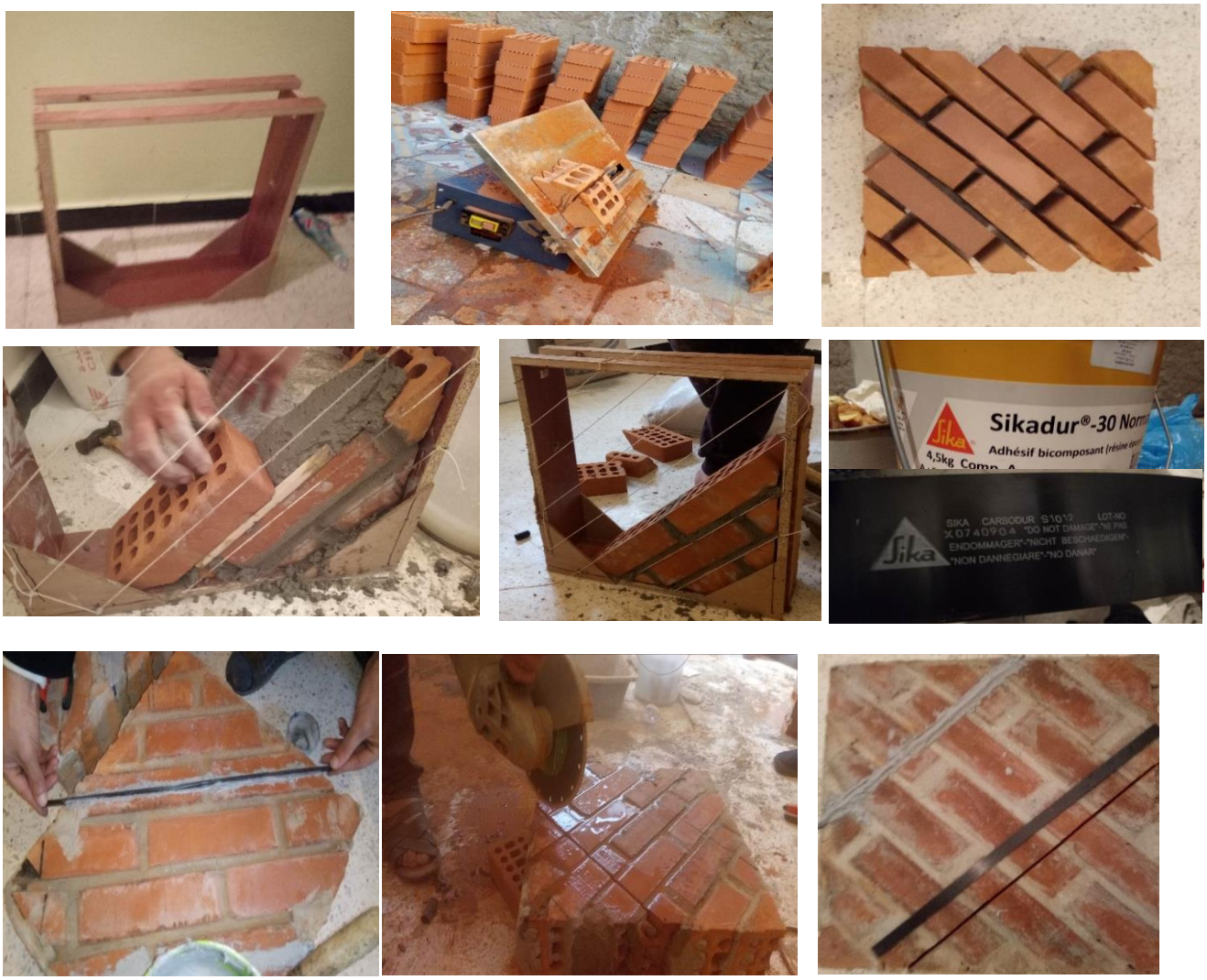

(d) fabrication of specimens and installation of CFRP

Figure 3.21 Test setup and reinforcement configuration of the masonry panels (θ=90° and θ=45°)

Table 3.11 walls dimensions and FRP retrofit details

Stage	Walls code	Walls Detail	Orientation (θ°)	Mortar Type	Dimensions walls (mm)	Joint thickness (mm)	Retrofit details
1	MCA MCB	Panels control	90°	A B	400*400*105	10	Without
2	MTA MTB	Panels control	45°	A B	400*400*105	10	without
3	MHA	Reinforced panels	45°	A	400*400*105	10	Two horizontals strips on one side
	MVA						Two verticals strips on one side
	MR2A						Two verticals strips on one side and two horizontals strips on the other side
4	MHB	Reinforced panels	45°	B	400*400*105	10	Two horizontals strips on one side
	MVB						Two vertical strips on one side
	MR2B						Two vertical strips on one side and two horizontals strips on the other side

3.2.5.2 Experimental results and discussion

- ***Unreinforced masonry panels subjected to uniaxial compression θ = 90° (MCA and MCB)***

1) Compressive strength of masonry panels:

Panels subjected to uniaxial compression perpendicular to bed joint (θ = 90°) failed due vertical cracking of the face shells of the masonry as shown in Figure 3.23 . The face-shell cracking occurred at a load close to 95% of the ultimate load. The vertical cracks on face-shell perpendicular to joints may be attributed to the different rates of lateral expansion of the units and mortar under compressive stresses, which causes tensile splitting of brick and perpendicular joints. The splitting cracks result in two face shells deform individually and become more

fragile .This failure pattern has been reported by other researchers such as Hamid and al [3]; Kaushik and al [18]. A decrease of mortar strength with increase in the proportion of sand in mortar is observed, whereas A slight increase was observed in the value of compressive strength for masonry panels MCB compared to masonry panels MCA (2.226MPa and 2.164 MPa respectively). This indicates the minor effect of mortar strength (3%) on the compressive strength of masonry wall. Therefore, the results confirm that the mortar compressive strength has only a slight influence on the masonry compressive strength.

The elastic modulus of the masonry wall is taken as the chord modulus of stress-strain curve obtained during a prism test between stress levels of 0.05 and 0.33 times σ_m. The values of Young's modulus of masonry panels obtained for each wall MC are summarized in Table 3.13.

The results show that the value of the modulus of linear deformation is low compared with the correlations between E and f_C provided by the codes: $E/f_c = 1000$ as in CSA 2004 [118] and $E/f_c = 850$ in EN 1052-1[119]. Most of the formulas that calculate the elastic modulus of the masonry give a value greater than the experimental value. This result was also found by Augenti and al, 2011[120] who found that the elastic modulus varies between 250-1100 times the compressive strength of masonry. They proposed an average value of Young's modulus equal to 550 times the compressive strength. The results obtained show that the measured values are closer to those found by internationally accepted documents and codes, e.g., FEMA306 [121], which also proposes $E_{,mac} \approx \approx 550\sigma_{c,\,mac}$, where, $\sigma_{c,\,mac}$ is the compressive strength of masonry units (see Table 3.12).

Venkatarama Reddy and Uday Vyas [122] studied the influence of bond strength on stress-strain characteristics of masonry using soil-cement blocks and cement-lime mortar. These studies show that when the masonry unit is stiffer than that of mortar (E_{block}/E_{mortar} ratio greater than one) the masonry compressive strength is not sensitive to bond strength variation and the modulus decreases with increase in bond strength. In addition, the modulus of masonry is less than that of the block and the mortar when E_{unit}/E_{mortar} ratio is less than one. However, the results of the present study indicated that the modulus of masonry is less than that of the block and the mortar although., for E_{unit}/E_{mortar} ratio greater than one (see Table 3.13).

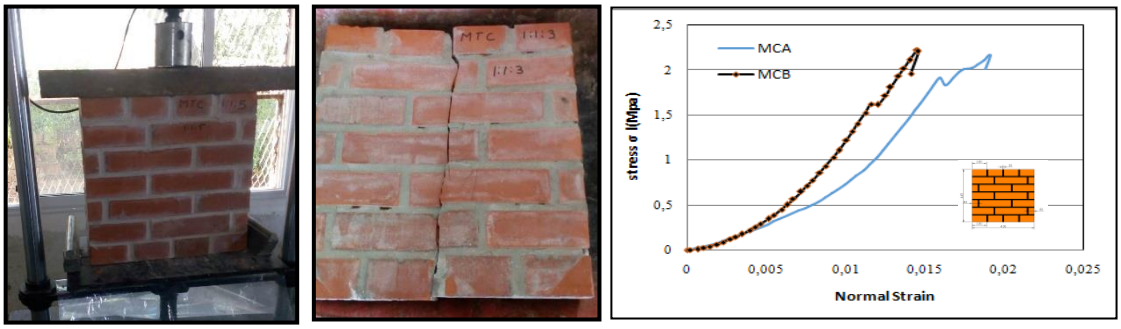

Figure 3.22 Failure modes and stress-strain response of masonry panels (MCA, MCB)

Table 3.12 Comparison of past Experimental Results on Masonry Prisms with Analytical Predictions

Calculation formula of, E_{mac} (MPa)	Calculated values, E_{mac} (MPa)		Experimental values, E_{mac} (MPa)	
	Mortar type A	Mortar type B	Mortar type A	Mortar type B
(Augenti et al, 2011) $E_{,mac} \approx 550\sigma_{c,mac}$	1245.2	1224.3	1082.071 ($E_{,mac} \approx 500\sigma_{c,mac}$)	1391.256 ($E_{,mac} \approx 600\sigma_{c,mac}$)
(EN 1052-1,1998) $E_{,mac} \approx 1000\sigma_{c,mac}$	2226	2164		
(CSA 2004) $E_{,mac} \approx 850\sigma_{c,mac} \leq 20000$MPa	1839	1892.1		
(Drysdale et al.,1994) $E_{,mac} \approx (500\text{-}600)\sigma_{c,mac}$	1082-1298.4	1113-1335.6		

Table 3.13 Compressive strength of masonry panels

θ°	Wall panels	$E_{unit}/E_{mortar} = \beta$ β =2.7 (Mortar type A)			$E_{unit}/E_{mortar} = \beta$ β =5.403 (Mortar type B)		
		Shear strength (MPa)	Compressive strength (MPa)	Young's modulus E(MPa)	Shear bond strength (MPa)	Compressive strength (MPa)	Young's modulus E(MPa)
θ=90°	MC	-----	2.164	1082.071	-----	2.226	1391.256
θ=45°	MT	0.8235	1.647	300.08	1.0836	2.167	324.6
	MRH	1.0129	2.00	100.944	1.5441	3.09	138.96
	MRV	1.08045	2.16	117.2	1.6131	3.226	165.94
	MR2	1.525	3.05	156.72	2.117	4.234	458.308

Note: E_{unit}: Young's modulus of Brick

E_{mortar}: Young's modulus of Mortar

- ***Unreinforced masonry panels subjected to uniaxial compression θ = 45°***

On the planes of the bed and head joints, the combined shear and normal stresses play an important role in its deformation and failure modes. For a uniaxial state of stress that is inclined relative to the x-axis at an angle θ, if angle θ varies, the normal stress σ_n decreases and shear stress τ_n arises on an inclined plane. The maximum shear stress of magnitude τ_{max} occurs on the planes oriented at 45° to the x-axis. Using equilibrium Equations along the bed and perpendicular joints respectively, the applied vertical compressive stress σ_y can be converted to compressive and shear stresses (σ_n, τ_{np}) and (σ_p, τ_{np}). The three linear strains (ε_x, ε_y, ε_{45}) can be used to determine the normal and parallel strains (ε_n, ε_p) and the shear strain (γ_{np}) on the plane of the specimen using the strain transformation equations in which θ is the angle of bed joint to the *x* axis (Figure 3.23).

$$\sigma_n = \sigma_y \sin^2 \theta \tag{3.8}$$

$$\sigma_p = \sigma_y \cos^2 \theta \tag{3.9}$$

$$\tau_{np} = \sigma_y \sin\theta \cos\theta \tag{3.10}$$

In case θ equals 45°, the shear stress (τ) equals the normal stress (σ_n) on the sliding surface. The shear modulus (G) is calculated using:

$$\tau = G\,\gamma \tag{3.11}$$

the shear angle γ is calculated following:

$$\gamma = arctang\,\frac{\Delta h * \sin(\alpha)}{h * \sin(\alpha)} \tag{3.12}$$

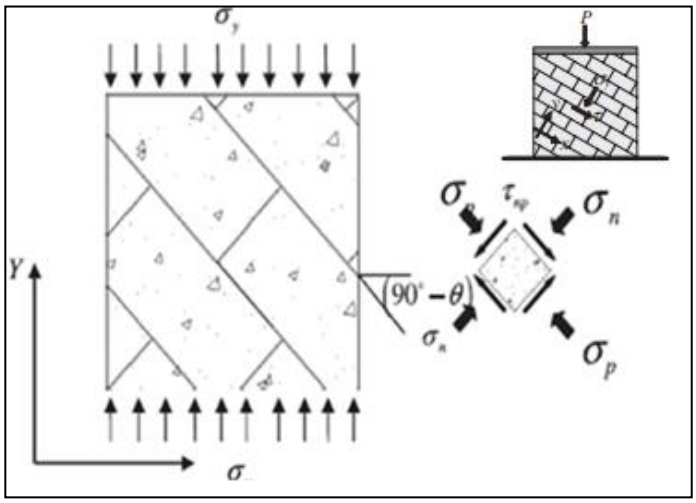

Figure 3.23 Masonry assemblage under combined shear and compression

1) Failure modes

In wall panels MTA and MTB cracking occurred predominately through the mortar joints in a diagonal, followed by a rapid decrease in load capacity. With load increasing, the wall exhibited a gradual increase in the width of predominately diagonally oriented crack, followed by sliding along the formed cracks (see Figure 3.24.a). With further increase in load, multiple cracks were observed in the panel MTB before failure as shown in Figure 3.24.b.

The ultimate loads of MTA and MTB panels were measured as 69.17 kN and 91.03 kN, respectively (see Table 7). The shear stress-strain response of the tested unreinforced wall panels (MTA and MTB) is summarized in Figure 3.24.c. For the comparison between the two responses, the shear strength value of masonry panel constructed with mortar type A was lower than the shear strength value of masonry panel constructed with mortar type B. Both MTA and MTB wall panels exhibited an approximately linear shear stress-strain response until cracking, followed by rapid degradation of shear strength once cracking propagated, followed by a slight increase in shear strength and deformation capacity before the rupture (see Figure 3.24.c).

The wall panel tested with an orientation of bed joint by 45° failed at lower load compared to the wall panel tested when its bed joint makes 90° with loading axis. The same remark was reported for young's modulus, for these orientations, the capacity was affected by the brick strength and the shear bond characteristics of the joints. The $f_{45°}/f_{90°}$ ratios, was at a range of 0.38 to 0.48 which is highly orthotropic representing a reduction of strength by up to 62%. Consequently, the failure load of the unreinforced wall panels was highly dependent on the bed joint orientation. As the orientation changes from 90° to 45°, the average strength value reduced from 2.22MPa to 1.0836MPa for masonry panels MTB and from 2.164MPa to 0.8235MPa for masonry panels MTA, which represented about 40% of the strength reduction. The shear modules of wall panel A and wall panel B were determined as 125.034MPa and 137.25 MPa, respectively.

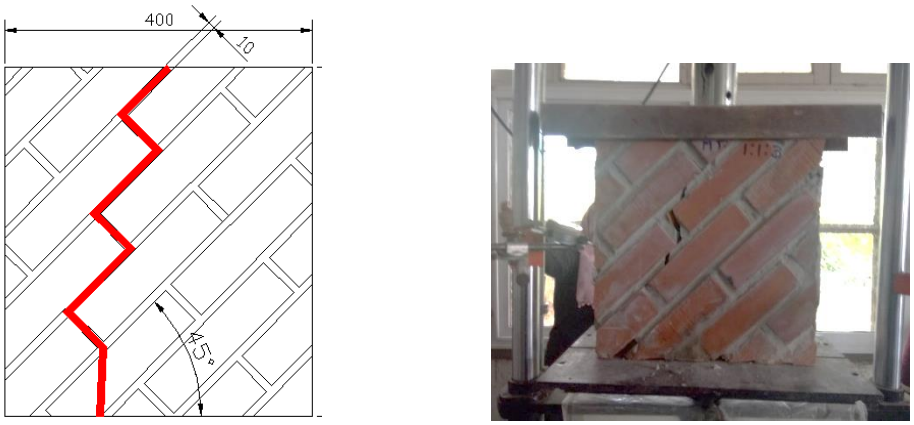

(a) Failure modes of unstrengthened masonry panels **45° (**MTA)

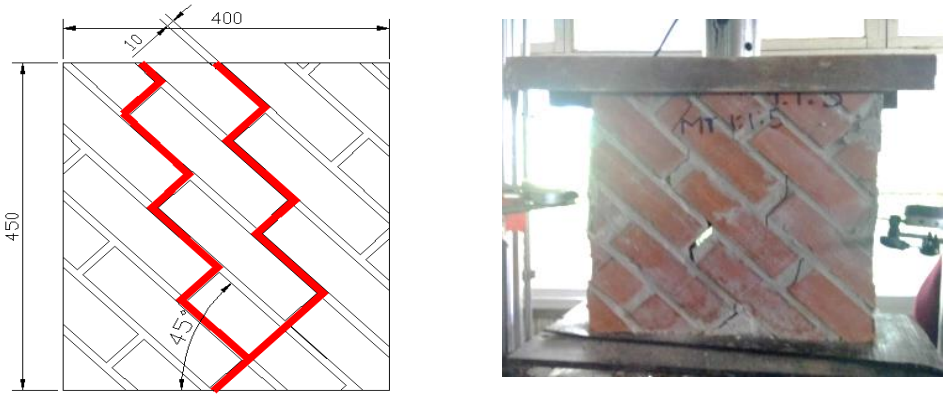

(b) Failure modes of unstrengthened masonry panels **45° (**MTB)

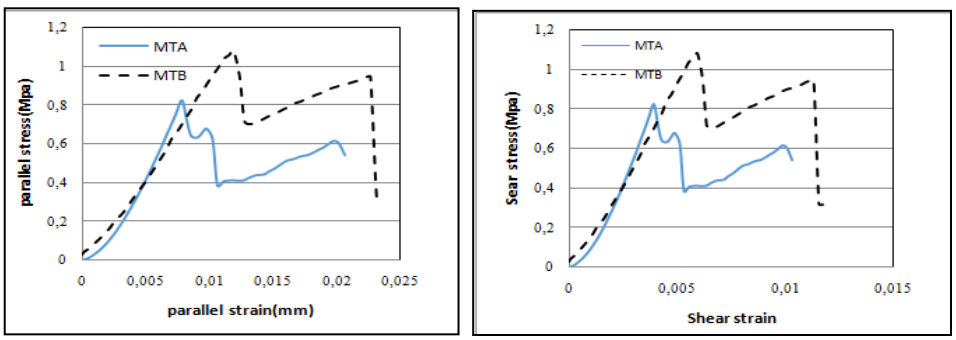

c) Parallel and shear Stress–strain relationships for masonry panels

Figure 3.24 Failure modes and Stress–strain relationships for masonry panels (MTA and MTB)

- **Reinforced masonry panels subjected to uniaxial compression (θ = 45°)**

The reinforcement schemes used for the strengthening of wall panels are summarized in Fig. 1c in which:

- Panels MRVA and MRVB were reinforced with two vertical strips on one side of the panel.

- Panels MRHA and MRHB were reinforced with two horizontal strips on one side of the panel.

- Panels MR2A and MR2B were reinforced with two vertical strips on one side of the panel and two horizontal strips on the other side. The distance between the staggered vertical reinforcement was 135mm.

1) Displacement ductility

The criteria that established by Park (1989) was used to calculate the displacement ductility factor of all tested panels. The displacement ductility factor (μ) is defined as the ratio between the ultimate displacement to the yield displacement. Or:

$$\mu = \frac{\delta_u}{\delta_y} \tag{3.13}$$

Where,

δ_u = displacement at ultimate load

δ_y = displacement at the load causing yield condition

2) **Failure modes**

In unreinforced walls, the tensile stress causes an appearance of cracks leading to a complete destruction. However, in the case of walls strengthened with CFRP strips, the tensile stresses are transferred to these strips results in a significant reduction of stress in the masonry wall. As the load increases, the maximum tensile stress occurs in the corner of the wall. Wall panels reinforced by NSM CFRP strip technique presented more ductile behavior compared with the control wall panels for each type of mortar (see Figure 3.26). The result showed that, when the ratio E_{unit}/E_{mortar} increased by the double, the compressive strength of masonry panels increased by 102% and the shear strength increased by 132%. Furthermore, the E_{unit}/E_{mortar} ratio found to have a deep impact on the in-plane shear capacity of the shear walls. Likewise, it was found

that the improvement in shear strength for strengthened wall panels type A ranged from 123% to 185%, whereas for wall panels type B it ranged between 142% to 196% (see Table 3.15). Concerning the behavior of the reinforced panels, the ultimate load in the (MRVA, MRVB) panels reinforced with vertical CFRP strips on one side only had an increase up to 149%, Furthermore, the displacement increased to 200% which led to an increase of ductility by 384 % (see Table 3.14). This result show that all the reinforced wall revealed a significant improvement of ductility when compared with the corresponding control wall panel (μ_u / μ_o). They showed a substantial increase in deformation capacity which remained between 2.26 and 4.27 times (or of 222% up to 392% as a percentage). Approximately, similar results were also reported in literature as by Dizhur et al [10]. The vertical reinforcement contributed more to strength enhancement as compared to horizontal reinforcement. Wall panel reinforced using horizontal CFRP strips as shown in Figure 3.25.f failed by sliding along the bed joint (sliding shear failure mode) that resulted in a substantially lower increase in shear strength when compared with wall panels having vertical oriented reinforcement. The reinforced walls with two horizontal CFRP strips showed a brittle failure with a sudden loss of strength. On the other hand, the reinforced walls using vertical CFRP strips revealed less brittle failure mode with larger deformation (see Figure 3.25.g). Likewise, the studies performed by Parvin and Syed Shah [123] and Seracino and C Wylie [124] detailed the efficiency of used vertical oriented discrete FRP strips. These studies have shown that the panels reinforced using vertical CFRP strips showed an increase in vertical moment capacity and deformation capacity of walls under out-of-plane loading or in-plane loading. The reinforced walls (MR2A and MR2B) exhibited a vertical splitting of the interior webs followed by a gradual increase in the load up to the peak load. After reaching the peak load the blocks webs completely broke off the face shells as shown in (Figure 3.25.a,b,c,d). Petersen et al [9] reported that the vertical reinforcement was very effective in restraining sliding and diagonal cracking and hence preventing the URM failure mode. The non-symmetrical reinforcement schemes caused out-of-plane deformations and therefore, it could not be avoided by reinforcing the panels at both sides (see Figure 3.25.e). Higher strains in vertical and horizontal directions were recorded for the MR2B panel while lower values were obtained for MRHA panel as shown in Figure 3.26. The strain values recorded in masonry panels of type B were much higher than that in panels of type A. The higher shear stress-strain values for masonry panels MR2 were primarily due to confinement of masonry on both sides of the wall. No rupture of the CFRP strips was observed during testing

or when the CFRP strips were exposed during demolition of the wall panels. With increasing wall panel deformation, the debonding and pull out of the middle CFRP strips was not observed.

Table 3.14 Comparison of shear stress for test results of masonry panels.

Wall panels	Young's modulus E(MPa)	Shear modulus G(MPa)	γ_e	γ_u	μ	$(\mu_u/\mu_0(\mu_u/\mu_o)$
MCA	1082.07	483.13	0.0142	0.0151	1.06	-----
MTA	300.08	125.03	0.0093	0.00531	1.12	-----
MRHA	100.94	42.10	0.00522	0.02	3.83	342%
MRVA	117.20	49.01	0.0059	0.0227	3.85	343%
MR2A	156.72	65.34	0.0045	0.0197	4.38	391%
MCB	1391.26	570.18	0.0113	0.0125	1.09	------
MTB	324.60	137.25	0.0082	0.00637	1.21	------
MRHB	138.96	57.90	0.0063	0.0169	2.68	222%
MRVB	165.94	69.13	0.006	0.0272	4.60	384%
MR2B	458.31	76.98	0.0052	0.0244	4.70	392%

(μ_u/μ_o) : ration ductility of reinforced wall panels when compared to the corresponding control wall panel.

Table 3.15 Comparison of uniaxial compressive stress of unstrengthened and strengthened masonry panels

Bed joint orientation	Type of Mortar	Wall panels	F_{max} (kN)	σ_1 (MPa)	Age increase%	σ_{nn} (MPa)	σ_p (MPa)	τ_{np} (MPa)
θ=90°	Type A	MCA	97.711	2.164	----	2.164	------	0
	Type B	MCB	100.51	2.226	-----	2.226	------	0
θ=45°	Type A	MTA Panel control	69.17	1.647	-----	0.8235	0.8235	0.8235
		MRHA Single side	85.08	2.00	123%	1.0129	1.0129	1.0129
		MRVA Single side	90.04	2.16	131%	1.0805	1.0805	1.08045
		MR2A both sides	178.98	3.05	185%	1.5247	1.5247	1.5247
	Type B	MTB Panel control	91.03	2.167	----	1.0836	1.0836	1.0836
		MRHB Single side	129.70	3.09	142%	1.5441	1.5441	1.5441
		MRVB Single side	135.50	3.226	149%	1.6131	1.6131	1.6131
		MR2B both sides	180.10	4.234	196%	2.117	2.117	2.117

Note: F_{max} : ultimate load; σ_1: Average uniaxial compressive strength; σ_n: Stress normal to bed joint;
σ_p: Stress parallel to bed joint; τ_{np}: Shear stresses on bed joint.
Age increase%: the ratio of F_{max} of a reinforced panel to the control panel

(a) Front face wall panel MR2A

(b) Back face wall panel MR2A

(c) Front face wall panel MR2B

(d) Back face wall panel MR2B

(e) Lateral view of panel MR2A and MR2B

(f) Failure modes of strengthened panels MRHA and MRHB

(g) Failure modes of strengthened panels MRVA, MRVB

Figure 3.25 Failure modes of all strengthened masonry panels

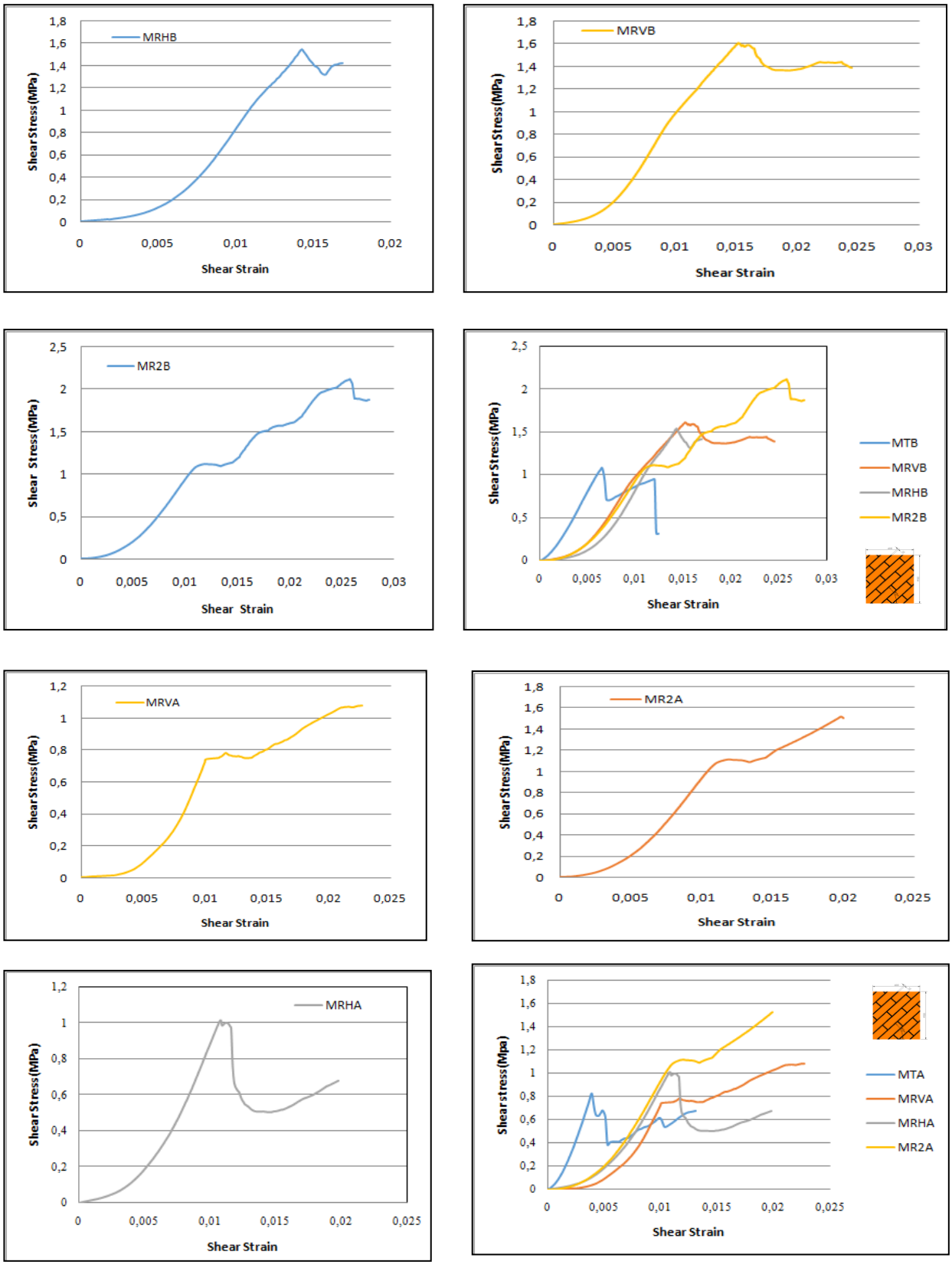

Figure 3.26 shear stress-strain relationship for MRA and MRB masonry panels

Chapter 4

Modelling and fracture mechanism of Unreinforced Masonry assemblages reinforced with CFRP composites/strips under in-plane loading

---

4.1 Introduction

The literature has clearly focus on the importance of including all the mechanisms of masonry rupture in the modeling to understand its behavior, in terms of ductility and ultimate load. The damage is usually found concentrated in the mortar interface. In microscopic models, only a tensile breaking of the bricks is sometimes considered, most studies relying only on a linear elastic behavior of the bricks. In these models, the authors assent to the need to introduce the post-peak softening behavior of the mortar. The softening behavior laws, which are thus essential in modeling, however, rely on the definition of many parameters whose values are difficult to appreciate a priori, This modeling is therefore only feasible if it is coupled with a several experimental test for best description of the material and their interactions.

The purposes of this study are to develop an accurate predictive FE model, eliminating the above-mentioned deficiencies. In order to model the behaviour of masonry walls, the detailed micro-modelling (DMM) approach was adopted (see figure 4.1), which is implemented in ABAQUS program to perform a numeric simulation of different masonry assemblages.

To demonstrate the effectiveness of this proposed approach the results from experimental tests on masonry assemblages were compared to those obtained from the developed numerical model. Information gained from developing the model and comparisons with the results of experiments are presented below.

4.2 Material parameters

The units and mortar joints were modelled using eight node 3D continuum elements with four glass controls and reduced integration (C3D8R). The nonlinear behaviour of brick masonry was simulated with the Concrete Damage Plasticity (CDP) model. The Shell elements S4R are used to represent the CFRP because there are six degrees of freedom per node.The linear elastic response of CFRP is defined by using the lamina model needed to define the elastic modulus, the shear modulus in two directions, and Poisson's ratio. The debonding of CFRP and the contact region between CFRP and the masonry wall was modelled using surface based cohesive behaviour. To capture the behaviour of the bond between FRP and the masonry wall, especially those that debonded, an interface model was chosen in order to accurately model the masonry wall strengthened with FRP. The unit-mortar interface was modelled as a cohesive interface with zero thickness to represent the initiation and propagation of cracks via the Extended Finite Element Method (XFEM). To model cohesive behaviour, the normal and tangential stiffness of the traction and separation law in kn and ks was introduced. The Coulomb-friction parameter was added so that another source of dissipation (sliding) could be assumed. It was introduced as a coefficient of friction of 1.04 for the shear triplet model and 0.8 for the diagonal shear wall. The interaction between unit-mortar and the CFRP masonry assembly was modelled using the surface to surface contact option available in ABAQUS/implicit or the contact general in ABAQUS/Explicit.

The results obtained from the experimental characterization of materials carried out in the present study were admitted (values of fc, c and μ). the dilatancy angle was assumed to be zero to avoid a non-conservative shear strength prediction. For the tensile fracture energy (Mode I) of the interface, data available in the literature (Pluijm) recommend values in the range of 0.005 to 0.2 N/mm for a tensile strength range from 0.3 to 0.9 N/mm^2. This is confirmed by Almeida et al (2002) when they found that for different types of brick-mortar interfaces the average mode I fracture energy was around 0.008 N/mm when the average bond tensile strength was in the order of 2 N/mm^2.

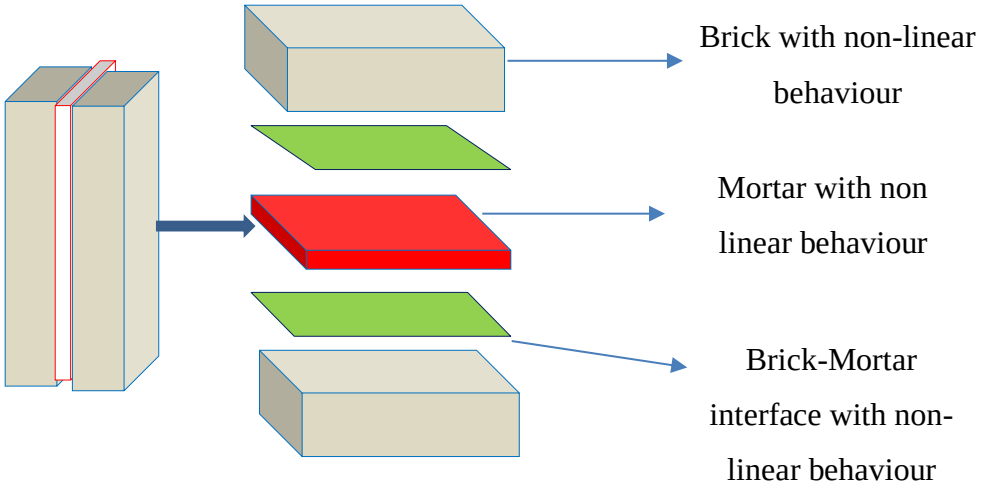

Figure 4.1 Adopted detailed micro-modelling approach (DMM)

4.2.1 Constitutive behavior of units and mortar:

4.2.1.1 Concrete Damage Plasticity (CDP) model:

The concrete damage plasticity model (CDP) used here to simulate the nonlinear behaviour of brick and mortar is available in ABAQUS. It was used here to predict the two main types of failure modes, cracking in tension and crushing in compression. The CDP models assume a non-associated potential plastic flow which is an adoption of Drucker-Prager hyperbolic function for flow potential (show Figure 4.2). Damage Plastic Model is the only constitutive model that takes into consideration the degradation of the elastic stiffness caused by plastic straining in both tension and compression as well as the stiffness recovery effects under cyclic loading, This model has been provided by Lubliner & al in 1989 [125] to identify the complex behavior of concrete. In this model, the softening/hardening parameter "k" in the overall form of classical plasticity was substituted by the damage parameter "d" where the plastic damage parameter takes an upward value beginning from zero when the concrete is totally undamaged until it reaches one where the concrete is totally damaged with full loss of cohesion.

When applied the load and exceeded the elastic region, a stiffness degradation occurs due to the appearance of plastic deformation. This degradation can be determined by unloading the material, calculating the unloading modulus of elasticity, and comparing it to the initial modulus

of elasticity. As a simplification, it was assumed that this behavior occurs just in the post- peak stress–strain curve. The decrease of the slope is ruled by two independent variables, dc (damage in uniaxial compression) and dt (damage in uniaxial tensile). those variables can be defined using the equations (4.26) and (4.27).

The modelling of components of masonry (brick and mortar) in all models was established through two steps. the elastic modulus and Poisson's ratio were introduced in the first step (see Table 4.1). whereas the damage plasticity model was adopted in the second step to define the nonlinear part of the stress-strain curve.

Additionally, there are other parameters that are needed for the application of the CDP technique in ABAQUS. These parameters are represented as follows:

- The dilation angle (ψ) takes the value of 12° to 30°. In this study, the value of the dilation angle was chosen equal to 20°.
- Eccentricity parameter (e) this value ranges from 0 to 0.1(theory of Drucker prager) which is assumed to be 0.1 (default value in ABAQUS).
- Viscosity parameter =0.001
- $(\frac{f_{bo}}{f_{co}})$ the ratio between the initial equilbiaxial compressive strength and uniaxial compressive strength of masonry when the default value was used (1.16).
- (k) the ratio of second stress invariant on the tensile meridian when the default value was used (0.67).

The plastic parameters used in masonry model are tabulated here in Table 4.2. All these properties are assigned to the model in the plasticity table in ABAQUS.

Table 4.*3* and Table 3.20 are used to assigned values to "concrete damage plasticity model". the stress- strain curves in tension and compression can be divided into several segments (show Figure 4.3), in which, the compression stress-strain curve of brick unit has three different regions, and the formulations for each region are shown from equations (4.1) to (4.6) derived [126, 127]. the stress- strain curves in tension is composed by two regions. The formulation that composes each region is given by equations (4.7) to (4.11).

In many cases, it is difficult to obtain stress-strain curves experimentally. To get the stress-strain curve, two main strategies can be adopted which are:

- The stress-inelastic strain curve can be provided directly by the user basing on experimental tests, then converted to the stress-strain curve such as ABAQUS do basing in the correlation between strain and inelastic strain (User data).
- The stress-inelastic strain data can be estimated by using codes presents empirical formulations, in which the researcher only includes parameters that are generally easy to determine. Such as the characteristic value of concrete compressive strength (Auto-estimation).

The equivalent uniaxial stress-strain relationship and corresponding damage parameter used in this study were determined automatically by the Excel program. it considers the elastic region until 30% of the ultimate load, where the modulus of elasticity is the slope of the stress-strain diagram. The inelastic region is defined by equations (4.21) to (4.24).

1) For Brick:

- **Compressive Behavior**

i. The First Region: Elastic Region (A to B)

$$\sigma_c = E_{ib} \times \varepsilon_c \quad (4.1)$$

ii. The Second Region: Inelastic Region (B to C i.e.$x \leq 1$)

$$\sigma_c = (\alpha_a x + (3 - 2\alpha_a)x^2 + (\alpha_a - 2)x^3) \times f_b \quad (4.2)$$

iii. The third region: inelastic region (C to D i.e. $x \leq 1$)

$$\sigma_c = \frac{(f_b)}{(\alpha_d x(x-1)^2)} \quad (4.3)$$

$$x = \frac{\varepsilon_c}{\varepsilon_{c1}} \quad (4.4)$$

$$\alpha_a = \frac{E_{ib}}{E_b} \quad (4.5)$$

$$1.5 \leq \alpha_d \leq 3 \quad (4.6)$$

- **Tensile Behavior**

i) The First Region: Elastic Region (A to B):

$$f_{tb} = E_{ib} \times \varepsilon_{cr} \quad (4.7)$$

$$f_{tb} = 0.3 \times (f_b)^{\frac{2}{3}} \quad (4.8)$$

ii) The Second Region: Inelastic Region (B to C):

$$\sigma_t = \frac{(f_{tb} \times x)}{(\alpha_t (x-1)^{1.7} + x)} \quad (4.9)$$

$$x = \frac{\varepsilon_t}{\varepsilon_{cr}} \quad (4.10)$$

$$\alpha_t = 0.312 f_{cb} \quad (4.11)$$

2) For mortar:

The tensile strength of the mortar was not determined experimentally but equations (4.12) to (4.14) was used to calculate this.

- **Tensile Behavior**

$$f_{ctm} = 0.3 \times (f_{cm})^{\frac{2}{3}} \quad (4.12)$$

$$\sigma_t = E_{cm} \times \varepsilon_t \quad si \quad \varepsilon_t \leq \varepsilon_{cr} \quad (4.13)$$

$$\sigma_t = f_{cm} \times \left(\frac{\varepsilon_{cr}}{\varepsilon_t}\right)^{0.4} \quad si \quad \varepsilon_t > \varepsilon_{cr} \quad (4.14)$$

- **Compressive Behavior**

$$\sigma_c = \frac{f_{cm}(k\eta - \eta^2)}{(1+(k-2)\eta)} \quad (4.15)$$

$$k = 1.05 E_{cm} \times \left(\frac{\varepsilon_{c1}}{f_{cm}}\right) \quad (4.16)$$

$$\eta = \frac{\varepsilon_c}{\varepsilon_{c1}} \quad (4.17)$$

$$E_{cm} = 22 \times \left(\frac{f_{cm}}{10}\right)^{0.3} \quad (4.18)$$

$$\varepsilon_{c1} = 0.7 \times (f_{cm})^{0.31} \quad (4.19)$$

In the CDP constitutive model, elastic and inelastic deformation (ε_{c0}^{el} and ε_c^{in} , respectively) are calculated independently, and subsequently summed to obtain the total deformation (ε). ε_{c0}^{el} depends only on the materials' modulus of elasticity and Poisson's ratio and ε_c^{in} is obtained from their stress-strain curve.

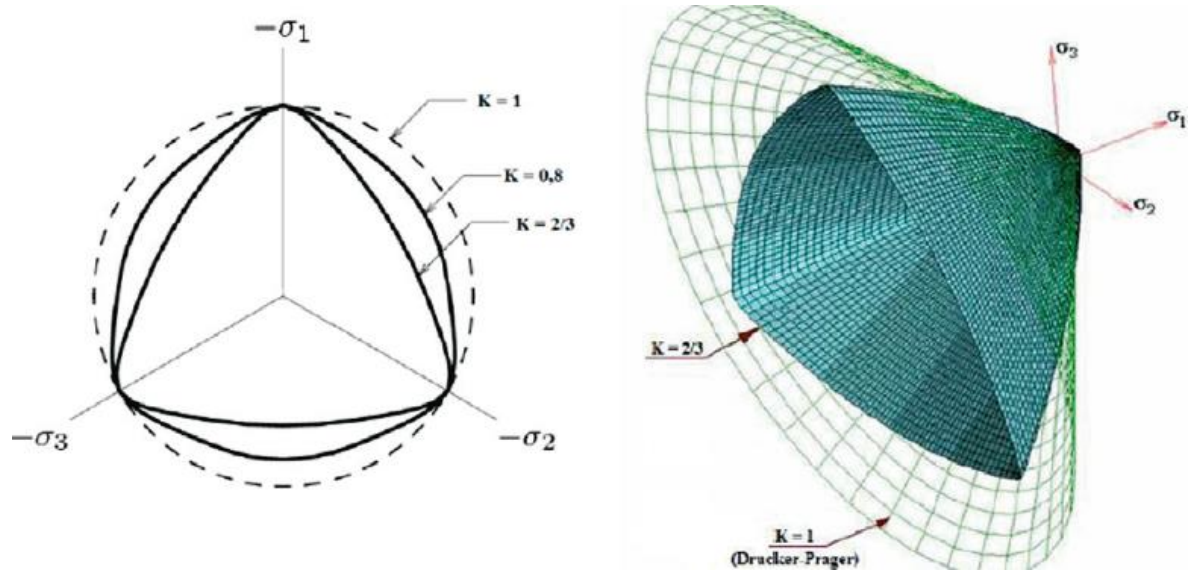

Figure 4.2 Influence of the Kc parameter on the shape of the yield surface Aguiar (2014).

Plastic strains are determined automatically from inelastic strains. Compressive elastic strains are determined by an equation (4.20).

$$\varepsilon_{c0}^{el} = \frac{\sigma_c}{E_0} \qquad (4.20)$$

Inelastic strains can be determined using equation (4.21)

$$\varepsilon_c^{in} = \varepsilon_c - \varepsilon_{c0}^{el} \qquad (4.21)$$

Plastic strains are calculated using equation (5.22)

$$\varepsilon_c^{pl} = \varepsilon_c^{in} - \frac{d_c}{(1-d_c)} \cdot \frac{\sigma_c}{E_0} \qquad (4.22)$$

In the absence of compression damage, it comes $\tilde{\varepsilon}_c^{pl} = \varepsilon_c^{in}$

Similar to the compression strain, tensile inelastic strains can be determined using equation (4.23)

$$\tilde{\varepsilon}_t^{pl} = \tilde{\varepsilon}_t^{ck} - \frac{d_t}{(1-d_t)} \frac{\sigma_t}{E_0} \qquad (4.23)$$

Where, $\tilde{\varepsilon}_t^{ck} = \varepsilon_t - \varepsilon_{0t}^{el}$ (4.27) and /Or $\varepsilon_{0t}^{el} = \frac{\sigma_t}{E_0}$ (4.24)

The damage plasticity constitutive model was based on the following stress–strain relationship:

$\sigma = (1 - d_t)\bar{\sigma}_t + (1 - d_c)\bar{\sigma}_c$ (4.25)

where $d_c$and d_t were two scalar damage variables, ranging from 0 to 1.

the damaged parameter (d_c) is calculated by:

$\mathrm{d_c} = 1 - \frac{\sigma_c}{\sigma'_c}$ (4.26)

Were σ'_c The compressive strength of masonry

Damaged parameter (d_t) can be calculated by equation (4.27)

$\mathrm{d_t} = 1 - \frac{\sigma_t}{\sigma'_t}$ (4.27)

were σ'_t Masonry tensile strength

The damage variables $\mathrm{d_t}$ and / or $\mathrm{d_c}$ are the maximum values of the history of the values of the damage in tension or compression, taking care not to exceed the maximum value of 0.99 (which corresponds to a reduction of 99% of rigidity) to avoid numerical problems of convergence of the solution.

The uniaxial compressive and tensile responses of mortar and brick with respect to the concrete damage plasticity model subjected to compression and tension load were given by equation (4.1) to (4.27) and shown in Figure 4.4 .

$\sigma_t = (1 - d_t)E_0\left(\varepsilon_t - \tilde{\varepsilon}_t^{pl}\right)$ (4.28)

$\sigma_c = (1 - d_c)E_0\left(\varepsilon_c - \tilde{\varepsilon}_c^{pl}\right)$ (4.29)

the effective uniaxial stress $\bar{\sigma}_t$ and $\bar{\sigma}_c$ were derived as follows:

$\bar{\sigma}_t = \frac{\sigma_t}{(1-d_t)}E_0\left(\varepsilon_t - \tilde{\varepsilon}_t^{pl}\right)$ (4.30)

$\bar{\sigma}_c = \frac{\sigma_c}{(1-d_c)}E_0\left(\varepsilon_c - \tilde{\varepsilon}_c^{pl}\right)$ (4.31)

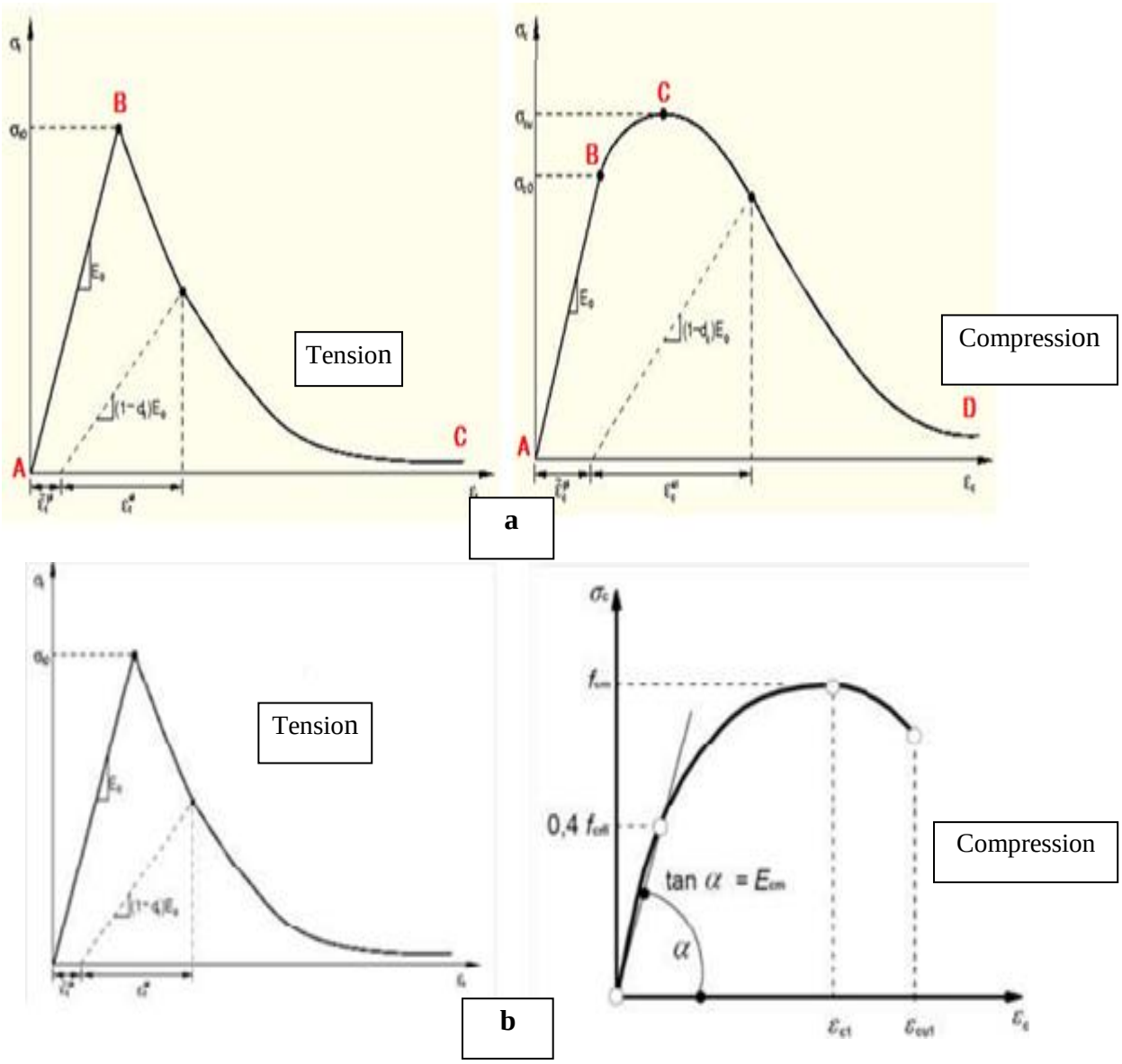

Figure 4.3 Response of concrete to uniaxial loading; (a) for Brick: in tension and compression; (b) for Mortar: in tension and compression. [19]

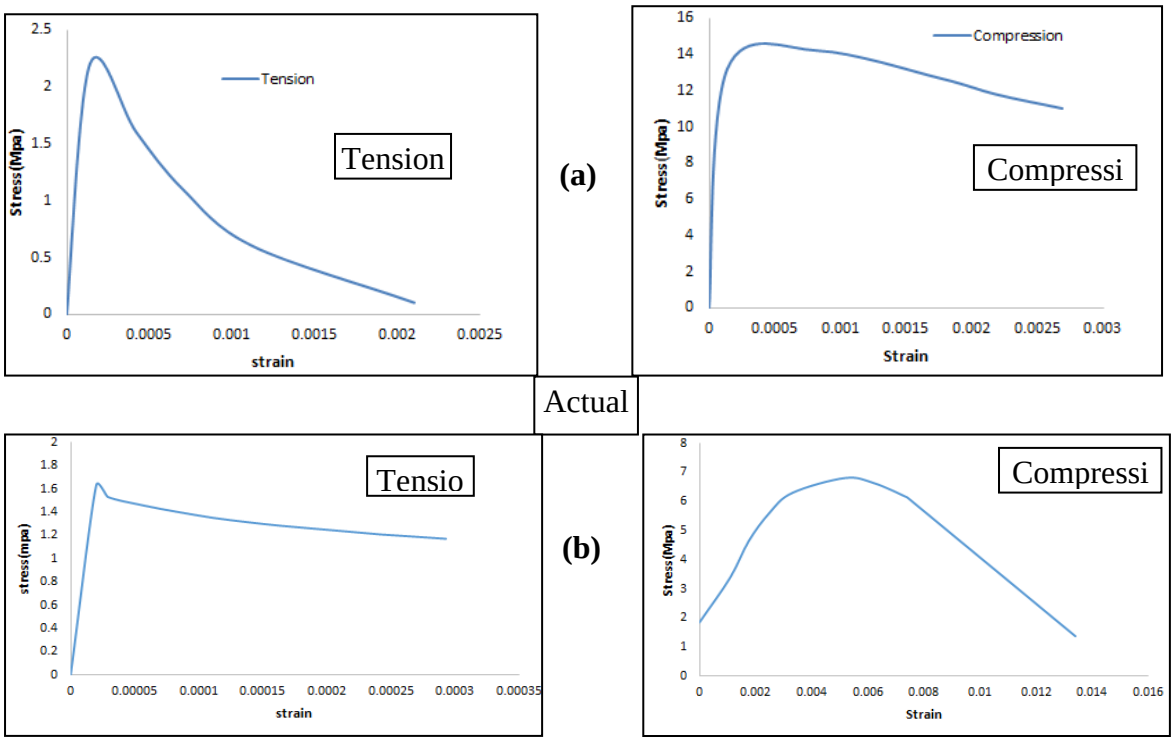

Figure 4.4 Brick and Mortar response to uni-axial loading; (a) for Brick: in tension and compression; (b) for Mortar: in tension and compression (present work).

4.2.1.2 Constitutive behavior of brick-mortar interface

The interaction module of Abaqus/implicit analysis was used to make the contact between units and mortar through the option surface-to surface contact. In this step, three contact properties should be defined: Normal contact, Tangential behavior, cohesive behavior and damage.

Normal behavior: the hard contact behaviour normal to the surfaces is chosen. The goal is to prevent interpenetration of surfaces, and also to permit a separation between them once a contact has been established.

Tangential behavior: the analysis needs to take frictional forces because when the surfaces are in contact, they habitually transmit shear and normal forces athwart their interface. which resist the relative sliding of the surfaces.in this case, the Coulomb friction was adopted to describe the interaction of contacting surfaces. This model characterizes the frictional behaviour between the surfaces employing a coefficient of friction (μ). (Figure 4.5)

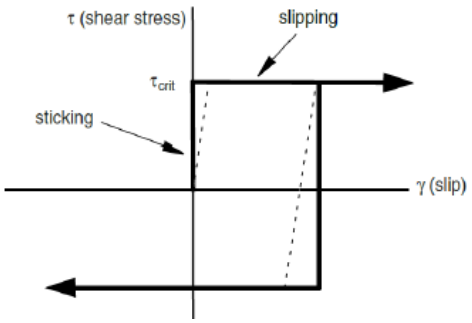

Figure 4.5 Friction behavior (Simulia,2014)

The cohesive behaviour of the surface was used to model the interface between units and mortar with zero thickness. The uncoupled cohesive behavior having three stiffness components in normal (K_{nn}), and the two-local shear (K_{ss}) & (K_{tt}) directions are considered. This kind of contact causes a stiffness degradation called Damage, in which it is only necessary to provide the interface's fracture energy.

In ABAQUS, the traction–separation model has three criteria, linear elastic behaviour, the damage initiation criterion, and the damage evolution law [128]. Before there is any damage, the initial response of the joint interfaces has a linear traction–separation relationship (Figure 4.6). In the elastic part the general linear behaviour is defined according to the relationship between the nominal traction stress (t) and nominal strain (δ) through the interface. The relationship between the elastic stiffness matrix (K), the traction stress vector (t), and the separation vector (δ) through the interface can be expressed in standard form as in equation (4.32). The components ($t_n, t_s\ t_t$) represent the fracture modes (shown in Figure 4.7).

$$t = \begin{pmatrix} t_n \\ t_s \\ t_t \end{pmatrix} = \begin{bmatrix} K_{nn} & 0 & 0 \\ 0 & K_{ss} & 0 \\ 0 & 0 & K_{tt} \end{bmatrix} \begin{Bmatrix} \delta_n \\ \delta_s \\ \delta_t \end{Bmatrix} \tag{4.32}$$

The generalized stresses and strains can be written in a linear elastic relation in the standard form as

$$\sigma = D\varepsilon \tag{4.33}$$

$\sigma = D\varepsilon(2)$ For a 2D configuration:

$$D = diag\{k_n, k_s\} \quad (4.34)$$

$$\varepsilon = \{\Delta u_n, \Delta u_s\}^T \quad (4.35)$$

$\mathrm{D} = \mathrm{diag}\{\mathrm{k_n}, \mathrm{k_s}\}(3)$

$\varepsilon = \{\Delta \mathrm{u_n}, \Delta \mathrm{u_n}\}^{\mathrm{T}}(4)$ Where, n and s denote normal and shear components respectively.

The equivalent stiffness for joint interfaces is represented as a function of the unit and mortar elastic modulus, and the thickness of the mortar (see Eqn.4.37 and Eqn.4.38) [13][9].

$$k_n = \frac{E_u E_m}{h_m(E_u - E_m)} \quad (4.37)$$

$$k_s = k_t = \frac{G_u G_m}{h_m(G_u - G_m)} \quad (4.38)$$

Where,

h_m = thickness of mortar

E_u and E_m = $\mathrm{E_m}$The Young's modules for unit and mortar respectively.

$\mathrm{G_m}$, G_u and $\mathrm{G_m}$ = The shear modules for mortar and unit respectively.

The damage evolution of cohesive behaviour represents the progressive degradation of cohesive stiffness or the dissipation of energy; it is called fracture energy and depends on the fracture mode that resulted from the failure method. The opening of the interface in a normal direction is called mode I, and the second and third modes are shearing modes known as mode II and mode III.

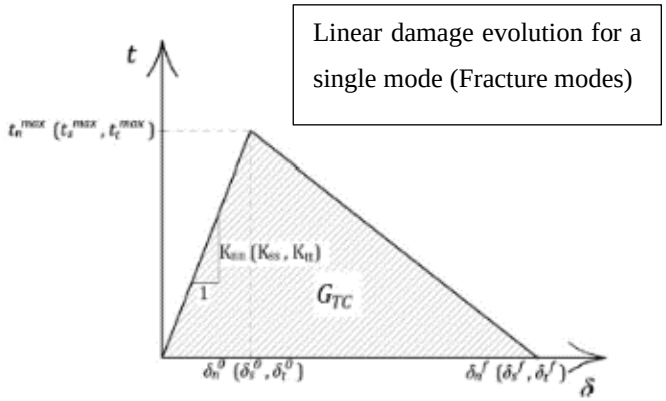

Figure 4.6 Typical traction–separation behavior of masonry joint interfaces in tension and Shear [9]

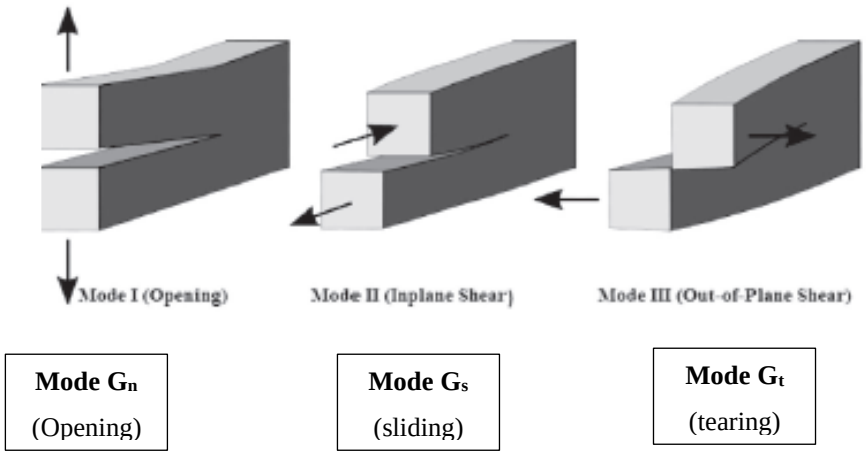

Figure 4.7 Fracture modes [9]

4.2.1.3 Constitutive behavior of the CFRP-masonry interface

The interface was modelled using the cohesive zone. The bond between the composite and the masonry was modelled with cohesive behaviour to represent the masonry-composite interface with the initial stiffness presented in equation (4.39) [128].

$$k_0 = \frac{1}{\frac{t_i}{G_i}+\frac{t_c}{G_c}} \tag{4.39}$$

Where: t_i is the thickness of the resin, t_c is the thickness of the masonry wall, and G_i, G_c are the shear modulus of resin and masonry wall respectively.

Two criteria were used to evaluate the initial debonding of the FRP masonry interface. One criterion assumed that the mode I and Mode II debonding was independent, while the other criterion assumed that normal and shear stress have couplet effects and thus mixed mode interface debonding will begin when the following stress condition is reached.

The quadratic function is used to indicate the initial damage of the interface and presented in equation (4.40):

$$\left(\frac{\sigma_n}{\sigma_n^0}\right)^2 + \left(\frac{\tau_n}{\tau_s^0}\right)^2 + \left(\frac{\tau_t}{\tau_t^0}\right)^2 \begin{cases} < 1 \; no \; failure \\ = 1 \; failure \end{cases} \quad (4.40)$$

σ_n is the tensile stress, τ_s and τ_t are the shear stresses of the interface, and n, s, t are the directions of the components of the constraint. The values used in this study for epoxy resin are σ_{no}=1.81 MPa τ_{s0}= τ_{t0}= 1.5 MPa [129].

The evolution of the damage of the interface is expressed by the term of energy dissipation. The model description is available in the Abaqus materials library. The dependence of the fracture energy on the fracture mode (opening in normal direction and shearing modes respectively calling sliding and tearing).

The opening fracture is denoted by Gn and the shearing modes are Gs and Gt respectively.

$$\left(\frac{G_I}{G_1^f}\right)^2 + \left(\frac{G_{II}}{G_2^f}\right)^2 = 1 \quad (4.41)$$

Where G_i^f and G_2^f are fracture energies of interface under pure mode I and Mode II respectively.

4.2.2 Extended finite element method (X-FEM)

Mathematically the crack propagation and fracture analysis problems might be solved. In the last few decades, a numerical method was developed. Such method is the Partition of Unity (PU), which is first produced by Melenk and Babuska, 1996. In this method, a set of functions are defined on a certain domain, and the enrichment method, which is developed by Gifford and Hilton, 1978, depends on the enriching region. The displacement approximation in this method is considered to be the summation of the finite element's standard solution u_{std} and the enrichment solution u_{enr} as can be seen in Eq. (4.42) below:

$$u = u_{std} + u_{enr} \quad (4.42)$$

Belytschko [130] proposed an enrichment method that is specialized in the enriching of localized regions. The Extended Finite Element Method (XFEM) developed by Belytschko and Black [131] is an enrichment method that is used for discontinuities problems such as crack propagation in concrete. It employs the PU technique for the numerical solution. These discontinuities might be a result of crack interface produced from the fracture of the material in

a certain region of the domain, or might be a material interface that produced in a composite material located at the interface zone between the two materials.

The Extended Finite Element Method (XFEM), is a numerical technique used to solve the discontinuities problems that occur in brittle materials such as concrete. The XFEM is an extension of the conventional finite element method based on the PU method. In spite the XFEM uses a localized enrichment function, an enrichment of nodes is developed nearby the discontinuity. The enrichment is done mathematically by the use of the enrichment functions. The analysis of crack propagation using an enriched FEM approach was originally introduced by Moës and al [132] and Fries et al [133]. In this method, the elements around the crack tip and along the crack path are enriched by adding to the leading singular crack tip asymptotic displacement fields through the partition of unity approach (PUM) for modeling of the crack. The method of partition of unity (PUFEM) proposed by Melenk and Babuska [134] represents one of the mathematical bases of the X-FEM. It has been experienced by some authors as Sukumar et al [135], Stolarska and al [136], particularly in the field of fracture mechanics. The main idea of this method is to enrich the standard approximation of the finite elements by appropriate functions.

The XFEM introduces in the approximation of the displacement field two types of enrichments(show Figure 4.8) [131]:

-A discontinuous function H (Heaviside function) that enriches the split nodes:

$$H(x) = \begin{cases} +1 & if \quad \varphi(x) \geq 0 \\ -1 & if \quad \varphi(x) \leq 0 \end{cases} \qquad (4.43)$$

Where φ *i*s the level set function that determines the normal position of node *(x)* from the crack.

-Four singular functions for each tip node:

$$F(x) = \sqrt{r}\{sin(\theta / 2), sin(\theta / 2)\, sin(\theta), cos(\theta / 2), cos(\theta / 2)\, sin(\theta)\} \qquad (4.44)$$

It allows the presence of discontinuities in an element by enriching degrees of freedom with special displacement functions. It is possible to model by X-FEM a crack whatever its position in the mesh, made from elements with 4 nodes. The approximate displacement fields are as follows:

$$u = \sum_{I=1}^{N} N_I(x)\left[u_I + H(x)a_I + \sum_{\alpha=1}^{4} f_\alpha(x)b_I^\alpha\right]$$

Applies to all nodes in the model

Applies to nodes whose shape function support is cut by the crack interior

Applies to nodes whose shape function support is cut by the crack tip

I: is the set of nodes of the mesh

u = Displacement vector

u_I = Nodal displacement vector.

$H(x)$ = Jump function

$\alpha_I = a_I$ Nodal enriched degree of freedom vector

$N_I(x)$ = Shape function

$f_\alpha(x)$ = Asymptotic crack-tip functions

b_I^α = Nodal enriched degree of freedom vector

By the level set method, ABAQUS can automatically find the position of the crack; this method defines the crack by using the isophanes ΦandΨ. In ABAQUS, Ψ defines the front of the crack and ϕ defines the face of the crack face, it is called PHILSM. The term STATUSXFEM indicates the cracking status of the element.

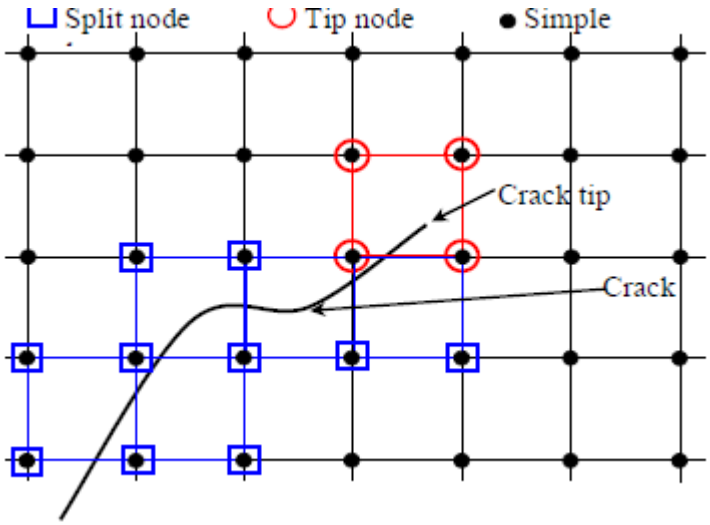

Figure 4.8 Type of XFEM enrichements of meshed domain [131]

4.3 Model input parameters

The ABAQUS/standard implicit algorithms solutions are very accurate in terms of mechanical behaviour when nonlinearities are considered because more realistic behaviour can be assumed and evaluated, but numerical stability suffers because a large set of linear equations must be solved. This can cause long CPU times and convergence is not guaranteed for highly nonlinear problems. For this reason, this type of algorithms was used to solve the shear triplet model. In the other hand, the explicit algorithm was used to simulate the two model of unreinforced and reinforced masonry wallette). For these problems typically involve contact or material complexities that cause convergence difficulties in ABAQUS /standard.

To model cohesive behaviour, the normal and tangential stiffness kn and ks of the traction and separation law were introduced. The average compressive strength of masonry prism of 2.19 N/mm^2 was employed in order to model the normal damage initiation. The masonry assemblages were modeled according to the materials properties reported in Table 4.5.

.

Table 4.1 Mechanical properties of masonry unit and mortar

Elastic Parameters	Brick	Mortar
Mass density (γ) (kg/m^3)	2200	1800
Young Modulus (E)(N/mm^2)	10000	1880
Poisson's ratio (μ)	0.2	0.18

Table 4.2 Damage plasticity of masonry brick

Plasticity parameters	
Dilation angle (ψ)	20
Eccentricity parameter (e)	0.1
Bi and unidirectional compression resistance ratio ($\frac{f_{bo}}{f_{co}}$)	1.16
Stress ratio in the meridian in tension (k)	0.67
Viscosity setting (ν) (m^2/s)	0.0001

Table 4.3 Stress-Strain relationship in tension and compression of masonry brick

Compressive uniaxial nonlinear beaviour		Tensile uniaxial nonlinear behaviour	
Stress (N/mm²)	Inelastic strain	Stress (N/mm²)	Cracking strain
12.1	0	2.5	0
13.2	0.00014	2.2	0.00014
14.19	0.00083	1.6	0.00042
12.65	0.00177	1.1	0.0007
11.77	0.00219	0.6	0.00112

Table 4.4 Compressive and tensile Behavior of mortar

Compressive uniaxial nonlinear behavior		Tensile uniaxial nonlinear behavior	
Stress (N/mm²)	Inelastic strain	Stress (N/mm²)	cracking strain
5.9825	0	1.63125	0
6.0525	0.001075	1.5328125	0.000590613
6.108125	0.00115	1.43671875	0.000694829
6.21	0.0018	1.25625	0.001320188
6.275625	0.002025	1.13671875	0.002293084
6.363125	0.002775	1.13203125	0.003150326

Table 4.5 Mechanical properties of brick-mortar interface and CFRP interface (contact cohesive behavior)

Sample	Contact										
	Tangential behavior	Normal behavior	Cohesive behavior								
			Stiffness coefficient (MN/m)			Damage initiation (N/mm^2)			Damage evolution		
	Friction coefficient		K_{nn}	K_{ss}	K_{tt}	Normal	ShearI	ShearII	Fracture energies (N/mm)		
									GFc	GFI	GFII
Compression triplet prism	1.04	Hard Contact	40	-	-	9.2	0	0	5	-	-
Shear triplet prism	1.04	Hard Contact	40	16	16	2	0.44	0.44	-	0.018	0.2
Reinforced Shear triplet prism											
Unreinforced and reinforced masonry Wallette	0.85	Hard contact	40	16	16	5	0.56	0.56	-	0.018	0.2
CFRP interface	-----	------	90	35	35	3	1.5	1.5	0.969	1.791	1.791

4.4 finite elements modelling and comparison with experimental results

4.4.1 Numerical behavior of brick masonry prism in compression

4.4.1.1 FE model description

The same masonry prism in compression described in chapter 3 is modelled using ABAQUS (2017).

The finite element mesh, boundary conditions, and loading of masonry assemblages are shown in Figure 4.9. For this model, the incremental load was applied at the top surface of prism as displacement. The mortar surface was considered as master surface due to its higher modulus of elasticity and the brick surface was considered as a slave surface.

In this analysis (DMM), both the brick and mortar were modeled using eight-node 3D continuum elements with four glass controls and reduced integration (C3D8R). The nonlinear behaviour of brick and mortar was simulated with CDP model.

For applicate the XFEM approach modeling, the mortar was modeled as solid cohesive elements; this procedure was implemented in ABAQUS using the cohesive behavior parameters. The size of the elements used for modeling the mortar is uniform with a thickness of 10mm which represented the real thickness of the joint. The unit-mortar interface was modelled as a cohesive interface with zero thickness using the surface-to-surface contact option available in ABAQUS /implicit.

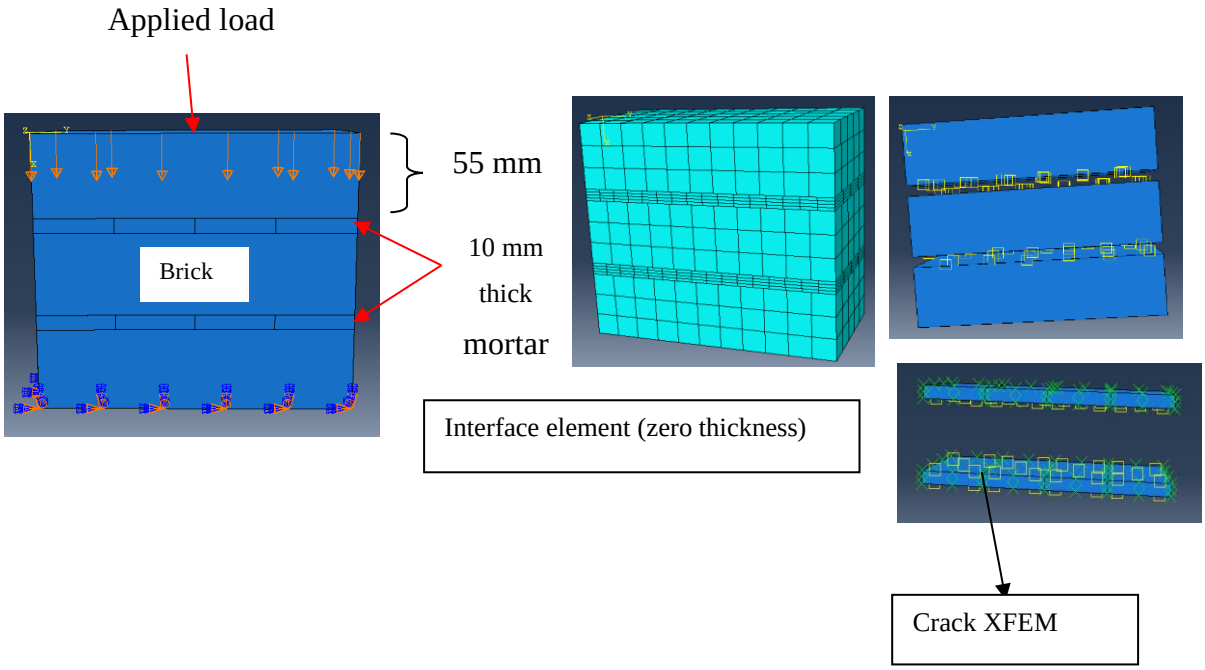

Figure 4.9 masonry Compression prism test: Geometry of assemblages, boundary and loading conditions; meshing, surface-based Interaction

4.4.1.2 Results and discussions

- ***Stresses and failure modes***

Figure 4.10 shows the maximum principal stress, the final von Mises, and the damage at failure for a compression prism. In the initial step the maximum tensile damage is located in the middle of the prism, whereas in the final step, tensile damage occurred at the bottom edges of the prism. This means that vertical tensile splitting cracks began in the middle of the prism and then propagated to the top and bottom of the brick, as was found experimentally. Therefore, the resulting failure mode in the vertical plane was tensile splitting in the middle of the top brick; this is the usual mode when the mortar joint is weaker than the units. The maximum stress for the numerical model was 2.35 N/mm^2, a difference of 7%.

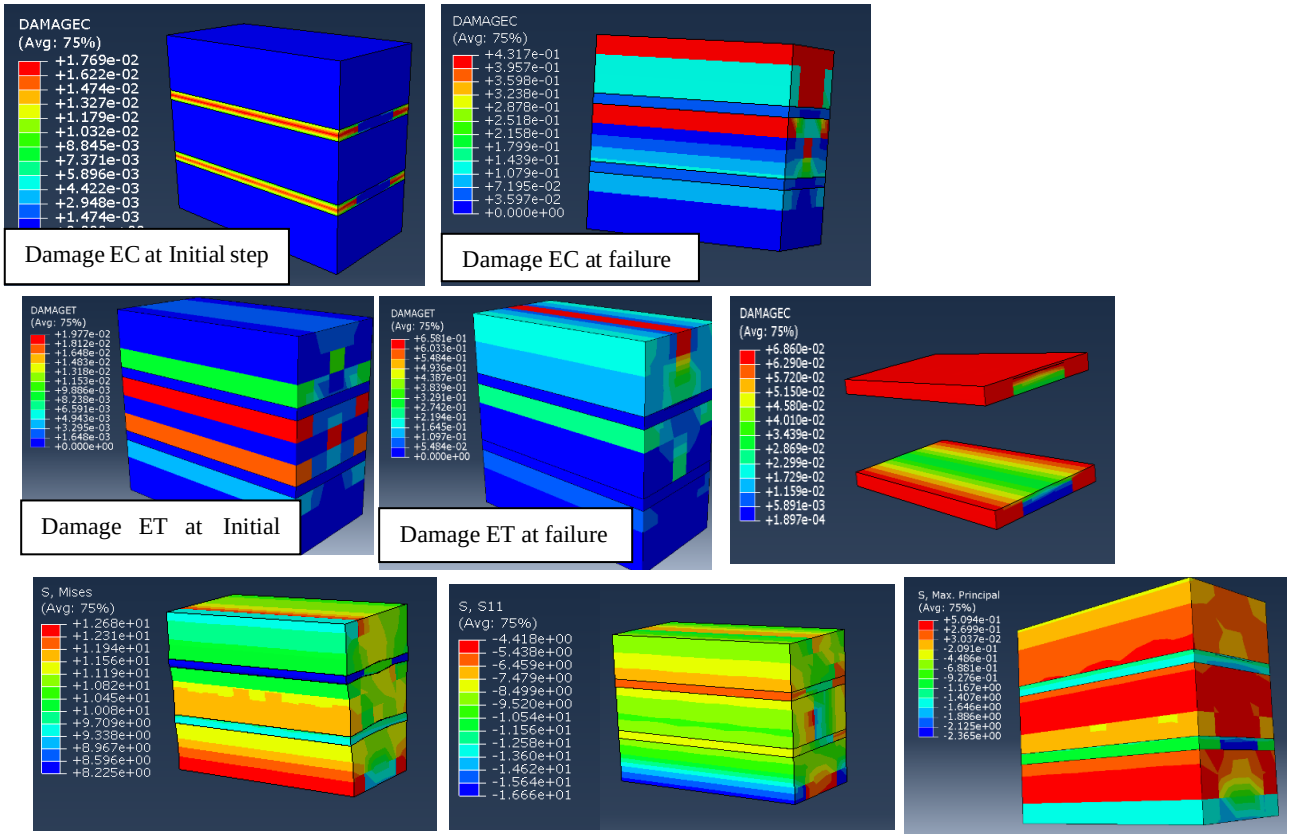

Figure 4.10 Stress contours for Masonry Compression prism : (a) Von Mises stresse ; (b) compressive stresses ; (c) maximal stresses

- ***Comparison between numerical and experimental results***

Figure 4.11 shows a comparison between the crack pattern developed in the numerical model and experimental test. These patterns that occurred in the mortar joint during the experiment and as predicted by the present model, are very similar, which is why the crack pattern of mortar and brick was in agreement. This proves that this proposed model of analysis can capture the compressive behaviour of masonry with sufficient accuracy in terms of the crack pattern (as confirmed by the damage contours) and the compressive strength (as demonstrated by the stress-strain curve).

A comparison between the results from the numerical model and experimental tests is given in **Erreur ! Source du renvoi introuvable.**in terms of stress-strain curves.Therefore, the resulting failure mode in the vertical plane was tensile splitting in the middle of the top brick; this is the usual mode when the mortar joint is weaker than the units.

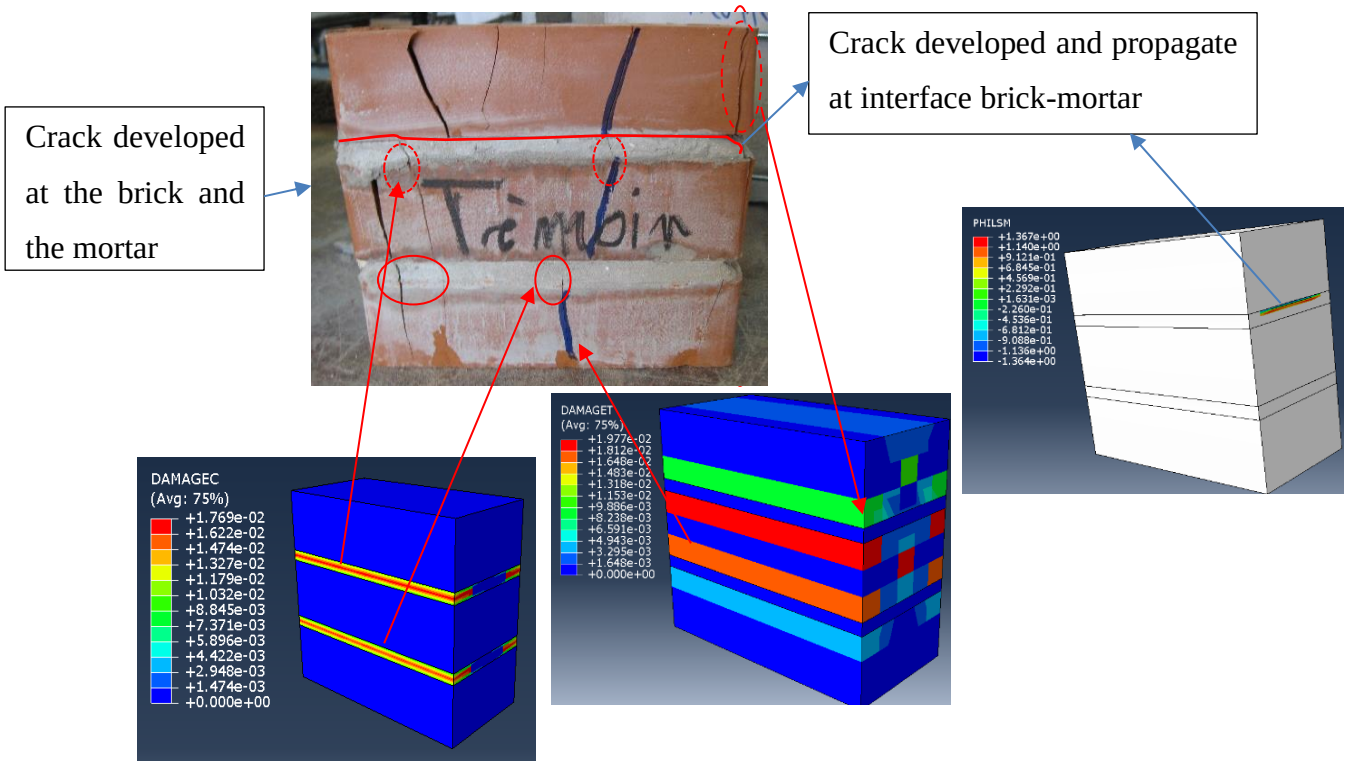

Figure 4.11 Comparison of failure modes developed in the numerical and experimental test.

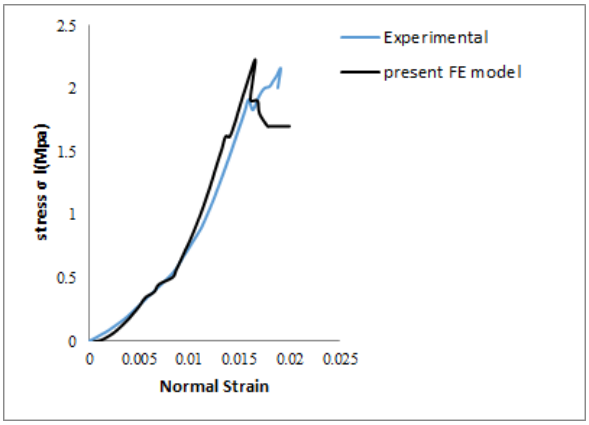

Figure 4.12 comparison of stress-strain values obtained from numerical simulation for compressive test

4.4.2 Finite element modeling of shear triplet prism (Unreinforced and reinforced shear triplet)

4.4.2.1 FE model descriptions

For the detailed micro-model of shear triplets, the incremental compressive load was applied at the top surface of the middle brick in terms of displacement. The bottoms of prism such as the bottoms of right and left units are restrained in the directions against the loading.The finite element mesh, boundary conditions, and loading of masonry assemblages are shown in Figure 4.13.

In this analysis (DMM), both the brick and mortar were modeled using eight-node 3D continuum elements with four glass controls and reduced integration (C3D8R). The nonlinear behaviour of brick and mortar was simulated with CDP model.

For applicate the XFEM approach modeling, the mortar was modeled as solid cohesive elements using the cohesive behavior parameters. The size of the elements used for modeling the mortar is uniform with a thickness of 10mm which represented the real thickness of the joint. The unit-mortar interface was modelled as a cohesive interface with zero thickness using the surface-to-surface contact option available in ABAQUS /implicit.

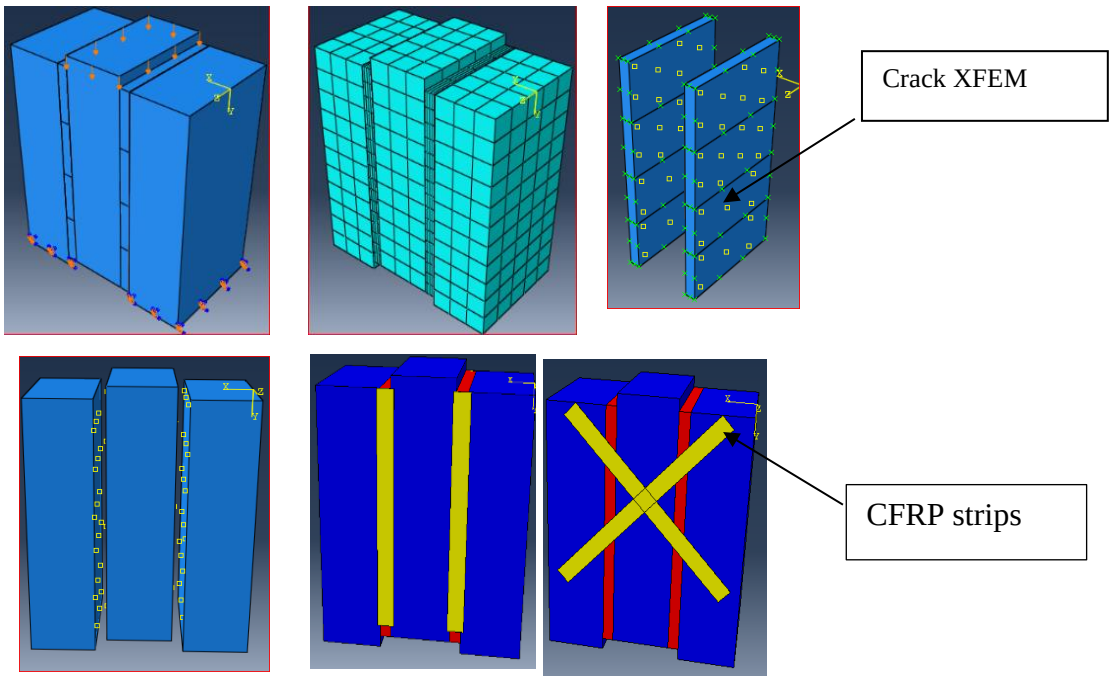

Figure 4.13 Shear triplet test: Geometry of assemblages, boundary and loading conditions; meshing, surface-based Interaction

- ***Comparison between numerical and experimental results***

As shown in Table 4.6, the numerical models could predict the shear strength of the shear triplet test, but not when the compressive stress was 1 MPa; here the numerical value was greater than the experimental value. This error is probably due to the bricks being cracked before use.

Figure 4.14 shows the distribution of shear stress and principal stress, and the damage and STUXFEM of unreinforced shear triplets at different levels of pre -compressive normal stress. There was no splitting at the mortar joint when the pre-compression was 0.6 and 1 MPa, however, the tensile damage at the bottom of the right-hand brick increased when the pre-compressive stress increased.

Figure 4.15 shows a comparison between the failure modes developed in the numerical model and experimental test. In this figure the initiation and propagation of cracks obtained experimentally by Abdou et al [38], Fouchal [137] and numerically by Sarhosis and Lemos [138] were compared with the present work. The crack patterns observed in the mortar joint during the experiment and predicted by proposed model were similar, which is why the pattern of cracks in the mortar and the bricks was similar; this means the numerical model can capture the failure mode with sufficient accuracy.

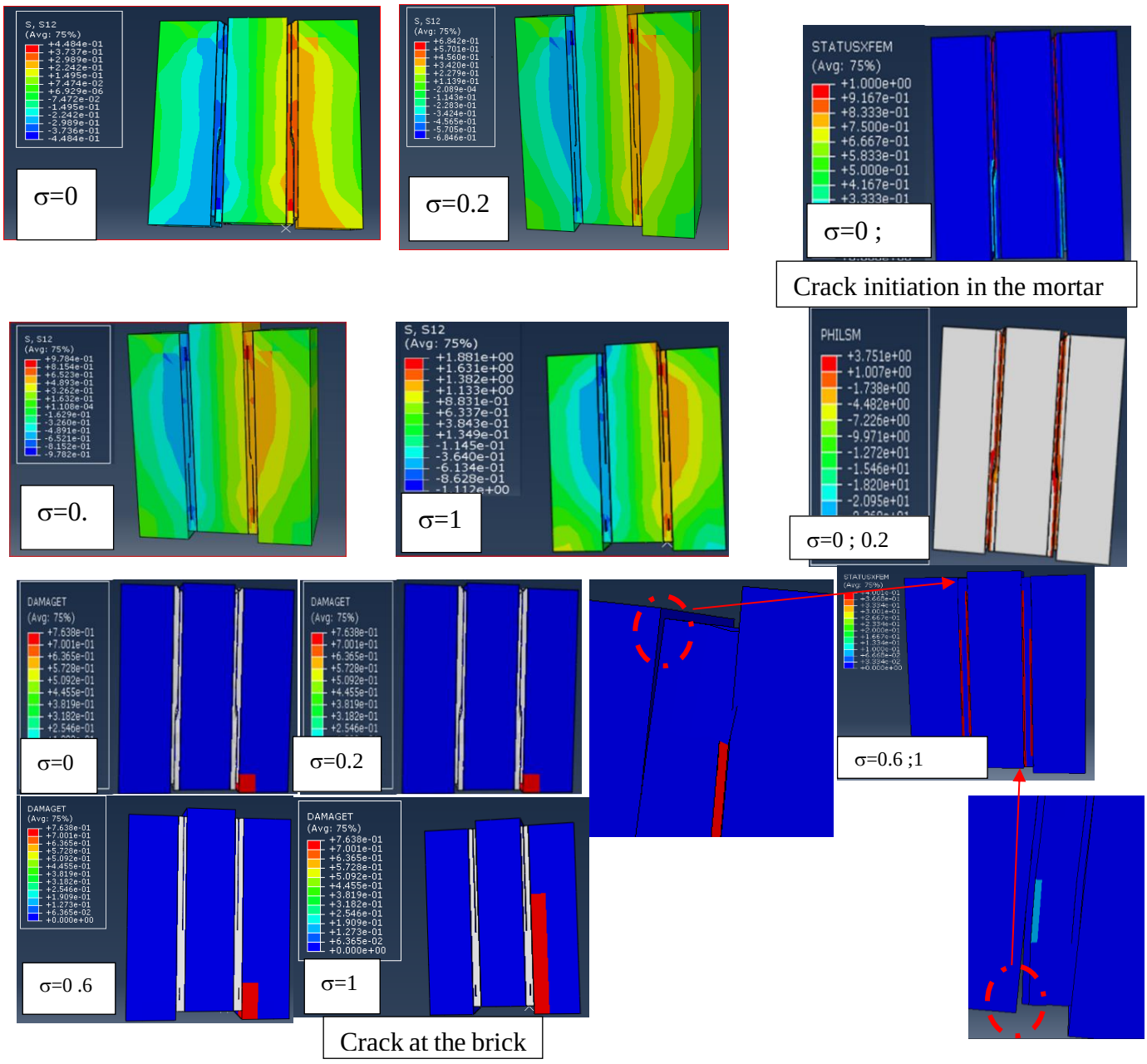

Figure 4.14 shear stress distribution σ12, principal stress, DAMAGET and STUXFEM for unreinforced shear triplets for different levels of compressive normal stress (0, 0,2; 0.6 ;1) MPa respectively

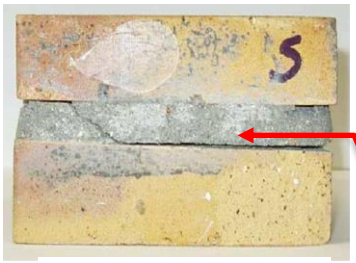

a. Characteristics of shear strength tests
(Abdou et al,2006)

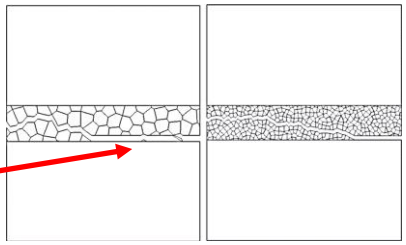

b. Failure mode as obtained from the numerical
for different in size Voronoi elements
(V. Sarhosis and al,2018)

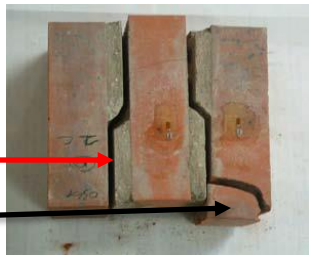

c . Shear test on the hollow brick triplet
(Fazia Fouchal 2006)

Crack of diagonal

Crushing of the brick

d . failure mode obtained in present work

e . failure mode obtained in this work

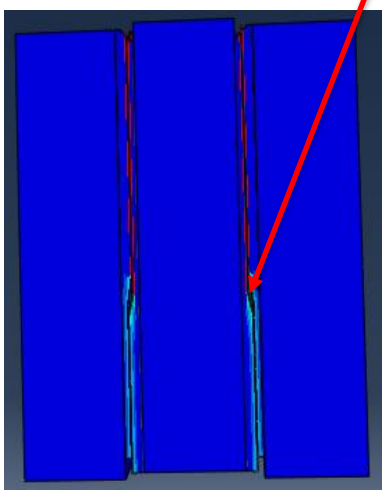

f. failure mode obtained in the present work
(Numerical model)

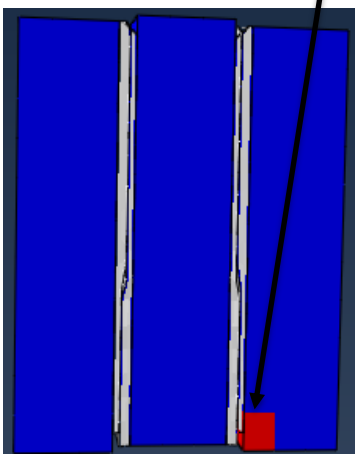

g . failure mode obtained in the present work
(Numerical model)

Figure 4.15 Comparison of failure modes developed in the numerical and experimental test:(a,b,c) experimental and numerical failure patterns cited in the literature ;(d,e,f,g) experimental and numerical failure modes for present work

- ***The Effect of energies fracture and mesh size of the mortar joint***

A finer mesh will give more accurate results but the CPU time will increase accordingly, therefore a sensitivity analysis was carried out to find a mesh that would considers accuracy and CPU time. The bricks were given a coarser mesh and a dense mesh was given to the mortar. Three different size meshes were proposed for the sensitivity analysis. The stress-strain response obtained for each mesh is shown in Figure 4.16. this figure shows the effect of element size on the predicted maximum shear strength in the controlled shear triplet. The different load-displacement curves converged well when the mesh sizes varied between 1mm, 2mm and 2.5mm. The difference between the 1mm mesh and the 2.5mm mesh is 0.22%. The results indicate (see Table 4.7), that the simulations are very sensitive to the varying values of the mesh size, so on a scale of accuracy the 2mm mesh was used for all the modelling in the remainder of the study. For non-linear analysis, a mesh that is too dense (<1mm) requires a long run time and a lot of computer memory so the analyses were aborted after failure due to convergence errors. This analysis also showed that when the number of mesh sizes (MS>5) increases there are convergence problems in the numerical solutions and the results are wrong. The effect of fracture energy shown in Figure 4.17 indicates that the maximum shear strength obtained in the numerical analyses is not sensitive to the variation of fracture energy (mode I and mode II). Nevertheless, when the value in each pure mode (I and II) was reduced, there was a slight change in the level of principal crack propagation.

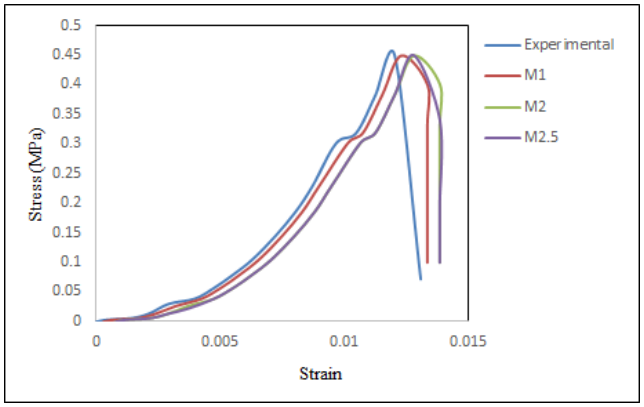

Figure 4.16 Mesh Sensitivity Analysis of shear triplet with zero confining stress

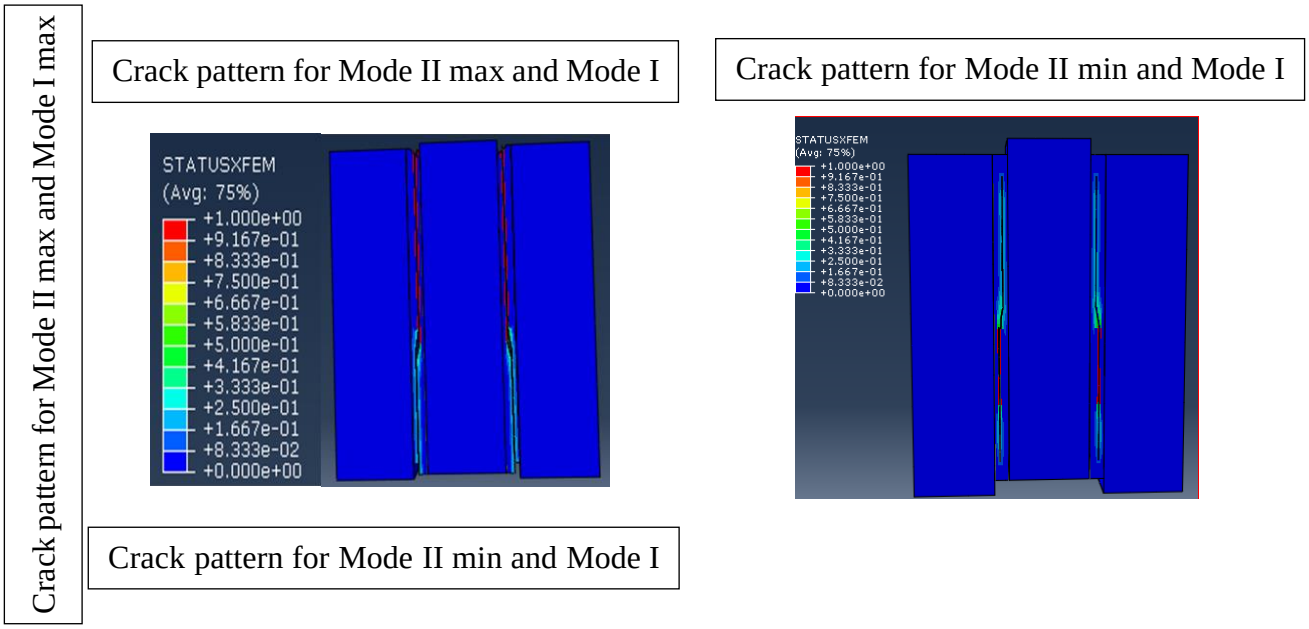

Figure 4.17 effect of energies Fracture in the location of damage in shear triplet model

The shear stress and principal stress distribution at the CFRP reinforced triplet is shown in Figure 4.18. It can be seen that the shear failure of this masonry specimen can be eliminated CFRP reinforcement; this proves that that CFRP reinforcement helped to support the tensile force at the bed joints. With the reinforced shear triplet, some cracks observed in the numerical study differed from the experimental program. This was probably due to numerical simplification because all the mortar joints with mechanical properties and the same thickness cannot be done experimentally. The debonding of CFRP composite was predicted by the contact opening parameter (COPEN), in fact according to this parameter the proposed contact models performed well enough to capture the location of debonding of the CFRP composites.

The STUXFEM for all the reinforced specimens shown in Figure 4.18 shows that CFRP reinforcement prevented the cracks from extending through the mortar joint; this increased the bearing capacity by transferring the rupture to the brick units. The ductility obtained in the experimental test was less than predicted by the numerical model, as

Table 4.*8* indicates. Moreover, the numerical model overestimated the shear strength but by less than 17%, possibly due to the selected contact model between the CFRP and masonry elements. The fracture energy and mesh size for mortar were considered in the analysis, with the fracture

energy Gf_1 (mode I) and fracture energy Gf_2 (mode II) being in the following ranges, 0.005 to 0.02 and 0.2 to 0.25N/mm. The mesh sizes used for the model were in 1mm, 2mm and 2.5mm intervals, depending on the thickness of the mortar.

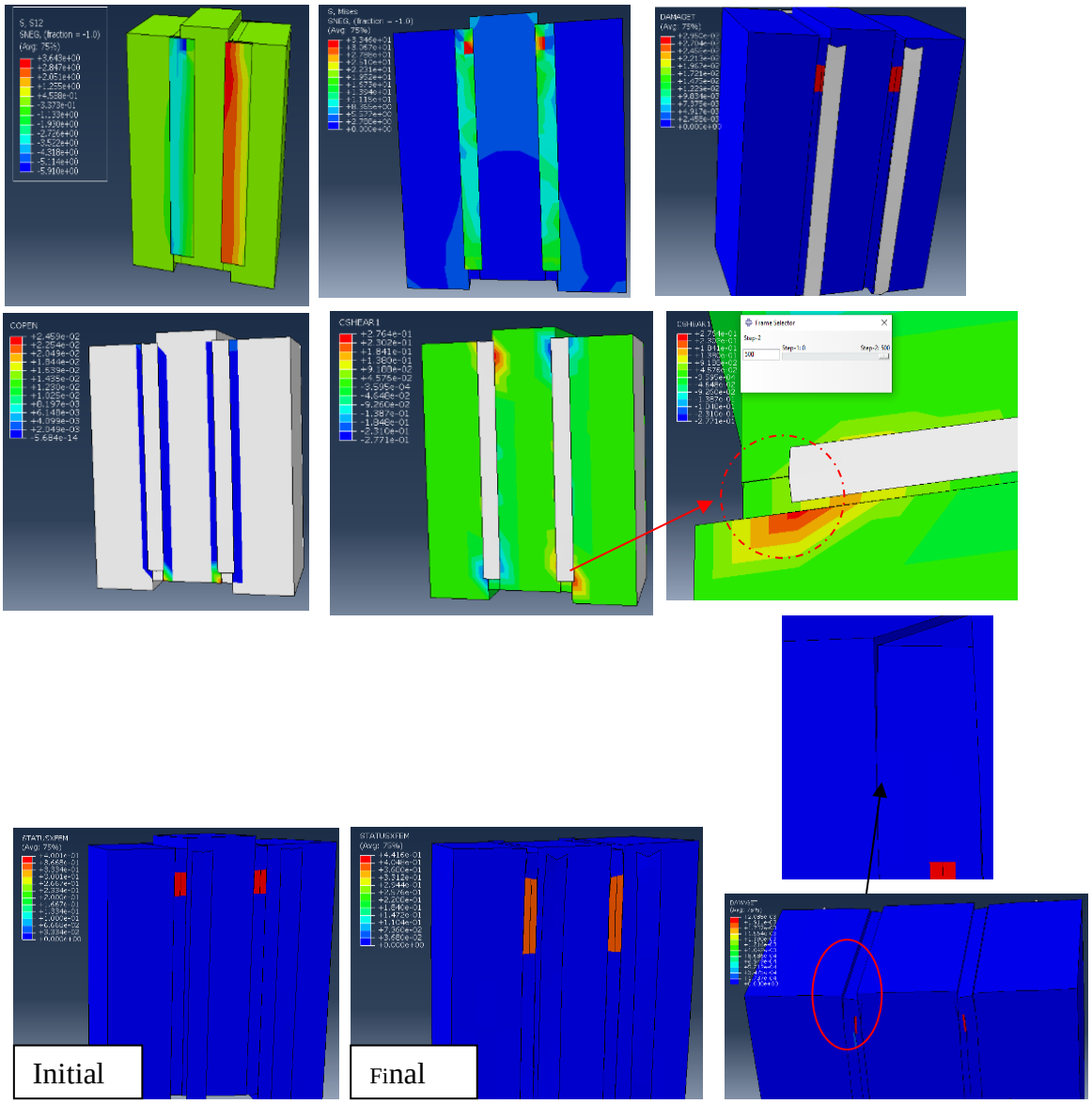

(a) Retrofitted with CFRP strips parallel to mortar joint

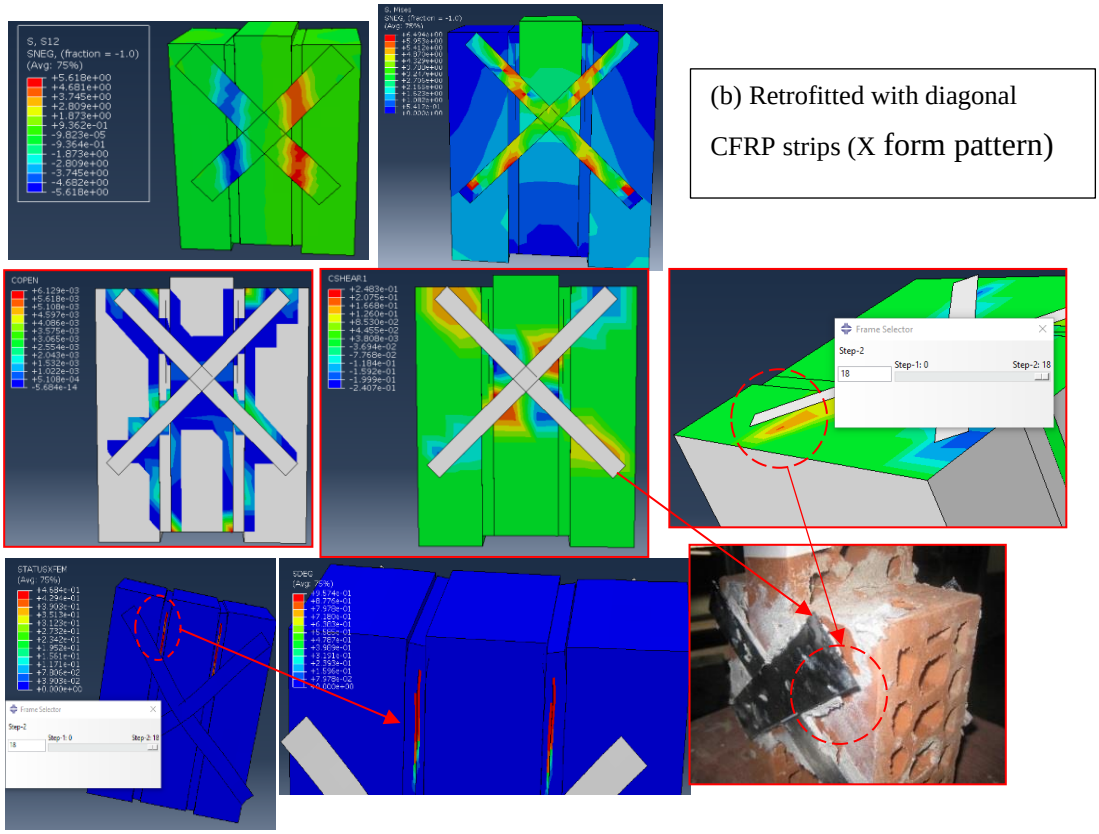

Figure 4.18 Shear stress distribution σ_{12}, principal stress; Contact opening (COPEN); contact shear (CSHEAR) and STUXFEM for reinforced masonry walls with different configuration of FRP strips

Table 4.6 Comparison between numerical result with experiment data

Horizontal stress σ_n (N/mm^2)	Experimental results τ (N/mm^2)	Numerical results τ [N/mm^2]	Difference (%)
0 N/mm^2	0.44	0.44	0 %
0.4 N/mm^2	0.9	0.86	4.65 %
0.8N/mm^2	1.06	0.97	9.27 %
1 N/mm^2	1.62	1.88	16 %

Table 4.7 Mesh convergence results

Mesh size (mm)	Numerical results τ (MPa)	Experimental results τ (MPa)	Time(secs)	Difference (%)
2.5	0.439	0.44	3600	-0.22 %
2	0.447	0.44	1200	1.59 %
1	0.440	0.44	7200	0 %

Table 4.8 Numerical and experimental results of shear triplet without /with retrofitting CFRP strips

Specimens	Experimental				Numerical			
	τ_u (N/mm^2)	δ_u (mm)	δ_e (mm)	$\mu = \frac{\delta_u}{\delta_e}$	τ_u (N/mm^2)	δ_u (mm)	δ_e (mm)	$\mu = \frac{\delta_u}{\delta_e}$
ST	0.44	0.012	0.012	0	0.44	0.012	0.012	0
SRV	0.5	0.014	0.015	0,93	3.64	0.018	0.015	1.2
SRX	0.6	0.017	0.009	1,88	4.11	0.02	0.01	2.0
SR2X	1.1	0.019	0.008	2,37	5.61	0.03	0.01	3.0
ST	0.44	0.012	0.012	0	0.44	0.012	0.012	0

Where,
τ_u = ultimate shear strength
δ_u = Maximum shear deformation
δ_e = elastic shear deformation
μ = ductility

4.4.3 FE model of CFRP reinforced brick masonry Wallette (square panel) subjected to diagonal compression (MTB)

4.4.3.1 Presentation of the numerical model

To validate the model proposed in this study, the same masonry wallette that which was studied in the experimental part was chosen (MTB).

In this model, the specimens wallettes were modeled using eight-node 3D continuum elements with four glass controls and reduced integration (C3D8R). Different mesh sizes were utilized for wallettes to predict the ultimate post-peak response. However, coarser meshes with element size in the order of 20–30 mm resulted in a better prediction of post-peak response.

The nonlinear behaviour of brick and mortar was simulated with CDP model. The CFRP composite fabric/sheet was modeled using four noded 3D shell elements (S4R) with three translational and rotational degrees of freedom at each node. It was modelled in ABAQUS using the lamina material properties.

To capture the behaviour of the bond between FRP and the masonry wall, especially those that debonded, an interface model was chosen in order to accurately model the masonry wall strengthened with FRP. The debonding of CFRP and the contact region between CFRP and the masonry wallette was modelled using surface-based cohesive behavior. The unit-mortar interface was modelled as a cohesive interface with zero thickness using the contact general available in ABAQUS /explicit.

Figure 4.19 shows the geometry and loading condition for the FE model that has been implemented using ABAQUS. in this section, the ABAQUS/ explicit method was adopted to solve the models proposed.

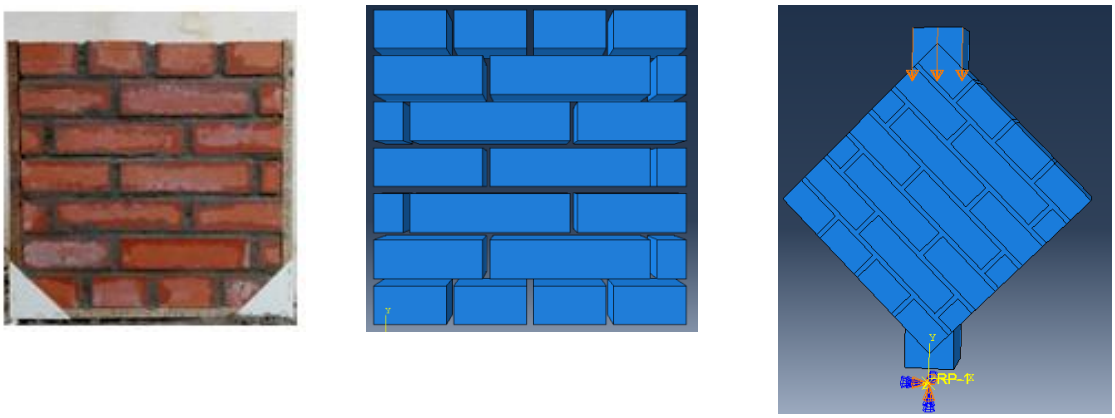

Figure 4.19 numerical Model (DMM) and boundary conditions of unreinforced brick masonry wall

It is meriting to notice that for the estimation of lateral in-plane shear strength of wallette a correction factor is used to the Mohr-Coulomb parameters i.e. c and μ. It is due to the experience

that these parameters are obtained from tests at the local level. Their correction for resistance evaluation of wallette is necessary ([34]).

$$k = \frac{1}{\left(1 + 2\mu\frac{\Delta_y}{\Delta_x}\right)} \qquad (4.45)$$

where k denotes the correction factor; Δx represents the length of the brick; Δy represents the height of the brick; μ represents the friction coefficient. The new parameters can be determined then as follow: $c_{new} = c \times k$ and $\mu_{new} = \mu \times k$.

4.4.3.2 Comparison of results and discussion

The response obtained from developed model is illustrated by predict of ultimate shear stress, collapse mechanism and failure mode of CFRP-reinforced wallette. Figure 4.20 shows the numerical and experimental curves of the stress-strain relationship of unreinforced walls (MTB). The numerical results show a good agreement with the experimental results concerning not only at the initial rigidity of the elastic phase but also from the non-linear phase to the post peak response corresponding, but with a value from the numerical stress to the higher peak than the experimental value. Through these results show that the technique proposed in this study gives a good result to analysis the brick masonry wall behavior.

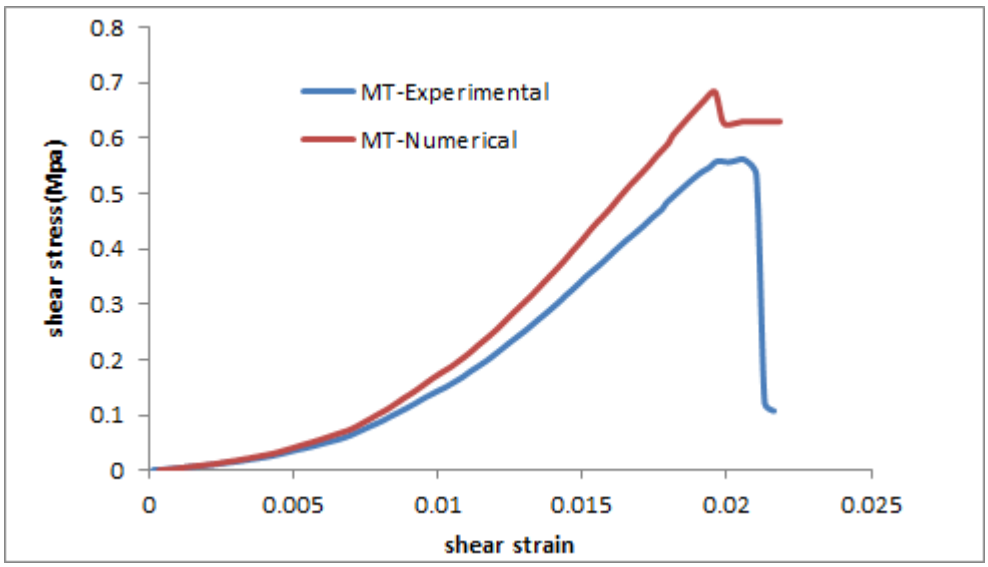

Figure 4.20 Confrontation of curves (σ – ε)

- **Crack pattern and mode failure**

Figure 4.21 shows the initial cracking occurs along the bed and head mortar joints in a diagonal (initial step). As the vertical loads increase, more cracks occur in the mortar joints of wall from top to down. After that, cracks appear and propagate in the brick directly in final step. same mode of rupture was found experimentally.

Figure 4.22 show a comparison of the crack pattern developed in the numerical and experimental test for the masonry wall MTB. The crack patterns observed in the mortar joint and brick during the experiment test and predicted by FE model resemble each other to a good extent. A good confrontation was found not only at the crack pattern of mortar but also from the brick. However, sometimes there are position of numerical cracks at the brick differs from experiments test, this can be explained by the numerical simplification which consists in considering that all the mortar joints have the same thickness, the same mechanical characteristics, which is not assured experimentally.

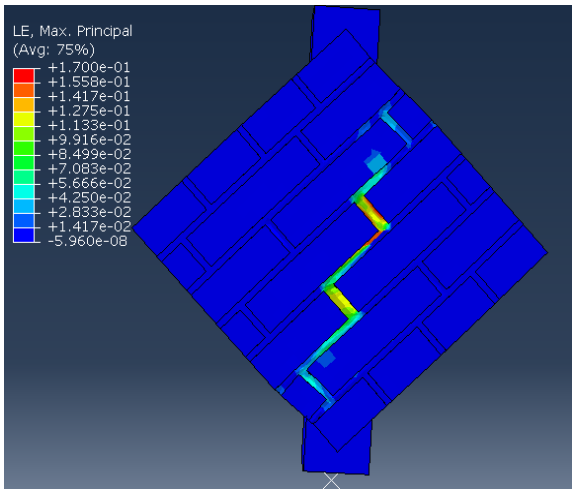
LE, Max. Principal
(Avg: 75%)
+1.700e-01
+1.558e-01
+1.417e-01
+1.275e-01
+1.133e-01
+9.916e-02
+8.499e-02
+7.083e-02
+5.666e-02
+4.250e-02
+2.833e-02
+1.417e-02
-5.960e-08

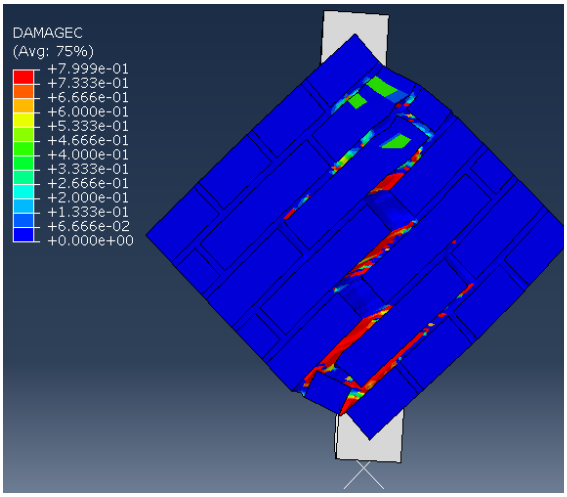
DAMAGEC
(Avg: 75%)
+7.999e-01
+7.333e-01
+6.666e-01
+6.000e-01
+5.333e-01
+4.666e-01
+4.000e-01
+3.333e-01
+2.666e-01
+2.000e-01
+1.333e-01
+6.666e-02
+0.000e+00

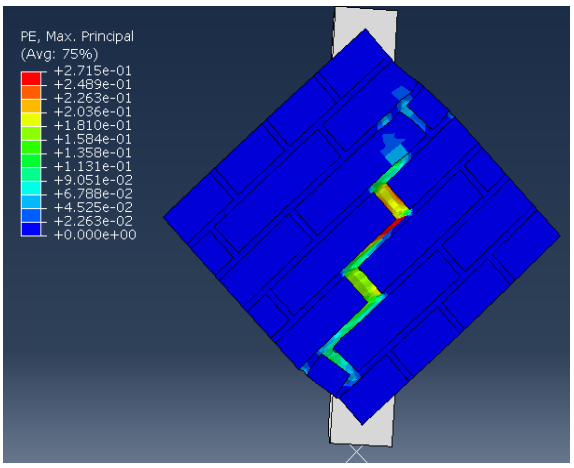
PE, Max. Principal
(Avg: 75%)
+2.715e-01
+2.489e-01
+2.263e-01
+2.036e-01
+1.810e-01
+1.584e-01
+1.358e-01
+1.131e-01
+9.051e-02
+6.788e-02
+4.525e-02
+2.263e-02
+0.000e+00

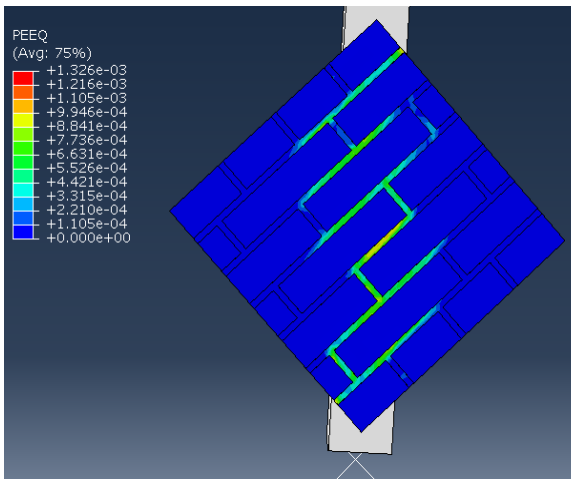
PEEQ
(Avg: 75%)
+1.326e-03
+1.216e-03
+1.105e-03
+9.946e-04
+8.841e-04
+7.736e-04
+6.631e-04
+5.526e-04
+4.421e-04
+3.315e-04
+2.210e-04
+1.105e-04
+0.000e+00

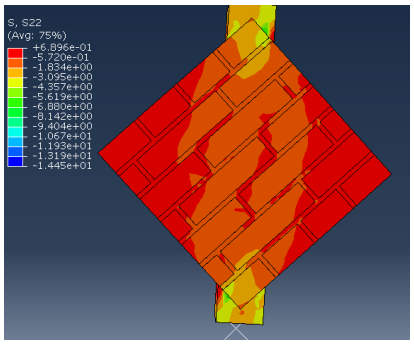
S, S22
(Avg: 75%)
+6.896e-01
-5.720e-01
-1.834e+00
-3.095e+00
-4.357e+00
-5.619e+00
-6.880e+00
-8.142e+00
-9.404e+00
-1.067e+01
-1.193e+01
-1.319e+01
-1.445e+01

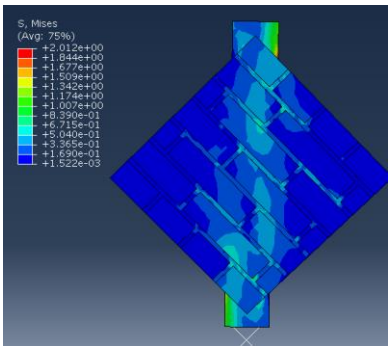
S, Mises
(Avg: 75%)
+2.012e+00
+1.844e+00
+1.677e+00
+1.509e+00
+1.342e+00
+1.174e+00
+1.007e+00
+8.390e-01
+6.715e-01
+5.040e-01
+3.365e-01
+1.690e-01
+1.522e-03

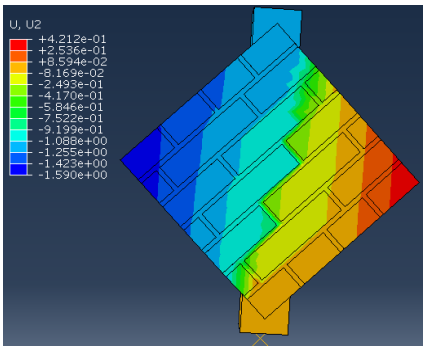
U, U2
+4.212e-01
+2.536e-01
+8.594e-02
-8.169e-02
-2.493e-01
-4.170e-01
-5.846e-01
-7.522e-01
-9.199e-01
-1.088e+00
-1.255e+00
-1.423e+00
-1.590e+00

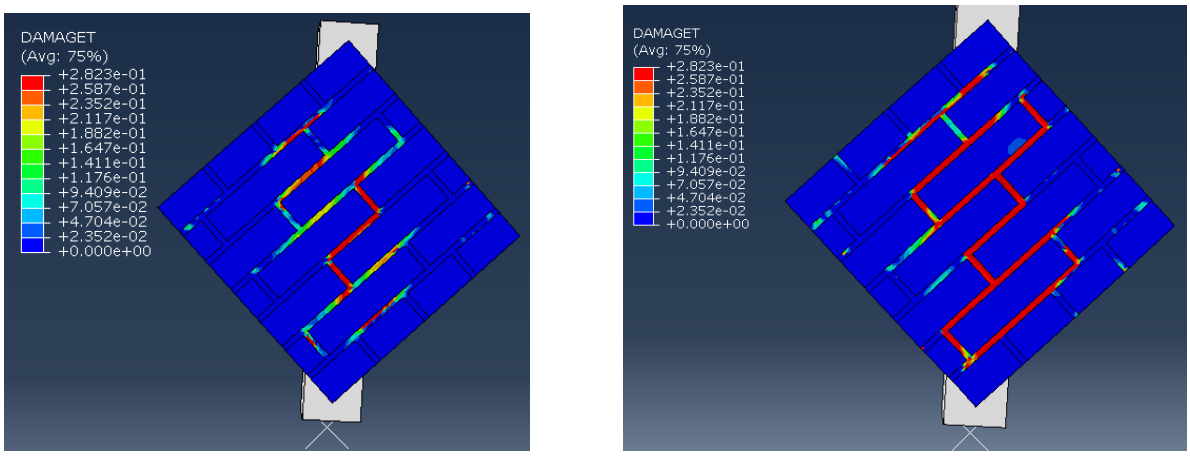

DAMAGET for Brick and Mortar at the initial of the step

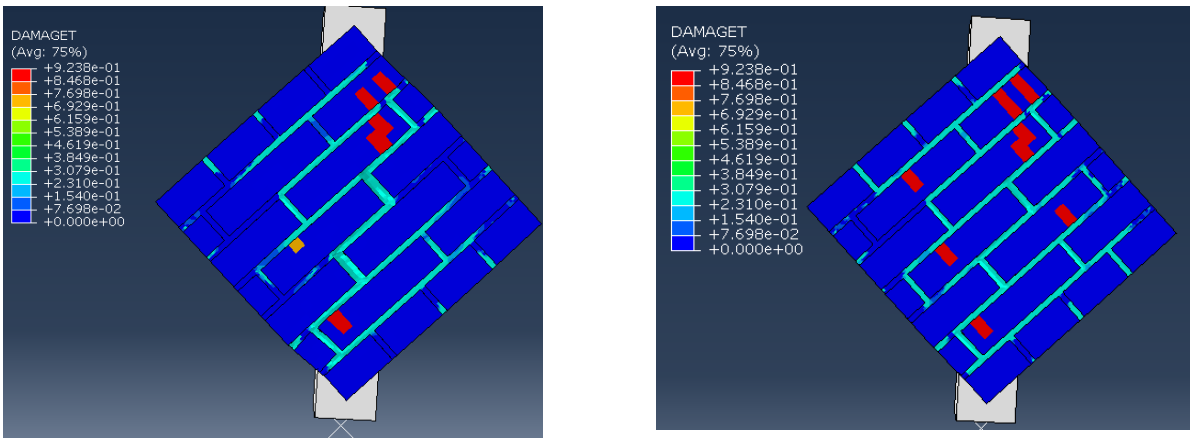

DAMAGET for Brick and Mortar at the end of the step

Figure 4.21 Von misses stress distributions, normal stress in the direction y (S22), Plastic strain distributions and evolution of damage (DAMAGET, DAMAGEC) in the unreinforced brick masonry wall MT

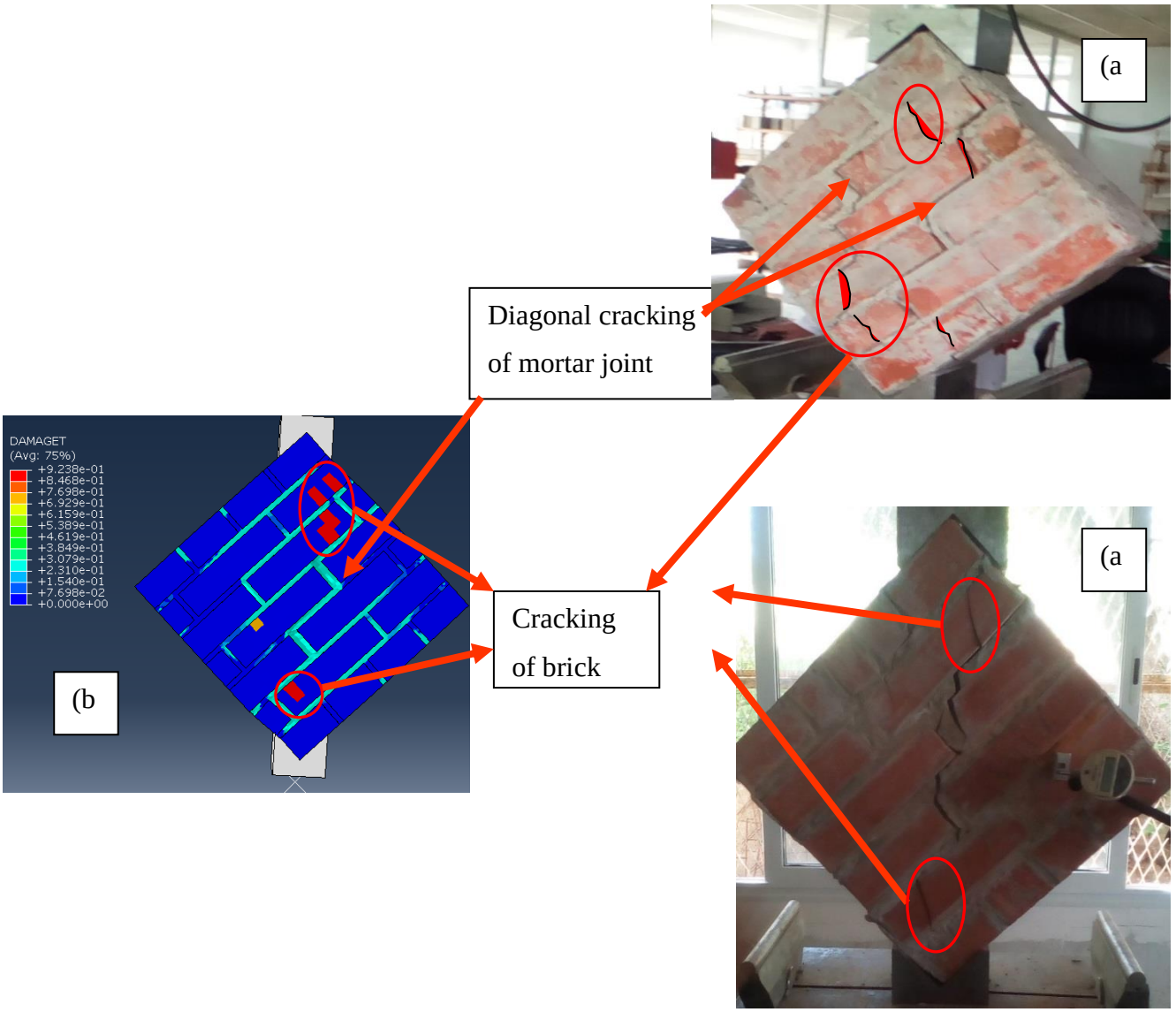

Figure 4.22 Comparison between the numerical and experimental results concerning the crack pattern for the unreinforced wall MT: (a) expérimentale crack pattern; (b) numérique crack pattern

- **Reinforced masonry wallettes**

The response obtained from developed model is illustrated by predict of ultimate shear stress, collapse mechanism and failure mode of CFRP-reinforced Wallette.

The improvements in ultimate shear stress of retrofitted masonry Wallette in comparison with controlled specimens is illustrated in Table 4.9. where reinforcement ratio is also shown. these results indicate that the proposed numerical models can well predict the ultimate shear strength of unreinforced masonry Wallette.in case of reinforced specimens, this model provide results higher than experimental model in terms of stress and displacement while the collapse mechanism was similar. this can be explained by inadequate Implementation method test for connecting the CFRP to masonry interface, and among them, preparation and brushing of a surface of contact before the application of epoxy resin. that required for this purpose more skilled labor by which is not assured experimentally. which might affect significantly the overall structural performance of the CFRP composite.

The typical cracking pattern at failure observed in the experimental test and that was obtained with a proposed model for all reinforced wallets (scheme 1, scheme 2, and scheme 3) is illustrated in Figure 4.24.This figure showing that the failure mode of all reinforced specimens was characterized by vertical tensile splitting cracks initiated at the middle web and spreading to the top and bottom of the specimen. Cracking initiation was observed to appear near the ultimate load (around 90% of ultimate load). as well a failure by tensile is localized in the support zone as result of brick and mortar failure. particularly for the specimens reinforced with scheme1 where a diagonal crack as well has appeared which progressed towards the supports in compressed diagonal direction. diagonal Cracking disappeared in both configuration (scheme 1, scheme 2) assures us the composite material limits the cracking propagation in masonry wallets.

The Predicted crack pattern of CFRP-to masonry interface with cohesive surface damage (CSDMG) distribution are show in Figure 4.24, for scheme 1 the failure of superficial layers of the bricks due to the use of shorter CFRP strips produces the pull-out of the CFRP strips. For the scheme 2 and scheme 3 the debonding starts to propagate rapidly at the end near to the external support. on the other hand, no debonding was observed in the CFRP composite which is placed at the middle of the wallet. these results evidencing that the detailed micro modeling strategy was able to reproduce the exact cracking pattern observed during the tests.

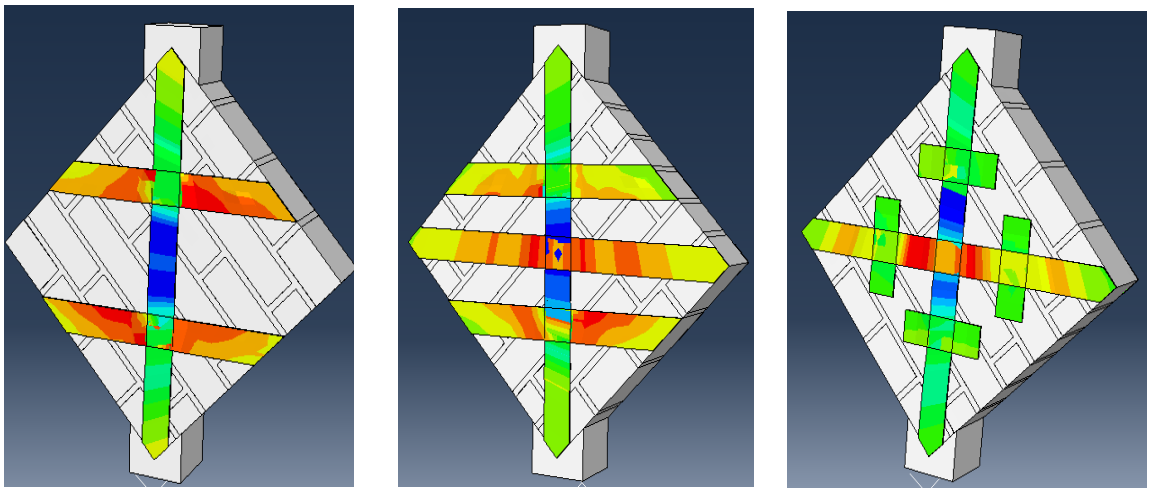

Figure 4.23 Principal stress distribution before the failure in all configurations of CFRP strengthened Wallette under diagonal compression

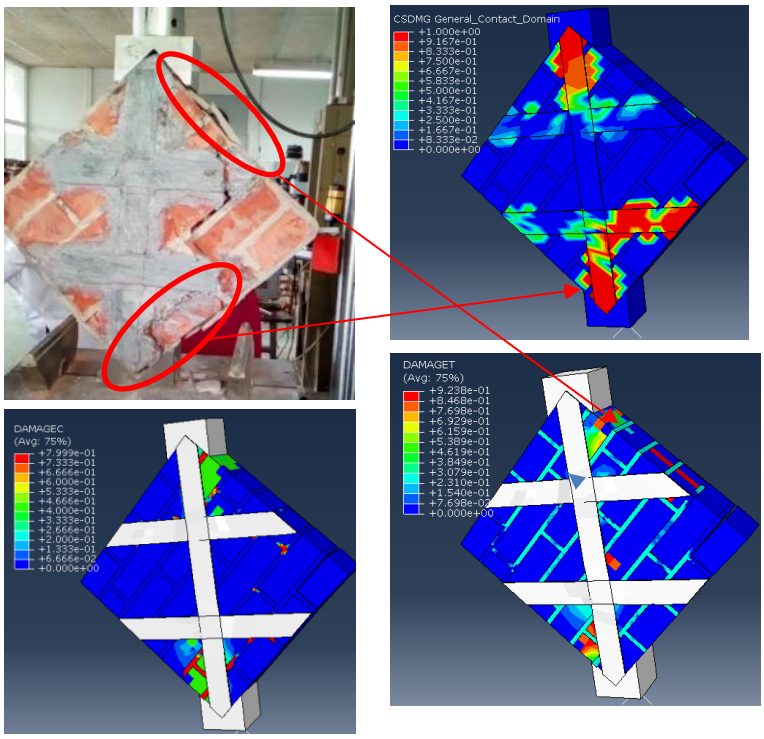

(a)

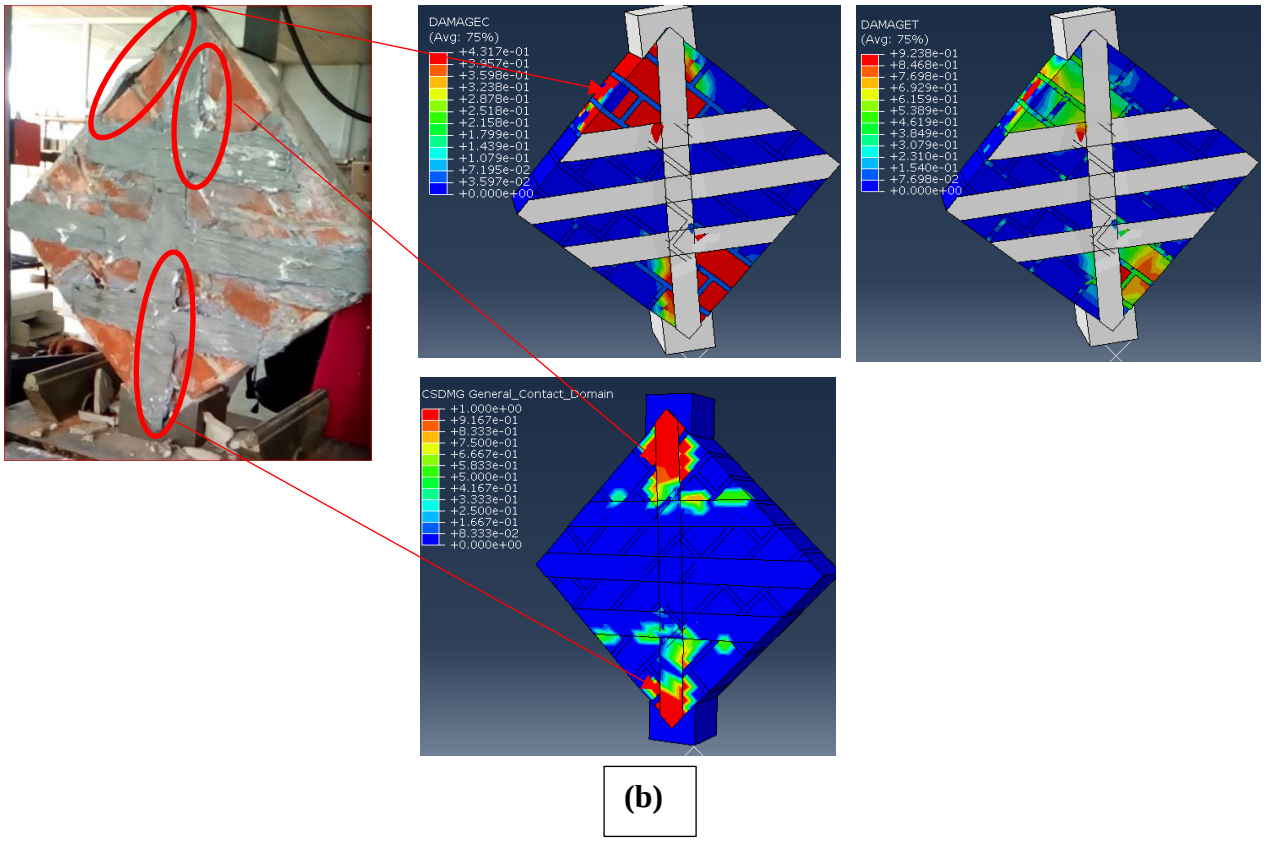

Figure 4.24 Predicted crack pattern of CFRP reinforced masonry Wallette at different configuration : (a) scheme 1, (b) scheme 2, (c) scheme 3

Table 4.9 comparisons of numerical result with experiment data

		Experimental results			Numerical results		
panels	fibers ٪	Fmax(KN)	τ(MPA)	εmax (%)	τ(MPA)	εmax (%)	Error %
MTA	0 ٪	35.063	0.56	0.019	0.56	0.02	0
MRH	54.68٪	57.583	1.85	0.058	2.64	0.07	0.42
MRX	54.06 ٪	55.274	1.82	0.022	2.58	0.023	0.41
MRI	22.91٪	50.455	1.59	0.028	2.08	0.033	0.30

4.4.4 FE model Unreinforced masonry panels subjected to uniaxial compression (θ = 90° and 45°)

4.4.4.1 Material parameters

The units and mortar joints are modelled using eight-noded 3D continuum elements with hour glass control and reduced integration (C3D8R), and the unit-mortar interface was modeled as a cohesive interface with zero thickness using the contact available in ABAQUS/explicit analysis. Furthermore, coulomb-frictional contact behavior is defined in this model. In this step, it is necessary to define two contact properties: Normal contact and tangential behavior. The nonlinear behavior of brick and mortar was simulated by using the CDP model.

4.4.4.2 Presentation of the numerical model

The numerical study will be limited to analysis the identical unreinforced brick masonry wallette (MCB and MTB) which was studied in the experimental part. Figure 4.25 shows the numerical simulation, the geometry, interaction surfaces between units and mortar and loading condition for the FE model that has been implemented using ABAQUS.

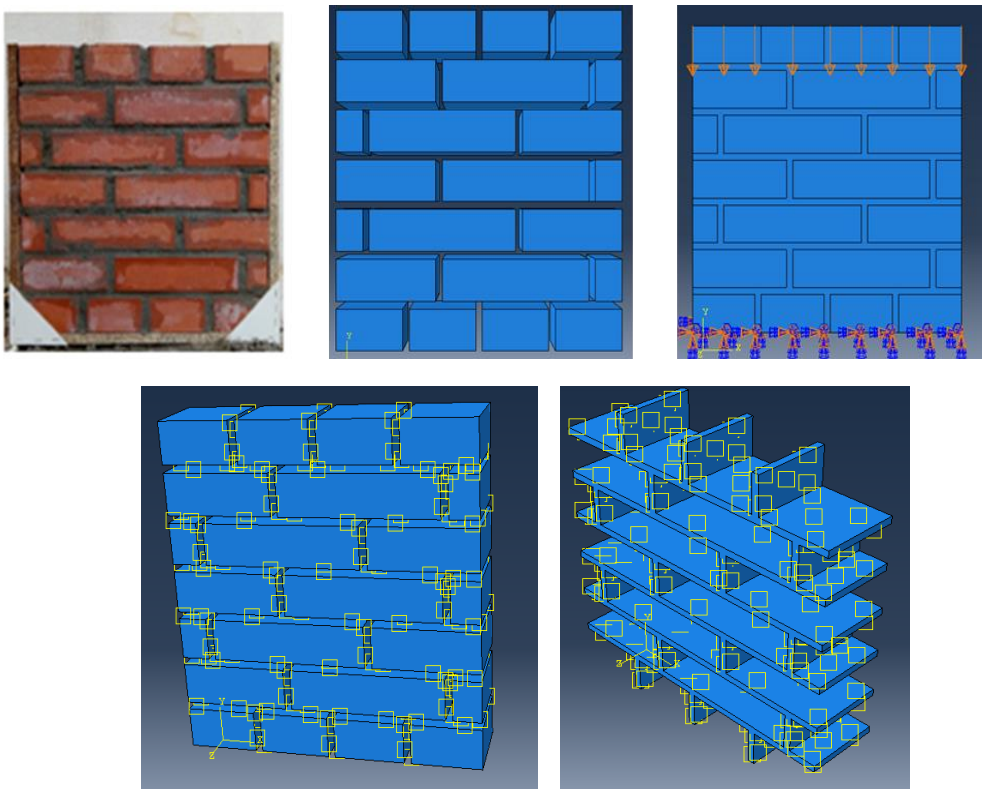

(a)

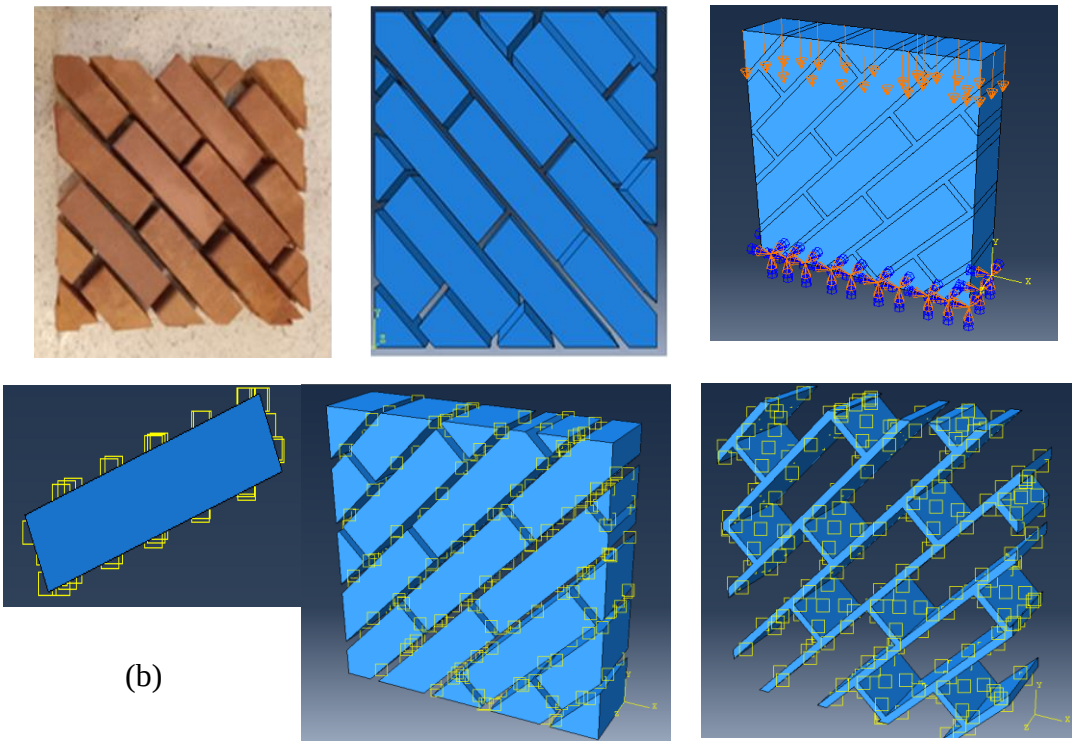

(b)

Figure 4.25 numerical model (DMM) and boundary conditions and interface contact of unreinforced brick masonry wall :(a) wall MCB (θ=90°); (b) wall MTB (θ=45°).

4.4.4.3 Comparison of results and discussion

The numerically predicted deformations and peak loads for each panel compared to the averaged experimental results are shown in Table 4.10.

Figure 4.26 shows the numerical and experimental curves of the stress-strain relationship of unreinforced walls (MCB, MTB). The numerical results show a good agreement with the experimental results concerning not only at the initial rigidity of the elastic phase but also from the non-linear phase to the post peak corresponding response. However, the values of numerical modeling are somewhat higher than that of the experimental results except the result of maximum strain for the wall sample MTB (θ=45°).

- **Crack pattern and mode failure**

For the wall subjected to uniaxial compression perpendicular to bed joint (MCB), the initial cracking occurs along the vertical mortar joint as an initial response. As the vertical loads increase, more cracks occur in the vertical mortar joints of wall from top to down. After that, cracks appear and propagate in the brick units directly as a final response which causes failure due to vertical cracking of the face shells of the wall masonry (see Figure 4.27). The same mode of rupture was found experimentally.

In wall panels MTB cracking occurred predominately through the bed and head mortar joints extended diagonally. With load increasing, the wall exhibited a gradual increase in the width of predominately diagonally oriented crack, followed by sliding along the diagonal parallel to bed joints. On the other hand, many cracks appeared at the level of brick (see Figure 4.28).

Table 4.10 comparisons of numerical result with experiment data

Wall	Experimental results			Numerical results		
	$F_{max}(KN)$	$\sigma_{max}(MPa)$	ε_{max}	$F_{max}(KN)$	$\sigma_{max}(MPa)$	ε_{max}
θ=90°(MCB)	100.11	2.226	0.0161	88.60	1.97	0.0159
θ=45°(MTB)	80.76	1.92	0.0143	67.20	1.60	0.0221

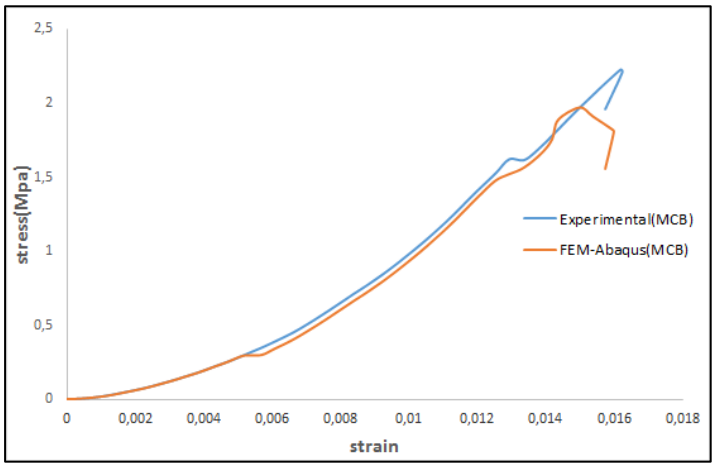

(a) unreinforced brick masonry wall MCB (θ = 90°)

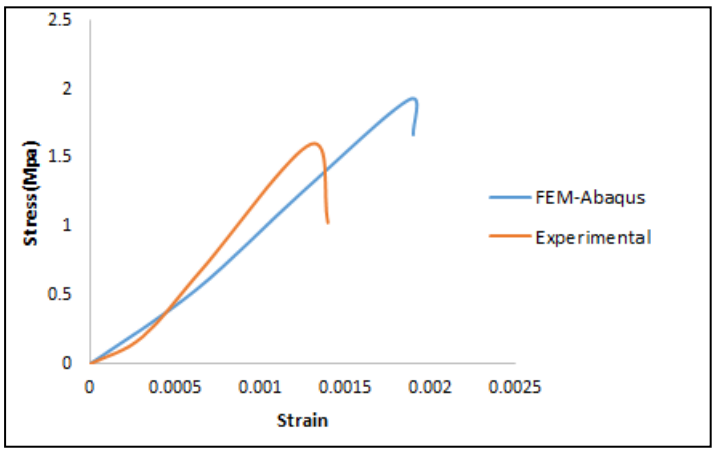

(b) unreinforced brick masonry wall MTB (θ = 45°)

Figure 4.26 Confrontation of curves (σ – ε)

Figure 4.29 shows a comparison of the crack pattern developed in the numerical and experimental test for the masonry wall MTB. The crack patterns observed in the mortar joint during the experiment and predicted by FE model resemble each other to a good extent. A good confrontation was found not only for the crack pattern of mortar but also for the brick units. However, sometimes there are position of numerical cracks at the brick differs from the experimental results, among them, crushing in the two extremities of the diagonal. This can be explained by the numerical simplification which comprises considering that all the mortar joints have the same thickness, the same mechanical characteristics, which is not assured experimentally.

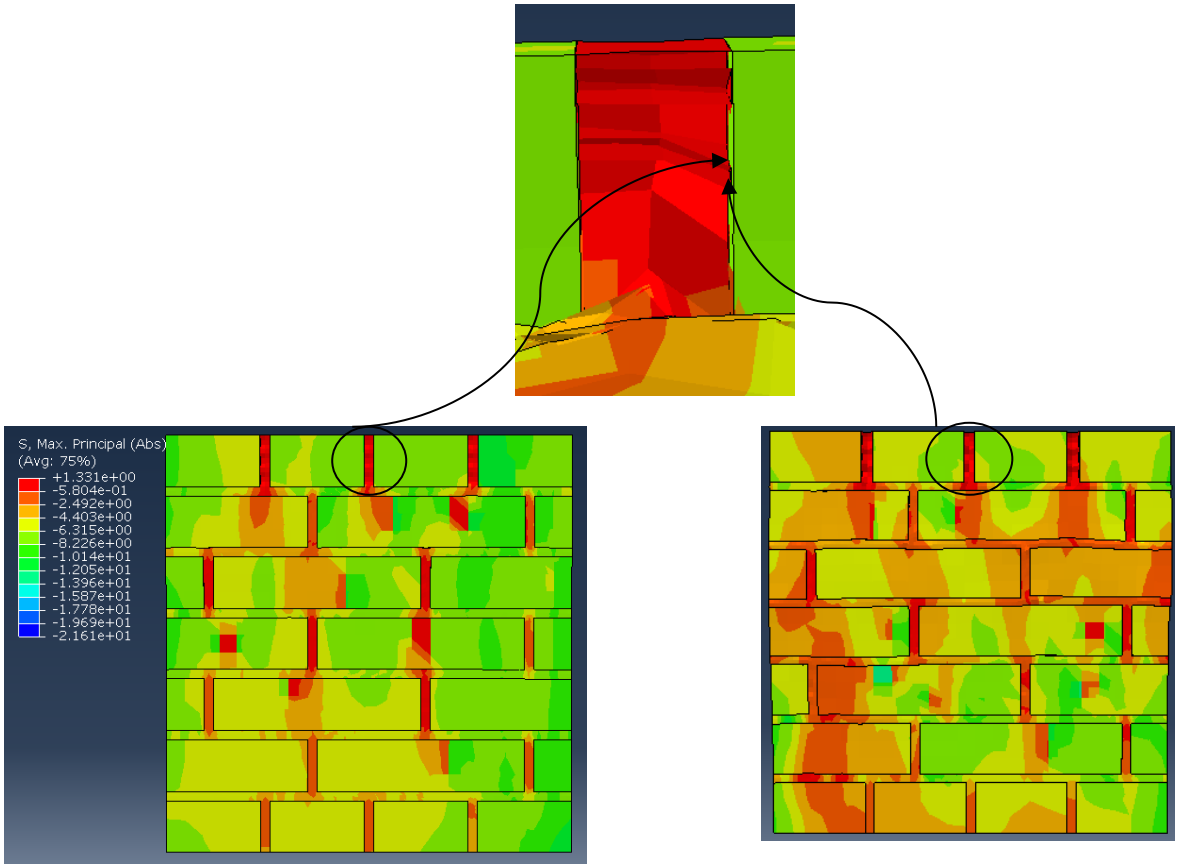

(a) (b)

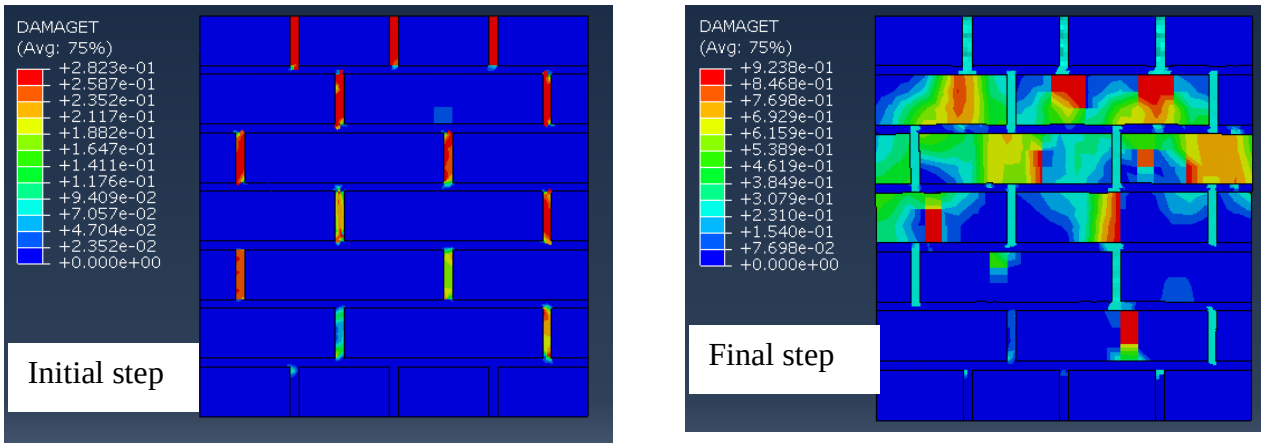

(c)

Figure 4.27 principal stress, normal stress in the direction y (S22) and evolution of damage (DAMAGET) in the unreinforced brick masonry wall θ = 90° (MCB)

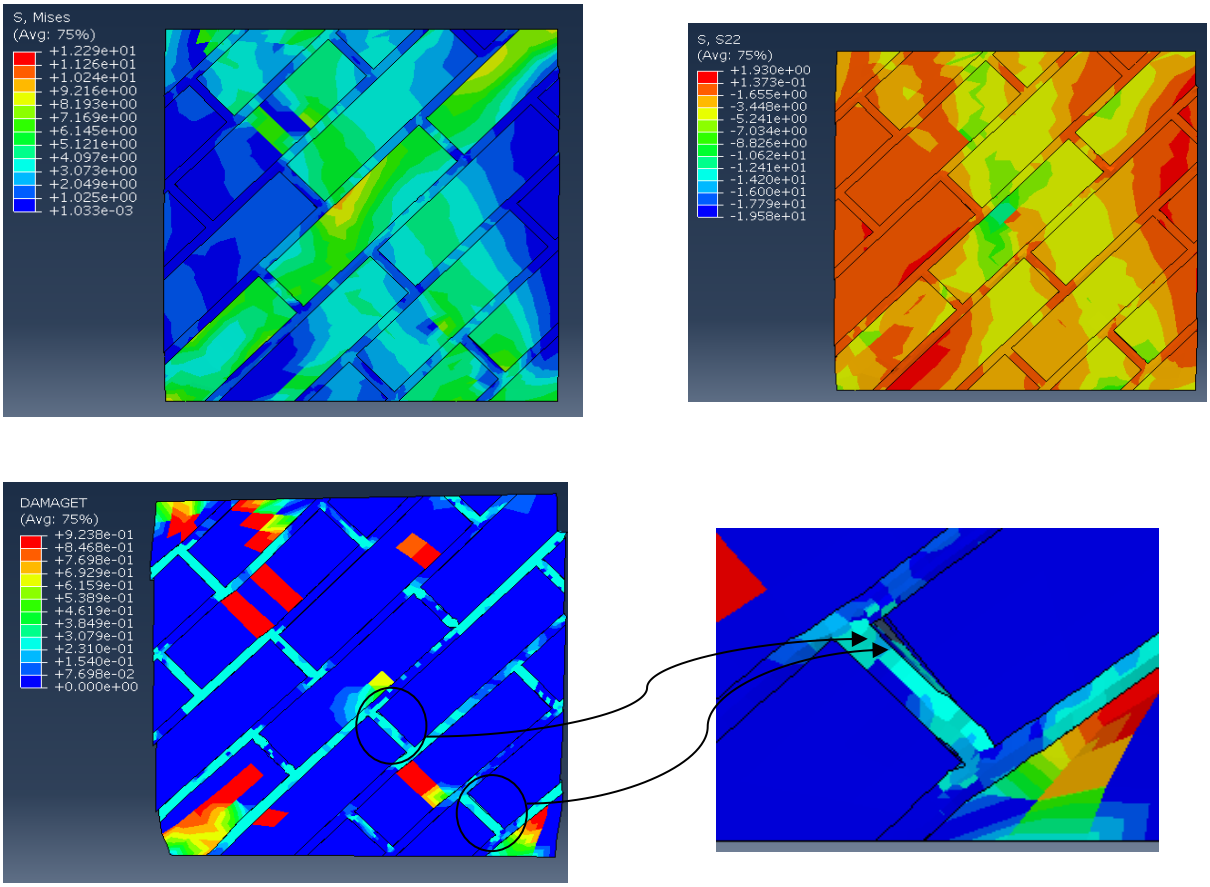

Figure 4.28 Von Mises stress, normal stress in the direction y (S22) and evolution of damage (DAMAGET) in the unreinforced brick masonry wall

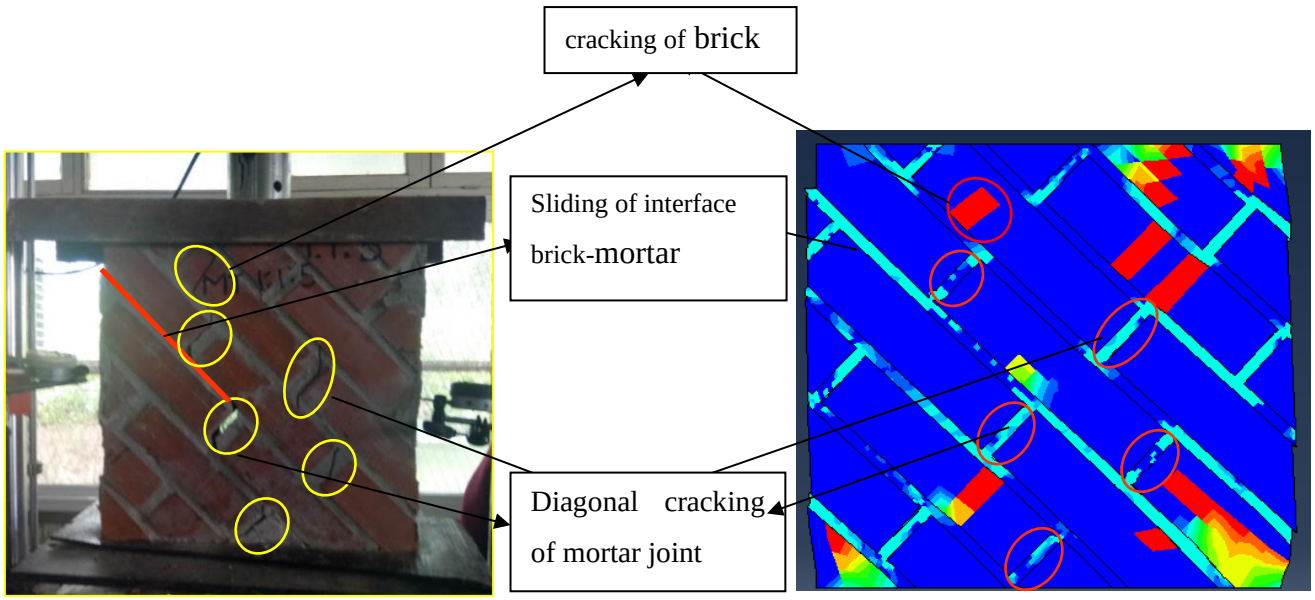

Figure 4.29 Comparison between the numerical and experimental results concerning the crack pattern for the unreinforced wall (MTB): (a) exprimental crack p4.30attern; (b) numerical crack pattern.

4.5 Conclusions

This chapter has presented a numerical model based on DMM approach using a concrete damage plasticity to simulate the unreinforced and CFRP reinforced masonry assemblages. the CFRP-masonry bonded joint was modelled using zero thickness interface elements. The FE model was calibrated using data obtained from the experimental test to validate the adapted FE modeling approach.

The comparison between FE model and test results indicates that the proposed model shows a considerable accuracy for the prediction of maximum shear load and failure mode.in addition, a good confrontation was found not only at the crack pattern of mortar and brick but also the model can accurately predict the CFRP-to masonry bond behavior.

Chapter 5

Conclusions and Recommendations

- **Summary of research**

There is significant potential for the use of FRP in the masonry industry, both in the construction and rehabilitation of older structures. In this thesis, two technique of reinforcing were used to study the behavior of strengthened brick masonry walls reinforced with externally bonded (EB-FRP) and NSM-FRP technique. The experimental program of this thesis focused on the in-plane shear behavior of FRP strengthened brick masonry assemblages under in-plane loading. For this purpose, four stages of testing were carried out.

The first stage three triplet specimens tested under axial compression. the compressive strength of three test specimen and value of elastic modulus were determined.

The second stage contains sixteen unreinforced and reinforced shear triplet specimens under different normal compressive stress levels, the frictional parameters shear (initial strength and friction angle of the unit-mortar interface), the fracture energy (mode II), the shear strength and the failure mode of unreinforced and strengthened masonry specimen were determined.

The third stage of experimental investigation consists of twenty masonry wallette tested under diagonal compression load to evaluate the influence of the type of joint mortar and location of the CFRP composites in the EB-FRP strengthened masonry walls.

At the final stage, the influence of the type of joint mortar, the behavior of unreinforced brick masonry under uniaxial loading with different orientations of the bed joints (45°, 90°), and NSM-CFRP reinforced brick masonry wall was studied.

Finally, a numerical model based on DMM approach was developed using FE software. The FE model was calibrated using data obtained from the experimental test to validate the adapted FE modeling approach. The constitutive models include surface-based cohesive behavior to capture the elastic / plastic behaviour of unit-mortar interface, cohesive element to simulate the FRP-to masonry bond behavior, and CDP model to simulate the cracking and crushing of masonry units and mortar. The Extended Finite Element Method (XFEM) was used to simulate cracks propagation in the mortar without an initial definition of crack location.

Note that, the stress-strain response, ductility response in all specimens tested and failure patterns were determined at each stage. The results are in close agreement with test results.

This chapter presents a summary of and conclusions drawn from the work presented in this thesis. Suggestions for further work in this research area are proposed.

- **Conclusions**

The results obtained from both the experimental and numerical studies led to the following main findings:

1. The increase in the proportion of sand in the mortar from 3 to 5 led to an increase in the shear strength and the ductility of the masonry panels, especially in the case of reinforcement masonry walls.
2. In the diagonal test, the improvement in shear strength for EB-FRP strengthened wall panels doubled from 3 to 4 times with a rate 65% to 270%.
3. All reinforced wall panels showed a considerable increase in the ductility from 73% to 88% compared to unreinforced wall panels.
4. The most important increase in ductility was achieved in wall panels reinforced by X shape with heels (MRX) on both sides. In addition, for the shear triplet test, the significant increase in ductility and bearing capacity was achieved by diagonal (X pattern) of CFRP reinforcement at both sides.
5. The developed model was proved to obtain the crack patterns and the stress distribution patterns in both brick and mortar.
6. The behavior of the masonry is strongly governed by that of the interface. The Coulomb friction criterion is important for the correct simulation of the load transmission between brick and mortar.

7. The good correlation between experimental and numerical results allows this model to be used in further studies of all types of unreinforced or reinforced masonry structures.
8. The shear strength of unreinforced and reinforced masonry wall panels oriented by 45° was mainly related to their compressive strength.
9. The compressive strength and shear strength of masonry panels were affected by E_{unit}/E_{mortar} ratio, even when this ratio was greater than one.
10. As the horizontal reinforcement restrained the opening of diagonal cracks, the sliding failures along single mortar bed joints caused by the horizontal reinforcement were prevented by the vertical reinforcement.
11. The use of CFRP strips improved the ductility and the bond strength of wall masonry, especially in the case of reinforcement on both sides of the panel.
12. The improvement in shear strength of strengthened wall panels with NSM CFRP strips increased from 1.3 to 2 times, i.e. an improvement rate from 123% to 196%.
13. The most significant increase in ductility was achieved by vertical NSM-FRP reinforcement on both sides of the wall panel.
14. The FRP did not completely separate at the ultimate load from the masonry wallette reinforced with (EB-FRP) technique, but remained attached at both ends.
15. From the masonry wallette reinforced with (NSM-FRP) technique no rupture of the CFRP strips was observed during testing or when the CFRP strips were exposed during demolition of the wallette. With increasing wall panel deformation, the debonding and pull out of the middle CFRP strips was not observed.
16. The Finite Element model proposed in this thesis showed a considerable accuracy for the prediction of maximum shear load and failure mode. The contact elements with cohesive behavior is suitable for the modeling of shear failure at interface.
17. The XFEM approach is suitable for the modeling of shear failure at interface and the crack propagation in the mortar.
18. The Concrete Damage Plasticity (CDP) model can effectively represent the damage and the compressive non-linear behavior of masonry brick units.
19. The results indicate that, the tensile stress is transferred from masonry to the CFRP strips leading to a decrease in masonry stress.
20. An overestimation of shear strength was reported for numerical models simulating reinforced masonry Wallette, while the collapse mechanism was similar, possibly due to the selected contact model between the CFRP and masonry elements.

21. The numerical models developed in ABAQUS enable the investigation the behavior of unreinforced and reinforced brick masonry. It also helps recognize the region where crashing occurs on the brick and locating the failure in the mortar.

- **Recommendations for further research**

An Experimental and numerical study was carried out in extensive research to investigate the behavior of unreinforced and reinforced masonry structures under in-plane loading. In this section, recommendations for future work are listed:

From an experimental point of view:

- It would be necessary to study in more detail the effects of E_{unit}/E_{mortar} ratio and different types of mortar on the shear strength and the ductility of strengthened masonry panels under in-plane loading.
- Investigate the bond behavior between CFRP and masonry Wallette.
- Identity the parameters, which influence the shear behavior of masonry walls such as panel aspect ratio (H/L), material properties, pre-compression, type of loading and boundary condition of the wall.

From a numerical point of view:

- In order to study the damage and the bond mechanism between the CFRP strips and the surface of masonry walls, it would be necessary to introduce a non-linear constitutive law for CFRP composites.
- Damaged masonry panels could be studied in more detail and numerical model could be suggested using XFEM approaches.
- Develop a new analytical model for the prediction of in-plane shear capacity of strengthened masonry walls.

Finally, it is hoped that, the procedure presented in this thesis would help researchers to develop a future numerical model to analyze the behavior of brick masonry wall reinforced with FRP composite with considering the non-linear behavior of the composite to study the bond mechanism of FRP-to masonry interface. In addition, several factors such as type of loading, geometric, the characteristics of the brick units and mortar, and strengthening conditions should

be considered in future studies to develop a suitable design approach for CFRP strengthened masonry walls.

Reference

[1] M. Haroun, A. Mosallam, K. Allam, Cyclic in-plane shear of concrete masonry walls strengthened by FRP laminates, ACI Specia l Publication 230(19) (2005) 327-340.

[2] J. Tumialan, A. Morbin, A. Nanni, C. Modena, Shear strengthening of masonry walls with FRP composites, Composites (2001) 3-6.

[3] A.A. Hamid, W.W. El-Dakhakhni, Z.H. Hakam, M. Elgaaly, Behavior of composite unreinforced masonry–fiber-reinforced polymer wall assemblages under in-plane loading, Journal of composites for Construction, 2005, pp. 73-83.

[4] T. Li, P. Silva, A. Belarbi, A. Nanni, J. Myers, Retrofit of un-reinforced infill masonry walls with FRP, Journal of composites for Construction 5 (2001) 559-563.

[5] M.A. ElGawady, P. Lestuzzi, M. Badoux, In-plane seismic response of URM walls upgraded with FRP, Journal of composites for Construction, 2005, pp. 524-535.

[6] Y. Korany, R. Drysdale, Rehabilitation of masonry walls using unobtrusive FRP techniques for enhanced out-of-plane seismic resistance, Journal of composites for Construction 10(3) (2006) 213-222.

[7] J.C. Wylie, Experimental Testing of Unreinforced Masonry Walls Strengthened with Orthogonal Near-Surface Mounted CFRP Subjected to Out-of-Plane Loading, (2009).

[8] M.R. Valluzzi, D. Tinazzi, C. Modena, Shear behavior of masonry panels strengthened by FRP laminates, Construction and building Materials 16(7) (2002) 409-416.

[9] R.B. Petersen, M.J. Masia, R. Seracino, In-plane shear behavior of masonry panels strengthened with NSM CFRP strips. I: Experimental investigation, Journal of composites for Construction 14(6) (2010) 754-763.

[10] D. Dizhur, M. Griffith, J. Ingham, In-plane shear improvement of unreinforced masonry wall panels using NSM CFRP strips, Journal of composites for Construction 17(6) (2013) 04013010.

[11] H. Maljaee, B. Ghiassi, P.B. Lourenço, Bond behavior in NSM-strengthened masonry, Engineering Structures 166 (2018) 302-313.

[12] P. Lourenço, Computational strategies for masonry structures [Ph. D. thesis], Delft University, The Netherlands (1996).

[13] P.B. Lourenço, Structural masonry analysis: recent developments and prospects, (2008).
[14] A. Mandara, D. Scognamiglio, Prediction of collapse behavior of confined masonry members with ABAQUS, ABAQUS Users' Conference, Munich (2003).
[15] E. LST, Specification for masonry units-Part 1: Clay masonry units, LST EN (2005) 771-1.
[16] C. ASTM, 270. Standard Specification for Mortar for Unit Masonry, Especificación Estándar del Mortero para Unidades de Mampostería (2003).
[17] C.-E.C.f. Standardization, EN 1052-1: 1998-Methods of tests for masonry–Part 1: Determination of compressive strength, (1999).
[18] H.B. Kaushik, D.C. Rai, S.K. Jain, Stress-strain characteristics of clay brick masonry under uniaxial compression, Journal of materials in Civil Engineering 19(9) (2007) 728-739.
[19] N. EN, 196-1, Méthodes d'essais des ciments-Partie 1: détermination des résistances mécaniques, French Standard (2006).
[20] A. Page, The biaxial compressive strength of brick masonry, Proceedings of the Institution of Civil Engineers 71(3) (1981) 893-906.
[21] A. Page, The strength of brick masonry under biaxial tension-compression, International journal of masonry construction 3(1) (1983) 26-31.
[22] W. Samarasinghe, A. Hendry, The tensile of brickwork under biaxial tensile and compressive stress, Proc. 7 th International Symposium on Load Bearing Brickwork, London, 1980, pp. 129-139.
[23] A.W. Page, Finite element model for masonry, Journal of the Structural Division 104(8) (1978) 1267-1285.
[24] A. Zucchini, P.B. Lourenço, Mechanics of masonry in compression: Results from a homogenisation approach, Computers & structures 85(3-4) (2007) 193-204.
[25] L. Binda, A. Fontana, G. Frigerio, Mechanical behaviour of brick masonries derived from unit and mortar characteristics, Brick and Block Masonry(8 th IBMAC) London, Elsevier Applied Science 1 (1988) 205-216.
[26] C.C. Fishburn, Effect of mortar properties on strength of masonry, US Department of Commerce, National Bureau of Standards1961.
[27] K. Wesche, A. Ilantzis, General recommendations for methods of testing loadbearing walls, Mater. Struct./Res. Test. 13(78) (1980) 433.
[28] E. -1-1, Eurocode 6. Design of masonry structures. Part 1-1: General rules for reinforced and unreinforced masonry structures, European Committee for Standardization Brussels, 2005.

[29] H. Backes, On the behavior of masonry under tension in the direction of the bed joints, Dissertation, Aachen University of Technology, Aachen, Germany (1985).
[30] H. Ganz, B. Thürlimann, Tests on the biaxial strength of masonry, Rep. No. 7502 3 (1982).
[31] R. Guggisberg, B. Thürlimann, Experimental determination of masonry strength parameters, Report, 1987.
[32] F. Lurati, H. Graf, B. Thürlimann, Experimental determination of the strength parameters of concrete masonry, Rep. No. 8401 2 (1990).
[33] E. ASTM, 519-02. Standard test method for diagonal tension (shear) in masonry assemblages, CD, American Society for Testing and Materials: Philadelphia (2002).
[34] G. Magenes, G.M. Calvi, In-plane seismic response of brick masonry walls, Earthquake engineering & structural dynamics 26(11) (1997) 1091-1112.
[35] M. Tomaževič, Earthquake-resistant design of masonry buildings, World Scientific1999.
[36] M.A. ElGawady, P. Lestuzzi, M. Badoux, Static cyclic response of masonry walls retrofitted with fiber-reinforced polymers, Journal of composites for Construction 11(1) (2007) 50-61.
[37] R. Van der Pluijm, Shear behaviour of bed joints, (1993).
[38] L. Abdou, R.A. Saada, F. Meftah, A. Mebarki, Experimental investigations of the joint-mortar behaviour, Mechanics research communications 33(3) (2006) 370-384.
[39] N. EN, 1052-3 Norme européenne, norme française: Méthode d'essai de la maçonnerie, Partie, 2003.
[40] C. Calderini, S. Cattari, S. Lagomarsino, The use of the diagonal compression test to identify the shear mechanical parameters of masonry, Construction and building Materials 24(5) (2010) 677-685.
[41] A. Gabor, E. Ferrier, E. Jacquelin, P. Hamelin, Analysis and modelling of the in-plane shear behaviour of hollow brick masonry panels, Construction and building Materials 20(5) (2006) 308-321.
[42] T. Rilem, LUM B6 Diagonal tensile strength tests of small wall specimens, 1991, RILEM Recommendations for the testing and use of constructions materials (1994) 488-489.
[43] L. Pelà, Continuum damage model for nonlinear analysis of masonry structures, (2009).
[44] T.C. Triantafillou, Strengthening of masonry structures using epoxy-bonded FRP laminates, Journal of composites for Construction 2(2) (1998) 96-104.
[45] A. Nanni, J.G. Tumialan, Fiber-reinforced composites for the strengthening of masonry structures, Structural engineering international 13(4) (2003) 271-278.

[46] T. Zhao, J. Xie, H. Li, Strengthening of cracked concrete block masonry walls using continuous carbon fiber sheet, 9th NAMC (2003) 156-167.
[47] J. Cadei, T. Stratford, L. Hollaway, W. Dcukett, Strengthening metallic structures using externally bonded fibre-reinforced polymers, Ciria2004.
[48] H. Mahmood, J.M. Ingham, Diagonal compression testing of FRP-retrofitted unreinforced clay brick masonry wallettes, Journal of composites for Construction 15(5) (2011) 810-820.
[49] O.S. Marshall, S.C. Sweeney, In-plane shear performance of masonry walls strengthened with FRP, International SAMPE Symposium and Exhibition, 万方数据资源系统, 2002, pp. 929-940.
[50] G. Marcari, G. Manfredi, A. Prota, M. Pecce, In-plane shear performance of masonry panels strengthened with FRP, Composites Part B: Engineering 38(7-8) (2007) 887-901.
[51] S.-W. Chuang, Y. Zhuge, T. Wong, L. Peters, Seismic Retrofitting of Unreinforced Masonry Walls by Frp Strip, New Zealand Society for Earthquake Engineering, 2003.
[52] J. Kubica, I. Galman, Comparison of two ways of AAC block masonry strengthening using CFRP strips-diagonal compression test, Procedia Engineering 193 (2017) 42-49.
[53] R.B. Petersen, In-plane shear behaviour of unreinforced masonry panels strengthened with fibre reinforced polymer strips, University of Newcastle, 2009.
[54] C.R. Willis, Q. Yang, R. Seracino, M. Griffith, Bond behaviour of FRP-to-clay brick masonry joints, Engineering Structures 31(11) (2009) 2580-2587.
[55] K. Konthesingha, M.J. Masia, R.B. Petersen, N. Mojsilovic, G. Simundic, A.W. Page, Static cyclic in-plane shear response of damaged masonry walls retrofitted with NSM FRP strips–An experimental evaluation, Engineering Structures 50 (2013) 126-136.
[56] M. Ehsani, H. Saadatmanesh, A. Al-Saidy, Shear behavior of URM retrofitted with FRP overlays, Journal of composites for Construction 1(1) (1997) 17-25.
[57] W.W. El-Dakhakhni, A.A. Hamid, M. Elgaaly, Seismic retrofit of concrete-masonry-infilled steel frames with glass fiber-reinforced polymer laminates, Journal of Structural Engineering 130(9) (2004) 1343-1352.
[58] F. Campanaro, R. Drysdale, A. Hamid, USE OF FIBRE REINFORCED POLYMER TO ENHANCE THE SLIDING SHEAR RESISTANCE OF UNREINRORCED CONCRETE MASONRY.
[59] G. Pavan, K. Nanjunda Rao, Behavior of Brick–Mortar Interfaces in FRP-Strengthened Masonry Assemblages under Normal Loading and Shear Loading, Journal of materials in Civil Engineering 28(2) (2016) 04015120.

[60] P.B. Lourenço, Computations on historic masonry structures, Progress in Structural Engineering and Materials 4(3) (2002) 301-319.
[61] P.G. Asteris, D.M. Cotsovos, C. Chrysostomou, A. Mohebkhah, G. Al-Chaar, Mathematical micromodeling of infilled frames: state of the art, Engineering Structures 56 (2013) 1905-1921.
[62] I. Caliò, M. Marletta, B. Pantò, A new discrete element model for the evaluation of the seismic behaviour of unreinforced masonry buildings, Engineering Structures 40 (2012) 327-338.
[63] P.B. Lourenço, J.G. Rots, Multisurface interface model for analysis of masonry structures, Journal of engineering mechanics 123(7) (1997) 660-668.
[64] D.V. Oliveira, Experimental and numerical analysis of blocky masonry structures under cyclic loading, (2003).
[65] A. Mohebkhah, A. Tasnimi, H. Moghadam, Nonlinear analysis of masonry-infilled steel frames with openings using discrete element method, Journal of constructional steel research 64(12) (2008) 1463-1472.
[66] L.A.S. Kouris, A.J. Kappos, Detailed and simplified non-linear models for timber-framed masonry structures, Journal of Cultural Heritage 13(1) (2012) 47-58.
[67] J. Pina-Henriques, P.B. Lourenço, Masonry compression: a numerical investigation at the meso-level, Engineering computations (2006).
[68] G. van Zijl, A discrete crack modelling strategy for masonry structures, Structural Engineering, Mechanics and Computation, Elsevier2001, pp. 745-752.
[69] P.A. Cundall, A computer model for simulating progressive, large-scale movement in blocky rock system, Proceedings of the International Symposium on Rock Mechanics, 1971, 1971.
[70] P.A. Cundall, O.D. Strack, A discrete numerical model for granular assemblies, geotechnique 29(1) (1979) 47-65.
[71] J. Idris, T. Verdel, M. Al-Heib, Numerical modelling and mechanical behaviour analysis of ancient tunnel masonry structures, Tunnelling and Underground Space Technology 23(3) (2008) 251-263.
[72] V. Sarhosis, K. Tsavdaridis, I. Giannopoulos, Discrete element modelling (DEM) for masonry infilled steel frames with multiple window openings subjected to lateral load variations, Open Construction and Building Technology Journal 8 (2014) 93-103.

[73] T. Bui, A. Limam, Q. Bui, Characterisation of vibration and damage in masonry structures: experimental and numerical analysis, European journal of environmental and civil engineering 18(10) (2014) 1118-1129.
[74] Y. Rashed, M. Abdalla, M. Youssef, Boundary element analysis of masonry structures, WIT Transactions on Modelling and Simulation 19 (1970).
[75] J. Heyman, The safety of masonry arches, International Journal of Mechanical Sciences 11(4) (1969) 363-385.
[76] R.K. Livesley, Limit analysis of structures formed from rigid blocks, International Journal for Numerical Methods in Engineering 12(12) (1978) 1853-1871.
[77] M. Gilbert, C. Melbourne, Rigid-block analysis of masonry structures, Structural engineer 72(21) (1994).
[78] A.ı.n. Orduña, P.B. Lourenço, Cap model for limit analysis and strengthening of masonry structures, Journal of Structural Engineering 129(10) (2003) 1367-1375.
[79] A. Zucchini, P.B. Lourenço, Homogenization of masonry using a micro-mechanical model: Compressive behaviour, (2006).
[80] A. Gabor, Contribution à la caractérisation et à la modélisation des maçonneries non-renforcées et renforcées par matériaux composites, PhD thesis, Université Claude-Bernard Lyon I, 2002.
[81] A.M. Avossa, P. Malangone, A new model for the seismic performance assessment of masonry structures, IX international Forum Le Vie Dei Mercanti, SAVE Heriatage, Aversa, Capri, 2011, pp. 9-11.
[82] P.J.B.B. Lourenço, Computational strategies for masonry structures, (1997).
[83] J.A. Barros, J. Almeida, P.B. Lourenço, Characterization of brick and brick–mortar interface under uniaxial tension, (2002).
[84] L. Abdou, Modélisation du comportement mécanique des murs en maçonnerie charges dans leur plan, Marne-la-Vallée, 2005.
[85] K.J. Willam, Constitutive model for the triaxial behaviour of concrete, Proc. Intl. Assoc. Bridge Structl. Engrs 19 (1975) 1-30.
[86] P. Kohnke, Ansys Inc, Theory manual—Twelfth Edition. SAS IP Inc (2001).
[87] E. Papa, A. Nappi, Numerical modelling of masonry: A material model accounting for damage effects and plastic strains, Applied Mathematical Modelling 21(6) (1997) 319-335.
[88] A.T. Vermeltfoort, T. Raijmakers, Deformation controlled tests in masonry shear walls, part, 1993.

[89] G. Giambanco, L. Di Gati, A cohesive interface model for the structural mechanics of block masonry, Mechanics research communications 24(5) (1997) 503-512.
[90] K.F. Abdulla, L.S. Cunningham, M. Gillie, Simulating masonry wall behaviour using a simplified micro-model approach, Engineering Structures 151 (2017) 349-365.
[91] P.B. Lourenço, Recent advances in masonry modelling: micromodelling and homogenisation, Multiscale modeling in solid mechanics: computational approaches, World Scientific2010, pp. 251-294.
[92] S.-Y. Chen, F. Moon, T. Yi, A macroelement for the nonlinear analysis of in-plane unreinforced masonry piers, Engineering Structures 30(8) (2008) 2242-2252.
[93] M. Annecchiarico, F. Portioli, R. Landolfo, Micro and macro finite element modeling of brick masonry panels subject to lateral loadings, Proc., COST C26 Action Final Conf, 2010, pp. 315-320.
[94] A. Drougkas, P. Roca, C. Molins, Experimental analysis and detailed micro-modeling of masonry walls subjected to in-plane shear, Engineering Failure Analysis 95 (2019) 82-95.
[95] C. Belghiat, J.-P. Plassiard, P. Perrotin, O. Plé, M. Guenfoud, A. Messabhia, Contribution à la modélisation dynamique de la maçonnerie chainée, Academic Journal of Civil Engineering 34(1) (2016) 261-268.
[96] B. Luccioni, V.C. Rougier, In-plane retrofitting of masonry panels with fibre reinforced composite materials, Construction and building Materials 25(4) (2011) 1772-1788.
[97] B. Luccioni, V.C. Rougier, Numerical analysis of fibre reinforced polymer retrofitted masonry panels, Engineering Structures 49 (2013) 360-372.
[98] M. kabir, a. Kalali, In-plane Numerical Modelling of Sterngthened Perforated Masonry Walls Using FRP under Cyclic Loading, (2013).
[99] A. Gabor, A. Bennani, E. Jacquelin, F. Lebon, Modelling approaches of the in-plane shear behaviour of unreinforced and FRP strengthened masonry panels, Composite structures 74(3) (2006) 277-288.
[100] E. Grande, G. Milani, E. Sacco, Modelling and analysis of FRP-strengthened masonry panels, Engineering Structures 30(7) (2008) 1842-1860.
[101] S. Zhang, D. Yang, Y. Sheng, S.W. Garrity, L. Xu, Numerical modelling of FRP-reinforced masonry walls under in-plane seismic loading, Construction and building Materials 134 (2017) 649-663.
[102] L. Ascione, L. Feo, F. Fraternali, Load carrying capacity of 2D FRP/strengthened masonry structures, Composites Part B: Engineering 36(8) (2005) 619-626.

[103] P. Carrara, D. Ferretti, F. Freddi, Debonding behavior of ancient masonry elements strengthened with CFRP sheets, Composites Part B: Engineering 45(1) (2013) 800-810.
[104] Y. Zhuge, Numerical study of URM walls retrofitted with cable and FRP, Proc., 14th Int. Brick and Block Masonry Conf, 2008.
[105] G. Van Zijl, P. De Vries, Masonry wall crack control with carbon fiber reinforced polymer, Journal of composites for Construction 9(1) (2005) 84-89.
[106] L. Schueremans, Probabilistic evaluation of structural unreinforced masonry, (2001).
[107] R. Van der Pluijm, Out-of-plane bending of masonry: behaviour and strength, (1999).
[108] A.A.A. Hamid, Behaviour characteristics of concrete masonry, (1978).
[109] N. Mojsilovic, P. Marti, Tests on masonry walls subjected to combined actions, Report No. 203 (1994).
[110] M. Dhanasekar, A. Page, P. Kleeman, The failure of brick masonry under biaxial stresses, Proceedings of the Institution of Civil Engineers 79(2) (1985) 295-313.
[111] B. EN, 771-1 (2003), Specification for Masonry Units-Part 1: Clay Masonry Units, British Standards Institute.
[112] G. Vasconcelos, P. Lourenço, Experimental characterization of stone masonry in shear and compression, Construction and building Materials 23(11) (2009) 3337-3345.
[113] B. EN, 1015-11: 1999, Methods of test for mortar for masonry. Determination of flexural and compressive strength of hardened mortar (1999).
[114] T. RILEM, 76-LUM-B. 1, Compressive strength of small walls and prisms (1991).
[115] B. EN, 1052-3.(2002), Methods of test for masonry, Part 3: Determination of initial shear strength.
[116] T. Paulay, M.N. Priestley, Seismic design of reinforced concrete and masonry buildings, (1992).
[117] M. Saghafi, S. Safakhah, A. Kheyroddin, M. Mohammadi, In-plane shear behavior of FRP strengthened masonry walls, APCBEE procedia 9 (2014) 264-268.
[118] C.S. Association, CSA S304. 1-04: Design of masonry structures, CSA, Mississauga, ON, Canada (2004).
[119] E. CEN, 1052-1: 1998 Methods of test for masonry-Part 1: Determination of compressive strength, Comité Européen de Normalisation, Brussels (2001).
[120] N. Augenti, F. Parisi, Constitutive modelling of tuff masonry in direct shear, Construction and building Materials 25(4) (2011) 1612-1620.
[121] F. 306, Evaluation of earthquake damaged concrete and masonry wall buildings: Basic procedures manual, FEMA, Washington, DC, 1998.

[122] B.V. Reddy, C.V.U. Vyas, Influence of shear bond strength on compressive strength and stress–strain characteristics of masonry, Materials and structures 41(10) (2008) 1697-1712.
[123] A. Parvin, T. Syed Shah, Fiber reinforced polymer strengthening of structures by near-surface mounting method, Polymers 8(8) (2016) 298.
[124] R. Seracino, J.C. Wylie, FRP Strengthening and Repair of Unreinforced Brick Masonry Walls.
[125] J. Lubliner, J. Oliver, S. Oller, E. Oñate, A plastic-damage model for concrete, Int. J. Solids and Structures (1989).
[126] C. Santos, R. Alvarenga, J. Ribeiro, L. Castro, R. Silva, A. Santos, G. Nalon, Numerical and experimental evaluation of masonry prisms by finite element method, Revista IBRACON de Estruturas e Materiais 10(2) (2017) 477-508.
[127] V. Abaqus, 6.14-1. Abaqus/standard user's manual and Abaqus CAE manual, Providence, RI, USA: Dassault Systemes Simulia Corp (2014).
[128] F. Abaqus, Analysis User's Manual 6.14, Dassault Systemes Simulia Corp., Providence, RI (2011).
[129] Y.T. Obaidat, S. Heyden, O. Dahlblom, G. Abu-Farsakh, Y. Abdel-Jawad, Retrofitting of reinforced concrete beams using composite laminates, Construction and building Materials 25(2) (2011) 591-597.
[130] T. Belytschko, J. Fish, B.E. Engelmann, A finite element with embedded localization zones, Computer methods in applied mechanics and engineering 70(1) (1988) 59-89.
[131] T. Belytschko, T. Black, Elastic crack growth in finite elements with minimal remeshing, International Journal for Numerical Methods in Engineering 45(5) (1999) 601-620.
[132] N. Moës, J. Dolbow, T. Belytschko, A finite element method for crack growth without remeshing, International Journal for Numerical Methods in Engineering 46(1) (1999) 131-150.
[133] T.P. Fries, T. Belytschko, The extended/generalized finite element method: an overview of the method and its applications, International Journal for Numerical Methods in Engineering 84(3) (2010) 253-304.
[134] J.M. Melenk, I. Babuška, The partition of unity finite element method: basic theory and applications, Research Report/Seminar für Angewandte Mathematik, Eidgenössische Technische Hochschule, Seminar für Angewandte Mathematik, 1996.
[135] N. Sukumar, N. Moës, B. Moran, T. Belytschko, Extended finite element method for three-dimensional crack modelling, International Journal for Numerical Methods in Engineering 48(11) (2000) 1549-1570.

[136] M. Stolarska, D.L. Chopp, N. Moës, T. Belytschko, Modelling crack growth by level sets in the extended finite element method, International Journal for Numerical Methods in Engineering 51(8) (2001) 943-960.
[137] F. Fouchal, Contribution à la modélisation numérique des interfaces dans les structures maçonnées, Reims, 2006.
[138] V. Sarhosis, J. Lemos, A detailed micro-modelling approach for the structural analysis of masonry assemblages, Computers & structures 206 (2018) 66-81.